A Nanoscale Blueprint of the Human Kinetochore and the Functional Limits of Its Design

by

Alexander A. Kukreja

A dissertation submitted in partial fulfillment
of the requirements for the degree of
Doctor of Philosophy
(Biophysics)
in the University of Michigan
2021

Doctoral Committee:

Associate Professor Ajit Joglekar, Chair
Associate Professor Julie Biteen
Associate Professor Uhn-Soo Cho
Professor Janet Smith
Professor Yukiko Yamashita, Massachusetts Institute of Technology
Assistant Professor Qiong Yang

Alexander A. Kukreja

akukreja@umich.edu

ORCID iD: 0000-0003-1066-9958

Acknowledgments

Thanks to Ajit Joglekar, whose lab I ended up in by accidental circumstances. Many great things in my life I stumbled into while trying to pursue other goals. I, therefore, count myself fortunate to have recognized that my 'other goals' during the start of graduate school were flexible enough to accommodate a lab that was completely counter-intuitive to my 'research ideals'. Ajit was accidentally the perfect mentor for me during these past years of growth and learning. His lab was accidentally an incredible environment for me to learn about science. The research goals of his lab were accidentally ideal. And perhaps the most rewarding part of these past six years working with Ajit is that I think we may accidentally have become really good friends in the process.

I also need to thank my first research mentor, Adam Zlotnick at Indiana University. My journey to graduate school at the University of Michigan comes with a long back-story of struggle which was put to an end in Adam's lab. When I came to Adam's lab, I was defeated by a lack of self-confidence, a sense of failure for having previously dropped out of a life sciences PhD program, and a lack of practical bench and critical thinking skills. Fortunately, Adam's lab was a place where second chances could not only be born but also thrive. I was given the space and patience to set down of a lot of the self-defeating habits I walked into his lab with and in exchange I picked up a passion and direction for my life. I should also mention, when I was struggling to choose between labs after my first year at the University of Michigan, Adam may have accidentally pushed me towards Ajit's lab.

I could spend an eternity thanking the myriads of other people that have helped me throughout graduate school, both in the context of science and in the broader category of life. However, I will opt to severely condense my acknowledgements by ending on a special thanks to the three who have provided me with my most profound lessons in patience, forgiveness, dedication, hard work, loyalty, unconditional love, and having fun: my dogs Ruby Roo, Eddie Vedder, and Clarabella Puppydog.

Table of Contents

List of Tables

List of Figures

Abstract

Cellular duplication is the cornerstone of all life, allowing organisms to replicate and develop through the creation of genetically identical cells. Proper duplication requires cells to accurately segregate copies of their DNA so that the resulting sister cells each receive a full complement of the genome. In eukaryotes, the segregation process is accomplished by the kinetochore, a large multi-protein structure built upon the centromeric DNA of chromosomes. To segregate chromosomes with high fidelity, the kinetochore executes three principal functions: (1) spindle assembly checkpoint (SAC) signaling, where unattached kinetochores pause the cell cycle until they attach to the spindle; (2) error correction, where kinetochores destabilize incorrect attachments that may otherwise lead to missegregation; and (3) force generation, where kinetochores physically move chromosomes by coupling to the energy of microtubule depolymerization. To implement these functions, the kinetochore incorporates a large, interconnected network of multicopy proteins. While the biochemical and structural properties of many of these proteins are known, a mechanistic understanding of how these proteins integrate to give rise to the emergent functions of chromosome segregation is lacking. To achieve such insights, the number and spatial arrangement, or 'architecture', of kinetochore proteins must be solved.

In this thesis, I develop a Förster Resonance Energy Transfer-based microscopy method to map the nanoscale organization of human kinetochore proteins relative to its ~20 microtubule attachments. I focus my studies on the Ndc80 complex (Ndc80C), the central microtubule-

binding molecule of the kinetochore with important roles in all its principal functions. I find that Ndc80C molecules cluster during microtubule attachment despite being recruited by centromeric proteins which are separated by ≥10 nm. Furthermore, Ndc80C clustering depends on microtubule attachment and reduces significantly in unattached kinetochores. I also discover that Ndc80C clustering increases with centromeric tension and provide evidence that this correlation relies on the ability of centromeric tension to promote Ndc80C binding. Additionally, I show that Ndc80C clustering persists when its centromeric receptors are significantly diminished, suggesting a 'lawn-like' model of human kinetochore function. I synthesize these data into an architectural framework of human kinetochore-microtubule attachments, highlighting the potential functional implications of this architecture.

In a second project, I investigate the architecture/function relationship of the human kinetochore by asking: what is the minimum number of the human kinetochore's ~250 Ndc80C molecules needed for proper chromosome segregation? To answer this question, I perform a series of 'stress tests' to determine the failure limits of kinetochore function by titrating human kinetochores with microtubule-binding mutants of Ndc80C. These tests reveal that the SAC is activated in a sigmoidal, switch-like manner when the number of functional Ndc80C molecules falls below 60%. This all-or-nothing response suggests that the human kinetochore rapidly extinguishes SAC signaling beyond a threshold number of microtubule-bound Ndc80C molecules. Additionally, severe chromosome alignment and segregation errors occur when kinetochores contain as little as 20% of a non-regulatable, strong-binding Ndc80C mutant. Thus, the kinetochore achieves proper chromosome segregation through a remarkably acute ability to fine-tune the attachment strength of Ndc80C. Overall, these stress tests demonstrate that the

human kinetochore incorporates an excess of Ndc80C, allowing it to operate with definable margins of error.

As a final summary, my work highlights the reciprocal relationship between kinetochore architecture and function, each influencing the other to ultimately converge on the principles of accurate chromosome segregation.

CHAPTER 1:

How Kinetochore Architecture Shapes the Mechanisms of Its Function

This chapter is from a peer-reviewed article:

How Kinetochore Architecture Shapes the Mechanisms of Its Function

Ajit P. Joglekar and Alexander A. Kukreja. *Curr Biol*, *2017*, *27*(16), R816-R824.

doi:10.1016/j.cub.2017.06.012 *originally published online August 21, 2017*

1.1 Abstract

The eukaryotic kinetochore is a sophisticated multi-protein machine that segregates chromosomes during cell division. To ensure accurate chromosome segregation, it performs three major functions using disparate molecular mechanisms. It operates a mechanosensitive signaling cascade known as the spindle assembly checkpoint (SAC) to detect and signal the lack of attachment to spindle microtubules, and delay anaphase onset in response. In addition, after attaching to spindle microtubules, the kinetochore generates the force necessary to move chromosomes. Finally, if the two sister kinetochores on a chromosome are both attached to microtubules emanating from the same spindle pole, they activate another mechanosensitive mechanism to correct the monopolar attachments. All three of these functions maintain genome

stability during cell division. The outlines of the biochemical activities responsible for these functions are now available. How the kinetochore integrates the underlying molecular mechanisms is still being elucidated. In this review, we discuss how the nanoscale protein organization in the kinetochore, which we refer to as kinetochore 'architecture', organizes its biochemical activities to facilitate the realization and integration of emergent mechanisms underlying its three major functions. For this discussion, we will use the relatively simple budding yeast kinetochore as a model and extrapolate insights gained from this model to elucidate functional roles of the architecture of the much more complex human kinetochore.

1.2 Introduction

Multi-protein assemblies and machines assume tremendously diverse composition and organization to perform complex cell biological functions. An excellent example of a protein assembly is the endocytic coat, which is a transient, continuously evolving assemblage of many interacting proteins (Picco, Mund, Ries, Nedelec, & Kaksonen, 2015). At the other extreme is the nuclear pore. The core scaffold of the nuclear pore is a long-lived structure containing precisely organized copies of many proteins (Alber et al., 2007). In both cases, the protein 'architecture', defined as the nanoscale spatial organization of component proteins within the protein assembly or machine, influences how they cooperate with one another to realize their functions. Reductionist methods have been extremely successful in defining structure-function relationships for individual proteins. However, to fully understand multi-protein machines, integrative approaches that define how individual components give rise to emergent functions, and establish 'architecture-function' relationships, are also necessary. The eukaryotic kinetochore presents an excellent case to study architecture-function relationships.

Much is now known about the structures, biochemical activities, and the biophysics of the component proteins of the kinetochore that execute its three major functions (Figure 1.1A) (Musacchio & Desai, 2017). However, this knowledge does not fully reveal the underlying molecular mechanisms, explain how the kinetochore integrates these mechanisms into one framework, or predict the possibility of cross-talk among its functions (Nezi & Musacchio, 2009). For this, the spatial organization of the biochemical activities must be considered. Complicating this analysis, however, is the fact that most eukaryotic kinetochore bind multiple microtubules dynamically. For example, the human kinetochore simultaneously interacts with the plus-ends of ~20 microtubules that exist as a mixed population of both polymerizing and depolymerizing microtubules. Furthermore, the ~200 nm diameter disk-shaped human

kinetochore is densely populated with a large and diverse set of proteins, most of which are present in multiple copies. In this context, the kinetochore found in the budding yeast *Saccharomyces cerevisiae* is a particularly suitable model because it stably binds to the plus-end of one microtubule in metaphase (McIntosh et al., 2013; Winey et al., 1995). It thus represents the basic functional unit of the eukaryotic kinetochore – one kinetochore-microtubule attachment. Important aspects of the architecture of the yeast kinetochore-microtubule attachment in metaphase have been quantified. Models of kinetochore architecture created from these and structural data provide the starting point needed to study architecture-function relationships (Aravamudhan, Felzer-Kim, Gurunathan, & Joglekar, 2014; Aravamudhan, Goldfarb, & Joglekar, 2015).

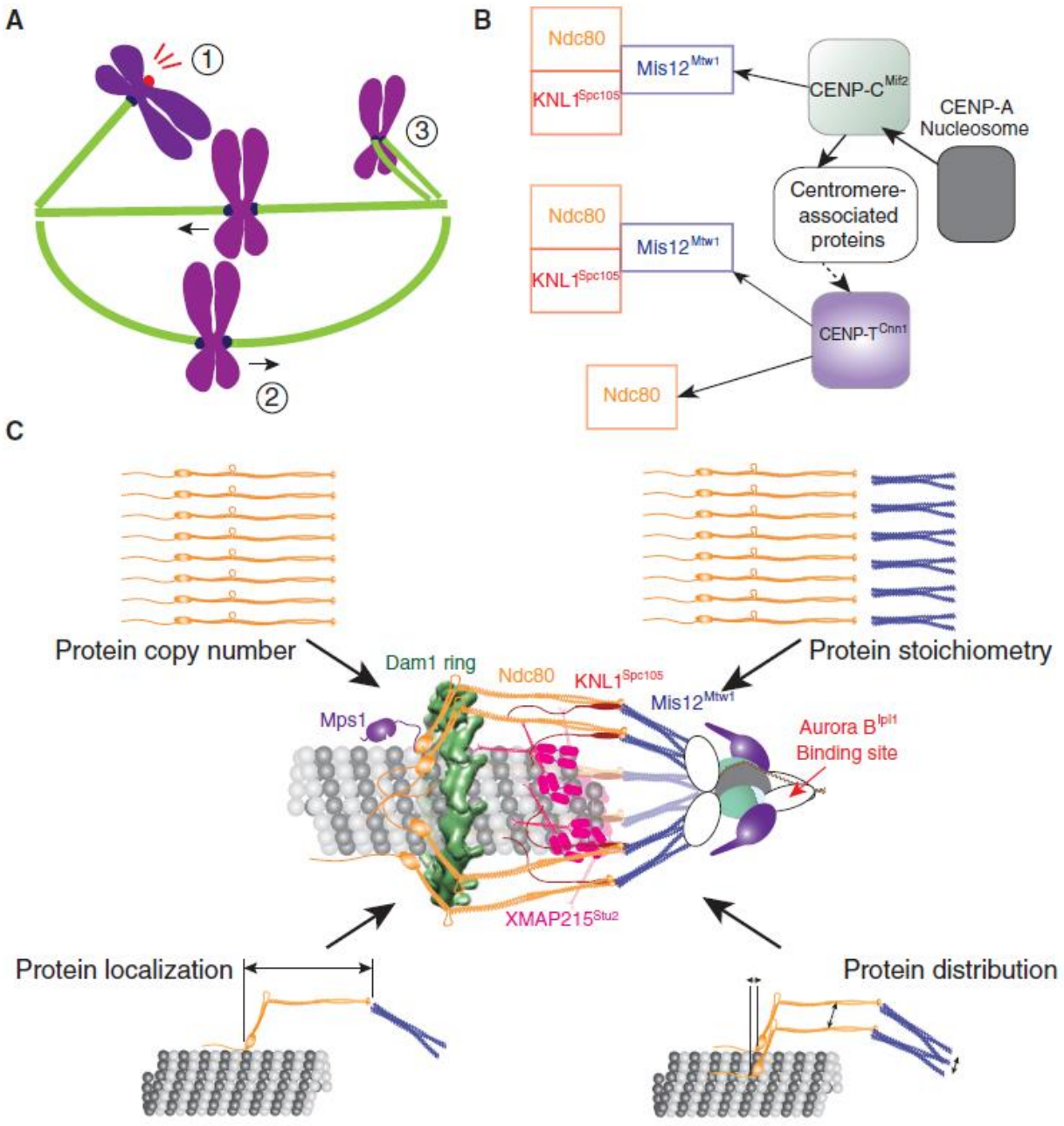

Figure 1.1 The function and protein architecture of the kinetochore
(A) Cartoon of a mitotic spindle displaying the three main kinetochore functions: (1) activation of the spindle assembly checkpoint, (2) generation of bidirectional chromosome movement that is coupled to microtubule polymerization and depolymerization, and (3) correction of monopolar attachment of sister kinetochores. (B) (left to right = microtubule plus-end to centromere) The conserved dual pathways (solid arrows, direct interaction; dashed arrow, indirect interaction) that assemble the KMN network, which forms the interface of the kinetochore with the microtubule plus-end. (C) Reconstruction of the protein architecture of the budding yeast kinetochore using fluorescence microscopy measurements and protein structures (Aravamudhan et al., 2014; Aravamudhan et al., 2013; Aravamudhan et al., 2015; Ayaz et al., 2012; Ciferri et al., 2008; Dimitrova et al., 2016; Joglekar et al., 2009; Joglekar et al., 2006; Petrovic et al., 2016; Westermann et al., 2005). Centromere-associated proteins are represented by white, oblong shapes.

The core protein machinery of the yeast kinetochore is conserved. Therefore, the architecture-function relationships derived from budding yeast will provide insight into the operation of the highly complex human kinetochore. Indeed, a recent study proposed an elegant conceptualization of the human kinetochore as the two-dimensional convolution of multiple yeast kinetochore-like subunits over a disk-shaped surface (Weir et al., 2016). Nevertheless, the human kinetochore is built for entirely different performance specifications – it must coordinate the activities of its multiple microtubule binding sites to move the chromosome over longer distances (~5 μm *versus* < 0.5 μm in budding yeast) (Magidson et al., 2011), against much larger opposing forces (> 100 pN *versus* < 7 pN in yeast) (Akiyoshi et al., 2010; Nicklas, 1983). In this Review, we will use the budding yeast kinetochore as a starting point for the discussion of architecture-function relationships. We will then highlight how these relationships may fit into the complex architecture of the human kinetochore, and the areas in which the two kinetochores likely diverge.

1.3 The Composition, Assembly Pathways, and Biochemical Activities of the Kinetochore

We begin the discussion by briefly describing the essential biochemical activities that execute the three major functions of the kinetochore (please see the recent review by Musacchio and Desai (Musacchio & Desai, 2017) for a comprehensive discussion of the molecular biology of the kinetochore). We will refer to each protein by the name for the human ortholog followed by a super-scripted name of the corresponding budding yeast protein, if it is different. From the functional perspective, the protein composition and assembly of the kinetochore can be simplified as follows (Figure 1.1B). The kinetochore interacts with the microtubule and with SAC signaling proteins through a network of three protein complexes: KNL1^{Spc105}, Mis12^{Mtw1}, and Ndc80, collectively referred to as the KMN network (Cheeseman, Chappie, Wilson-Kubalek, & Desai, 2006; Dimitrova, Jenni, Valverde, Khin, & Harrison, 2016; Petrovic et al., 2016). This interface is assembled by two parallel pathways initiated by the proteins CENP-C^{Mif2} and CENP-T^{Cnn1} (Gascoigne et al., 2011; Huis In 't Veld et al., 2016; Kim & Yu, 2015; Nishino et al., 2012; Rago, Gascoigne, & Cheeseman, 2015). CENP-C^{Mif2} and CENP-T^{Cnn1} are assembled on a well-defined territory on each chromosome, known as the centromere, through their interactions with the centromere-specific histone H3 variant CENP-A^{Cse4} (Gascoigne et al., 2011; Klare et al., 2015; Weir et al., 2016). Although the CENP-C^{Mif2} and CENP-T^{Cnn1} pathways are conserved, their contribution to kinetochore function is species-specific – both pathways are required for the function of the human kinetochore, whereas only the CENP-C^{Mif2} pathway is required in budding yeast (Schleiffer et al., 2012).

Remarkably, the three kinetochore mechanisms of end-on microtubule attachment, SAC signaling, and error correction ultimately focus on just two proteins that directly interface the kinetochore with the microtubule and the SAC signaling machinery – Ndc80 and KNL1^{Spc105}. To activate the SAC, the calponin-homology (CH) domains of Ndc80, which are globular domains

located at the microtubule-binding end of the complex, bind the SAC activator, Mps1 kinase (Aravamudhan et al., 2015; Hiruma et al., 2015; Ji, Gao, & Yu, 2015; Kemmler et al., 2009). Mps1 phosphorylates conserved motifs within KNL1^{Spc105} to enable these motifs to recruit a number of SAC signaling proteins and form the mitotic checkpoint complex (Faesen et al., 2017; Ji, Gao, Jia, Li, & Yu, 2017; London & Biggins, 2014; London, Ceto, Ranish, & Biggins, 2012; Shepperd et al., 2012). KNL^{Spc105} also recruits phosphatases that antagonize Mps1 to facilitate SAC silencing (London et al., 2012). In addition to the crucial role of recruiting Mps1 for SAC signaling, the CH-domains of Ndc80 also function as the primary binding site that establishes end-on microtubule attachment (Ciferri et al., 2008; DeLuca et al., 2006). To maintain end-on attachments and to generate force, Ndc80 recruits several accessory microtubule-associated proteins (e.g., Dam1 complex in fungi; Ska complex, Astrin/SKAP, etc. in metazoa (Manning et al., 2010; Welburn et al., 2009; Westermann et al., 2005)). Finally, the kinetochore destabilizes monopolar attachments by directing the Aurora B^{Ipl1} kinase toward the microtubule-binding domains of Ndc80 and other proteins, thereby weakening their affinity for the microtubule (Chan, Jeyaprakash, Nigg, & Santamaria, 2012; Liu, Vader, Vromans, Lampson, & Lens, 2009; Pinsky, Kung, Shokat, & Biggins, 2006; Schmidt et al., 2010; Shang et al., 2003; Tien et al., 2010; Welburn et al., 2010). This description of the biochemical activities of kinetochore proteins does not fully explain the underlying molecular mechanisms – knowledge of kinetochore architecture is required to elucidate how these activities cooperate. Furthermore, the functional roles of any reorganization of the kinetochore induced by microtubule attachment or dynamic changes within the architecture during kinetochore movement must also be studied.

1.4 The Protein Architecture in the End-On Kinetochore-Microtubule Attachment

The end-on morphology of the kinetochore-microtubule attachment is highly conserved in all eukaryotes that have been studied to date (McIntosh et al., 2013). Kinetochore researchers recognized early on that this morphology plays an integral role in its functional mechanisms and proposed generalized models centered on the end-on morphology to explain the functional mechanisms (Hill, 1985; Inoue & Salmon, 1995; McIntosh, 1991). To test the implementation of these model mechanisms, however, it is necessary to first define the biochemical properties and structures of kinetochore components and then their organization within the end-on kinetochore-microtubule attachment. The latter part has proven to be a significant challenge. The kinetochore is a network of several protein components, most of which are present in multiple copies. Many of these components contain inherently flexible domains and linkages (Musacchio & Desai, 2017). Additionally, the microtubule plus-end likely re-organizes this protein network in a functionally significant manner (Dong, Vanden Beldt, Meng, Khodjakov, & McEwen, 2007; Magidson et al., 2016). These issues pose a major obstacle for structural biological approaches in defining its architecture. Resolving the positions of individual molecules in the densely packed kinetochore is also beyond the capabilities of super-resolution microscopy. Therefore, alternative approaches are necessary to determine the architecture.

One such approach is to re-construct kinetochore architecture by answering simpler questions pertaining to its key features (Figure 1.1C). How many molecules of each protein component does one kinetochore incorporate, and how variable is this number? What is the average position of each component, and are these positions variable? What is the axial and circumferential distribution of protein molecules about their average positions? Quantitative answers to these questions obtained from diverse fluorescence microscopy methods and combined with the known structures of kinetochore proteins established a detailed model of the

architecture of the KMN network in the budding yeast kinetochore-microtubule attachment (Aravamudhan et al., 2014; Aravamudhan, Felzer-Kim, & Joglekar, 2013; Joglekar, Bloom, & Salmon, 2009; Joglekar, Bouck, Molk, Bloom, & Salmon, 2006). Although this architecture invokes certain assumptions, specifically the circular symmetry of kinetochore proteins around the microtubule diameter and the relative positions of the CH-domains and the Dam1 ring, it has enabled powerful predictions regarding the emergent mechanisms of kinetochore function (discussed in the sections below).

Much work is still needed to synthesize a similar understanding of the architecture of the human kinetochore. The average copy numbers of KMN network molecules per kinetochore, and their organization along the axis of the microtubule in metaphase are known (Suzuki, Badger, & Salmon, 2015; Wan et al., 2009). However, their distribution about the average positions and over the disk-shaped surface of the centromere is unknown, a problem that is significantly complicated by the fact that human kinetochores contain multiple microtubule binding sites (Figure 1.2A). Identification of the CENP-A^{Cse4} nucleosome as the minimal foundation for assembling the KMN network will simplify to some extent (Huis In 't Veld et al., 2016; Weir et al., 2016). This finding is useful for proposing a model for the 'local' kinetochore architecture, defined as the organization of kinetochore proteins in one kinetochore-microtubule attachment. The bilateral symmetry of the CENP-A^{Cse4} nucleosome will impose an orientation and spacing on the two CENP-C^{Mif2} molecules that it recruits (Figure 1.2B, top). This patterning of CENP-C^{Mif2} will then direct the spatial organization of other centromeric proteins, including CENP-T^{Cnn1}. Thus, the spatial organization of centromeric proteins will ultimately dictate the patterning of KMN network molecules, and hence the architecture of the interface of the human kinetochore with the microtubule plus-end (Figure 1.2B, bottom). Beyond the local architecture

of KMN molecules within one attachment lies the broader architecture of the kinetochore – the distribution of many such attachments across the disk-shaped surface of the centromere. This broader architecture will influence the ability of the kinetochore to interact simultaneously with many microtubule plus-ends. Defining both the local and broader architecture of the human kinetochore remains a major challenge for the field.

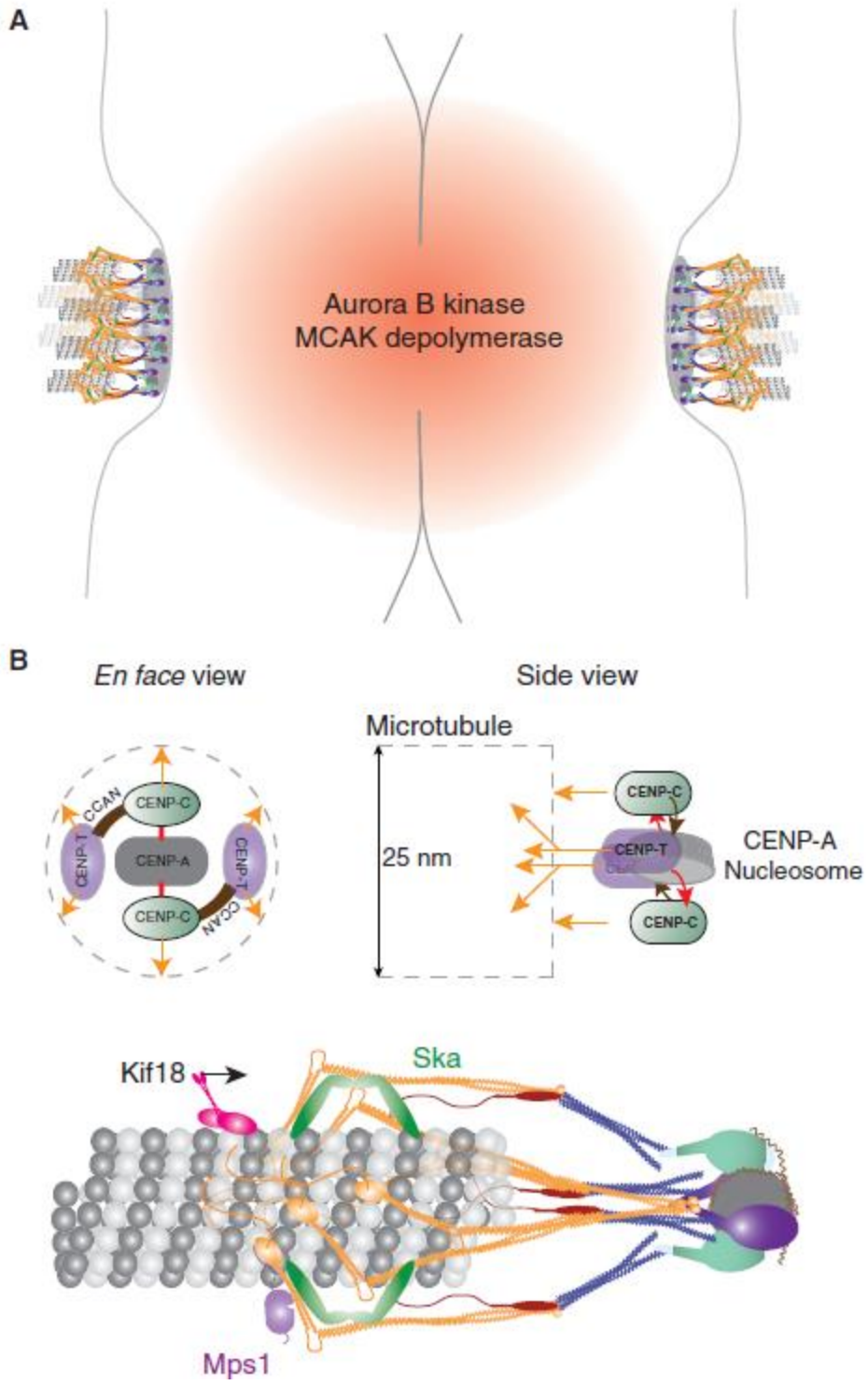

Figure 1.2 Protein architecture of the human kinetochore
(A) Cartoon of the organization of sister kinetochores on a human chromosome. The inter-centromeric localization of Aurora B^{Ipl1} and MCAK is highlighted. (B) Top: schematic displays a hypothetical spatial manifestation of the biochemical pathways of kinetochore assembly. Orange arrows indicate pathways of Ndc80 recruitment; grey dashed lines represent the microtubule. Note that CENP-T^{Cnn1} recruits two Ndc80 molecules. Bottom: cartoon of a hypothetical local architecture of the kinetochore-microtubule attachment in humans.

1.5 Kinetochore Architecture Encodes a Mechanism for Sensing End-On Attachment

In most eukaryotes, the kinetochore is unattached at the beginning of mitosis. To avoid chromosome missegregation, it delays cell division by activating the SAC. Typically, the kinetochore first binds laterally to the microtubule lattice, and then converts this interaction into a stable end-on attachment. SAC inactivation occurs once end-on attachments form (Hiruma et al., 2015; Krefman, Drubin, & Barnes, 2015). Recent work reveals two mechanisms that the kinetochore can use to detect end-on attachment and silence the SAC in response (Aravamudhan et al., 2015; Hiruma et al., 2015; Ji et al., 2015). Both mechanisms rely on the dual role of the CH-domains of Ndc80 as the Mps1 binding and as the interface for end-on attachment. The first mechanism, studied in human cells, proposes that Mps1 and the microtubule plus-end compete for binding to the CH-domains of Ndc80 (Hiruma et al., 2015; Ji et al., 2015). Consequently, end-on attachments displace Mps1 from the kinetochore so that it can no longer phosphorylate KNL^{Spc105}. The second mechanism, which comes from studies in budding yeast, suggests an integral role for kinetochore architecture in implementing the attachment-mediated SAC silencing (Aravamudhan et al., 2015).

The signaling state of the yeast kinetochore is determined by a single change in its architecture that is elicited by end-on attachment. In the unattached, SAC active kinetochore, the CH-domains of Ndc80 are located within 10 nm of the phosphodomain of $KNL1^{Spc105}$ (Figure 1.3A, top). Therefore, Mps1 bound to the CH-domains robustly phosphorylates $KNL1^{Spc105}$ and the SAC proteins that it recruits, initiating the SAC. In the attached, SAC inactive kinetochore, the CH-domains and $KNL1^{Spc105}$ phosphodomain are ~30 nm apart (Joglekar et al., 2009). This prevents Mps1 from phosphorylating $KNL1^{Spc105}$, thereby disrupting SAC signaling (Figure 1.3A, bottom). If the 30 nm gap is experimentally abridged, the yeast kinetochore becomes unable to sense end-on attachment, and the SAC becomes constitutively active (Aravamudhan et

al., 2015). Thus, the yeast kinetochore relies on the separation between Mps1 and its target to detect end-on attachments.

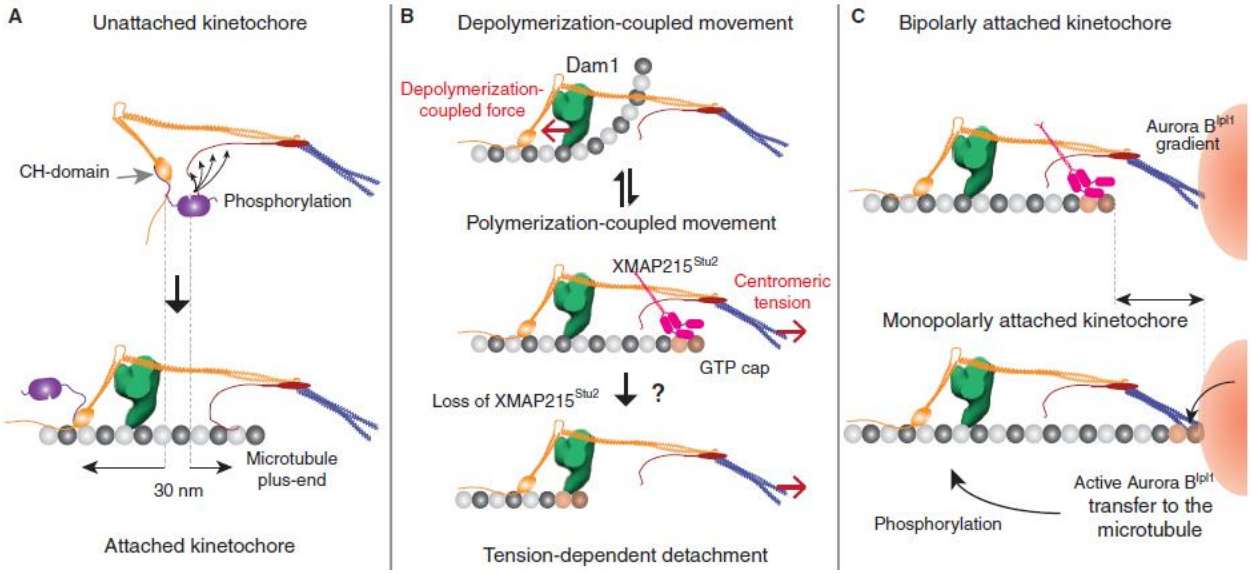

Figure 1.3 Proposed architecture-function relationships for the yeast kinetochore
1D representations of the kinetochore shown. (A) Role of kinetochore architecture in SAC inactivation. Separation of the CH-domains of Ndc80 and the phosphodomain of KNL1^{Spc105} by end-on attachment (highlighted by dashed lines) disrupts the phosphorylation of KNL1^{Spc105} by the Mps1 kinase (purple) bound to the CH-domain. (B) Proposed roles of the architecture of microtubule-binding proteins in generating bidirectional movement. Top: When the plus-end is depolymerizing, the Dam1 ring (green) mechanically opposes the curling of tubulin protofilaments and experiences a pushing force (red arrow). Middle panel: A proposed scenario where XMAP215^{Stu2} localizes to the kinetochore by recognizing the GTP-tubulin cap on the polymerizing plus-end. Its microtubule-destabilizing activity reverts the plus-end back to the depolymerizing state. Bottom panel: In the absence of XMAP215^{Stu2} activity, centromeric tension can slide the kinetochore off the growing plus-end. (C) Potential roles for kinetochore architecture in correcting monopolar attachment. The position of the plus-end may be significantly different in kinetochores with bipolar and monopolar attachment (highlighted by the arrow and accompanying dashed lines). The proximity of the lattice to the centromere may facilitate the transport of hyper-activated Aurora B^{Ipl1} kinase to its targets – microtubule-binding kinetochore proteins.

Despite recent progress, two significant questions about the mechanism of SAC silencing remain unresolved. The first question is whether the silencing mechanism exclusively relies on the presence of end-on attachment, or whether it also requires force generation by such an attachment. Recent observations suggest that force generation is not necessary for SAC silencing (Etemad, Kuijt, & Kops, 2015; Tauchman, Boehm, & DeLuca, 2015). This conclusion is consistent with the biochemical competition mechanism for SAC silencing, which does not require any force. It is also consistent with the architecture-based model of SAC silencing: the

displacement of two protein domains is unlikely to require a large force (Aravamudhan et al., 2015; Joglekar, 2016). Future biophysical analyses of SAC silencing by the kinetochore will unequivocally establish whether SAC silencing requires significant force generation by end-on attachment. The second question relates to the assumption of the binary, switch-like activation and inactivation of the SAC in the two models. This description is superficially valid for the yeast kinetochore, which can exist in only one of two states – attached or unattached. The binary state description does not apply to the human kinetochore because it attaches dynamically to ~20 microtubule plus-ends that turn over completely in about 4 minutes (Godek, Kabeche, & Compton, 2015). Furthermore, study of metaphase kinetochores in Potaroo kidney (PtK1) cells suggest that the kinetochore possesses ~15% excess microtubule-binding capacity that is unused even in metaphase (McEwen, Heagle, Cassels, Buttle, & Rieder, 1997). To distinguish between partial attachment from a complete lack of attachments, the human kinetochore may use either additional regulation or more complex mechanisms to silence the SAC. For example, to inactivate the SAC, the human kinetochore may use either a temporal threshold defined by a minimum time period that the kinetochore must spend in the attached state, or a number threshold defined by the minimum number of microtubules bound by the kinetochore. Very little is known about the existence or nature of such mechanisms.

1.6 The Role of Kinetochore Architecture in Driving Persistent, Bidirectional Chromosome Movement

As suggested by its name, the major function of the kinetochore is to drive chromosome movement. It produces the force necessary for generating movement by harnessing microtubule polymerization dynamics. It is reasonable to expect that the architecture of the microtubule-binding kinetochore proteins is tailored to suit the changing form and position of tubulin dimers

at the plus-end. The kinetochore also recruits motor proteins and microtubule-associated proteins (MAPs) as accessory factors for attachment and force generation. These proteins are expected to occupy positions dictated by their interactions with kinetochore proteins and the microtubule. The relatively simple and well-defined microtubule-binding machinery of the yeast kinetochore and its persistent interaction with one microtubule plus-end in metaphase provide the ideal opportunity to study the significance of its architecture to force generation.

Ndc80 is the linchpin of end-on kinetochore-microtubule attachment (Figure 1.3B). It uses three microtubule-binding domains: a positively-charge disordered amino-terminal tail of the $Hec1^{Ndc80}$ subunit and the CH-domains of the $Hec1^{Ndc80}$ and Nuf2 subunits (Wei, Sorger, & Harrison, 2005). The disordered tail binds to the negatively-charged tubulin tails. This binding assists in the initial contact between the kinetochore and the microtubule lattice (Tanaka, 2010). The CH-domains bind in the groove between tubulin monomers along a straight tubulin protofilament in the microtubule lattice, but they cannot do so if this groove is distorted, as in a curling, depolymerizing protofilament (Alushin et al., 2010; Ciferri et al., 2008). This property of the CH-domains is essential for forming end-on kinetochore-microtubule attachments (Cheeseman et al., 2006; Wei, Al-Bassam, & Harrison, 2007). Ndc80 structure appears to be tailored for both lateral and end-on attachment – it contains a flexible hinge in its front section to enable the CH-domains access to the binding groove between tubulin monomers by making a 40° angle to the microtubule axis (Wang et al., 2008). The conformation of Ndc80 in metaphase yeast kinetochores suggests that they can assume the preferred orientation for the CH-domains to bind to the lattice (Figure 1.3B, top) (Aravamudhan et al., 2014).

Ndc80 positions the kinetochore at the plus-end, but it cannot hold on to a dynamic plus-end against high opposing forces (Powers et al., 2009). In budding yeast, the Dam1 complex,

which is recruited by Ndc80, is essential for force generation (Lampert, Hornung, & Westermann, 2010; Tien et al., 2010). Dam1 molecules likely assemble in the form of an oligomeric ring encircling the microtubule (Aravamudhan et al., 2014; Umbreit et al., 2014; Westermann et al., 2005). The Dam1 ring mechanically opposes the outward curling of tubulin protofilaments during depolymerization, and thus experiences a poleward force (Grishchuk, Molodtsov, Ataullakhanov, & McIntosh, 2005; Grishchuk et al., 2008). However, to generate force in this manner, the Dam1 ring must be positioned at the edge of the microtubule lattice, where it can encounter curling protofilaments (Efremov, Grishchuk, McIntosh, & Ataullakhanov, 2007). Therefore, it is not surprising that Dam1 localizes in close proximity to the CH-domains of Ndc80, which likely bind to the microtubule lattice near the plus-end (Figure 1.3B, top) (Aravamudhan et al., 2014; Joglekar et al., 2009). It is reasonable to expect that the Dam1 ring is positioned on the centromeric side of the CH-domains so that it can transmit the force generated to the centromere through Ndc80 (Aravamudhan et al., 2014). The mechanical opposition to microtubule depolymerization offered by the Dam1 complex also institutes a crucial regulatory mechanism known as 'tension-dependent rescue' of the depolymerizing plus-end (Akiyoshi et al., 2010; Franck et al., 2007; Tien et al., 2010). As the opposing pull of sister kinetochores on the centromere increases, the Dam1 ring inhibits the conformational change that the tubulin dimers undergo to depolymerize. This force-dependent inhibition promotes the transition from microtubule depolymerization to polymerization. Consequently, the kinetochore switches its direction of movement and relieves centromeric tension in the process. Tension-dependent recue is necessary for persistent attachment of sister kinetochores to spindle microtubules.

The high combined affinity of the Ndc80-Dam1 ring assembly likely makes its diffusion along the microtubule lattice very slow (Grishchuk et al., 2008). If diffusion is much slower than

the rate of microtubule polymerization, then biased diffusion may not be able to keep pace with the polymerizing microtubule tip. The higher affinity of the Dam1 complex for GTP-tubulin, which is present only at the growing microtubule tip, over GDP-tubulin present in the lattice enables Dam1 monomers and small oligomers to track growing microtubule tips (Lampert, Mieck, Alushin, Nogales, & Westermann, 2013; Tien et al., 2010). However, whether Dam1 rings can also do this is unclear. Indeed, yeast kinetochore particles have not been observed to track polymerizing microtubule plus-ends *in vitro*, unless they are experimentally assisted by the imposition of an external force directed toward the plus-end (Akiyoshi et al., 2010). Centromeric strain will drag the kinetochore toward the plus-end *in vivo*, but this process depends on the magnitude of the strain, and it is independent of the growth of the plus-end (Figure 1.3B, middle). This means that the movement induced by high centromeric tension could potentially slide the kinetochore off the polymerizing microtubule tip, and additional mechanisms may be necessary to mitigate this possibility.

In this context, the involvement of XMAP215^{Stu2} in yeast kinetochore motility is noteworthy, but also perplexing. Although XMAP215^{Stu2} is a well-known tubulin polymerase, it destabilizes microtubules during mitosis in yeast cells (Ayaz, Ye, Huddleston, Brautigam, & Rice, 2012; Kosco et al., 2001). Consistent with this finding, XMPA215^{Stu2} localizes in a region within the yeast kinetochore where the polymerizing plus-end is expected to be located (Figure 1.3B, middle) (Aravamudhan et al., 2014). On the other hand, *in vitro* findings suggest that XMAP215^{Stu2} stabilizes attachment of yeast kinetochores to the microtubule tip in a tension-dependent manner (Miller, Asbury, & Biggins, 2016). We suggest a simple model to reconcile these observations (Figure 1.3B, middle & bottom panels). We propose that XMAP215^{Stu2} recognizes polymerizing microtubule plus-ends within yeast kinetochores and promotes their

transition to depolymerization. This prevents the plus-ends from outpacing the kinetochore and minimizes the possibility of the kinetochore sliding off a growing microtubule tip under high centromeric tension.

The conserved mechanics and biochemistry underlying microtubule plus-end dynamics suggest that the basic mechanisms of harnessing force and persistent bidirectional movement used by the budding yeast kinetochore will be conserved in human kinetochores. This is reflected in the similar organization of microtubule-binding activities in the yeast and human kinetochore (Joglekar et al., 2009; Wan et al., 2009). Ndc80 is similarly organized and required for end-on attachment in both kinetochores (Guimaraes, Dong, McEwen, & Deluca, 2008; Joglekar et al., 2009; Wan et al., 2009). However, the human kinetochore attaches to ~20 microtubule plus-ends on average, and these attachments are dynamic – they turn over with a half-life of ~4 minutes (in RPE-1 cells (Kabeche & Compton, 2013) compared to ~25-30 minutes duration of mitosis (Magidson et al., 2011)). The human kinetochore also employs a much larger array of accessory motors and MAPs to elaborate on the basic mechanisms of force generation. The motors include MCAK, Kif18A, Dynein, and CENP-E (Stumpff, von Dassow, Wagenbach, Asbury, & Wordeman, 2008; Varma, Monzo, Stehman, & Vallee, 2008; Vitre et al., 2014; Wordeman, Wagenbach, & von Dassow, 2007). The MAPs include the Ska complex, Astrin/SKAP, CLASP, EB1, and XMAP215^{Stu2} (Cassimeris, Becker, & Carney, 2009; Draviam, Shapiro, Aldridge, & Sorger, 2006; Manning et al., 2010; Pereira et al., 2006; Tirnauer, Canman, Salmon, & Mitchison, 2002; Welburn et al., 2009). The mechanisms of kinetochore recruitment and organization of some of these accessory proteins are similar to the corresponding mechanisms in yeast (Stumpff et al., 2008; Varma et al., 2008; Vitre et al., 2014; Wan et al., 2009; Wordeman et al., 2007; Zhang et al., 2012). For example, the recruitment and location of the Ska complex in

the human kinetochore appears similar to that of Dam1 in the yeast kinetochore (Zhang et al., 2012). The collective activities of these proteins in microtubule-biding and in modulating plus-end polymerization dynamics establish and maintain end-on kinetochore-microtubule attachment, generate force, and coordinate the activities of sister kinetochores to drive persistent, bidirectional chromosome movement.

One puzzling aspect of the large array of accessory motors and MAPs employed by the human kinetochore is the apparent redundancy in their activities and kinetochore-specific functions. For example, Ska and XMAP215^{Stu2} are involved in microtubule attachment and force generation; EB1, CLASP, and Astrin/SKAP promote plus-end polymerization (Draviam et al., 2006; Friese et al., 2016; Maiato, Khodjakov, & Rieder, 2005; Miller et al., 2016; Welburn et al., 2009). This redundancy may be necessary in part to achieve robust kinetochore functionality. However, it is also possible that the unique kinetochore position of some of these proteins assigns them with unique functions. For example, MCAK and Kif18A can both destabilize the plus-end (Mayr et al., 2007; Wordeman et al., 2007). However, MCAK improves the coordinated movement of sister kinetochores, whereas Kif18A promotes the mutually antagonistic activity of the sisters and reduces their coordinated movements (Mayr et al., 2007; Wordeman et al., 2007). In addition to differences in the biochemical activities of these motors, how they encounter the microtubule plus-end in the kinetochore may give rise to the differences in their function. MCAK localizes at the centromere, whereas Kif18A walks along the microtubule to reach the plus-ends (Figure 1.2A, B) (Andrews et al., 2004). Due to its centromeric localization, MCAK may selectively destabilize only those plus-ends that polymerize to extend more than usual towards the centromere. In contrast, Kif18A-mediated plus-end destabilization may be dependent on microtubule length/age (Stumpff et al., 2008; Varga, Leduc, Bormuth, Diez, & Howard,

2009). Thus, differences in function may arise from differences in protein position. Therefore, to fully understand how the human kinetochore brings about bidirectional chromosome movement, the biochemical activities as well as the nanoscale architecture of its microtubule-binding machinery must be studied. Additionally, any temporal coordination of these activities and dynamics of protein architecture are also likely to play key roles in kinetochore motility (Dumont, Salmon, & Mitchison, 2012). A major challenge in the field is to formulate a comprehensive model that explains how the human kinetochore synthesizes the activities of its microtubule-binding proteins to control plus-end dynamics, and generate persistent, bidirectional chromosome movement.

1.7 Potential Roles of Kinetochore Architecture in Correcting Monopolar Attachments

Although bipolar attachment of sister kinetochores to microtubules emanating from opposite spindle poles is strongly favored, two types of erroneous attachments occur frequently – merotelic and monopolar (Godek et al., 2015; Gregan, Polakova, Zhang, Tolic-Norrelykke, & Cimini, 2011; Lampson & Grishchuk, 2017). The first type of erroneous attachments is known as merotelic attachment, wherein a single kinetochore attaches to microtubules emanating from both poles. There is no kinetochore-based mechanism for the resolution of merotelic attachments; these attachments are destabilized, and bipolar attachments are stabilized, by a finely tuned regulation of the dynamicity of spindle microtubules (Cimini, Cameron, & Salmon, 2004; Godek et al., 2015). The second type of erroneous attachments are known as syntelic or monopolar attachments, wherein both sister kinetochores in a pair are attached to the same pole. These attachments are destabilized by a dedicated, kinetochore-based error correction process. Two elements of this process are clear. First, it directs Aurora B^{Ipl1} kinase activity toward

microtubule-binding kinetochore proteins to weaken their microtubule-binding affinity (Chan et al., 2012; Liu et al., 2009; Pinsky et al., 2006; Schmidt et al., 2010; Shang et al., 2003; Tien et al., 2010; Welburn et al., 2010; Zaytsev, Sundin, DeLuca, Grishchuk, & DeLuca, 2014). Second, the activity of the error correction process is strongly correlated with a sustained lack of centromeric tension, which is a characteristic unique to sister kinetochores with monopolar attachments (Liu et al., 2009). Interestingly, sister kinetochores with bipolar attachments also experience periodic and transient loss of centromeric tension, but they do not activate the error correction process. How the kinetochore senses a prolonged absence of centromeric tension, and activates Aurora B^{Ipl1} in response, is unclear. Potential mechanisms that can explain this error correction process have been discussed in excellent reviews (e.g., see (Lampson & Grishchuk, 2017; Sarangapani & Asbury, 2014)). Therefore, we will only describe the prevalent model, and focus on the potential role of kinetochore architecture in the error correction process.

The prevalent model postulates that centromeric tension in the human kinetochore separates Aurora B^{Ipl1} from its phosphorylation targets in a manner that is superficially similar to the mechanism of attachment-dependent SAC signaling (Liu et al., 2009; Zaytsev et al., 2016). Aurora B^{Ipl1} dynamically localizes to chromatin situated in between the sister centromeres (Figure 1.2A). Here, the high local concentration of Aurora B^{Ipl1} stimulates its auto-phosphorylation and hence hyper-activation. Super-imposition of a phosphatase activity on this Aurora B^{Ipl1} hyper-activation region creates a steep gradient in Aurora B^{Ipl1} kinase activity (Figure 1.3C) (Zaytsev et al., 2016). Sister kinetochores with monopolar attachment fall within the region of Aurora B^{Ipl1} hyper-activity, whereas kinetochores with bipolar attachment deform the centromere and emerge out of it. Consequently, the microtubule-binding proteins in bipolar kinetochores become dephosphorylated, and microtubule attachment is stabilized. Although this

elegant is strongly supported by data from vertebrate kinetochores, it does not explain a key observation from budding yeast. Budding yeast kinetochores correct monopolar attachments even when Aurora B^{Ipl1} is unable to localize to the centromere (Campbell & Desai, 2013). Therefore, additional mechanisms in the error correction process remain to be discovered in both yeast and humans.

Kinetochore architecture is clearly important in the prevalent model of the error-correction process because it determines the positions of Aurora B^{Ipl1} targets relative to the centromere-localized Aurora B^{Ipl1}. However, the architecture of kinetochores with monopolar and bipolar attachments is likely to be similar given that they both possess end-on attachment. A key differences in kinetochore architecture under the two scenarios may be that the plus-end is in close proximity to the centromere only in kinetochores with monopolar attachment (Figure 1.3C). One possibility is that the error correction mechanism uses the proximity between centromere-localized Aurora B^{Ipl1} and the microtubule plus-end to locally concentrate, and then effectively transport active Aurora B^{Ipl1} along the microtubule to microtubule-bound kinetochore proteins (Campbell & Desai, 2013). However, the role of kinetochore architecture, if any, in mechanisms that direct Aurora B^{Ipl1} activity selectively to kinetochores with monopolar attachments remains poorly understood.

1.8 Concluding Remarks

The nanoscale architecture of the kinetochore provides insight into how it integrates three truly disparate mechanisms in one molecular framework. Comparison of the yeast and human kinetochores reveals how the basic integration of these three mechanisms may be enhanced to meet species-specific functional requirements. In the integrative model of the eukaryotic

kinetochore, Ndc80 emerges as the focal point of all three mechanisms. It acts as the terminal of a switch that controls the SAC, the conformational sensor that positions the kinetochore at the plus-end, an organizer of microtubule-binding activities in the kinetochore, and a major target of phosphoregulation by Aurora B^{Ipl1}. Therefore, the spatial patterning of Ndc80 in the kinetochore and its architecture relative to the microtubule plus-end will play key roles in shaping the emergent mechanisms underlying all three kinetochore functions. Future studies of the kinetochore that explicitly test the role of kinetochore architecture in its functional and regulatory mechanisms will lead us to a comprehensive understanding of one of the most fascinating multi-protein machines in cell biology.

1.9 Acknowledgements

This chapter has been published in Current Biology and has been included in this dissertation with permission from the journal editors. This work was supported by R01 GM105948 to A.P. Joglekar. The authors thank Iain Cheeseman and Jennifer DeLuca for helpful discussions and a critical reading of the manuscript.

1.10 References

Akiyoshi, B., Sarangapani, K. K., Powers, A. F., Nelson, C. R., Reichow, S. L., Arellano-Santoyo, H., . . . Biggins, S. (2010). Tension directly stabilizes reconstituted kinetochore-microtubule attachments. *Nature, 468*(7323), 576-579. doi:10.1038/nature09594

Alber, F., Dokudovskaya, S., Veenhoff, L. M., Zhang, W., Kipper, J., Devos, D., . . . Rout, M. P. (2007). The molecular architecture of the nuclear pore complex. *Nature, 450*(7170), 695-701. doi:10.1038/nature06405

Alushin, G. M., Ramey, V. H., Pasqualato, S., Ball, D. A., Grigorieff, N., Musacchio, A., & Nogales, E. (2010). The Ndc80 kinetochore complex forms oligomeric arrays along microtubules. *Nature, 467*(7317), 805-810. doi:10.1038/nature09423

Andrews, P. D., Ovechkina, Y., Morrice, N., Wagenbach, M., Duncan, K., Wordeman, L., & Swedlow, J. R. (2004). Aurora B regulates MCAK at the mitotic centromere. *Dev Cell, 6*(2), 253-268. doi:10.1016/s1534-5807(04)00025-5

Aravamudhan, P., Felzer-Kim, I., Gurunathan, K., & Joglekar, A. P. (2014). Assembling the protein architecture of the budding yeast kinetochore-microtubule attachment using FRET. *Curr Biol, 24*(13), 1437-1446. doi:10.1016/j.cub.2014.05.014

Aravamudhan, P., Felzer-Kim, I., & Joglekar, A. P. (2013). The budding yeast point centromere associates with two Cse4 molecules during mitosis. *Curr Biol, 23*(9), 770-774. doi:10.1016/j.cub.2013.03.042

Aravamudhan, P., Goldfarb, A. A., & Joglekar, A. P. (2015). The kinetochore encodes a mechanical switch to disrupt spindle assembly checkpoint signalling. *Nat Cell Biol, 17*(7), 868-879. doi:10.1038/ncb3179

Ayaz, P., Ye, X., Huddleston, P., Brautigam, C. A., & Rice, L. M. (2012). A TOG:alphabeta-tubulin complex structure reveals conformation-based mechanisms for a microtubule polymerase. *Science, 337*(6096), 857-860. doi:10.1126/science.1221698

Campbell, C. S., & Desai, A. (2013). Tension sensing by Aurora B kinase is independent of survivin-based centromere localization. *Nature, 497*(7447), 118-121. doi:10.1038/nature12057

Cassimeris, L., Becker, B., & Carney, B. (2009). TOGp regulates microtubule assembly and density during mitosis and contributes to chromosome directional instability. *Cell Motil Cytoskeleton, 66*(8), 535-545. doi:10.1002/cm.20359

Chan, Y. W., Jeyaprakash, A. A., Nigg, E. A., & Santamaria, A. (2012). Aurora B controls kinetochore-microtubule attachments by inhibiting Ska complex-KMN network interaction. *J Cell Biol, 196*(5), 563-571. doi:10.1083/jcb.201109001

Cheeseman, I. M., Chappie, J. S., Wilson-Kubalek, E. M., & Desai, A. (2006). The conserved KMN network constitutes the core microtubule-binding site of the kinetochore. *Cell, 127*(5), 983-997. doi:10.1016/j.cell.2006.09.039

Ciferri, C., Pasqualato, S., Screpanti, E., Varetti, G., Santaguida, S., Dos Reis, G., . . . Musacchio, A. (2008). Implications for kinetochore-microtubule attachment from the structure of an engineered Ndc80 complex. *Cell, 133*(3), 427-439. doi:10.1016/j.cell.2008.03.020

Cimini, D., Cameron, L. A., & Salmon, E. D. (2004). Anaphase spindle mechanics prevent mis-segregation of merotelically oriented chromosomes. *Curr Biol, 14*(23), 2149-2155. doi:10.1016/j.cub.2004.11.029

DeLuca, J. G., Gall, W. E., Ciferri, C., Cimini, D., Musacchio, A., & Salmon, E. D. (2006). Kinetochore microtubule dynamics and attachment stability are regulated by Hec1. *Cell, 127*(5), 969-982. doi:10.1016/j.cell.2006.09.047

Dimitrova, Y. N., Jenni, S., Valverde, R., Khin, Y., & Harrison, S. C. (2016). Structure of the MIND Complex Defines a Regulatory Focus for Yeast Kinetochore Assembly. *Cell, 167*(4), 1014-1027 e1012. doi:10.1016/j.cell.2016.10.011

Dong, Y., Vanden Beldt, K. J., Meng, X., Khodjakov, A., & McEwen, B. F. (2007). The outer plate in vertebrate kinetochores is a flexible network with multiple microtubule interactions. *Nat Cell Biol, 9*(5), 516-522. doi:10.1038/ncb1576

Draviam, V. M., Shapiro, I., Aldridge, B., & Sorger, P. K. (2006). Misorientation and reduced stretching of aligned sister kinetochores promote chromosome missegregation in EB1- or APC-depleted cells. *EMBO J, 25*(12), 2814-2827. doi:10.1038/sj.emboj.7601168

Dumont, S., Salmon, E. D., & Mitchison, T. J. (2012). Deformations within moving kinetochores reveal different sites of active and passive force generation. *Science, 337*(6092), 355-358. doi:10.1126/science.1221886

Efremov, A., Grishchuk, E. L., McIntosh, J. R., & Ataullakhanov, F. I. (2007). In search of an optimal ring to couple microtubule depolymerization to processive chromosome motions. *Proc Natl Acad Sci U S A, 104*(48), 19017-19022. doi:10.1073/pnas.0709524104

Etemad, B., Kuijt, T. E., & Kops, G. J. (2015). Kinetochore-microtubule attachment is sufficient to satisfy the human spindle assembly checkpoint. *Nat Commun, 6*, 8987. doi:10.1038/ncomms9987

Faesen, A. C., Thanasoula, M., Maffini, S., Breit, C., Muller, F., van Gerwen, S., . . . Musacchio, A. (2017). Basis of catalytic assembly of the mitotic checkpoint complex. *Nature, 542*(7642), 498-502. doi:10.1038/nature21384

Franck, A. D., Powers, A. F., Gestaut, D. R., Gonen, T., Davis, T. N., & Asbury, C. L. (2007). Tension applied through the Dam1 complex promotes microtubule elongation providing a direct mechanism for length control in mitosis. *Nat Cell Biol, 9*(7), 832-837. doi:10.1038/ncb1609

Friese, A., Faesen, A. C., Huis in 't Veld, P. J., Fischbock, J., Prumbaum, D., Petrovic, A., . . . Musacchio, A. (2016). Molecular requirements for the inter-subunit interaction and kinetochore recruitment of SKAP and Astrin. *Nat Commun, 7*, 11407. doi:10.1038/ncomms11407

Gascoigne, K. E., Takeuchi, K., Suzuki, A., Hori, T., Fukagawa, T., & Cheeseman, I. M. (2011). Induced ectopic kinetochore assembly bypasses the requirement for CENP-A nucleosomes. *Cell, 145*(3), 410-422. doi:10.1016/j.cell.2011.03.031

Godek, K. M., Kabeche, L., & Compton, D. A. (2015). Regulation of kinetochore-microtubule attachments through homeostatic control during mitosis. *Nat Rev Mol Cell Biol, 16*(1), 57-64. doi:10.1038/nrm3916

Gregan, J., Polakova, S., Zhang, L., Tolic-Norrelykke, I. M., & Cimini, D. (2011). Merotelic kinetochore attachment: causes and effects. *Trends Cell Biol, 21*(6), 374-381. doi:10.1016/j.tcb.2011.01.003

Grishchuk, E. L., Molodtsov, M. I., Ataullakhanov, F. I., & McIntosh, J. R. (2005). Force production by disassembling microtubules. *Nature, 438*(7066), 384-388. doi:10.1038/nature04132

Grishchuk, E. L., Spiridonov, I. S., Volkov, V. A., Efremov, A., Westermann, S., Drubin, D., . . . McIntosh, J. R. (2008). Different assemblies of the DAM1 complex follow shortening microtubules by distinct mechanisms. *Proc Natl Acad Sci U S A, 105*(19), 6918-6923. doi:10.1073/pnas.0801811105

Guimaraes, G. J., Dong, Y., McEwen, B. F., & Deluca, J. G. (2008). Kinetochore-microtubule attachment relies on the disordered N-terminal tail domain of Hec1. *Curr Biol, 18*(22), 1778-1784. doi:10.1016/j.cub.2008.08.012

Hill, T. L. (1985). Theoretical problems related to the attachment of microtubules to kinetochores. *Proc Natl Acad Sci U S A, 82*(13), 4404-4408. doi:10.1073/pnas.82.13.4404

Hiruma, Y., Sacristan, C., Pachis, S. T., Adamopoulos, A., Kuijt, T., Ubbink, M., . . . Kops, G. J. (2015). CELL DIVISION CYCLE. Competition between MPS1 and microtubules at kinetochores regulates spindle checkpoint signaling. *Science, 348*(6240), 1264-1267. doi:10.1126/science.aaa4055

Huis In 't Veld, P. J., Jeganathan, S., Petrovic, A., Singh, P., John, J., Krenn, V., . . . Musacchio, A. (2016). Molecular basis of outer kinetochore assembly on CENP-T. *Elife, 5*. doi:10.7554/eLife.21007

Inoue, S., & Salmon, E. D. (1995). Force generation by microtubule assembly/disassembly in mitosis and related movements. *Mol Biol Cell, 6*(12), 1619-1640. doi:10.1091/mbc.6.12.1619

Ji, Z., Gao, H., Jia, L., Li, B., & Yu, H. (2017). A sequential multi-target Mps1 phosphorylation cascade promotes spindle checkpoint signaling. *Elife, 6*. doi:10.7554/eLife.22513

Ji, Z., Gao, H., & Yu, H. (2015). CELL DIVISION CYCLE. Kinetochore attachment sensed by competitive Mps1 and microtubule binding to Ndc80C. *Science, 348*(6240), 1260-1264. doi:10.1126/science.aaa4029

Joglekar, A. P. (2016). A Cell Biological Perspective on Past, Present and Future Investigations of the Spindle Assembly Checkpoint. *Biology (Basel), 5*(4). doi:10.3390/biology5040044

Joglekar, A. P., Bloom, K., & Salmon, E. D. (2009). In vivo protein architecture of the eukaryotic kinetochore with nanometer scale accuracy. *Curr Biol, 19*(8), 694-699. doi:10.1016/j.cub.2009.02.056

Joglekar, A. P., Bouck, D. C., Molk, J. N., Bloom, K. S., & Salmon, E. D. (2006). Molecular architecture of a kinetochore-microtubule attachment site. *Nat Cell Biol, 8*(6), 581-585. doi:10.1038/ncb1414

Kabeche, L., & Compton, D. A. (2013). Cyclin A regulates kinetochore microtubules to promote faithful chromosome segregation. *Nature, 502*(7469), 110-113. doi:10.1038/nature12507

Kemmler, S., Stach, M., Knapp, M., Ortiz, J., Pfannstiel, J., Ruppert, T., & Lechner, J. (2009). Mimicking Ndc80 phosphorylation triggers spindle assembly checkpoint signalling. *EMBO J, 28*(8), 1099-1110. doi:10.1038/emboj.2009.62

Kim, S., & Yu, H. (2015). Multiple assembly mechanisms anchor the KMN spindle checkpoint platform at human mitotic kinetochores. *J Cell Biol, 208*(2), 181-196. doi:10.1083/jcb.201407074

Klare, K., Weir, J. R., Basilico, F., Zimniak, T., Massimiliano, L., Ludwigs, N., . . . Musacchio, A. (2015). CENP-C is a blueprint for constitutive centromere-associated network assembly within human kinetochores. *J Cell Biol, 210*(1), 11-22. doi:10.1083/jcb.201412028

Kosco, K. A., Pearson, C. G., Maddox, P. S., Wang, P. J., Adams, I. R., Salmon, E. D., . . . Huffaker, T. C. (2001). Control of microtubule dynamics by Stu2p is essential for spindle orientation and metaphase chromosome alignment in yeast. *Mol Biol Cell, 12*(9), 2870-2880. doi:10.1091/mbc.12.9.2870

Krefman, N. I., Drubin, D. G., & Barnes, G. (2015). Control of the spindle checkpoint by lateral kinetochore attachment and limited Mad1 recruitment. *Mol Biol Cell, 26*(14), 2620-2639. doi:10.1091/mbc.E15-05-0276

Lampert, F., Hornung, P., & Westermann, S. (2010). The Dam1 complex confers microtubule plus end-tracking activity to the Ndc80 kinetochore complex. *J Cell Biol, 189*(4), 641-649. doi:10.1083/jcb.200912021

Lampert, F., Mieck, C., Alushin, G. M., Nogales, E., & Westermann, S. (2013). Molecular requirements for the formation of a kinetochore-microtubule interface by Dam1 and Ndc80 complexes. *J Cell Biol, 200*(1), 21-30. doi:10.1083/jcb.201210091

Lampson, M. A., & Grishchuk, E. L. (2017). Mechanisms to Avoid and Correct Erroneous Kinetochore-Microtubule Attachments. *Biology (Basel), 6*(1). doi:10.3390/biology6010001

Liu, D., Vader, G., Vromans, M. J., Lampson, M. A., & Lens, S. M. (2009). Sensing chromosome bi-orientation by spatial separation of aurora B kinase from kinetochore substrates. *Science, 323*(5919), 1350-1353. doi:10.1126/science.1167000

London, N., & Biggins, S. (2014). Mad1 kinetochore recruitment by Mps1-mediated phosphorylation of Bub1 signals the spindle checkpoint. *Genes Dev, 28*(2), 140-152. doi:10.1101/gad.233700.113

London, N., Ceto, S., Ranish, J. A., & Biggins, S. (2012). Phosphoregulation of Spc105 by Mps1 and PP1 regulates Bub1 localization to kinetochores. *Curr Biol, 22*(10), 900-906. doi:10.1016/j.cub.2012.03.052

Magidson, V., He, J., Ault, J. G., O'Connell, C. B., Yang, N., Tikhonenko, I., . . . Khodjakov, A. (2016). Unattached kinetochores rather than intrakinetochore tension arrest mitosis in taxol-treated cells. *J Cell Biol, 212*(3), 307-319. doi:10.1083/jcb.201412139

Magidson, V., O'Connell, C. B., Loncarek, J., Paul, R., Mogilner, A., & Khodjakov, A. (2011). The spatial arrangement of chromosomes during prometaphase facilitates spindle assembly. *Cell, 146*(4), 555-567. doi:10.1016/j.cell.2011.07.012

Maiato, H., Khodjakov, A., & Rieder, C. L. (2005). Drosophila CLASP is required for the incorporation of microtubule subunits into fluxing kinetochore fibres. *Nat Cell Biol, 7*(1), 42-47. doi:10.1038/ncb1207

Manning, A. L., Bakhoum, S. F., Maffini, S., Correia-Melo, C., Maiato, H., & Compton, D. A. (2010). CLASP1, astrin and Kif2b form a molecular switch that regulates kinetochore-microtubule dynamics to promote mitotic progression and fidelity. *EMBO J, 29*(20), 3531-3543. doi:10.1038/emboj.2010.230

Mayr, M. I., Hummer, S., Bormann, J., Gruner, T., Adio, S., Woehlke, G., & Mayer, T. U. (2007). The human kinesin Kif18A is a motile microtubule depolymerase essential for chromosome congression. *Curr Biol, 17*(6), 488-498. doi:10.1016/j.cub.2007.02.036

McEwen, B. F., Heagle, A. B., Cassels, G. O., Buttle, K. F., & Rieder, C. L. (1997). Kinetochore fiber maturation in PtK1 cells and its implications for the mechanisms of chromosome congression and anaphase onset. *J Cell Biol, 137*(7), 1567-1580. doi:10.1083/jcb.137.7.1567

McIntosh, J. R. (1991). Structural and mechanical control of mitotic progression. *Cold Spring Harb Symp Quant Biol, 56*, 613-619. doi:10.1101/sqb.1991.056.01.070

McIntosh, J. R., O'Toole, E., Zhudenkov, K., Morphew, M., Schwartz, C., Ataullakhanov, F. I., & Grishchuk, E. L. (2013). Conserved and divergent features of kinetochores and spindle microtubule ends from five species. *J Cell Biol, 200*(4), 459-474. doi:10.1083/jcb.201209154

Miller, M. P., Asbury, C. L., & Biggins, S. (2016). A TOG Protein Confers Tension Sensitivity to Kinetochore-Microtubule Attachments. *Cell, 165*(6), 1428-1439. doi:10.1016/j.cell.2016.04.030

Musacchio, A., & Desai, A. (2017). A Molecular View of Kinetochore Assembly and Function. *Biology (Basel), 6*(1). doi:10.3390/biology6010005

Nezi, L., & Musacchio, A. (2009). Sister chromatid tension and the spindle assembly checkpoint. *Curr Opin Cell Biol, 21*(6), 785-795. doi:10.1016/j.ceb.2009.09.007

Nicklas, R. B. (1983). Measurements of the force produced by the mitotic spindle in anaphase. *J Cell Biol, 97*(2), 542-548. doi:10.1083/jcb.97.2.542

Nishino, T., Takeuchi, K., Gascoigne, K. E., Suzuki, A., Hori, T., Oyama, T., . . . Fukagawa, T. (2012). CENP-T-W-S-X forms a unique centromeric chromatin structure with a histone-like fold. *Cell, 148*(3), 487-501. doi:10.1016/j.cell.2011.11.061

Pereira, A. L., Pereira, A. J., Maia, A. R., Drabek, K., Sayas, C. L., Hergert, P. J., . . . Maiato, H. (2006). Mammalian CLASP1 and CLASP2 cooperate to ensure mitotic fidelity by regulating spindle and kinetochore function. *Mol Biol Cell, 17*(10), 4526-4542. doi:10.1091/mbc.e06-07-0579

Petrovic, A., Keller, J., Liu, Y., Overlack, K., John, J., Dimitrova, Y. N., . . . Musacchio, A. (2016). Structure of the MIS12 Complex and Molecular Basis of Its Interaction with CENP-C at Human Kinetochores. *Cell, 167*(4), 1028-1040 e1015. doi:10.1016/j.cell.2016.10.005

Picco, A., Mund, M., Ries, J., Nedelec, F., & Kaksonen, M. (2015). Visualizing the functional architecture of the endocytic machinery. *Elife, 4*. doi:10.7554/eLife.04535

Pinsky, B. A., Kung, C., Shokat, K. M., & Biggins, S. (2006). The Ipl1-Aurora protein kinase activates the spindle checkpoint by creating unattached kinetochores. *Nat Cell Biol, 8*(1), 78-83. doi:10.1038/ncb1341

Powers, A. F., Franck, A. D., Gestaut, D. R., Cooper, J., Gracyzk, B., Wei, R. R., . . . Asbury, C. L. (2009). The Ndc80 kinetochore complex forms load-bearing attachments to dynamic microtubule tips via biased diffusion. *Cell, 136*(5), 865-875. doi:10.1016/j.cell.2008.12.045

Rago, F., Gascoigne, K. E., & Cheeseman, I. M. (2015). Distinct organization and regulation of the outer kinetochore KMN network downstream of CENP-C and CENP-T. *Curr Biol, 25*(5), 671-677. doi:10.1016/j.cub.2015.01.059

Sarangapani, K. K., & Asbury, C. L. (2014). Catch and release: how do kinetochores hook the right microtubules during mitosis? *Trends Genet, 30*(4), 150-159. doi:10.1016/j.tig.2014.02.004

Schleiffer, A., Maier, M., Litos, G., Lampert, F., Hornung, P., Mechtler, K., & Westermann, S. (2012). CENP-T proteins are conserved centromere receptors of the Ndc80 complex. *Nat Cell Biol, 14*(6), 604-613. doi:10.1038/ncb2493

Schmidt, J. C., Kiyomitsu, T., Hori, T., Backer, C. B., Fukagawa, T., & Cheeseman, I. M. (2010). Aurora B kinase controls the targeting of the Astrin-SKAP complex to bioriented kinetochores. *J Cell Biol, 191*(2), 269-280. doi:10.1083/jcb.201006129

Shang, C., Hazbun, T. R., Cheeseman, I. M., Aranda, J., Fields, S., Drubin, D. G., & Barnes, G. (2003). Kinetochore protein interactions and their regulation by the Aurora kinase Ipl1p. *Mol Biol Cell, 14*(8), 3342-3355. doi:10.1091/mbc.e02-11-0765

Shepperd, L. A., Meadows, J. C., Sochaj, A. M., Lancaster, T. C., Zou, J., Buttrick, G. J., . . . Millar, J. B. (2012). Phosphodependent recruitment of Bub1 and Bub3 to Spc7/KNL1 by Mph1 kinase maintains the spindle checkpoint. *Curr Biol, 22*(10), 891-899. doi:10.1016/j.cub.2012.03.051

Stumpff, J., von Dassow, G., Wagenbach, M., Asbury, C., & Wordeman, L. (2008). The kinesin-8 motor Kif18A suppresses kinetochore movements to control mitotic chromosome alignment. *Dev Cell, 14*(2), 252-262. doi:10.1016/j.devcel.2007.11.014

Suzuki, A., Badger, B. L., & Salmon, E. D. (2015). A quantitative description of Ndc80 complex linkage to human kinetochores. *Nat Commun, 6*, 8161. doi:10.1038/ncomms9161

Tanaka, T. U. (2010). Kinetochore-microtubule interactions: steps towards bi-orientation. *EMBO J, 29*(24), 4070-4082. doi:10.1038/emboj.2010.294

Tauchman, E. C., Boehm, F. J., & DeLuca, J. G. (2015). Stable kinetochore-microtubule attachment is sufficient to silence the spindle assembly checkpoint in human cells. *Nat Commun, 6*, 10036. doi:10.1038/ncomms10036

Tien, J. F., Umbreit, N. T., Gestaut, D. R., Franck, A. D., Cooper, J., Wordeman, L., . . . Davis, T. N. (2010). Cooperation of the Dam1 and Ndc80 kinetochore complexes enhances microtubule coupling and is regulated by aurora B. *J Cell Biol, 189*(4), 713-723. doi:10.1083/jcb.200910142

Tirnauer, J. S., Canman, J. C., Salmon, E. D., & Mitchison, T. J. (2002). EB1 targets to kinetochores with attached, polymerizing microtubules. *Mol Biol Cell, 13*(12), 4308-4316. doi:10.1091/mbc.e02-04-0236

Umbreit, N. T., Miller, M. P., Tien, J. F., Ortola, J. C., Gui, L., Lee, K. K., . . . Davis, T. N. (2014). Kinetochores require oligomerization of Dam1 complex to maintain microtubule attachments against tension and promote biorientation. *Nat Commun, 5*, 4951. doi:10.1038/ncomms5951

Varga, V., Leduc, C., Bormuth, V., Diez, S., & Howard, J. (2009). Kinesin-8 motors act cooperatively to mediate length-dependent microtubule depolymerization. *Cell, 138*(6), 1174-1183. doi:10.1016/j.cell.2009.07.032

Varma, D., Monzo, P., Stehman, S. A., & Vallee, R. B. (2008). Direct role of dynein motor in stable kinetochore-microtubule attachment, orientation, and alignment. *J Cell Biol, 182*(6), 1045-1054. doi:10.1083/jcb.200710106

Vitre, B., Gudimchuk, N., Borda, R., Kim, Y., Heuser, J. E., Cleveland, D. W., & Grishchuk, E. L. (2014). Kinetochore-microtubule attachment throughout mitosis potentiated by the elongated stalk of the kinetochore kinesin CENP-E. *Mol Biol Cell, 25*(15), 2272-2281. doi:10.1091/mbc.E14-01-0698

Wan, X., O'Quinn, R. P., Pierce, H. L., Joglekar, A. P., Gall, W. E., DeLuca, J. G., . . . Salmon, E. D. (2009). Protein architecture of the human kinetochore microtubule attachment site. *Cell, 137*(4), 672-684. doi:10.1016/j.cell.2009.03.035

Wang, H. W., Long, S., Ciferri, C., Westermann, S., Drubin, D., Barnes, G., & Nogales, E. (2008). Architecture and flexibility of the yeast Ndc80 kinetochore complex. *J Mol Biol, 383*(4), 894-903. doi:10.1016/j.jmb.2008.08.077

Wei, R. R., Al-Bassam, J., & Harrison, S. C. (2007). The Ndc80/HEC1 complex is a contact point for kinetochore-microtubule attachment. *Nat Struct Mol Biol, 14*(1), 54-59. doi:10.1038/nsmb1186

Wei, R. R., Sorger, P. K., & Harrison, S. C. (2005). Molecular organization of the Ndc80 complex, an essential kinetochore component. *Proc Natl Acad Sci U S A, 102*(15), 5363-5367. doi:10.1073/pnas.0501168102

Weir, J. R., Faesen, A. C., Klare, K., Petrovic, A., Basilico, F., Fischbock, J., . . . Musacchio, A. (2016). Insights from biochemical reconstitution into the architecture of human kinetochores. *Nature, 537*(7619), 249-253. doi:10.1038/nature19333

Welburn, J. P., Grishchuk, E. L., Backer, C. B., Wilson-Kubalek, E. M., Yates, J. R., 3rd, & Cheeseman, I. M. (2009). The human kinetochore Ska1 complex facilitates microtubule depolymerization-coupled motility. *Dev Cell, 16*(3), 374-385. doi:10.1016/j.devcel.2009.01.011

Welburn, J. P., Vleugel, M., Liu, D., Yates, J. R., 3rd, Lampson, M. A., Fukagawa, T., & Cheeseman, I. M. (2010). Aurora B phosphorylates spatially distinct targets to differentially regulate the kinetochore-microtubule interface. *Mol Cell, 38*(3), 383-392. doi:10.1016/j.molcel.2010.02.034

Westermann, S., Avila-Sakar, A., Wang, H. W., Niederstrasser, H., Wong, J., Drubin, D. G., . . . Barnes, G. (2005). Formation of a dynamic kinetochore- microtubule interface through assembly of the Dam1 ring complex. *Mol Cell, 17*(2), 277-290. doi:10.1016/j.molcel.2004.12.019

Winey, M., Mamay, C. L., O'Toole, E. T., Mastronarde, D. N., Giddings, T. H., Jr., McDonald, K. L., & McIntosh, J. R. (1995). Three-dimensional ultrastructural analysis of the Saccharomyces cerevisiae mitotic spindle. *J Cell Biol, 129*(6), 1601-1615. doi:10.1083/jcb.129.6.1601

Wordeman, L., Wagenbach, M., & von Dassow, G. (2007). MCAK facilitates chromosome movement by promoting kinetochore microtubule turnover. *J Cell Biol, 179*(5), 869-879. doi:10.1083/jcb.200707120

Zaytsev, A. V., Segura-Pena, D., Godzi, M., Calderon, A., Ballister, E. R., Stamatov, R., . . . Grishchuk, E. L. (2016). Bistability of a coupled Aurora B kinase-phosphatase system in cell division. *Elife, 5*, e10644. doi:10.7554/eLife.10644

Zaytsev, A. V., Sundin, L. J., DeLuca, K. F., Grishchuk, E. L., & DeLuca, J. G. (2014). Accurate phosphoregulation of kinetochore-microtubule affinity requires unconstrained molecular interactions. *J Cell Biol, 206*(1), 45-59. doi:10.1083/jcb.201312107

Zhang, G., Kelstrup, C. D., Hu, X. W., Kaas Hansen, M. J., Singleton, M. R., Olsen, J. V., & Nilsson, J. (2012). The Ndc80 internal loop is required for recruitment of the Ska complex to establish end-on microtubule attachment to kinetochores. *J Cell Sci, 125*(Pt 13), 3243-3253. doi:10.1242/jcs.104208

CHAPTER 2:

Microtubule Attachment and Centromeric Tension Shape the Protein Architecture of the Human Kinetochore

This chapter is from a peer-reviewed article:

Microtubule Attachment and Centromeric Tension Shape the Protein Architecture of the Human Kinetochore

Alexander A. Kukreja, Sisira Kavuri, and Ajit P. Joglekar. *Curr. Biol. 2020. Available online October 8, 2020. doi: 10.1016/j.cub.2020.09.038*

2.1 Abstract

The nanoscale protein architecture of the kinetochore plays an integral role in specifying the mechanisms underlying its functions in chromosome segregation. However, defining this architecture in human cells remains challenging because of the large size and compositional complexity of the kinetochore. Here, we use Förster resonance energy transfer to reveal the architecture of individual kinetochore-microtubule attachments in human cells. We find that the microtubule-binding domains of the Ndc80 complex cluster at the microtubule plus end. This clustering occurs only after microtubule attachment, and it increases proportionally with centromeric tension. Surprisingly, Ndc80 complex clustering is independent of the organization

and number of its centromeric receptors. Moreover, this clustering is similar in yeast and human kinetochores despite significant differences in their centromeric organizations. These and other data suggest that the microtubule-binding interface of the human kinetochore behaves like a flexible “lawn” despite being nucleated by repeating biochemical subunits.

2.2 Introduction

To accurately segregate chromosomes, the kinetochore performs two functions. When unattached, it acts as a signaling hub to delay the onset of anaphase, but, when attached to the plus ends of spindle microtubules, it acts as a force-generating machine. The nanoscale organization of kinetochore proteins relative to one another and relative to the microtubule plus end, referred to here as the "architecture" of the kinetochore, plays key roles in the molecular mechanisms underlying both of these functions (Aravamudhan, Felzer-Kim, Gurunathan, & Joglekar, 2014; Aravamudhan, Goldfarb, & Joglekar, 2015; McIntosh, 1991; Wan et al., 2009). However, the architecture of the human kinetochore has not yet been defined. This is partly because the human kinetochore is compositionally complex and large, built from hundreds of protein molecules distributed upon a 200 nm diameter disk-like chromatin foundation known as the centromere. Furthermore, it changes in response to microtubule attachment and force (Magidson et al., 2016; Magidson et al., 2015; Suzuki, Badger, Wan, DeLuca, & Salmon, 2014), making its architecture intractable.

Because no currently available method can define kinetochore architecture, it must be synthesized from data defining four of its aspects: (1) the structures of kinetochore proteins, (2) their copy numbers, (3) their average localizations along the kinetochore-microtubule axis, and (4) their nanoscale distribution around and along the plus end (Hinshaw & Harrison, 2018; A. P. Joglekar & Kukreja, 2017; Musacchio & Desai, 2017). For the human kinetochore, data regarding the first three aspects are available (Magidson et al., 2016; Smith, McAinsh, & Burroughs, 2016; Suzuki, Badger, & Salmon, 2015; Suzuki et al., 2014; Suzuki, Long, & Salmon, 2018; Wan et al., 2009). However, the nanoscale distributions of kinetochore proteins around microtubule plus ends remains unknown. Here, we apply Förster resonance energy

transfer (FRET) between fluorescently labeled kinetochore subunits to elucidate this aspect of the human kinetochore.

We designed FRET experiments to elucidate specific aspects of the human kinetochore's architecture. One primary goal was to determine the organization of the microtubule-binding Ndc80 complex (Ndc80C) around the microtubule plus end. Ndc80C forms end-on microtubule attachments, generates force, and regulates plus-end polymerization dynamics (Ciferri et al., 2008; DeLuca et al., 2006). The human kinetochore contains ~250 Ndc80C molecules and binds ~20 microtubule plus ends, suggesting that on average ~12 Ndc80C molecules engage one microtubule (Suzuki et al., 2015; Wendell, Wilson, & Jordan, 1993). The nanoscale distribution of these molecules around the 25 nm diameter and along the longitudinal axis of the microtubule will influence the persistence of kinetochore-microtubule attachments (Hill, 1985). The distribution of Ndc80C molecules is dictated by long, flexible centromere-bound protein linkages. Therefore, we extended our FRET analysis to members of the Constitutive Centromere-Associated Network (CCAN) of proteins involved in Ndc80C recruitment. Microtubule attachment- and tension-dependent changes in kinetochore architecture are at the heart of its ability to implement emergent mechanisms. Therefore, we also studied how the nanoscale distribution of Ndc80C changes in response to attachment, tension, and when its recruitment is perturbed. From our FRET data, we formulate a model of human kinetochore-microtubule attachments and contrast it with the yeast kinetochore.

2.3 Results

2.3.1 Implementation of a FRET imaging Strategy to Study Kinetochore Architecture

To determine protein proximities in HeLa kinetochores using FRET, we co-expressed EGFP- (donor fluorophore, referred to as GFP) and mCherry- (acceptor fluorophore) labeled kinetochore proteins (Materials & Methods, (Khandelia, Yap, & Makeyev, 2011)). To maximize the recruitment of labeled proteins to the kinetochore, we knocked down their endogenous, unlabeled counterparts using RNAi (Supplementary Figure 2.1). Depending on the position of the donor and acceptor fluorophores (fused to either the C or N terminus of the selected proteins), we expected FRET to occur within a single protein complex (intra-complex), between neighboring complexes (inter-complex), or both (Figure 2.1A).

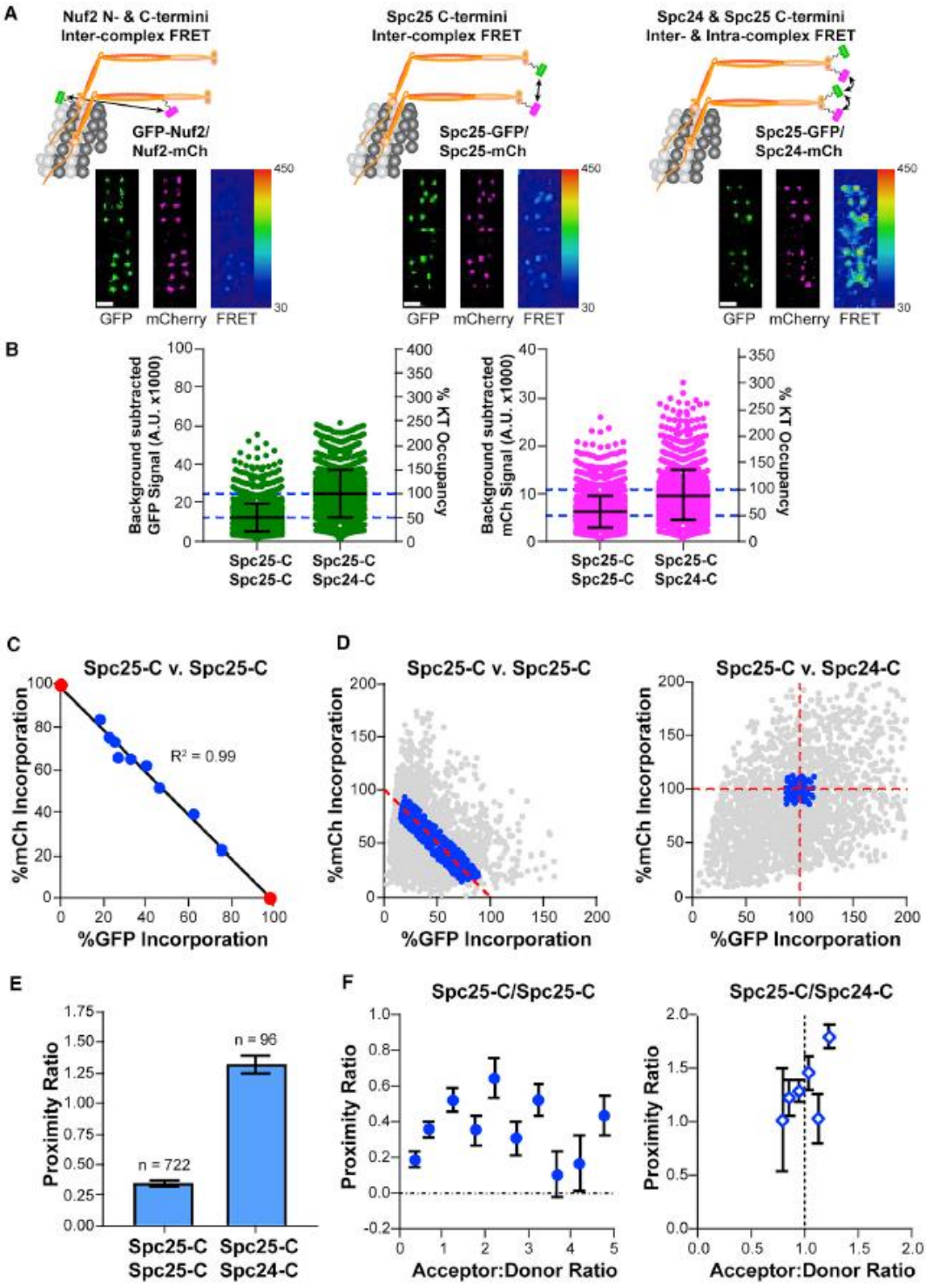

Figure 2.1 Design and Implementation of a FRET Imaging Strategy to Study Kinetochore Architecture
(A) Top: co-expression of GFP (FRET donor, green) and mCherry (mCh, FRET acceptor, magenta) fusions of the Ndc80 complex (Ndc80C, orange) reveal the proximity between adjacent Ndc80C molecules along the longitudinal axis (left), around the circumference of the microtubule (middle, right). For simplicity, only two Ndc80C molecules per microtubule are shown. Micrographs show representative metaphase plates from each cell line. FRET micrographs are scaled equivalently and pseudo-colored by the raw FRET values; GFP and mCherry micrographs

are scaled for ease of viewing. Scale bar, 1 μm. (B) Background subtracted GFP and mCherry signals of individual kinetochores in cells expressing Spc25-GFP/Spc25-mCherry and Spc25-GFP/Spc24-mCherry after siRNA-mediated knockdown of endogenous Spc25 or both Spc25 and Spc24, respectively. The y axis on the right shows the saturation level of the kinetochore by the GFP- and mCherry-labeled subunit, estimated from (Suzuki et al., 2015). (C) Correlation between Spc25-GFP and Spc25-mCherry signals measured from kinetochores from the dataset in (B). Data were binned by the ratio of mCherry to GFP fluorescence and further normalized by the X- and Y-intercepts of their linear regression (black line; see main text). Measurements of cells expressing Spc25-GFP or Spc25-mCherry in isolation are marked by red circles. From left to right: n = 398, 379, 109, 108, 131, 145, 170, 212, 491, 320, 499. (D) Normalized fluorescence signals for all kinetochores measured in Spc25-C/Spc25-C (left) and Spc25-C/Spc24-C (right) expressing cells. Only the data indicating complete saturation of the kinetochore by fluorophore-labeled proteins (blue circles) were used to measure FRET. Kinetochores from Spc25-C/Spc25-C expressing cells were further filtered by their acceptor to donor ratios (A:D) to include only the data within the range of 0.2–5 (see Materials & Methods). All other values are excluded (gray circles). (E) The proximity ratio for fully occupied, metaphase kinetochores in Spc25-C/Spc25-C and in Spc25-C/Spc24-C expressing cells. The number of kinetochores measured for each cell line is indicated above the bars. (F) Dependence of the proximity ratio on the A:D. In the absence of competition, the proximity ratio clusters around an A:D that reflects the inherent stoichiometry of the two fluorophore-labeled subunits involved (Spc25-C/Spc24-C cells, right). Data are binned by A:D (mean ± SEM; for Spc25-C/Spc25-C, n = 150, 192, 93, 62, 37, 53, 50, 36, 24, 25; for Spc25-C/Sp24-C, n = 2, 13, 32, 30, 14, 5). In (B), error bars are ± SD. In (C), (E), and (F), data represent the mean ± SEM. In (C), SEM error bars are too small to be seen. Data collected in (B)–(F) are from ≥ 3 experiments. See also Supplementary Figure 2.1, Supplementary Figure 2.2, Table 2.2, and Table 2.3.

For FRET to accurately reveal protein proximities, kinetochores must be saturated by donor- and acceptor-labeled proteins. However, in cells co-expressing GFP- and mCherry-labeled versions of Spc25, an Ndc80C subunit, we observed significant variability in kinetochore signals. This variability arises from several factors, including chromosome-specific differences in kinetochore size (Bodor et al., 2014; Cherry, Faulkner, Grossberg, & Balczon, 1989; Cherry & Johnston, 1987; Drpic et al., 2018; Dumont et al., 2020; Magidson et al., 2016; Magidson et al., 2015; McEwen, Ding, & Heagle, 1998), changes in fluorescence intensity that occur with depth from the coverslip, cell-to-cell variation in small interfering RNA (siRNA) efficiency, and overlapping signals from neighboring kinetochores. To minimize the effects of this variability, we established a filtering scheme as follows.

We quantified GFP and mCherry fluorescence signals per kinetochore in cells co-expressing Spc25-GFP and Spc25-mCherry (Figure 2.1B). Because the kinetochore has a limited protein capacity, we expected the donor- and acceptor-labeled versions of Spc25 to compete for kinetochore binding. Indeed, the Spc25-GFP and Spc25-mCherry signals per kinetochore were

anti-correlated (Figure 2.1C, blue circles). We performed linear regression of the data to determine the X- and Y-intercepts, which should correspond to intensities of kinetochores fully saturated with GFP or mCherry, respectively (Figure 2.1C, red circles; Supplementary Figure 2.2A). We used these values with the copy number for Ndc80C per kinetochore to define the single-molecule brightness of GFP and mCherry (Materials & Methods, (Suzuki et al., 2015)). Using these single-molecule brightness values, we converted the GFP and mCherry fluorescence intensities from each kinetochore into protein counts and retained only the measurements reflecting full kinetochore occupancy (Figure 2.1D, blue circles).

To quantify FRET, we determined the acceptor fluorescence due to FRET, which is known as "sensitized emission." The sensitized emission for each kinetochore was calculated by subtracting the contributions of GFP bleed-through and mCherry cross-excitation from the measured FRET signal (Supplementary Figure 2.2; Materials & Methods). Because sensitized emission is directly proportional to the average FRET efficiency and the total number of FRET pairs, we normalized it with respect to the number of donor and acceptor molecules per kinetochore. This normalization renders a FRET metric referred to as the "proximity ratio", which is proportional to the average FRET efficiency (A. Joglekar, Chen, & Lawrimore, 2013; Muller et al., 2005).

Using this methodology, the average inter-complex distance between neighboring Ndc80C molecules at their centromeric ends (Spc25-C/Spc25-C FRET, where -C refers to fluorophores fused to the C terminus) is <10 nm (Figure 2.1E). The higher FRET between Spc25 and Spc24 molecules indicates that these C termini are more densely organized than Spc25-C/Spc25-C, consistent with their ~2 nm intra-complex separation (Ciferri et al., 2008). We note that competition between donor- and acceptor-labeled Spc25 molecules in Spc25-C/Spc25-C

expressing cells yields kinetochores with varying acceptor to donor ratios (A:D; Figure 2.1D). This effect introduces variation in the measured proximity ratio for a given kinetochore (Figure 2.1F). Accounting for A:D, however, does not significantly change the trends of our FRET data (Table 2.2).

2.3.2 Ndc80C Molecules Cluster around the Microtubule and Are Staggered Relative to One Another

The nanoscale distribution of Ndc80C molecules around microtubule plus ends governs kinetochore-microtubule attachments and the polymerization dynamics of attached microtubules (DeLuca et al., 2006; Hill, 1985). Current evidence suggests that Ndc80C molecules are collinear with the microtubule-kinetochore axis (Roscioli et al., 2020; Suzuki et al., 2018), but their relative spacing and alignment are unknown. To reveal these aspects, we positioned fluorophores along Ndc80C's length to measure inter-complex FRET. We chose three locations along the Ndc80C molecule: proximal to its microtubule-binding end (i.e., N-Nuf2, wherein N- denotes fluorophores fused to the N terminus; we did not label the N terminus of Hec1 because this affects Ndc80C function (Mattiuzzo et al., 2011)), near the middle of its ~57 nm span (Nuf2-C, within its tetramerization domain), or near its centromeric end (Spc25-C). We detected FRET at all three positions, indicating that the average distance between adjacent Ndc80C molecules is <10 nm along its entire length (Figure 2.2A). Furthermore, the proximity ratio was higher at the microtubule-binding end (0.55 ± 0.02) and middle of Ndc80C (0.57 ± 0.03) than at its centromeric end (0.35 ± 0.02). Therefore, Ndc80C molecules are more tightly clustered on the microtubule lattice and at their tetramerization domains than at the ends which anchor them to the centromere.

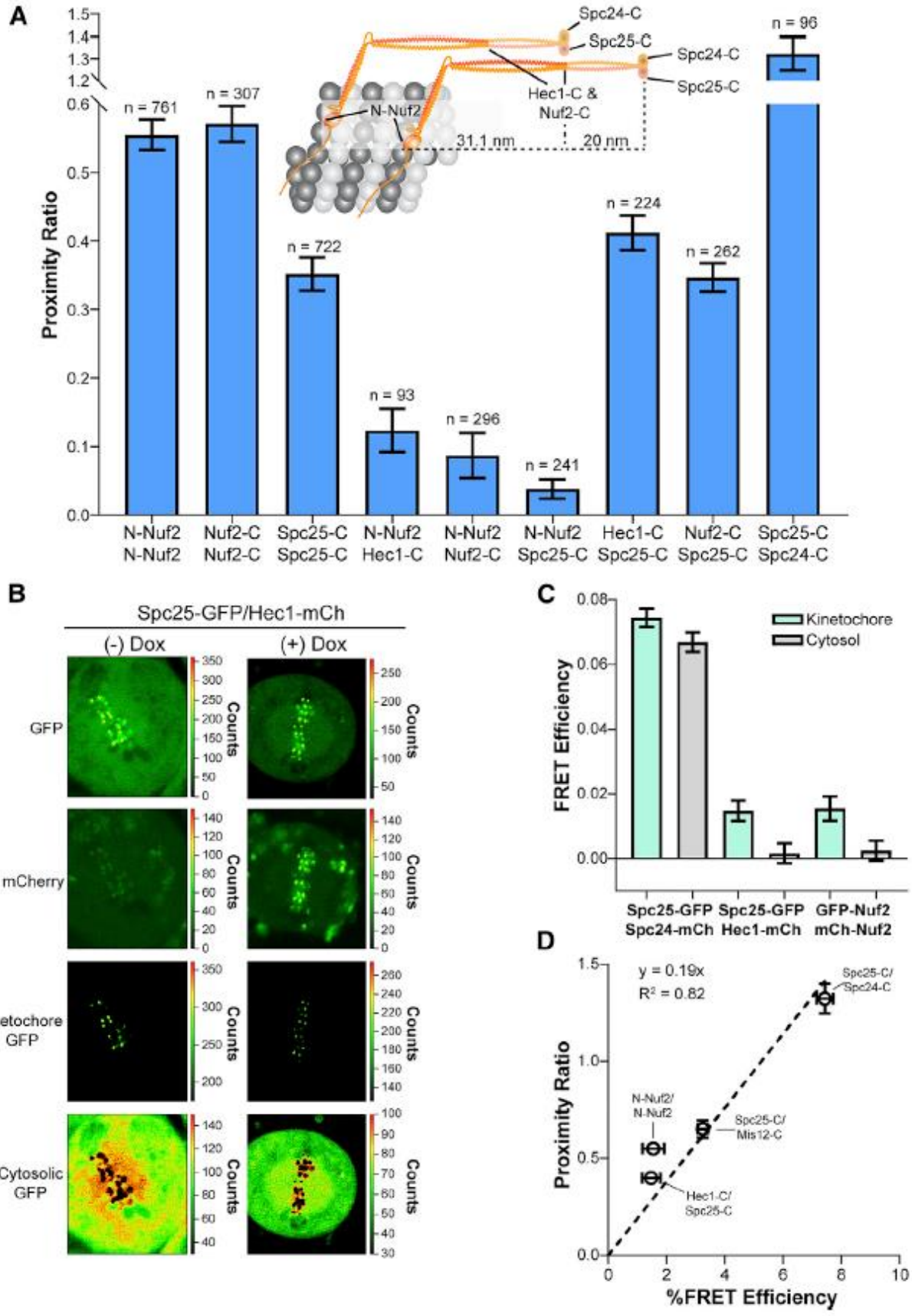
A
Proximity Ratio
n = 761
n = 307
n = 722
n = 93
n = 296
n = 241
n = 224
n = 262
n = 96
N-Nuf2
Spc24-C
Spc25-C
Hec1-C &
Nuf2-C
31.1 nm
20 nm
N-Nuf2 N-Nuf2
Nuf2-C Nuf2-C
Spc25-C Spc25-C
N-Nuf2 Hec1-C
N-Nuf2 Nuf2-C
N-Nuf2 Spc25-C
Hec1-C Spc25-C
Nuf2-C Spc25-C
Spc25-C Spc24-C
B
Spc25-GFP/Hec1-mCh
(-) Dox
(+) Dox
GFP
mCherry
Kinetochore GFP
Cytosolic GFP
Counts
C
FRET Efficiency
Kinetochore
Cytosol
Spc25-GFP Spc24-mCh
Spc25-GFP Hec1-mCh
GFP-Nuf2 mCh-Nuf2
D
y = 0.19x
R² = 0.82
Proximity Ratio
%FRET Efficiency
Spc25-C/ Spc24-C
Spc25-C/ Mis12-C
N-Nuf2/ N-Nuf2
Hec1-C/ Spc25-C

Figure 2.2 Ndc80C Molecules are Clustered along Their Entire Length and Staggered along the Microtubule Lattice in Metaphase Kinetochores
(A) FRET measurements for Ndc80C subunits in microtubule-attached metaphase kinetochores. The cartoon depicts the position and approximate distance between different anchoring points for donor and acceptor fluorophores as determined from structural data of Ndc80C (Cheeseman et al., 2006; Ciferri et al., 2008; Wang et al., 2008; Wei et al., 2005). For simplicity, only two Ndc80C molecules are shown. Bar graph displays the average proximity ratio ±SEM. The number of measurements is indicated above the bars. (B) FLIM micrographs of Spc25-GFP/Hec1-mCherry HeLa cells. Doxycycline (Dox) induces the expression of Hec1-mCherry. All images are scaled by the number of photons/pixel (scale to the right of images). Intensity thresholding was used to separate kinetochore-localized from cytosolic GFP pixels (bottom two rows). Note that GFP signal bleeds into the mCherry channel. (C) FRET efficiency of kinetochore-localized (light green bars) and cytosolic (gray bars) FRET pairs. Bars represent the average FRET efficiency ± SEM (n = 15, 14, and 13). (D) Plot of the average proximity ratio versus the average FRET efficiency for the indicated FRET pairs (dashed line, linear regression). Error bars are ± SEM. The N-Nuf2/N-Nuf2 data point deviates from the trend, likely due to our inability to assess the A:D ratio on the FLIM setup. For each FRET pair, ≥ 3 experiments were performed. See also Supplementary Figure 2.3, Table 2.2, and Table 2.3.

The clustering of Ndc80C molecules along their entire length suggests that adjacent molecules are aligned with one another as in the budding yeast kinetochore (Aravamudhan et al., 2014). To reveal the extent of this alignment, we co-expressed two different fluorophore-tagged Ndc80C subunits specifically chosen to avoid intra-complex FRET. Within a single Ndc80C molecule, fluorophores at N-Nuf2/Spc25-C, N-Nuf2/Hec1-C, and Hec1-C/Spc25-C are separated by ~51, 31, and 20 nm, respectively (Cheeseman, Chappie, Wilson-Kubalek, & Desai, 2006; Ciferri et al., 2008; Wang et al., 2008; Wei, Sorger, & Harrison, 2005). However, inter-complex FRET will occur if neighboring Ndc80C molecules are staggered along the kinetochore-microtubule axis such that the donor on one Ndc80C is within 10 nm of the acceptor on another. We detected very little FRET between the extremes of Ndc80C (N-Nuf2/Spc25-C; Figure 2.2A; Table 2.2 and Table 2.3). Interestingly, we detected low FRET at N-Nuf2/Hec1-C and higher FRET between Hec1-C/Spc25-C. These measurements were further confirmed by similar FRET values between N-Nuf2/Nuf2-C and Nuf2-C/Spc25-C (Figure 2.2A). Thus, a measurable fraction of Ndc80C molecules are staggered relative to one another along kinetochore-microtubule attachments. The extent of this staggering can be estimated by assuming that two Ndc80C molecules bind to the same protofilament. In such a scenario, two Ndc80C molecules would

need to be staggered by at least 21 nm, but no greater than 30 nm, to allow for the FRET between N-Nuf2/Hec1-C and Hec1-C/Spc25-C (see the cartoon diagram in Figure 2.2A). If neighboring molecules are bound to adjacent protofilaments (~6.2 nm separation), then the staggering would need to be between ~23 and 28 nm. Of note, these same FRET pairs did not produce FRET in budding yeast kinetochores (Aravamudhan et al., 2014). Thus, the staggered organization of Ndc80C molecules is a distinct feature of human kinetochore-microtubule attachments.

2.3.3 Fluorescence Lifetime Imaging Confirms Staggering of Ndc80c Molecules

Concluding that Ndc80C molecules are staggered along the microtubule lattice assumes that the detected FRET occurs between adjacent complexes. To confirm this, we measured FRET from kinetochore-localized Ndc80C molecules and from molecules freely diffusing in the cytosol. If the observed FRET arises due to staggering, then it should be detected within kinetochores but not in the cytosol. Conversely, if FRET occurs intra-complex, then it should be detectable at both the kinetochore and within the cytosol. We used fluorescence lifetime imaging (FLIM) to simultaneously measure FRET in both populations of kinetochore proteins. FLIM directly measures FRET efficiency from the decrease in the excited-state lifetime of the donor fluorophore due to the presence of an acceptor within 10 nm (Becker, 2012). Since the donor fluorescence lifetime can be determined accurately even at low fluorophore concentration, we could separately quantify FRET between kinetochore-localized and cytosolic Ndc80C molecules (Figure 2.2B and Supplementary Figure 2.3; Materials & Methods).

We first tested the validity of this approach by measuring the FRET efficiency at N-Nuf2/N-Nuf2 and Spc25-C/Spc24-C. In the former case, FRET is inter-complex and should be detected only within kinetochores. In the latter, FRET is predominantly intra-complex and

should occur within kinetochores and the cytosol (Ciferri et al., 2008). Fluorescence lifetime measurements for these two FRET pairs confirmed our expectations (Figure 2.2C). For Hec1-C/Spc25-C, the pair from which we deduced Ndc80C staggering by our fluorescence intensity-based method, FLIM detected FRET only within kinetochores and not within the cytosol (Figure 2.2C). Thus, intra-complex FRET does not occur with the Hec1-C/Spc25-C pair, supporting the conclusion that adjacent Ndc80C molecules are staggered along kinetochore-microtubule attachments in human kinetochores.

As a final note, the FRET efficiencies measured via FLIM were directly proportional to the fluorescence intensity-based proximity ratios (Figure 2.2D). Thus, the proximity ratio reflects the average proximity between kinetochore subunits.

2.3.4 The Ndc80C Recruitment Linkages Are Sparsely Distributed

The clustered and staggered organization of Ndc80C molecules in attached kinetochores may result from the spatial organization of its centromeric protein linkages. In human kinetochores, CenpC and CenpT recruit Ndc80C (Figure 2.3A; (Gascoigne et al., 2011; Huis In 't Veld et al., 2016; Klare et al., 2015; Nishino et al., 2013; Rago, Gascoigne, & Cheeseman, 2015; Screpanti et al., 2011; Weir et al., 2016)). These proteins bind to the centromere using their C-terminal domains and extend flexible N-terminal domains to bind one Mis12 complex (Mis12C). Mis12C is a ~20 nm long linker/adaptor that binds one Ndc80C. Additionally, the CenpT N-terminal domain directly recruits up to two additional Ndc80C molecules (Huis In 't Veld et al., 2016). Therefore, to better understand the spatial organization of Ndc80C, we measured FRET between these linkages.

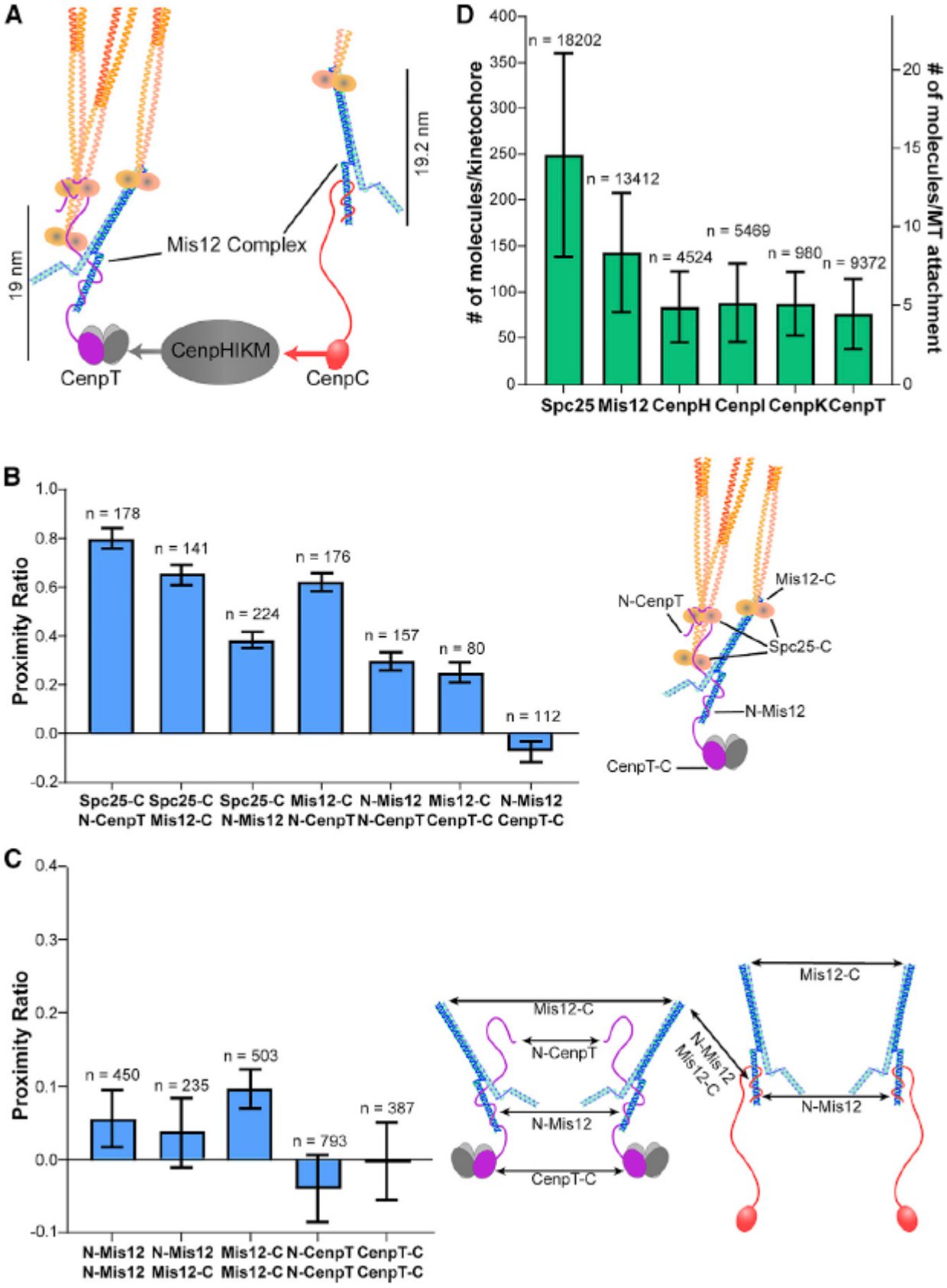
A
19 nm
19.2 nm
Mis12 Complex
CenpHIKM
CenpT
CenpC
D
# of molecules/kinetochore
# of molecules/MT attachment
n = 18202
n = 13412
n = 4524
n = 5469
n = 980
n = 9372
Spc25 Mis12 CenpH CenpI CenpK CenpT
B
Proximity Ratio
n = 178
n = 141
n = 224
n = 176
n = 157
n = 80
n = 112
Spc25-C N-CenpT
Spc25-C Mis12-C
Spc25-C N-Mis12
Mis12-C N-CenpT
N-Mis12 N-CenpT
Mis12-C CenpT-C
N-Mis12 CenpT-C
N-CenpT
Mis12-C
Spc25-C
N-Mis12
CenpT-C
C
Proximity Ratio
n = 450
n = 235
n = 503
n = 793
n = 387
N-Mis12 N-Mis12
N-Mis12 Mis12-C
Mis12-C Mis12-C
N-CenpT N-CenpT
CenpT-C CenpT-C
Mis12-C
N-CenpT
N-Mis12
CenpT-C
N-Mis12
Mis12-C
Mis12-C
N-Mis12

Figure 2.3 The Protein Linkages that Tether Ndc80C to the Centromere Are Sparsely Distributed
(A) Diagram of the biochemical recruitment pathway for Ndc80C (cartoon clipped). (B) FRET between proteins involved in Ndc80C recruitment. Diagram to the right shows the location of different fluorophore tags within the CenpT linkage. (C) The lack of FRET between neighboring Mis12C molecules and between neighboring CenpT molecules suggests that Ndc80C linkages are ≥10 nm apart. The potential FRET pathways are indicated by arrows. (D) Protein copy numbers for metaphase kinetochores, evaluated from unfiltered fluorescence signals of kinetochores in cells expressing GFP and/or mCherry-labeled versions of the indicated subunits. Bar graphs in (B) and (C) display the average proximity ratio ±SEM of fully occupied, metaphase kinetochores. Bar graph in (D) displays the average number of molecules per kinetochore (left axis) or per microtubule (right axis, assuming 17.1 microtubules per human kinetochore) ±SD. The number of kinetochores measured for each cell line is indicated above the bars in (B)–(D). All data are from ≥ 3 experiments. See also Supplementary Figure 2.4, Table 2.2, and Table 2.3.

FRET measurements characterizing the CenpT-Mis12C-Ndc80C linkage were consistent with its known organization (Huis In 't Veld et al., 2016; Nishino et al., 2013; Petrovic et al., 2016) (Figure 2.3B). Next, since Mis12C serves as a convenient proxy for CenpC and CenpT (each binds only one Mis12C), we measured FRET between neighboring Mis12C molecules. At most, we detected weak inter-complex FRET between adjacent Mis12C molecules, irrespective of fluorophore placement (Figure 2.3C). Thus, adjacent Mis12C molecules are, on average, ≥10 nm apart. Interestingly, we did not detect FRET between fluorophores fused to either the C or the N terminus of CenpT (Figure 2.3C). We note that, although the copy number of CenpT is low (~80 molecules/kinetochore), the lower signal-to-noise ratio did not affect our ability to detect FRET (see Materials & Methods and also Figure 2.5D and Supplementary Figure 2.6). Thus, neighboring CenpT molecules are spaced ≥10 nm apart. We did not include CenpC in these analyses due to technical difficulties. The absence of FRET between Mis12C molecules, however, indicates that the CenpC recruitment domains are also ≥10 nm apart.

An additional component that may influence the organization of Ndc80C is the CenpH, CenpI, CenpK, and CenpM (CenpHIKM) complex, a CCAN component (Basilico et al., 2014; Klare et al., 2015; McKinley et al., 2015). CenpHIKM organizes centromeric chromatin and bridges CenpT with CenpC (Figure 2.3A). Consistent with this role, we found a ~1:1 stoichiometry between three of the four CenpHIKM subunits with CenpT (average for CenpH,

CenpI, and CenpK = 86.3 ± 0.8 (SEM) molecules; Figure 2.3D). FRET measurements between neighboring CenpI subunits revealed that, like CenpT and Mis12C, these subunits are also ≥10 nm apart (Supplementary Figure 2.4). Additionally, most of the CenpHIKM subunits were proximal to the centromere and not within proximity of Ndc80C.

In sum, we find that the centromeric recruitment linkages for Ndc80C are ≥10 nm apart from one another. Nevertheless, Ndc80C molecules cluster and stagger along the microtubule lattice. Two factors may contribute to this Ndc80C organization. First, the multivalent recruitment of Ndc80C molecules by CenpT could place multiple Ndc80C molecules within 10 nm, allowing for both clustering and staggering. Second, the microtubule-binding domains of Ndc80C are ~50–70 nm from the CenpT and CenpC N termini. Thus, even though these recruitment domains are not within FRET proximity, this span may allow distantly spaced Ndc80C molecules to bind near each other on the same plus end.

2.3.5 Microtubule Attachment Clusters Ndc80C in Both Human and Budding Yeast Kinetochores

To examine the role of microtubule binding in Ndc80C organization, we destroyed the mitotic spindle by treating cells with nocodazole, a microtubule depolymerizing drug (Figure 2.4A, Figure 2.4C, and Supplementary Figure 2.5). In unattached human kinetochores, inter-complex FRET between Ndc80C molecules reduced significantly (Figure 2.4B). The strongest decrease occurred at the microtubule-binding end (N-Nuf2), with smaller decreases near the tetramerization domain (Nuf2-C) and its centromeric end (Spc25-C). The reduced FRET unlikely arises from structural rearrangement within Ndc80C because Spc25-C/Spc24-C FRET showed only a modest decrease (Figure 2.4B). Thus, binding to the microtubule plus end is the main

reason for the clustering of the microtubule-binding domains of Ndc80C in human metaphase kinetochores.

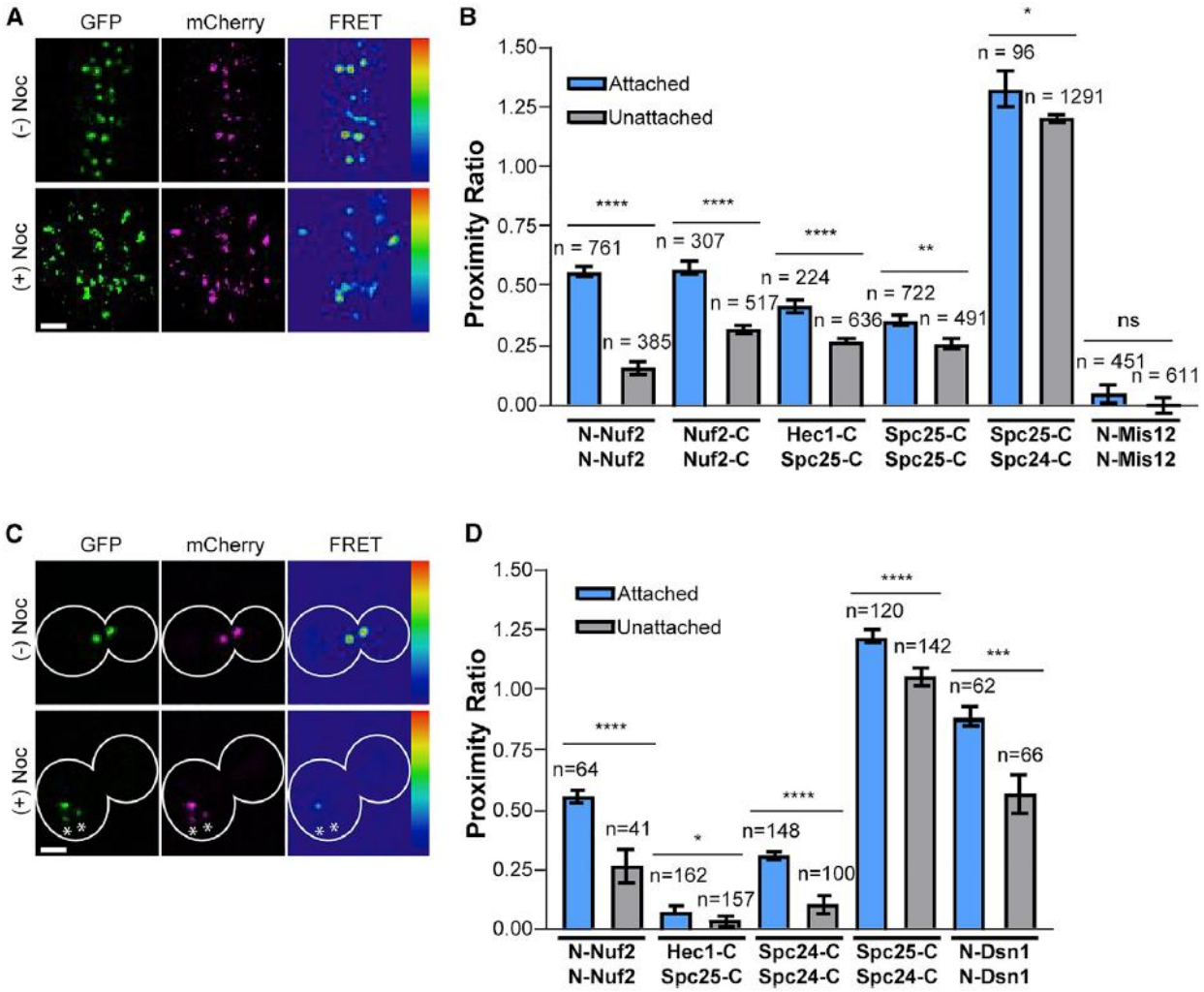

Figure 2.4 Microtubule Attachment Clusters Ndc80C in Both Human and Budding Yeast Kinetochores
(A) Micrographs of mitotic HeLa cells expressing N-Nuf2/N-Nuf2 with and without nocodazole (Noc) treatment. (B) Nocodazole treatment reduces FRET between Ndc80C subunits. Measurements are from metaphase (blue) and nocodazole-treated (gray) cells. (C) Micrographs of budding yeast metaphase cells expressing N-Nuf2/N-Nuf2, with or without nocodazole. Asterisks highlight clusters of unattached kinetochores. (D) Same as in (B) but for budding yeast kinetochores. For (A) and (C), FRET micrographs are scaled equivalently; GFP and mCherry micrographs are scaled for ease of viewing. Scale bar, 2 μm. For (D) and (B), bars are average proximity ratio ± SEM. The number of measurements is indicated above the bars. All data are from ≥ 3 experiments. Statistical significance was evaluated using the Mann-Whitney test, ns, not significant; $^{*}p < 0.05$; $^{**}p < 0.01$; $^{***}p < 0.001$; $^{****}p < 0.0001$. See also Supplementary Figure 2.5, Table 2.2, and Table 2.3.

Interestingly, the proximity ratio at the centromeric end of Ndc80C was only modestly reduced in unattached kinetochores. This observation suggests that the multivalent recruitment of

Ndc80C by CenpT is responsible for Ndc80C centromeric clustering (Huis In 't Veld et al., 2016). Moreover, Hec1-C/Spc25-C inter-complex FRET was also detectable in unattached kinetochores (Figure 2.4B). Therefore, Ndc80C staggering may also result from the multivalence of CenpT.

To understand the influence of multivalent CenpT interactions with Ndc80C in organizing the kinetochore, we adopted a comparative approach. In budding yeast, each centromeric linkage recruits only one Ndc80C (Dimitrova, Jenni, Valverde, Khin, & Harrison, 2016; Hornung et al., 2014; Malvezzi et al., 2013). The budding yeast CenpT homolog does not bind Ndc80C prior to anaphase (Bock et al., 2012; Dhatchinamoorthy et al., 2017; Malvezzi et al., 2013; Schleiffer et al., 2012). Therefore, we expected that the yeast and human kinetochore architectures may respond differently to the loss of microtubule attachment. Accordingly, the centromeric ends of Ndc80C molecules were clustered during attachment in both yeast and human kinetochores. This clustering vanished in unattached yeast kinetochores (compare Spc25-C/Spc25-C in human kinetochores with Spc24-C/Spc24-C in yeast; Figure 2.4B and D). Furthermore, Hec1-C/Spc25-C FRET was undetectable in yeast kinetochores, consistent with a lack of Ndc80C staggering. The centromeric end of Mis12C (marked by N-Mis12 in the human kinetochore and N-Dsn1 in the yeast kinetochore (Aravamudhan et al., 2014; Dimitrova et al., 2016; Petrovic et al., 2016)) showed a significant degree of clustering in budding yeast kinetochores but not in human kinetochores. Interestingly, the degree of clustering at the Ndc80C microtubule-binding ends was similar in both kinetochores, implying similar distribution relative to the plus end.

These data reveal the influence of centromere organization on kinetochore architecture. They strengthen our proposal that the multivalent CenpT linkage is the main source of Ndc80C's

clustered centromeric ends and its longitudinal staggering in human kinetochores. Importantly, despite these differences both kinetochores adopt similar organization at the microtubule-binding ends of Ndc80C.

2.3.6 Centromeric Tension and Microtubule Dynamics Promote Ndc80C Clustering

The sensitivity of Ndc80C clustering to microtubule attachment prompted us to study whether Ndc80C architecture is also sensitive to centromeric tension. Centromeric tension arises from the opposing forces generated by bioriented sister kinetochores. To reveal the relationship between Ndc80C clustering and centromeric tension, we plotted inter-complex FRET between Ndc80C molecules at their microtubule binding ends (N-Nuf2/N-Nuf2) and at their centromeric ends (Spc25-C/Spc25-C) against the sister kinetochore separation, a proxy for the centromeric tension (referred to as the K-K distance, Figure 2.5A). The proximity ratio in both cases showed a weak positive correlation, in part because of measurement noise and a smaller number of observations at high K-K distance values (Pearson's correlation coefficients of 0.17 for N-Nuf2/N-Nuf2 and 0.09 for Spc25-C/Spc25-C, see Materials & Methods). To expose the relationship between the proximity ratio and K-K distance, we binned the dataset according to the K-K distance, revealing positive linear correlations at both ends of Ndc80C (Figure 2.5A). Thus, the proximity between Ndc80C molecules increases with centromeric tension at both the microtubule-binding and centromere-anchored ends of Ndc80C.

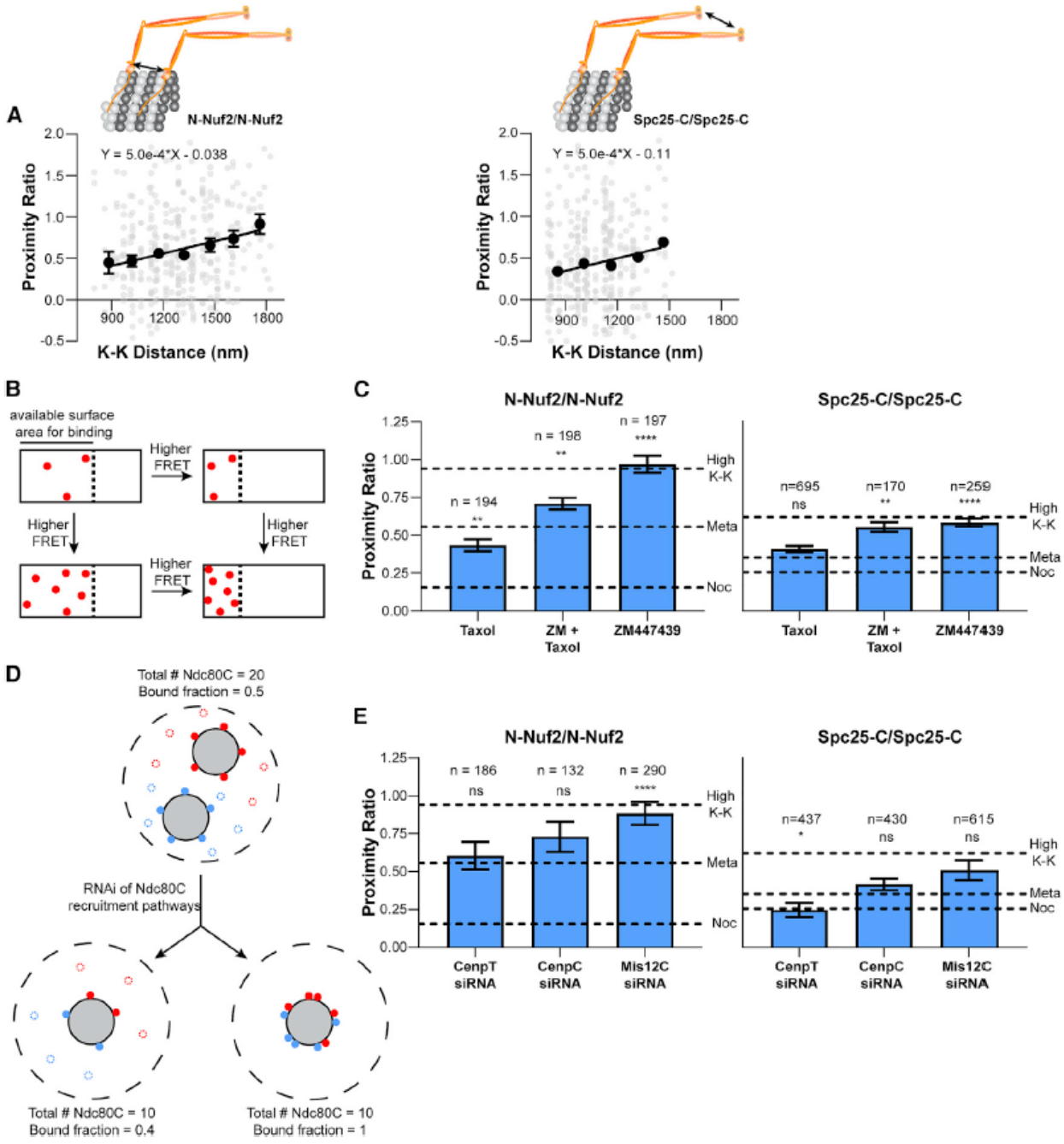

Figure 2.5 Centromeric Tension and Microtubule Dynamics Promote Ndc80C Clustering
(A) Correlation between the proximity ratio and sister kinetochore separation for N-Nuf2/N-Nuf2 (left) and Spc25-C/Spc25-C (right) expressing HeLa cells Proximity ratio measurements are from fully occupied, metaphase kinetochores. The unbinned data are in gray, and the average value of each bin is shown in black. Bins were defined in ranges of 150 nm K-K separation and are the mean ± SEM. For N-Nuf2/N-Nuf2, n = 23, 52, 92, 83, 63, 30, 20 kinetochores; Pearson correlation coefficient = 0.17 for the unbinned data. For Spc25-C/Spc25-C, n = 82, 103, 108, 41, 14 kinetochores; Pearson correlation coefficient = 0.09 for the unbinned data. Solid lines, linear regression of the binned data. (B) The diagram depicts the relationship between the binding density of Ndc80C and the FRET produced by a kinetochore. White rectangles represent the microtubule lattice, where the dashed line demarcates the region of the microtubule plus end available for Ndc80C binding. Red dots represent bound Ndc80C molecules. (C) N-Nuf2/N-Nuf2 and Spc25-C/Spc25-C FRET in response to the microtubule-stabilizing drug Taxol, the Aurora B

kinase inhibitor ZM447439, or both. (D) Cartoon depicting two potential effects of siRNA-mediated knockdown of Ndc80C recruitment pathways on the organization of Ndc80C molecules. The dashed outer circle denotes a portion of the kinetochore in an *en face* view. Blue and red circles indicate Ndc80C molecules linked to individual CenpA nucleosomes. Filled circles are molecules bound to microtubules (gray circles). Unfilled circles indicate unbound molecules. (E) N-Nuf2/N-Nuf2 and Spc25-C/Spc25-C FRET after siRNA-mediated knockdown of members of the Ndc80C recruitment pathways. In (C) and (E), data are the average proximity ratio ± SEM. The dashed lines indicate the average proximity ratio for untreated metaphase (Meta), nocodazole-treated (Noc), and for high tension kinetochores (High K-K). The number of kinetochores measured is indicated above the bars. All data are from ≥ 3 experiments. Statistical significance between untreated metaphase cells and each of the measurements in (C) and (E) was evaluated by the Mann-Whitney test, ns, not significant; $^{*}p < 0.05$; $^{**}p < 0.01$; $^{***}p < 0.001$; $^{****}p < 0.0001$. See also Supplementary Figure 2.6, Table 2.2, and Table 2.3.

Ndc80C clustering at the microtubule-binding ends can increase in response to tension because the number of microtubule-bound molecules increases, the spacing between bound molecules decreases, or both (Figure 2.5B). These two parameters can change due to Aurora B kinase mediated phosphoregulation of Ndc80C molecules (Yoo et al., 2018), via Ndc80C's numerous protein-protein interactions (e.g., oligomerization, accessory microtubule-binding proteins, etc.), and by changes in the available microtubule binding surface (Alushin et al., 2012; Alushin et al., 2010; Helgeson et al., 2018; Janczyk et al., 2017; McEwen, Heagle, Cassels, Buttle, & Rieder, 1997).

To understand the role of phosphoregulation on Ndc80C clustering, we treated HeLa cells with ZM447439, a small-molecule inhibitor of the Aurora B kinase. ZM447439 treatment increased inter-complex FRET at both N-Nuf2 and Spc25-C such that the average value of the proximity ratio was equivalent to its value in kinetochores under the highest centromeric tension (Figure 2.5C). ZM447439 treatment did not affect the range of K-K distances as compared to untreated cells, eliminating any potential role of tension in this experiment (Supplementary Figure 2.6; (Yoo et al., 2018)). Thus, an increase in the number of microtubule-bound molecules results in more Ndc80C clustering at the plus end.

To reveal how microtubule plus-end dynamics affects Ndc80C clustering, we treated cells with Taxol. Taxol stabilizes kinetochore-bound plus ends by dampening tubulin

polymerization dynamics, causing an increase in the number of kinetochore-bound microtubules (Fanara et al., 2004; Kumar, 1981; McEwen et al., 1997). Therefore, Ndc80C molecules will have a larger microtubule surface area for binding. Accordingly, we measured a small decrease in inter-complex FRET at N-Nuf2 in Taxol-treated cells as compared to untreated metaphase cells (Figure 2.5C). Interestingly, FRET at Spc25-C did not change with Taxol treatment, showing that plus-end stabilization has little effect on the organization of Ndc80C's centromere-anchored ends. As an aside, we note that Taxol also lowers the turnover rate of kinetochore-bound microtubules (i.e., the k-fiber, (McEwen et al., 1997)). Therefore, k-fiber stabilization may play a role in Ndc80C clustering. To test this, we measured N-Nuf2/N-Nuf2 FRET in anaphase cells. During anaphase, the turnover rate of kinetochore-microtubule attachments is reduced (Zhai, Kronebusch, & Borisy, 1995). However, N-Nuf2/N-Nuf2 FRET did not change in anaphase kinetochores as compared to metaphase kinetochores (proximity ratio = 0.58 ± 0.05 versus 0.55 ± 0.02, respectively), suggesting that k-fiber stabilization plays an insignificant role in the organization of Ndc80C's microtubule-binding ends.

Finally, we simultaneously treated cells with Taxol and ZM447439 to study the distribution of maximally bound Ndc80C molecules. Under this condition, N-Nuf2/N-Nuf2 FRET was intermediate between what we measured with either Taxol or ZM447439 alone (Figure 2.5C). However, Spc25-C/Spc25-C FRET was unchanged from ZM447439 treatment alone, consistent with the observation that Taxol does not influence Ndc80C centromeric clustering. Overall, these observations show that the number of microtubule-bound Ndc80C molecules and microtubule dynamics influence the relationship between centromeric tension and Ndc80C clustering.

2.3.7 Kinetochores Depleted of Ndc80C Recruitment Linkages Maintain Ndc80C Clustering and Form Load-Bearing Microtubule Attachments

Our data demonstrate that Ndc80C clustering occurs despite a ≥10 nm separation between its centromeric receptors (Figure 2.3C). To determine each receptor's contribution to Ndc80C clustering, we used RNAi of either CenpT, CenpC, or Mis12C. Knockdown of these proteins reduces the number of Ndc80C molecules per kinetochore by 60–70% (Supplementary Figure 2.6; (Rago et al., 2015; Suzuki et al., 2015). The lower copy number should lower the centromeric surface density of Ndc80C (Figure 2.5D). Additionally, because CenpT recruits multiple Ndc80C molecules, these experiment should also reveal the contribution of CenpT in clustering Ndc80C molecules (Figure 2.2A; (Huis In 't Veld et al., 2016; Rago et al., 2015; Volkov, Huis In 't Veld, Dogterom, & Musacchio, 2018)).

RNAi treatments caused minor perturbations in chromosome alignment and cell-cycle timing. However, most sister kinetochores aligned at the metaphase plate and exhibited K-K separations similar to untreated cells (Supplementary Figure 2.6). We only analyzed aligned kinetochores. We first measured Spc25-C/Spc25-C inter-complex FRET. CenpC and Mis12C siRNA treatments did not significantly influence centromeric clustering (Figure 2.5E). However, CenpT depletion caused a modest decrease consistent with its multivalent Ndc80C recruitment domain (Huis In 't Veld et al., 2016). Although CenpC depletion reduces CenpT by ~40%, the remaining CenpT molecules should still recruit multiple Ndc80C molecules, explaining why CenpC RNAi may have little effect on Ndc80C's centromeric clustering (Suzuki et al., 2015). Finally, CenpT depletion does not completely eliminate centromeric clustering, suggesting that under this condition Ndc80C molecules recruited by CenpC come within 10 nm of each other.

We next assessed Ndc80C clustering at its microtubule-binding ends by quantifying N-Nuf2/N-Nuf2 FRET. In addition to lowering Ndc80C's centromeric surface density, reduced

numbers of Ndc80C also decreases the number of microtubules per kinetochore (Suzuki et al., 2015). Therefore, RNAi-mediated knockdown of Ndc80C should reduce Ndc80C clustering at its microtubule-binding end (Figure 2.5D). Alternatively, the fraction of microtubule-bound Ndc80C molecules and/or the proximity between them may increase to compensate for the lower number of Ndc80C molecules (Figure 2.5D and Supplementary Figure 2.6D). Surprisingly, N-Nuf2/N-Nuf2 FRET was either unchanged or increased significantly (Figure 2.5E and Supplementary Figure 2.6B). Thus, Ndc80C clustering at the plus end is either unchanged or increased during knockdowns of its recruitment linkages. This feature may explain how these kinetochores effectively formed load-bearing attachments despite reduced Ndc80C copy numbers (Figure 2.5D).

2.4 Discussion

Our analysis adds a new dimension to the emerging model of human kinetochore architecture by defining the distribution of key proteins around the plus end and along the longitudinal axis of attached microtubules. We synthesized this information with protein structures and interactions to construct a model of the organization of human kinetochore-microtubule attachments (Figure 2.6). In synthesizing this model, we considered the structure and interactions of the human kinetochore's repeating ~26-subunit core seeded by the centromeric CenpA nucleosome (Gascoigne et al., 2011; Klare et al., 2015; McKinley et al., 2015; Pesenti et al., 2018; Weir et al., 2016). The number and centromeric distribution of CenpA nucleosomes dictates CenpC, CenpT, and Ndc80C distribution within the kinetochore. Current estimates suggest that ~44 CenpA nucleosomes participate directly in nucleating the human kinetochore (Bodor et al., 2014; Logsdon et al., 2015). Our quantitation of CenpHIK (Figure

2.3D) is consistent with this: one CenpA nucleosome recruits two copies of the CCAN; hence, ~44 CenpA nucleosomes will recruit ~88 CCAN subunits (Weir et al., 2016).

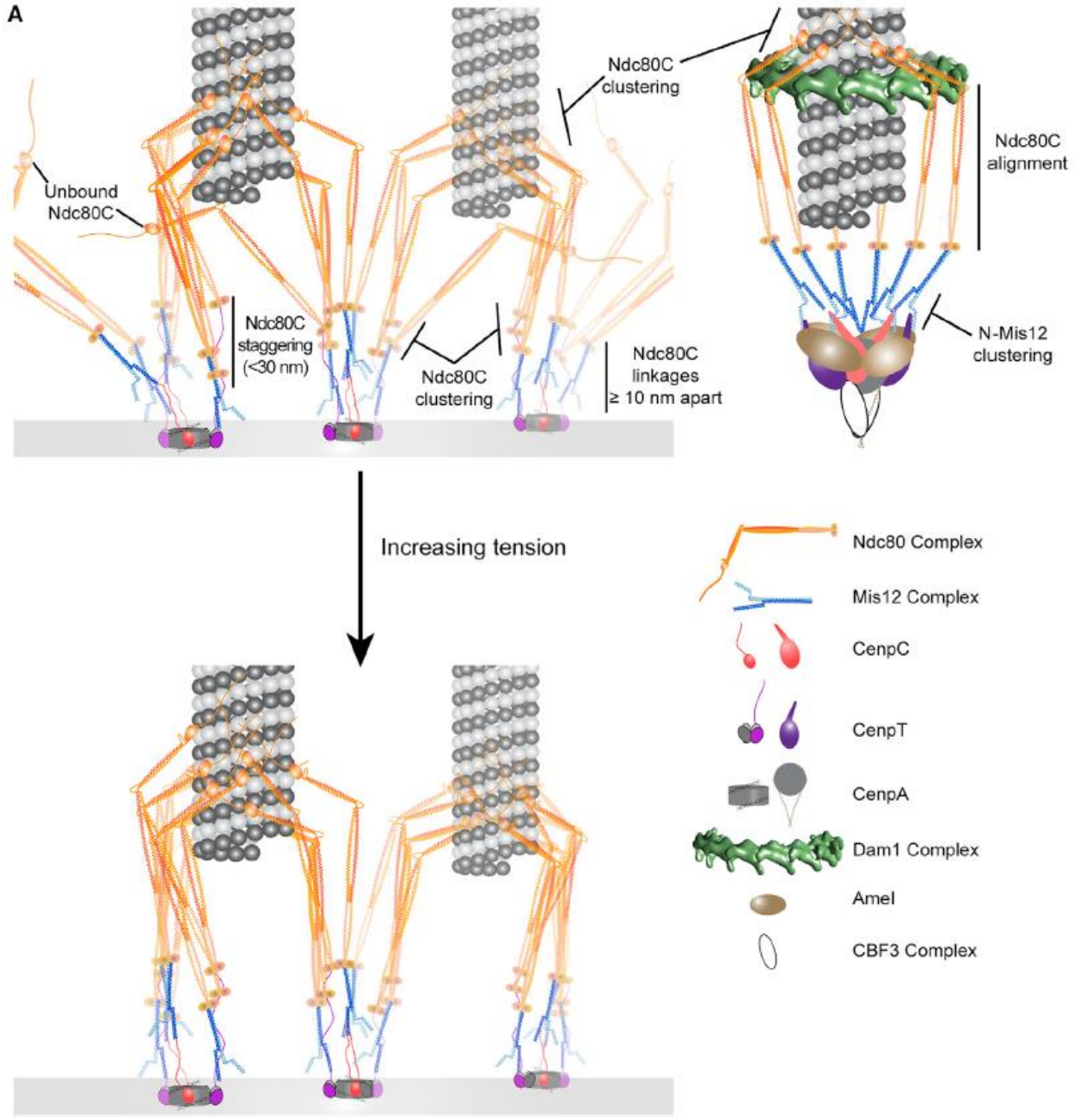

Figure 2.6 Architectural Models of Human and Budding Yeast Kinetochore Microtubule Attachments
(A) The protein organization of human kinetochore-microtubule attachment sites (left) is responsive to physical attachment to the microtubule lattice and to centromeric tension, both of which act to increase the density of microtubule-bound Ndc80C molecules. For comparison, we include a model of the budding yeast kinetochore (top right). The legend (bottom right) identifies proteins for both models. Key architectural details are emphasized. See text for further details.

The human kinetochore binds 17–20 microtubules on average. Therefore, there are at least two CenpA-nucleated kinetochore subunits for every microtubule attachment. Whether the Ndc80C molecules recruited by a single CenpA-nucleated subunit interact exclusively with one microtubule plus end, like yeast kinetochores, is unknown (McIntosh et al., 2013). Our measurements of Ndc80C clustering upon depletion of its centromeric linkages suggest this is not the case (Figure 2.5D and E). These RNAi treatments reduce the number, and hence the surface density, of Ndc80C molecules per kinetochore by up to 60% (Suzuki et al., 2015). Accordingly, each CenpA-nucleated subunit will recruit as few as 2 Ndc80C molecules, and the number of microtubules per kinetochore will see a proportionate decrease. Nevertheless, inter-complex FRET between Ndc80C's microtubule-binding ends persists or even increases indicating that Ndc80C's reduced surface density does not hinder its microtubule binding activity. Conceivably, the loss of centromeric structural integrity that accompanies CenpC and CenpT depletion may affect kinetochore/spindle interactions (Suzuki et al., 2014). However, this concern does not apply to Mis12C RNAi. Mis12C does not bind the centromere and yet its depletion results in the highest clustering of Ndc80C molecules. These observations support the model that Ndc80C molecules in the human kinetochore operate as a lawn, allowing several neighboring CenpA-nucleated kinetochore subunits to cooperate in the formation of microtubule attachments despite their sparse centromeric distribution (Dong, Vanden Beldt, Meng, Khodjakov, & McEwen, 2007; Zaytsev et al., 2015; Zaytsev, Sundin, DeLuca, Grishchuk, & DeLuca, 2014) (Figure 2.6).

The sensitivity of Ndc80C FRET to microtubule attachment reveals the adaptability of kinetochore architecture to its mechanical state. Upon attachment, Ndc80C molecules become

clustered (Figure 2.2 and Figure 2.4). This behavior resembles a recent model wherein Ndc80C molecules align along the spindle axis upon microtubule attachment (Roscioli et al., 2020). Ndc80C clustering also increases proportionally with centromeric tension, suggesting that centromeric tension and the number of microtubule-bound Ndc80C molecules are correlated (Figure 2.5A). This hypothesis is supported by the significant increase in Ndc80C clustering upon Aurora B kinase inhibition, which promotes maximal Ndc80C binding (Figure 2.5C; (Yoo et al., 2018)). The correlation between the number of microtubule-bound Ndc80C molecules and centromeric tension may also play a role in the persistent clustering of Ndc80C observed in our RNAi experiments. In these experiments, the force per Ndc80C molecule increases because Ndc80C numbers reduce without a change in the range of K-K distances (Supplementary Figure 2.6). The higher force per Ndc80C may promote binding and clustering despite their lower centromeric surface density. Our studies also reveal that microtubule plus-end dynamics play a role in Ndc80C clustering. This is most clearly seen when Aurora B activity and plus-end dynamics are inhibited simultaneously: Ndc80C clustering decreases at its microtubule-binding domains compared to Aurora B inhibition alone (Figure 2.5C). How plus-end dynamics affect Ndc80C clustering is unclear. However, it is possible that dynamicity limits Ndc80C distribution at the plus end (Long, Udy, & Dumont, 2017). Aurora B inhibition may also affect the function of key microtubule-binding proteins (e.g., the Astrin-SKAP complex) and indirectly affect Ndc80C architecture (Manning et al., 2010; Redli, Gasic, Meraldi, Nigg, & Santamaria, 2016; Schmidt et al., 2010).

Finally, our study highlights the similarities and differences in kinetochore architectures built upon point centromeres (budding yeast) and regional centromeres (humans). Unlike the human kinetochore, the yeast kinetochore is nucleated by just one CenpA nucleosome, forming a

persistent attachment with only one microtubule (Figure 2.6; (McIntosh et al., 2013)). Therefore, all Ndc80C molecules interact with the same microtubule plus end in budding yeast kinetochores. Consistent with this picture, both the Ndc80C microtubule-binding domains and the Mis12C centromere-binding ends cluster together in the yeast kinetochore (Figure 2.4D; (Aravamudhan et al., 2014; Dimitrova et al., 2016)). In contrast, only Ndc80C molecules cluster in the human kinetochore; Mis12C molecules do not (Figure 2.4B). Furthermore, Ndc80C molecules are aligned with one another in yeast kinetochores but stagger along the microtubule axis in human kinetochores. For yeast, Ndc80C alignment is likely enforced by the point centromere and the Dam1 ring-like structure (Ng et al., 2019). In humans, the staggered organization of Ndc80C arises because of the multivalence of CenpT and the flexibility of the centromeric linkages. We estimate that Ndc80C staggering is no greater than 30 nm, although we cannot rule out the possibility that non-adjacent Ndc80C molecules are staggered by even larger distances. The staggered arrangement of Ndc80C molecules will enhance the attachment persistence and tip-tracking ability of human kinetochores (Hill, 1985). Given the significant differences in the organization of the human and yeast centromeres, it is remarkable that both kinetochores achieve similar degrees of Ndc80C clustering. This similarity in the kinetochore-microtubule interfaces of yeast and humans may represent a generally conserved feature of kinetochore architecture.

2.5 Materials & Methods

2.5.1 Key Resources and Resource Availability

For a list of key resources used in this study, see Table 2.1. For a list of plasmids used for the dual-expression of fluorophore-tagged kinetochore proteins in Hela cells, see Table 2.4. For a list of siRNA sequences used for the knockdown of endogenous human kinetochore proteins, see Table 2.5.

2.5.2 Construction of HeLa Cell Lines

For the co-expression of fluorophore-tagged kinetochore proteins, HeLa cell lines were generated containing a stable chromosomal insertion of a dual-expression vector. The HeLa A12 cell line (gift from the Lampson lab) contains a lentiviral-based chromosomal insertion of a pair of incompatible Cre/Lox sites in front of the human EF-1α promoter (see (Khandelia et al., 2011) for details). Using standard molecular cloning, we created cassettes capable of Cre recombinase-mediated integration at this chromosomal locus that were based on the pERB131 plasmid backbone (gift from the Lampson lab). Briefly, the pERB131 backbone contains two open-reading frames (ORFs), one that becomes under the control of the constitutive EF-1α promoter upon successful integration (ORF1) and a second (ORF2) which is controlled by a tetracycline responsive promoter (Tet-ON). All proteins examined in this study were cloned into one of these two ORFs. The cassette also contains a gene for puromycin resistance which aided in the selection of HeLa cells with successful integration. All HeLa cell lines generated for this study are listed in Table 2.4.

Integration was performed using the Lipofectamine 3000 Reagent kit (Thermo Fisher Scientific) to co-transfect cells with the pERB131 cassette of interest and a Cre-expression

plasmid (gift from the Lampson lab). Two days post-transfection, 2 μg/mL puromycin was added to the cell media for selection over the course of two weeks. Successful transformants were then maintained in media containing 1 μg/mL puromycin.

Owing to the large number of cell lines generated for this study, we did not conduct a detailed analysis of cell cycle duration or mitotic defects. Uninduced cell lines were maintained at 37°C/5% CO_2 for 1 – 2 weeks without any obvious increases in cell death or mitotic index. Cells induced for dual protein expression by doxycycline were maintained for, at most, 3 days and under these conditions we also did not observe obvious increases in cell death or mitotic index. Additionally, the average sister kinetochore distances were in the normal range for all FRET pairs (see Table 2.3).

2.5.3 Fluorescence Microscopy

All fluorescence and FRET imaging was performed on a Nikon Ti-E inverted microscope with a 1.4 NA, 100x, oil immersion objective. A Lumencor LED light engine (472/20 nm GFP excitation, 543/20 nm mCherry excitation) served as the laser power source. All filters are from Chroma and included: 1) a dual-band excitation filter ET/GFP-mCherry (59002x); 2) an excitation dichroic (89019bs); 3) an emission-side dichroic (T560lpxr); 4) and emission filters ET525/50 m and ET595/50 m. Images were acquired on an Andor iXon3 EMCCD camera (pixel size = 160 nm, 16-bit A/D converter). Cell images were either 20 or 10 plane z stack image series for HeLa and budding yeast cells, respectively. The step size between planes was 0.25 μm. For most experiments, the acquisition rate for GFP and mCherry was set at 400 ms. Occasionally, when the copy number of fluorophore-tagged proteins was low (e.g., CCAN proteins or during siRNA mediated knockdowns) the acquisition rate was increased to obtain

higher fluorescence signal. A simple linear correction was applied to normalize fluorescence intensity values to a 400 ms acquisition rate.

To account for fluctuations in laser power and other artifacts in our microscopy setup, we collected images of ~20 anaphase budding yeast cells expressing Ndc80-GFP and Spc25-mCherry before all experiments. Since budding yeast incorporate a stable number of proteins per kinetochore, any changes in GFP and mCherry brightness in these cells should be a result of instrument-derived fluctuations. In this way, ratiometric correction factors were derived for each day of imaging to normalize all FRET measurements throughout the course of this study.

For HeLa, cells were plated in multi-chamber glass-bottomed dishes (Lab-Tek®II) in DMEM media (GIBCO) supplemented with 10% FBS (Corning), and 100 U/mL penicillin and 100 μg/mL streptomycin (GIBCO). Cells were treated with 1 – 2 μg/mL doxycycline for 48 hr to induce the expression of ORF2 proteins. Treatments with siRNA were performed using the Lipofectamine RNAiMAX kit (Invitrogen), using 30 pmol of each protein-specific siRNA and an incubation period of at least 48 hr (siRNAs listed in Table 2.5). During imaging, cell media was changed to DMEM without any phenol red and supplemented with 10% FBS and 100 U/mL penicillin and 100 μg/mL streptomycin. During imaging, the microscope stage is fitted with a heated chamber with CO_2 respirator and objective warmer (Live Cell Instrument). For several experiments, we employed double-thymidine synchronization with 2.5 mM thymidine. For imaging unattached kinetochores, cells were treated with 100 ng/mL nocodazole and incubated at least 30 min before imaging. For imaging attached, tensionless kinetochores, cells were treated with 10 μM Taxol and incubated at least 10 min before imaging. For experiments with the Aurora B inhibitor, ZM447439, we added 10 μM MG132 and incubated 5 min before adding 3 μM of the ZM447439 drug. Cells were incubated an additional 10 min before imaging. For

imaging with both ZM447429 and Taxol, the same procedure was followed as above, adding MG132 and ZM447439 first, incubating 10 min, then adding Taxol. Attached kinetochores were distinguished from unattached kinetochores by their positioning at the spindle mid-zone. Unattached kinetochores were often dispersed through the cell body with random orientations with respect to the spindle and greatly reduced (~800 nm) sister kinetochore separation.

For budding yeast, cells were grown at 30°C to mid-log phase in yeast peptone (YP) media supplemented with 2% glucose. For strains with galactose-inducible promoters, the YP media was supplemented with 2% raffinose and varying concentrations of galactose. The appropriate galactose concentration was determined as that which produced average fluorescence signals at kinetochores that were equal to the fluorescence signal in strains without inducible-promoters. Prior to imaging, cells were rinsed and concentrated in synthetic drop-out media. For imaging of unattached kinetochores, mid-log phase cells were treated with 15 μg/mL nocodazole for 1.5 hr before rinsing and concentrating cells in synthetic media supplemented with 15 μg/mL nocodazole. Metaphase kinetochore clusters were designated by sister pairs with a separation of ~0.8 to 1 μm. For nocodazole-treated cells, unattached kinetochores were identified as the dimmer fluorescent puncta separate from the brighter, spindle-localized attached kinetochores. Cells were imaged on 22x22 mm glass coverslips. All yeast strains used in this study are from (Aravamudhan et al., 2014).

2.5.4 Intensity-Based FRET Quantification

To measure FRET, a semi-automated graphical user interface written in MATLAB was used to analyze cell images. The implementation of this program is described in (A. Joglekar et al., 2013). The raw FRET intensity, measured as the fluorescence intensity observed in the mCherry channel upon excitation with the GFP-specific laser, contains contaminating signal

from GFP bleed-through and mCherry cross-excitation. The contribution of these signals was measured in HeLa cells expressing either Spc25-GFP or Spc25-mCherry alone (Supplementary Figure 2.2; GFP bleed-through = 5.79 ± 0.17%, mCherry cross-excitation = 6.64 ± 0.18%). Subtracting these values from the raw FRET intensity yields the sensitized emission due to FRET. Given the variable number and stoichiometry of kinetochore protein subunits, the sensitized emission was further normalized by the sum of the GFP bleed-through and mCherry cross-excitation. Since these values are proportional to the number of fluorophore-tagged molecules, this normalization essentially yields the sensitized emission/molecule, a metric we refer to as the proximity ratio:

Equation 2.1

$$\text{Proximity ratio} = \frac{\text{Sensitized emission}}{\text{GFP Bleed-through} + \text{mCherry cross-excitation}}$$

2.5.5 Filtering for Kinetochore Protein Occupancy

To accurately measure FRET at HeLa kinetochores, we needed to ensure that our datasets contained only those kinetochores that are maximally occupied by donor- and acceptor-labeled proteins. To meet this requirement, we first defined the single molecule brightness values of GFP and mCherry. To do this, we measured the average background subtracted fluorescence signals for HeLa cells that co-expressed Spc25-GFP and Spc25-mCherry. For these measurements, HeLa cells were treated with Spc25 siRNA which specifically targets endogenous, unlabeled Spc25 but not the fluorophore-tagged versions of Spc25. The dataset of fluorescence signal per kinetochore from these cells were first binned by their mCherry:GFP ratios. This binning suppresses the effect of variations in kinetochore size, which was noted in previous reports (Bodor et al., 2014; Cherry et al., 1989; Cherry & Johnston, 1987; Drpic et al., 2018; Dumont et al., 2020; McEwen et al., 1998). A plot of the bin average Spc25-mCherry v. Spc25-GFP

fluorescence signals was fit by a linear regression, yielding the linear equation $y = -0.4418x + 11010$. The x- and y-intercepts of this equation predict the fluorescence intensity corresponding to kinetochores fully occupied by GFP or mCherry labeled Spc25 molecules, respectively (x-intercept = 24,921 a.u.; y-intercept = 11,010 a.u.; the data in Figure 2.1C are normalized by these values). These intensity values reflect the average number of Spc25 molecules per kinetochore. A prior study by Suzuki et al. found that there are 244 molecules of the Ndc80C per kinetochore (Spc25 is a subunit of the Ndc80 complex) (Suzuki et al., 2015). Using this information, we determined the single molecule brightness of GFP and mCherry to be 102.1 ± 5.0 and 45.1 ± 0.9 a.u.

Using these single molecule brightness values, we converted all subsequent fluorescence signals per kinetochore into a molecular count. Only these brightness values that reflected the appropriate molecule counts for a given kinetochore subunit were retained. The following table defines the filtering bounds we used for each of the kinetochore protein complexes measured in this study:

Protein Complex	Measurement Type	Filtering Bounds (# of molecules)	Reference
The Ndc80 complex	Untreated/Metaphase	212 – 276	(Suzuki et al., 2015)
	Nocodazole	>212	(Suzuki et al., 2015)
	Taxol	212 – 488	(Suzuki et al., 2015)
	ZM447439	212 – 276	(Suzuki et al., 2015)
	ZM447439 + Taxol	212 – 488	(Suzuki et al., 2015)
	CenpT siRNA	73 – 107	(Suzuki et al., 2015)
	CenpC siRNA	83 – 117	(Suzuki et al., 2015)
	Mis12C siRNA	40 – 146	(Suzuki et al., 2015)
The Mis12 complex	Untreated/Metaphase	130 – 172	(Suzuki et al., 2015)
	Nocodazole	>130	(Suzuki et al., 2015)
CenpT	Untreated/Metaphase	64 – 110	This study & (Suzuki et al., 2015)
	Nocodazole	>64	This study & (Suzuki et al., 2015)
CenpHIKM	Untreated/Metaphase	64 – 110	This study
	Nocodazole	>64	This study

For nocodazole measurements, we adhered to the lower limits determined from (Suzuki et al., 2015), but did not place an upper limit on these values for two reasons: 1) it has been

previously noted elsewhere and in our studies that nocodazole-treated, unattached kinetochores recruit greater numbers of molecules than attached, metaphase kinetochores (Supplementary Figure 2.6C and (Magidson et al., 2016; Magidson et al., 2015; Wynne & Funabiki, 2015, 2016)); and 2) the disorganized spindles and reduced sister kinetochore separation made it difficult to measure single kinetochores accurately (Supplementary Figure 2.6D, Table 2.2, and Table 2.3). Similarly, due to the reduced sister kinetochore separation upon Taxol treatment, we filtered Taxol measurements between 212-488 molecules (the upper-limit being twice the average number of molecules at a single kinetochore). Therefore, a small fraction of nocodazole and Taxol measurements may represent more than one kinetochore. For the purposes of quantifying FRET, however, this is not a problem as the proximity ratio is normalized by the total number of molecules (see "2.5.4 Intensity-Based FRET Quantification").

The number of Ndc80 complex molecules after siRNA mediated knockdown of CenpT or CenpC is documented (Suzuki et al., 2015). For siRNA mediated knockdown of the Mis12 complex, however, we have defined our filter bounds for the Ndc80 complex indirectly by assuming that every Mis12 complex recruits exactly one Ndc80 complex (Huis In 't Veld et al., 2016; Petrovic et al., 2016; Rago et al., 2015; Suzuki et al., 2015). Thus, Mis12 complex knockdown should reduce the total number of Ndc80 complexes by 130 – 172 molecules.

The filter bounds for members of the CenpHIKM complex and CenpT were, in part, defined from the average of the unfiltered intensity values of CenpH, CenpI, CenpK, and CenpT (~87 molecules/kinetochore; Figure 2.3D). Since the CenpHIKM complex aids in the recruitment of CenpT, we set the lower limit of CenpHIKM molecules the same as for CenpT (i.e., 64 molecules/kinetochore; (Suzuki et al., 2015)). The upper limit was then set at 110 molecules/kinetochore to place the average value as the midpoint of these extremes.

An additional filter was used when two versions of the same protein compete for binding to the kinetochore (e.g., Spc25-C/Spc25-C FRET). In addition to filtering for full kinetochore occupancy, we further eliminated kinetochores with acceptor-to-donor ratios outside of the range of 0.2 – 5.0. Such filtering removes kinetochores that are saturated with only donor-labeled or acceptor-labeled molecules (i.e., incapable of FRET). As discussed in the main text and as demonstrated in Table 2.2, changing the bounds on this acceptor-to-donor ratio filter only mildly affects the value of the proximity ratio and the overall trends between different FRET pairs does not change.

In budding yeast measurements, nocodazole treatment creates unattached kinetochore clusters of variable size. Therefore, for consistency between metaphase attached and the unattached nocodazole-treated kinetochores, all measurements were filtered to contain only data points with an mCh:GFP ratio of 0.5 – 2.

2.5.6 Fluorescence Lifetime Imaging Microscopy

Fluorescence lifetime imaging (FLIM) data were collected on an ISS ALBA time-resolved laser-scanning confocal system. This setup consists of: 1) an Olympus IX-81 microscope with a U-Plan S-APO 60X 1.2 NA water immerision objective; 2) an SPC-830 time-correlated single photon counting (TCSPC) board (Becker & Hickl); 3) an SC-400-6-PP supercontinuum laser (Fianium); 4) and two photomuliplier tubes (PMT) detectors (Hamamatsu H7422P-40). During data collection, the objective was also equipped with a 37°C temperature-controlled sleeve. HeLa cells were plated in 35 mm glass-bottomed dishes (MatTek) and imaged in DMEM media without any phenol red supplemented with 10% FBS and 100 U/mL penicillin and 100 µg/mL streptomycin. GFP and mCherry excitation were performed with 488 nm and 561 nm lasers, interleaved with 20 MHz frequency and 256 ADC resolution. The pixel-dwell

time was 0.2 ms and laser power was adjusted to keep photon counts between 500,000 – 1,000,000 per pixel.

FLIM data were analyzed using the VistaVision software analysis program (ISS). To distinguish between cytosolic versus kinetochore-localized GFP, we employed intensity threshold masks. This method proved effective since kinetochore-localized GFP always provided higher counts/pixel than cytosolic GFP. Additionally, kinetochore pixels were further isolated by cropping the images to contain only the cellular region corresponding to the metaphase plate. At minimum, cytosolic GFP had a lower threshold of 30 photon counts/pixel to distinguish from background. We also maintained a buffer of at least 25 photon counts/pixel between the upper threshold for the cytosolic GFP and the lower threshold for the kinetochore-localized GFP to prevent cross-contamination of signals. After appropriate thresholding, photon counts from all pixels were summed. As the GFP excitation laser was pulsed first during the interleaved excitation, only photons collected between the first 6.6 – 24.8 ns of each pulse were included. GFP lifetimes were estimated by fitting the histograms of the photon arrival times to single-component exponential decays, using a software generated instrument response function (IRF). The FRET efficiency was calculated by comparing the difference between the GFP lifetime in the absence and presence of an mCherry acceptor ($1 - (\tau_{\text{with mCherry}}/\tau_{\text{without mCherry}})$). We note that the GFP lifetime in the absence of an mCherry acceptor was highly dependent on the protein subunit to which it was attached and on temperature. Therefore, for all FRET pairs the GFP lifetimes without an mCherry acceptor were measured independently.

2.5.7 Western Blot Analysis

HeLa cell lysates were collected from cultures grown in 6-well plates (Corning), seeding at a density of ~100K cells/well. Cells were grown for 3 days with the appropriate drug and

siRNA treatments applied, after which cells were rinsed and aspirated. Lysates were collected in 200 µL SDS-PAGE buffer containing 2-mercaptoethanol using a cell scarper. Lysates were denatured at 95°C, vortexed and centrifuged before loading onto a 4% stacking/10% resolving SDS-PAGE gel. After running, PAGE gels were transferred to PVDF membranes (pre-activated by soaking in methanol) via electrophoresis in transfer buffer (1.4% glycine, 0.3% Tris-base in H_2O). Blots were blocked with 5% milk in tris-buffered saline (TBS) for 30 min. and then incubated with primary antibody overnight at 4°C with shaking (primary antibodies prepared in either 5% BSA or 5% milk in TBS + 0.1% Triton X-100). After rinsing, blots were incubated with secondary antibody prepared in 5% BSA in TBS-T for 30 min. After rinsing, blots were developed via chemiluminescence (Immobilon Western reagent from Millipore) and imaged with an Azure c600 gel imager (Azure Biosystems). All antibodies used in this study are provided in Table 2.1.

2.5.8 Quantification and Statistical Analysis

Intensity-based FRET fluorescence microscopy images were measured using a semi-automated graphical user interface in MATLAB (A. Joglekar et al., 2013). Fluorescence lifetime imaging microscopy data were analyzed using the VistaVision software analysis program (ISS). Statistical analyses were performed in GraphPad Prism. Details of statistical analyses performed in this study are provided in the figure legends and in Table 2.3.

2.6 Acknowledgments

This chapter has been published in Current Biology and has been included in this dissertation with permission from the journal editors. This work was supported by NIGMS of the National Institutes of Health under award number: R35GM126983 to A.P.J. The authors also thank the Single Molecule Analysis in Real-Time (SMART) Center of the University of Michigan, seeded by NSF MRI-R2-ID award DBI-0959823 to Nils G. Walter; Damon Hoff for training, technical advice, and use of the ALBA time-resolved confocal microscope; and Shih-Chu "Jeff" Liao for his help in debugging and running the VistaVision software.

2.7 Author Contributions

Conceptualization, Methodology, Writing – Original Draft, Writing – Review & Editing, Visualization, and Supervision, A.A.K. and A.J.P.; Formal Analysis and Investigation, A.A.K., S.K., and A.J.P.; Software, Resources, and Funding Acquisition, A.J.P.

2.8 Tables

Table 2.1 Key Resources Table

REAGENT or RESOURCE	SOURCE	IDENTIFIER
Antibodies		
Mouse monoclonal anti-β-tubulin	Sigma-Aldrich	Cat# T7816; RRID: AB_261770
Mouse monoclonal anti-DsRed2	Santa Cruz Biotechnology	Cat# sc-101526; RRID: AB_1562589
Rabbit polyclonal anti-Spc25	Atlas Antibodies	Cat# HPA047144; RRID: AB_2679952
Rabbit polyclonal anti-Nuf2	Bethyl	Cat# A304-319A; RRID: AB_2620515
Mouse monoclonal anti-GFP	Takara Bio	Cat# 632381; RRID: AB_2313808
Goat monoclonal anti-mouse, horseradish peroxidase conjugated	Sigma-Aldrich	Cat# A4416; RRID: AB_258167
Goat monoclonal anti-rabbit, horseradish peroxidase conjugated	Sigma-Aldrich	Cat# A4914; RRID: AB_258207
Chemicals, Peptides, and Recombinant Proteins		
Nocodazole	Fisher	Cat# AC358240100; CAS: 31430-18-9
Taxol	Fisher	Cat# NC9507351; CAS: 33069-62-4
ZM447439	Fisher	Cat# 508279
Doxycycline	Fisher	Cat# BP26531; CAS: 10592-13-9
Thymidine	Millipore	Cat# 6060; CAS: 50-89-5
Puromycin	Fisher	Cat# ICN19453910
Experimental Models: Cell Lines		
HeLa A12	(Khandelia et al., 2011)	N/A
Experimental Models: Organisms/Strains		
S. cerevisiae: Strain background: YEF473	ATCC	ATTC:
Oligonucleotides		
For a list of all siRNAs used in this study, see Table 2.5		
Recombinant DNA		
pEM784 – pCAGGS-nls-Cre	(Khandelia et al., 2011)	N/A
pERB131 – Mis12-GFP-FKBPx3; inducible: mCh-Mps1	Lampson lab	N/A
For plasmids for the expression of FRET pairs in HeLa A12 cells, see Table 2.4	This study	N/A
For plasmids for the expression of FRET pairs in *S. cerevisiae*, please see the accompanying reference	(Aravamudhan et al., 2014)	N/A
Software and Algorithms		

Prism	Graphpad	Ver. 8
MATLAB	Mathworks	Ver. 2017b
VistaVision	ISS	Ver. 4.0
Other		
DMEM	Thermo Fisher	N/A
Lipofectamine 3000	Life Technologies	Cat# L3000008
Lipofectamine RNAiMAX	Life Technologies	Cat# 13778075

Table 2.2 List of Proximity Ratio Measurements for FRET Pairs

FRET pairs are grouped by the complexes to which they belong. "Measurement Type" indicates treatments applied to cells before measurements ("Metaphase" indicates untreated cells). For all measurement types except Nocodazole, only bioriented kinetochores were selected for analysis. [a]Average of all filtered measurements, where filtering discards kinetochores that are not fully occupied by the fluorophore-tagged proteins. [b]The Max Proximity Ratio indicates the average proximity ratio for all filtered measurements within an acceptor to donor ratio of 1 – 2. This is only done for FRET pairs that compete for binding to the kinetochore (i.e., acceptor and donor fluorophores on the same protein subunit).

Protein Complex	FRET Pair	Measurement Type	GFP Intensity[a] (Avg ± SD)	mCherry Intensity[a] (Avg ± SD)	Sensitized Emission[a] (Avg ± SEM)	Proximity Ratio[a] (Avg ± SEM)	# of Kinetochores[a]	Max Proximity Ratio[b] (Avg ± SEM)	# of Kinetochores[b] (A:D = 1 -2)
Ndc80 Complex	N-Nuf2 N-Nuf2	Metaphase	12567 ± 4697	5391 ± 2067	591 ± 23.4	0.55 ± 0.02	761	0.70 ± 0.04	222
		Nocodazole	16599 ± 7232	7347 ± 3630	202 ± 36.4	0.16 ± 0.03	385	0.26 ± 0.05	132
		Taxol	15633 ± 6185	5649 ± 2522	532 ± 51.5	0.43 ± 0.04	194	0.43 ± 0.07	51
		ZM447439	14004 ± 4871	4648 ± 2065	1057 ± 59.7	0.97 ± 0.06	197	1.47 ± 0.14	35
		ZM447439 + Taxol	16795 ± 7084	5914 ± 2982	924 ± 45.9	0.71 ± 0.04	198	0.77 ± 0.10	33
		CenpT siRNA	4955 ± 1427	1842 ± 563	246 ± 36.0	0.60 ± 0.09	186	0.63 ± 0.15	63
		CenpC siRNA	5135 ± 1584	2205 ± 720	312 ± 43.1	0.73 ± 0.10	132	0.85 ± 0.16	49
		Mis12C siRNA	5406 ± 2202	2137 ± 910	380 ± 30.0	0.88 ± 0.08	290	1.20 ± 0.13	97
	N-Nuf2 Hec1-C	Metaphase	24633 ± 1878	10741 ± 762	451 ± 68.4	0.12 ± 0.03	93	n/a	n/a
		Nocodazole	32837 ± 8532	13422 ± 3582	327 ± 48.1	0.12 ± 0.02	265	n/a	n/a
	N-Nuf2 Nuf2-C	Metaphase	12940 ± 4532	5230 ± 2011	90.7 ± 35.3	0.09 ± 0.03	296	0.22 ± 0.06	94
	N-Nuf2 Spc25-C	Metaphase	24643 ± 1815	10874 ± 836	80.6 ± 30.4	0.04 ± 0.01	241	n/a	n/a
		Nocodazole	26808 ± 4249	13265 ± 2719	72.2 ± 54.7	0.03 ± 0.02	84	n/a	n/a
	Nuf2-C Nuf2-C	Metaphase	11971 ± 5362	5546 ± 2351	591 ± 26.3	0.57 ± 0.03	307	0.71 ± 0.05	54
		Nocodazole	16328 ± 10461	8688 ± 4312	484 ± 25.4	0.32 ± 0.02	517	0.42 ± 0.04	89
	Spc25-C Hec1-C	Metaphase	24767 ± 2016	10914 ± 866	888 ± 54.6	0.41 ± 0.03	224	n/a	n/a
		Nocodazole	34597 ± 10733	15639 ± 4552	824 ± 36.6	0.27 ± 0.01	636	n/a	n/a

	Spc25-C Nuf2-C	Metaphase	25017 ± 1751	10930 ± 823	754 ± 45.5	0.35 ± 0.02	262	n/a	n/a
	Spc25-C Spc25-C	Metaphase	11748 ± 4904	5759 ± 2170	365 ± 25.3	0.35 ± 0.02	722	0.44 ± 0.05	155
		Nocodazole	19549 ± 10871	8406 ± 4387	429 ± 32.9	0.26 ± 0.02	491	0.28 ± 0.05	92
		Taxol	16431 ± 6576	6913 ± 2837	575 ± 28.7	0.41 ± 0.02	695	0.49 ± 0.04	254
		ZM447439	12410 ± 4718	5527 ± 2131	623 ± 28.0	0.58 ± 0.03	259	0.68 ± 0.05	81
		ZM447439 + Taxol	16289 ± 5652	6022 ± 2641	726 ± 39.0	0.55 ± 0.03	170	0.69 ± 0.06	52
		CenpT siRNA	4599 ± 1529	1921 ± 677	92.6 ± 17.7	0.25 ± 0.05	437	0.35 ± 0.07	171
		CenpC siRNA	5483 ± 1647	2085 ± 720	185 ± 17.0	0.42 ± 0.04	430	0.58 ± 0.07	141
		Mis12C siRNA	5477 ± 2204	1940 ± 942	215 ± 24.7	0.51 ± 0.06	615	0.58 ± 0.12	223
	Spc25-C Spc24-C	Metaphase	24595 ± 1727	10872 ± 810	2823 ± 161.1	1.32 ± 0.08	96	n/a	n/a
		Nocodazole	39566 ± 12479	18852 ± 6372	4238 ± 65.2	1.20 ± 0.02	1291	n/a	n/a
Mis12 Complex	Mis12-C Mis12-C	Metaphase	8454 ± 3572	2930 ± 1571	60.0 ± 17.3	0.10 ± 0.03	503	0.12 ± 0.07	61
		Nocodazole	12240 ± 6282	11541 ± 5678	110 ± 100	0.11 ± 0.08	255	0.13 ± 0.18	52
	N-Mis12 Mis12-C	Metaphase	7993 ± 2204	3204 ± 968	20.6 ± 31.1	0.04 ± 0.05	235	0.13 ± 0.07	104
	N-Mis12 N-Mis12	Metaphase	8355 ± 2783	3071 ± 1195	26.9 ± 26.4	0.06 ± 0.04	450	0.17 ± 0.07	140
		Nocodazole	12733 ± 5711	4454 ± 2093	-24.2 ± 28.3	-0.02 ± 0.03	609	0.04 ± 0.05	248
CenpT	N-CenpT N-CenpT	Metaphase	4431 ± 1639	1970 ± 694	-18.6 ± 17.1	-0.04 ± 0.05	793	-0.02 ± 0.08	279
		Nocodazole	6029 ± 2907	2995 ± 1330	-39.0 ± 23.7	-0.07 ± 0.05	543	-0.11 ± 0.08	239
	CenpT-C CenpT-C	Metaphase	4647 ± 1723	1756 ± 720	-2.21 ± 19.7	0.00 ± 0.05	387	0.15 ± 0.14	71

CenpHIKM	CenpI-C CenpI-C	Metaphase	4221 ± 1388	1934 ± 550	26.9 ± 29.3	0.07 ± 0.08	224	0.06 ± 0.11	111
Ndc80 Complex + Mis12 Complex	Spc25-C Mis12-C	Metaphase	20056 ± 5624	8918 ± 2456	1140 ± 72.0	0.65 ± 0.04	141	n/a	n/a
		Nocodazole	27709 ± 10985	16781 ± 7241	1057 ± 26.8	0.39 ± 0.01	1378	n/a	n/a
	Spc25-C N-Mis12	Metaphase	15517 ± 1152	10997 ± 830	621 ± 55.1	0.38 ± 0.03	224	n/a	n/a
		Nocodazole	26313 ± 8252	20253 ± 6701	664 ± 31.1	0.23 ± 0.01	1252	n/a	n/a
Ndc80 Complex + CenpT	Spc25-C N-CenpT	Metaphase	8234 ± 1272	11074 ± 868	967 ± 51.7	0.80 ± 0.04	178	n/a	n/a
		Nocodazole	12710 ± 4092	17428 ± 5998	1483 ± 45.2	0.80 ± 0.03	575	n/a	n/a
Mis12 Complex + CenpT	Mis12-C N-CenpT	Metaphase	9606 ± 1214	6582 ± 539	616 ± 36.4	0.62 ± 0.04	176	n/a	n/a
		Nocodazole	11851 ± 3733	7745 ± 1606	374 ± 30.0	0.32 ± 0.03	233	n/a	n/a
	N-Mis12 N-CenpT	Metaphase	9479 ± 1202	6588 ± 495	295 ± 35.6	0.30 ± 0.04	157	n/a	n/a
		Nocodazole	12130 ± 3707	7809 ± 1655	209 ± 20.2	0.17 ± 0.02	328	n/a	n/a
	Mis12-C CenpT-C	Metaphase	9429 ± 1302	6317 ± 393	241 ± 40.9	0.25 ± 0.04	80	n/a	n/a
		Nocodazole	12935 ± 4001	7592 ± 1452	159 ± 32.3	0.13 ± 0.03	184	n/a	n/a
	N-Mis12 CenpT-C	Metaphase	12153 ± 3762	4975 ± 1570	-66.8 ± 41.9	-0.07 ± 0.04	112	n/a	n/a
Ndc80 Complex + CenpHIKM	Hec1-C CenpI-C	Metaphase	15228 ± 7728	8013 ± 3516	50.2 ± 54.3	0.05 ± 0.04	120	n/a	n/a
		Nocodazole	17781 ± 11274	15918 ± 6826	204 ± 22.6	0.10 ± 0.01	850	n/a	n/a
	Spc25-C CenpI-C	Metaphase	8767 ± 1284	11018 ± 849	19.2 ± 63.1	0.02 ± 0.05	115	n/a	n/a
		Nocodazole	15309 ± 5895	19970 ± 7468	355 ± 27.7	0.15 ± 0.01	1109	n/a	n/a
	Spc25-C CenpH-C	Metaphase	15090 ± 8438	8074 ± 3857	88.4 ± 79.0	0.05 ± 0.06	104	n/a	n/a
	Spc25-C N-CenpI	Metaphase	9083 ± 1487	10879 ± 829	182 ± 54.3	0.15 ± 0.04	100	n/a	n/a

	Spc25-C N-CenpK	Metaphase	8385 ± 1188	11079 ± 804	125 ± 37.4	0.10 ± 0.03	184	n/a	n/a
	Spc25-C N-CenpH	Metaphase	8462 ± 1253	10983 ± 848	188 ± 59.5	0.16 ± 0.05	151	n/a	n/a
Mis12 Complex + CenpHIKM	Mis12-C CenpI-C	Metaphase	8801 ± 1205	6643 ± 540	-105 ± 77.8	-0.10 ± 0.08	61	n/a	n/a
	Mis12-C CenpH-C	Metaphase	10953 ± 3685	5961 ± 1560	-80.2 ± 96.9	-0.07 ± 0.10	110	n/a	n/a
	Mis12-C N-CenpI	Metaphase	9145 ± 1404	6772 ± 584	61.5 ± 67.2	0.06 ± 0.07	87	n/a	n/a
	Mis12-C N-CenpK	Metaphase	8989 ± 1327	6668 ± 556	192 ± 51.8	0.21 ± 0.05	98	n/a	n/a
	N-Mis12 CenpI-C	Metaphase	8828 ± 1245	6708 ± 543	172 ± 67.1	0.18 ± 0.07	54	n/a	n/a
	N-Mis12 CenpH-C	Metaphase	13436 ± 3232	4750 ± 1589	121 ± 55.3	0.12 ± 0.05	182	n/a	n/a
	N-Mis12 N-CenpI	Metaphase	14939 ± 1183	3583 ± 554	103 ± 46.6	0.09 ±0.04	80	n/a	n/a
		Nocodazole	22646 ± 7409	4872 ± 1531	172 ± 34.5	0.12 ± 0.02	160	n/a	n/a
	N-Mis12 N-CenpK	Metaphase	8940 ± 1334	6562 ± 549	228 ± 81.9	0.25 ± 0.09	58	n/a	n/a
CenpT + CenpHIKM	N-CenpT N-CenpI	Metaphase	9100 ± 1247	3785 ± 568	40.7 ± 36.1	0.05 ± 0.05	303	n/a	n/a
	CenpT-C N-CenpI	Metaphase	9355 ± 1223	3465 ± 454	268 ± 36.1	0.35 ± 0.05	107	n/a	n/a
	N-CenpT CenpI-C	Metaphase	9116 ± 1285	3731 ± 539	52.8 ± 25.0	0.06 ± 0.03	420	n/a	n/a
	CenpT-C CenpI-C	Metaphase	9040 ± 1502	3582 ± 579	71.6 ± 47.7	0.10 ± 0.06	48	n/a	n/a

Table 2.3 Measurement Statistics for FRET Pairs in This Study

FRET pairs are grouped by the complexes to which they belong. "Measurement Type" indicates treatments applied to cells before measurements ("Metaphase" indicates untreated cells). For all measurement types except Nocodazole, only bioriented kinetochores were selected for analysis. For all measurements, a one sample t test was used to evaluate if the proximity ratio was statistically different from zero (n.s. = not significant, with p values listed in parentheses; ∗ $p < 0.05$; ∗∗ $p < 0.01$; ∗∗∗ $p < 0.001$; ∗∗∗∗ $p < 0.0001$). [a]Average of all filtered measurements, where filtering discards kinetochores that are not fully occupied by the fluorophore-tagged proteins.

Protein Complex	FRET Pair	Measurement Type	K-K Distance (nm) (Avg ± SD)	Proximity Ratio[a] (Avg ± SEM)	One Sample T-Test: Proximity Ratio > 0	# of Experiments	# of Cells	# of Kinetochores[a]	Percent kinetochores retained after filtering
Ndc80 Complex	N-Nuf2 N-Nuf2	Metaphase	1321 ± 303	0.55 ± 0.02	****	19	237	761	24.5%
		Nocodazole	756 ± 155	0.16 ± 0.03	****	2	30	385	56.0%
		Taxol	851 ± 174	0.43 ± 0.04	****	5	76	194	28.0%
		ZM447439	1297 ± 327	0.97 ± 0.06	****	5	85	197	18.9%
		ZM447439 + Taxol	994 ± 252	0.71 ± 0.04	****	3	78	198	36.5%
		CenpT siRNA	1316 ± 271	0.60 ± 0.09	****	7	72	186	19.7%
		CenpC siRNA	1304 ± 278	0.73 ± 0.10	****	6	73	132	19.1%
		Mis12C siRNA	1376 ± 339	0.88 ± 0.08	****	4	48	290	48.6%
	N-Nuf2 Hec1-C	Metaphase	1322 ± 287	0.12 ± 0.03	***	4	105	93	6.1%
		Nocodazole	n/a	0.12 ± 0.02	****	2	48	265	24.2%
	N-Nuf2 Nuf2-C	Metaphase	1456 ± 313	0.09 ± 0.03	**	4	82	296	27.5%
	N-Nuf2 Spc25-C	Metaphase	1065 ± 207	0.04 ± 0.01	**	7	187	241	8.1%
		Nocodazole	n/a	0.03 ± 0.02	n.s. (p = 0.18)	1	30	84	26.2%
	Nuf2-C Nuf2-C	Metaphase	1295 ± 289	0.57 ± 0.03	****	5	99	307	21.5%
		Nocodazole	706 ± 173	0.32 ± 0.02	****	2	47	517	64.1%
	Spc25-C Hec1-C	Metaphase	1083 ± 224	0.41 ± 0.03	****	9	149	224	7.8%
		Nocodazole	692 ± 183	0.27 ± 0.01	****	3	54	636	48.4%

	Spc25-C Nuf2-C	Metaphase	1081 ± 242	0.35 ± 0.02	****	4	110	262	12.4%
	Spc25-C Spc25-C	Metaphase	1086 ± 269	0.35 ± 0.02	****	12	195	722	26.2%
		Nocodazole	692 ± 163	0.26 ± 0.02	****	3	42	491	76.6%
		Taxol	811 ± 216	0.41 ± 0.02	****	4	87	695	59.7%
		ZM447439	1050 ± 313	0.58 ± 0.03	****	2	70	259	22.7%
		ZM447439 + Taxol	814 ± 198	0.55 ± 0.03	****	1	45	170	40.5%
		CenpT siRNA	1124 ± 294	0.25 ± 0.05	****	8	131	437	34.3%
		CenpC siRNA	1118 ± 261	0.42 ± 0.04	****	8	199	430	22.9%
		Mis12C siRNA	992 ± 247	0.51 ± 0.06	****	3	70	615	75.4%
	Spc25-C Spc24-C	Metaphase	1160 ± 263	1.32 ± 0.08	****	6	115	96	4.7%
		Nocodazole	n/a	1.20 ± 0.02	****	4	97	1291	67.7%
Mis12 Complex	Mis12-C Mis12-C	Metaphase	1292 ± 310	0.10 ± 0.03	***	7	207	503	20.2%
		Nocodazole	n/a	0.11 ± 0.08	n.s. (p = 0.17)	1	31	255	89.2%
	N-Mis12 Mis12-C	Metaphase	1103 ± 254	0.04 ± 0.05	n.s. (p = 0.42)	4	82	235	23.0%
	N-Mis12 N-Mis12	Metaphase	1234 ± 355	0.06 ± 0.04	n.s. (p = 0.15)	11	165	450	26.3%
		Nocodazole	n/a	-0.02 ± 0.03	n.s. (p = 0.47)	3	49	609	82.3%
CenpT	N-CenpT N-CenpT	Metaphase	1131 ± 282	-0.04 ± 0.05	n.s. (p = 0.39)	4	146	793	51.6%
		Nocodazole	786 ± 160	-0.07 ± 0.05	n.s. (p = 0.14)	3	60	543	93.0%
	CenpT-C CenpT-C	Metaphase	1160 ± 319	0.00 ± 0.05	n.s. (p = 0.96)	4	100	387	49.1%

CenpHIKM	CenpI-C CenpI-C	Metaphase	1093 ± 265	0.07 ± 0.08	n.s (p = 0.37)	2	54	224	37.8%
Ndc80 Complex + Mis12 Complex	Spc25-C Mis12-C	Metaphase	1193 ± 293	0.65 ± 0.04	****	4	99	141	7.5%
		Nocodazole	n/a	0.39 ± 0.01	****	2	61	1378	68.1%
	Spc25-C N-Mis12	Metaphase	1145 ± 253	0.38 ± 0.03	****	6	134	224	8.8%
		Nocodazole	n/a	0.23 ± 0.01	****	2	60	1252	88.9%
Ndc80 Complex + CenpT	Spc25-C N-CenpT	Metaphase	1119 ± 250	0.80 ± 0.04	****	4	92	178	17.6%
		Nocodazole	n/a	0.80 ± 0.03	****	1	30	575	76.4%
Mis12 Complex + CenpT	Mis12-C N-CenpT	Metaphase	1254 ± 292	0.62 ± 0.04	****	3	83	176	10.9%
		Nocodazole	700 ± 179	0.32 ± 0.03	****	2	25	233	37.4%
	N-Mis12 N-CenpT	Metaphase	1207 ± 286	0.30 ± 0.04	****	3	82	157	8.9%
		Nocodazole	706 ± 182	0.17 ± 0.02	****	2	31	328	39.1%
	Mis12-C CenpT-C	Metaphase	1123 ± 271	0.25 ± 0.04	****	3	80	80	5.3%
		Nocodazole	734 ± 184	0.13 ± 0.03	****	2	26	184	31.0%
	N-Mis12 CenpT-C	Metaphase	1189 ± 293	-0.07 ± 0.04	n.s. (p = 0.09)	6	146	112	7.0%
Ndc80 Complex + CenpHIKM	Hec1-C CenpI-C	Metaphase	1061 ± 268	0.05 ± 0.04	n.s. (p = 0.25)	2	63	120	10.9%
		Nocodazole	n/a	0.10 ± 0.01	****	2	62	850	67.4%
	Spc25-C CenpI-C	Metaphase	1058 ± 242	0.02 ± 0.05	n.s. (p = 0.64)	2	50	115	19.9%
		Nocodazole	n/a	0.15 ± 0.01	****	2	60	1109	84.5%
	Spc25-C CenpH-C	Metaphase	1153 ± 255	0.05 ± 0.06	n.s. (p = 0.41)	2	67	104	11.2%
	Spc25-C N-CenpI	Metaphase	1150 ± 283	0.15 ± 0.04	***	1	49	100	13.6%

	Spc25-C N-CenpK	Metaphase	1039 ± 246	0.10 ± 0.03	**	2	69	184	18.8%
	Spc25-C N-CenpH	Metaphase	973 ± 222	0.16 ± 0.05	**	1	57	151	18.4%
Mis12 Complex + CenpHIKM	Mis12-C CenpI-C	Metaphase	1129 ± 251	-0.10 ± 0.08	n.s. (p = 0.22)	1	33	61	14.0%
	Mis12-C CenpH-C	Metaphase	1279 ± 250	-0.07 ± 0.10	n.s. (p = 0.45)	2	73	110	11.5%
	Mis12-C N-CenpI	Metaphase	1010 ± 226	0.06 ± 0.07	n.s. (p = 0.35)	2	79	87	7.7%
	Mis12-C N-CenpK	Metaphase	1207 ± 248	0.21 ± 0.05	***	1	31	98	18.5%
	N-Mis12 CenpI-C	Metaphase	1128 ± 264	0.18 ± 0.07	*	1	37	54	11.0%
	N-Mis12 CenpH-C	Metaphase	1250 ± 300	0.12 ± 0.05	*	2	82	182	13.9%
	N-Mis12 N-CenpI	Metaphase	1059 ± 236	0.09 ±0.04	*	2	40	80	12.8%
		Nocodazole	712 ± 139	0.12 ± 0.02	****	1	12	160	41.2%
	N-Mis12 N-CenpK	Metaphase	1146 ± 249	0.25 ± 0.09	**	1	24	58	14.2%
CenpT + CenpHIKM	N-CenpT N-CenpI	Metaphase	1055 ± 231	0.05 ± 0.05	n.s. (p = 0.29)	2	71	303	26.2%
	CenpT-C N-CenpI	Metaphase	1121 ± 263	0.35 ± 0.05	****	2	40	107	19.8%
	N-CenpT CenpI-C	Metaphase	1067 ± 246	0.06 ± 0.03	n.s. (p = 0.05)	2	89	420	24.9%
	CenpT-C CenpI-C	Metaphase	1147 ± 267	0.10 ± 0.06	n.s. (p = 0.11)	2	36	48	19.4%

Table 2.4 List of Dual-Expression Plasmids

These plasmids were stably integrated into the HeLa genome via Cre/Lox recombination. ORF1 indicates genes that are under the control of a constitutive promoter and ORF2 indicates genes that are under the control of a dox-inducible promoter.

Plasmid Name	Backbone	ORF1 gene (constitutive)	ORF2 gene (dox-inducible)
pHELA16	pERB131	Spc25-GFP	Spc25-mCherry
pHELA17	pERB131	Spc25-mCherry	Spc25-GFP
pAK003	pERB131	GFP-Nuf2	Spc25-mCherry
pAK008	pERB131	Spc25-mCherry	GFP-CenpT
pAK009	pERB131	mCherry-Nuf2	Spc25-GFP
pAK016	pERB131	GFP-Nuf2	mCherry-Nuf2
pAK017	pERB131	mCherry-Nuf2	GFP-Nuf2
pAK020	pERB131	mCherry-CenpT	GFP-CenpT
pAK022	pERB131	GFP-Mis12	Spc25-mCherry
pAK024	pERB131	mCherry-Mis12	GFP-Mis12
pAK025	pERB131	GFP-Mis12	mCherry-Mis12
pAK026	pERB131	Spc25-GFP	Hec1-mCherry
pAK027	pERB131	Spc25-mCherry	Hec1-GFP
pAK030	pERB131	GFP-Mis12	Mis12-mCherry
pAK031	pERB131	mCherry-Mis12	Mis12-GFP
pAK032	pERB131	Mis12-GFP	Mis12-mCherry
pAK033	pERB131	Mis12-mCherry	Mis12-GFP
pAK036	pERB131	GFP-Mis12	CenpT-mCherry
pAK037	pERB131	mCherry-Mis12	CenpT-GFP
pAK038	pERB131	CenpT-GFP	CenpT-mCherry
pAK039	pERB131	CenpT-mCherry	CenpT-GFP
pSK01	pERB131	Spc25-mCherry	Mis12-GFP
pAK051	pERB131	mCherry-Nuf2	Hec1-GFP
pSK02	pERB131	Spc25-GFP	Mis12-mCherry
pSK14	pERB131	Spc25-mCherry	Spc24-GFP
pAK057	pERB131	Spc25-GFP	Spc24-mCherry
pAK061	pERB131	Spc25-mCherry	CenpI-GFP
pAK062	pERB131	mCherry-Mis12	CenpI-GFP
pAK063	pERB131	Mis12-mCherry	CenpI-GFP
pAK064	pERB131	Spc25-mCherry	CenpH-GFP
pAK065	pERB131	mCherry-Mis12	CenpH-GFP
pAK066	pERB131	Mis12-mCherry	CenpH-GFP
pAK072	pERB131	CenpI-mCherry	CenpI-GFP
pAK073	pERB131	Spc25-GFP	CenpI-mCherry
pAK074	pERB131	GFP-CenpI	Spc25-mCherry
pAK075	pERB131	mCherry-CenpI	Spc25-mCherry
pAK076	pERB131	GFP-CenpH	Spc25-mCherry

pAK077	pERB131	mCherry-CenpH	Spc25-mCherry
pAK078	pERB131	mCherry-CenpT	CenpI-GFP
pAK084	pERB131	Spc25-GFP	CenpH-mCherry
pAK085	pERB131	GFP-Mis12	CenpH-mCherry
pAK086	pERB131	Mis12-GFP	CenpH-mCherry
pAK087	pERB131	mCherry-Mis12	GFP-CenpK
pAK088	pERB131	Mis12-mCherry	GFP-CenpK
pAK091	pERB131	CenpI-GFP	Hec1-mCherry
pAK092	pERB131	CenpI-mCherry	Hec1-GFP
pAK093	pERB131	CenpH-GFP	CenpH-mCherry
pAK094	pERB131	CenpH-mCherry	CenpH-GFP
pAK095	pERB131	CenpI-mCherry	GFP-CenpT
pAK099	pERB131	Spc25-mCherry	GFP-CenpK
pAK114	pERB131	Spc25-GFP	Nuf2-mCherry
pAK115	pERB131	Spc25-mCherry	Nuf2-GFP
pAK116	pERB131	GFP-Nuf2	Nuf2-mCherry
pAK117	pERB131	mCherry-Nuf2	Nuf2-GFP
pAK125	pERB131	Spc25-mCherry	GFP-CenpK
pAK126	pERB131	GFP-CenpI	Mis12-mCherry
pAK127	pERB131	mCherry-CenpI	GFP-CenpT
pAK129	pERB131	CenpI-GFP	CenpT-mCherry
pAK130	pERB131	GFP-CenpI	CenpT-mCherry
pAK131	pERB131	Mis12-mCherry	GFP-CenpT
pAK132	pERB131	mCherry-CenpT	Mis12-GFP
pAK133	pERB131	mCherry-Mis12	GFP-CenpT
pAK134	pERB131	CenpT-GFP	Mis12-mCherry
pAK135	pERB131	GFP-Mis12	mCherry-CenpI
pAK136	pERB131	Nuf2-GFP	Nuf2-mCherry
pAK137	pERB131	Nuf2-mCherry	Nuf2-GFP

Table 2.5 List of siRNAs

Target Protein	Sequence	Target Sequence	Source	Reference
Hec1	UGUCUAGCAGAUACUUGCACGGUUU	5' UTR	Invitrogen	This paper
Nuf2	CUAAAUUGCUGAAUGGUAAGAAGCC	ORF	Invitrogen	This paper
Spc25 (1)	UGCCUGCGAAGCAUUGUCCUACAUA	5' UTR	Invitrogen	This paper
Spc25 (2)	GCCUGCGAAGCAUUGUCCUACAUAA	5' UTR	Invitrogen	This paper
Spc24 (1)	CCAGUGGAGGCAAGUGGAACCACCU	5' UTR	Sigma Aldrich	This paper
Spc24 (2)	CAAGUGGAACCACCUUCUCUCUGCU	5' UTR	Sigma Aldrich	This paper
Mis12 (1)	GCAAAAUAAGCCAAGAUGUCU	ORF	Sigma Aldrich	This paper
Mis12 (2)	GUAUCUAUGCCAAAUUUGUUUU	ORF	Sigma Aldrich	This paper
Dsn1	GUCUAUCAGUGUCGAUUUA	ORF	Sigma Aldrich	(Kim & Yu, 2015)
Nsl1	CAUGAGCUCUUUCUGUUUA	ORF	Sigma Aldrich	(Kim & Yu, 2015)
CenpC (1)	GCACUCUUUCAGGUAGAAAGUCAA	ORF	Invitrogen	This paper
CenpC (2)	AACAUCUGGAAAUUUCAUCAUGACC	ORF	Invitrogen	This paper
CenpT (1)	AUCUCAAGAGCCUUCCUCUCCAUGG	ORF	Invitrogen	This paper
CenpT (2)	AACAGAGGCUGAGACUGUCAGUGUU	ORF	Invitrogen	This paper
CenpI (1)	GGUACAAGGUGAAUAAUUA	ORF	Sigma Aldrich	Sequence provided by the Stuckenberg lab
CenpI (2)	CAGCAAGACUUAUCAAGAA	ORF	Sigma Aldrich	Sequence provided by the Stuckenberg lab
CenpI (3)	GCUGGUAUUUGGACUAUUU	ORF	Sigma Aldrich	Sequence provided by the Stuckenberg lab
CenpI (4)	GUGAAGCAUUCCUGUAUAA	ORF	Sigma Aldrich	Sequence provided by the Stuckenberg lab
CenpH (1)	CGUUUGCCUGUUGAGUGGUAGCCUU	5' UTR	Sigma Aldrich	This paper
CenpH (2)	CAUUUCUGGCAAUCUCAACUCUUAU	3' UTR	Sigma Aldrich	This paper
CenpK (1)	CAAGAUCUUGAAAUGGUACUGUCCA	ORF	Sigma Aldrich	This paper
CenpK (2)	GGGAACAACGGUGGUUGGAUGAACA	ORF	Sigma Aldrich	This paper

2.9 Supplementary Figures

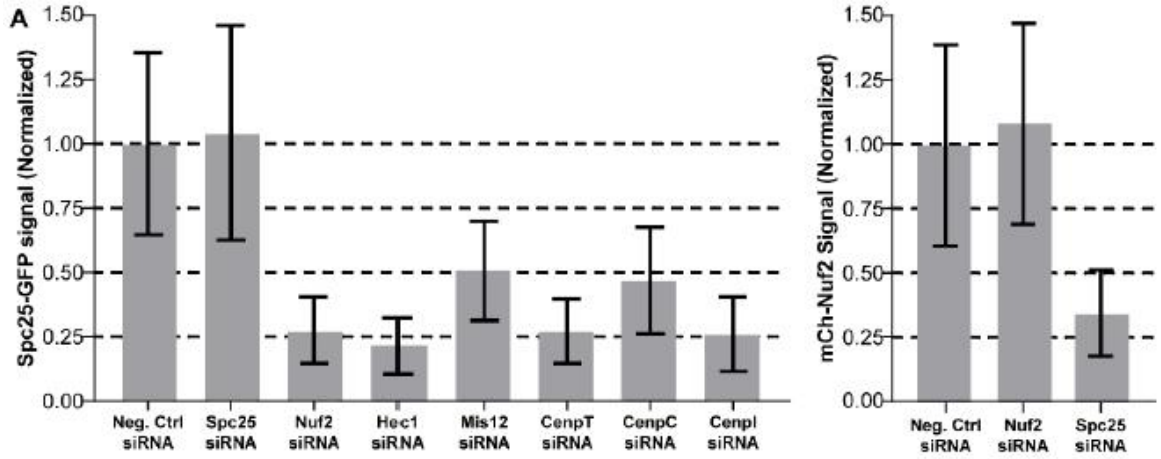

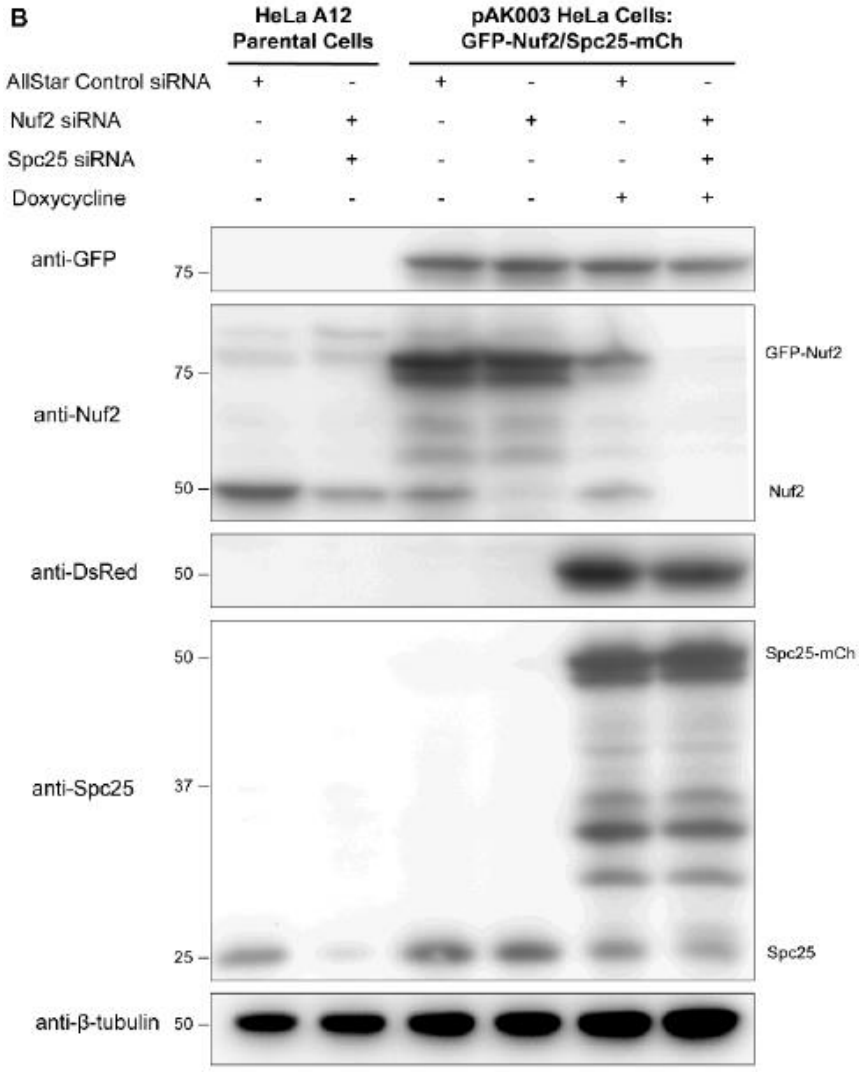

Supplementary Figure 2.1 Knockdown of Endogenous, Unlabeled Kinetochore Proteins via siRNA treatment, Related to Figure 2.1

(A) The recruitment of siRNA resistant Spc25-GFP (left) or mCherry-Nuf2 (right) to kinetochores was affected by siRNAs targeting the indicated subunits which are either directly or indirectly involved in Ndc80C recruitment. Bars are the average background subtracted fluorescence signal ± S.D. All measurements are normalized to negative control siRNA treated cells. (B) Assessment of the knock-in/knock-down strategy using Western blot analysis of HeLa A12 parental cells and of HeLa A12 cells stably transfected with the pAK003 plasmid (which confers cells with constitutive expression of siRNA resistant GFP-Nuf2 and doxycycline-inducible expression of siRNA resistant Spc25-mCherry). Treatments with negative control (AllStar siRNA), Spc25, or Nuf2 siRNAs as well as doxycycline induction are indicated. Cell lysates were probed with anti-GFP, anti-Nuf2, anti-DsRed (to detect mCherry), anti-Spc25, and anti-β-tubulin antibodies. Bands corresponding to fluorophore-labeled Nuf2 and Spc25 and to the endogenous, unlabeled versions are indicated. For unknown reasons, the anti-Nuf2 antibody detected only a faint GFP-Nuf2 band in the last lane of the blots. However, as evidenced by the blot with anti-GFP antibody (top), the level of GFP-Nuf2 is unaffected by the siRNA treatment.

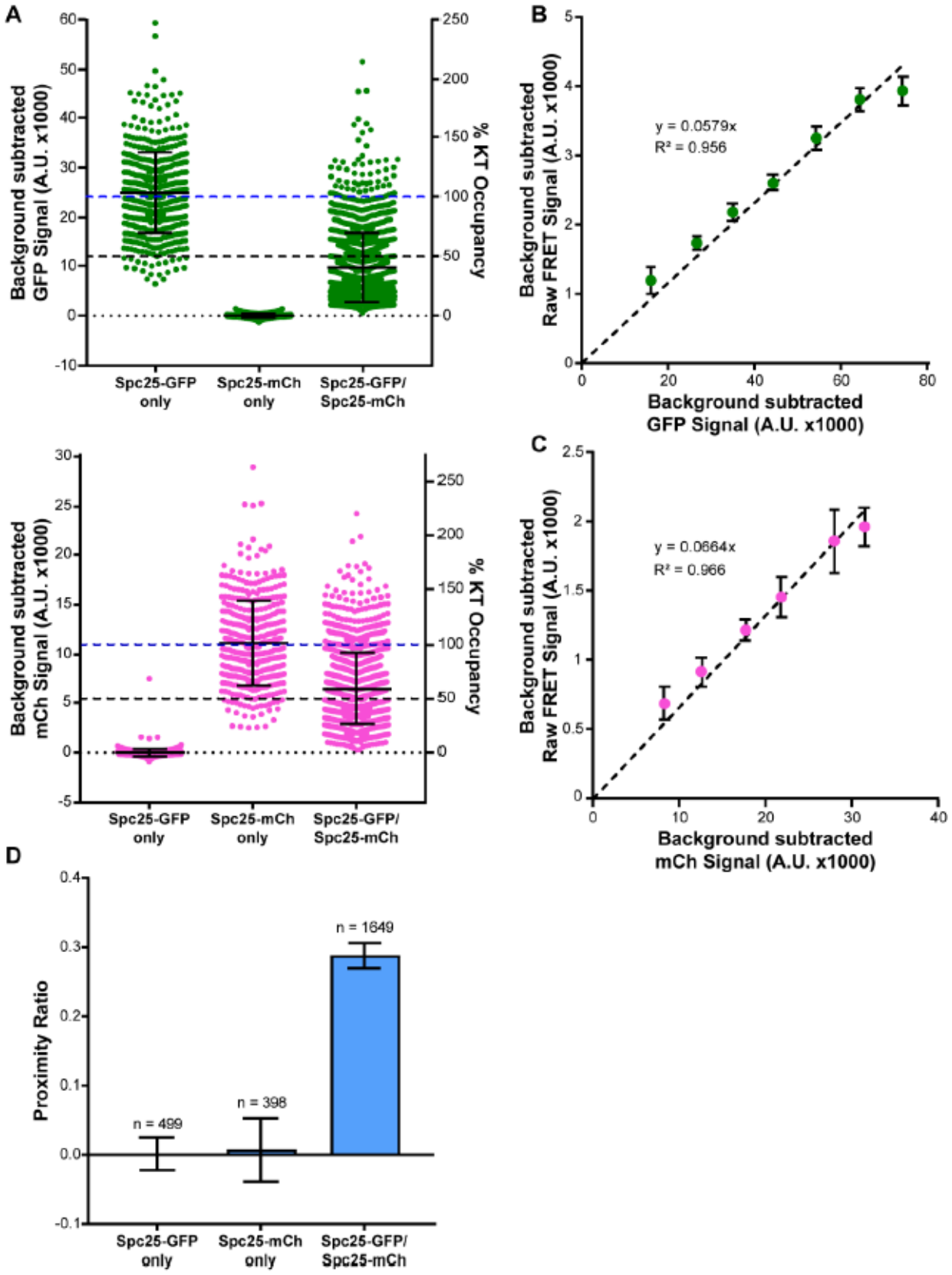
A
Background subtracted GFP Signal (A.U. x1000)
% KT Occupancy
Spc25-GFP only
Spc25-mCh only
Spc25-GFP/ Spc25-mCh
Background subtracted mCh Signal (A.U. x1000)
B
Background subtracted Raw FRET Signal (A.U. x1000)
y = 0.0579x
R² = 0.956
Background subtracted GFP Signal (A.U. x1000)
C
Background subtracted Raw FRET Signal (A.U. x1000)
y = 0.0664x
R² = 0.966
Background subtracted mCh Signal (A.U. x1000)
D
Proximity Ratio
n = 499
n = 398
n = 1649

Supplementary Figure 2.2 Calibrations for the Measurement of FRET in Live HeLa Cells, Related to Figure 2.1

(A) GFP and mCherry signals in HeLa cells expressing either Spc25-GFP, Spc25-mCherry, or co- expressing Spc25-GFP & Spc25-mCherry, after siRNA-mediated knockdown of the endogenous, unlabeled Spc25. Measurements are from unfiltered metaphase kinetochores. Data are average fluorescence signal ± S.D. Note that these average values are similar to the values predicted from the X- and Y- intercepts of main text Figure 2.1C. (B) Donor emission bleed-through was estimated from the slope of a linear regression fit to a plot of raw FRET signal versus GFP signal in HeLa cells expressing Spc25-GFP in isolation. Data are binned by the GFP signal. Error bars are ± S.E.M. (C) Similar to (B) but estimating acceptor cross-excitation from measurements in HeLa cells expressing Spc25-mCherry in isolation. (D) The donor bleed-through and acceptor cross-excitation ensure FRET is only measurable when the donor and acceptor fluorophores are co-expressed. Bars are the average proximity ratio at metaphase kinetochores ± S.E.M. The number of measurements is indicated above the bars. Measurements are from kinetochores before filtering for 100% occupancy.

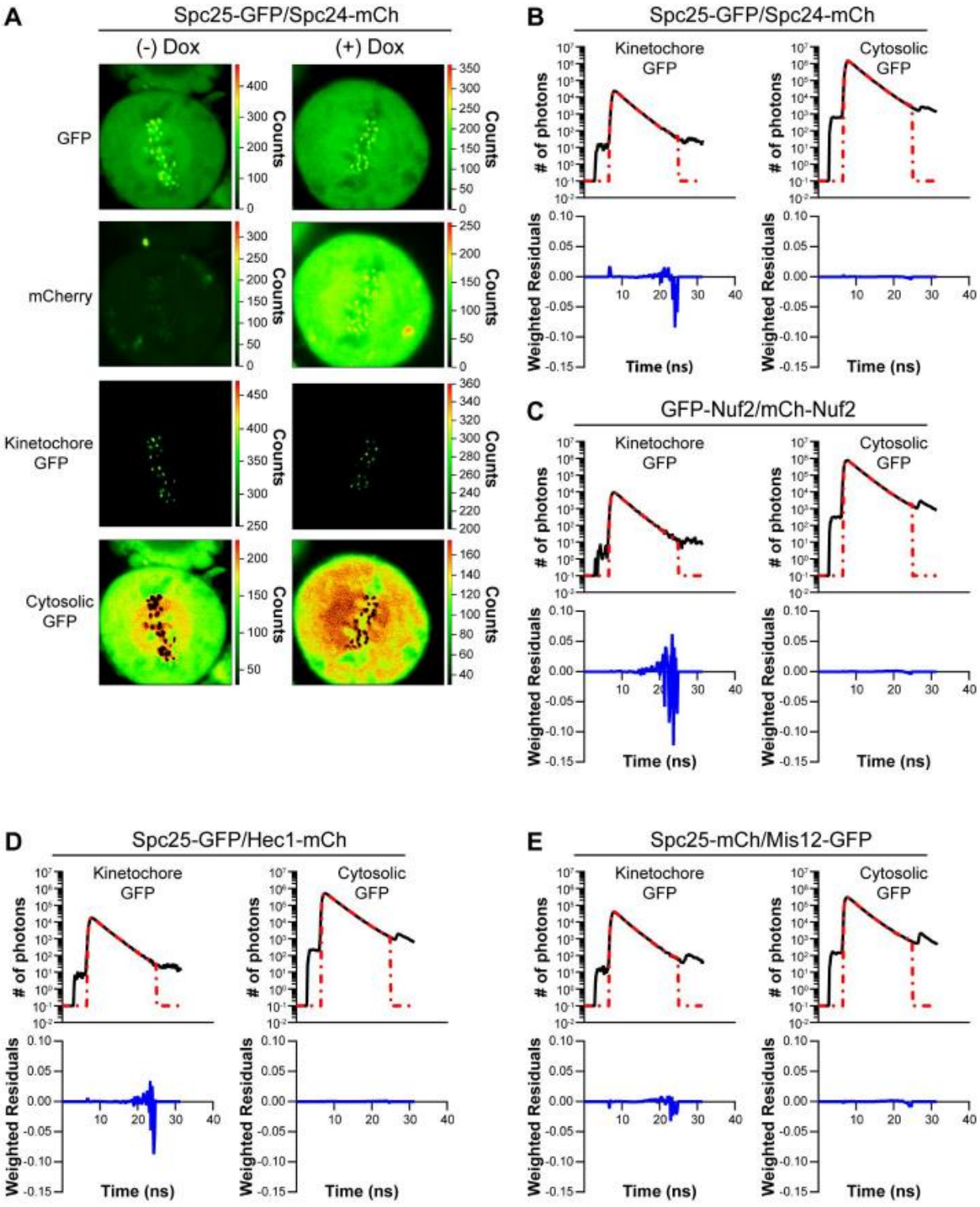

Supplementary Figure 2.3 FRET-induced Changes in Donor Lifetime Measured by FLIM Microscopy, Related to Figure 2.2

(A) Example confocal micrographs of Spc25-GFP/Spc24-mCherry HeLa cells for FLIM microscopy. Doxycycline (Dox) induces expression of the Spc24-mCherry protein. All images are scaled by the number of photons/pixel (scale to the right of images). Intensity thresholding was used to separate kinetochore-localized from cytosolic GFP pixels (bottom two rows). (B) – (E) Example photon arrival histograms for kinetochore-localized and cytosolic GFP

in HeLa cells co-expressing the indicated proteins. Histograms are fit with single component exponential decays (red dashed lines). Weighted residuals are below histograms.

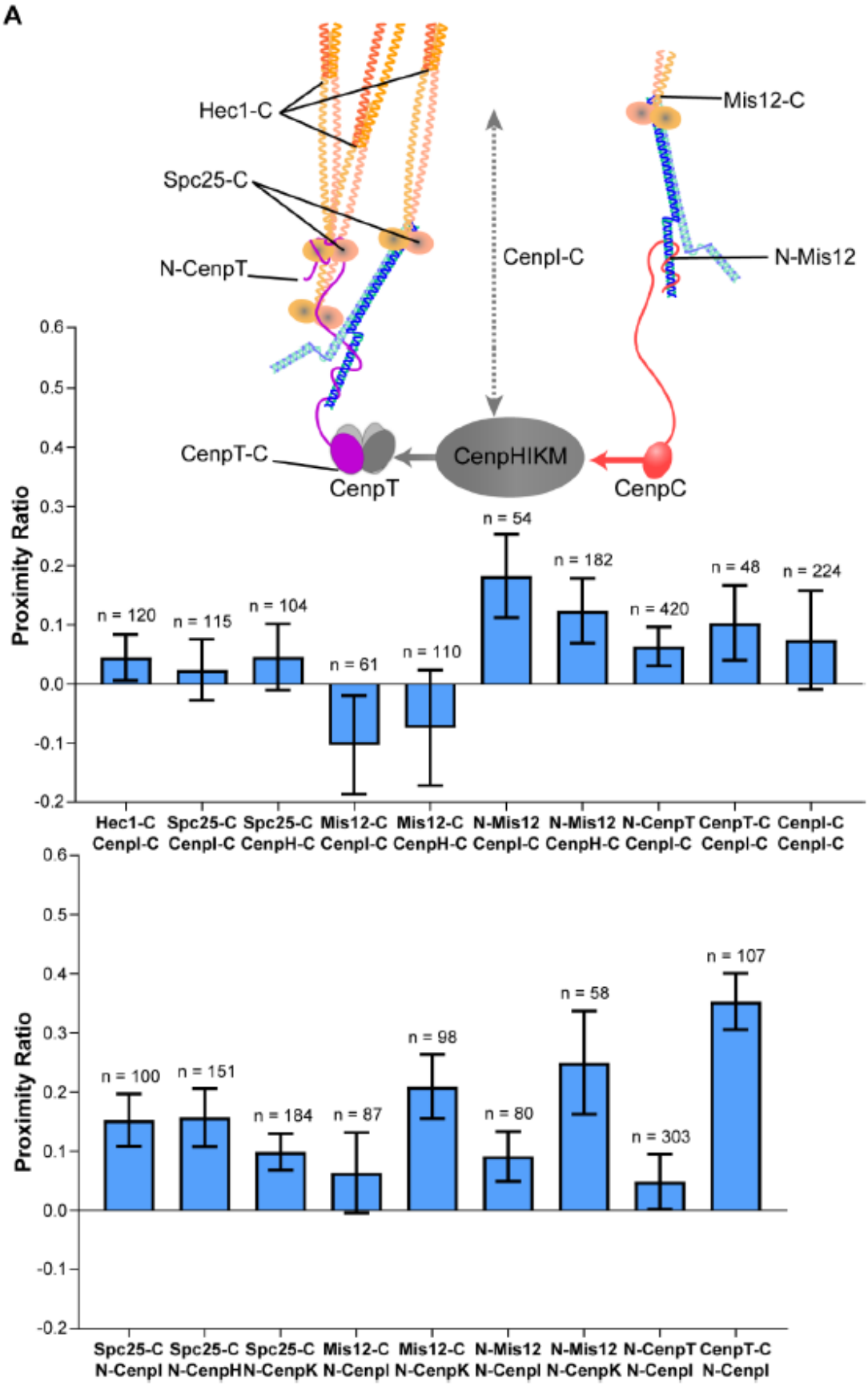
A
Hec1-C
Spc25-C
N-CenpT
CenpT-C
CenpT
CenpI-C
CenpHIKM
CenpC
Mis12-C
N-Mis12
Proximity Ratio
0.6
0.5
0.4
0.3
0.2
0.1
0.0
-0.1
-0.2
n = 120
n = 115
n = 104
n = 61
n = 110
n = 54
n = 182
n = 420
n = 48
n = 224
Hec1-C CenpI-C
Spc25-C CenpI-C
Spc25-C CenpH-C
Mis12-C CenpI-C
Mis12-C CenpH-C
N-Mis12 CenpI-C
N-Mis12 CenpH-C
N-CenpT CenpI-C
CenpT-C CenpI-C
CenpI-C CenpI-C
Proximity Ratio
n = 100
n = 151
n = 184
n = 87
n = 98
n = 80
n = 58
n = 303
n = 107
Spc25-C N-CenpI
Spc25-C N-CenpH
Spc25-C N-CenpK
Mis12-C N-CenpI
Mis12-C N-CenpK
N-Mis12 N-CenpI
N-Mis12 N-CenpK
N-CenpT N-CenpI
CenpT-C N-CenpI

Supplementary Figure 2.4 The N-termini, but not the C-termini, of Members of the CenpHIKM Complex Produce Low FRET with Ndc80C and Mis12C, Related to Figure 2.3

(A) Top: Diagram of the biochemical recruitment pathway for Ndc80C. The CenpHIKM bridges an interaction between CenpT and CenpC. Due to limited structural data, the location of the N- and C-termini for members of the CenpHIKM complex are unknown. Based on fluorescence co-localization data, the CenpI C-terminus is drawn as potentially extending toward the centromeric end of Ndc80C (gray, dashed arrow). Middle: FRET does not occur between the C-termini of either CenpI or CenpH and members of the outer kinetochore, CenpT, or between neighboring CenpI C-termini. Bottom: Weak FRET occurs between the N-termini of CenpI, CenpH, and CenpK and members of the outer kinetochore. Moderate to strong FRET is produced between the N-terminus of CenpI and the C-terminus of CenpT, consistent with the known biochemical interaction between these two complexes. Data are the average proximity ratio ± S.E.M of fully occupied, metaphase kinetochores. The number of measurements is indicated above each bar.

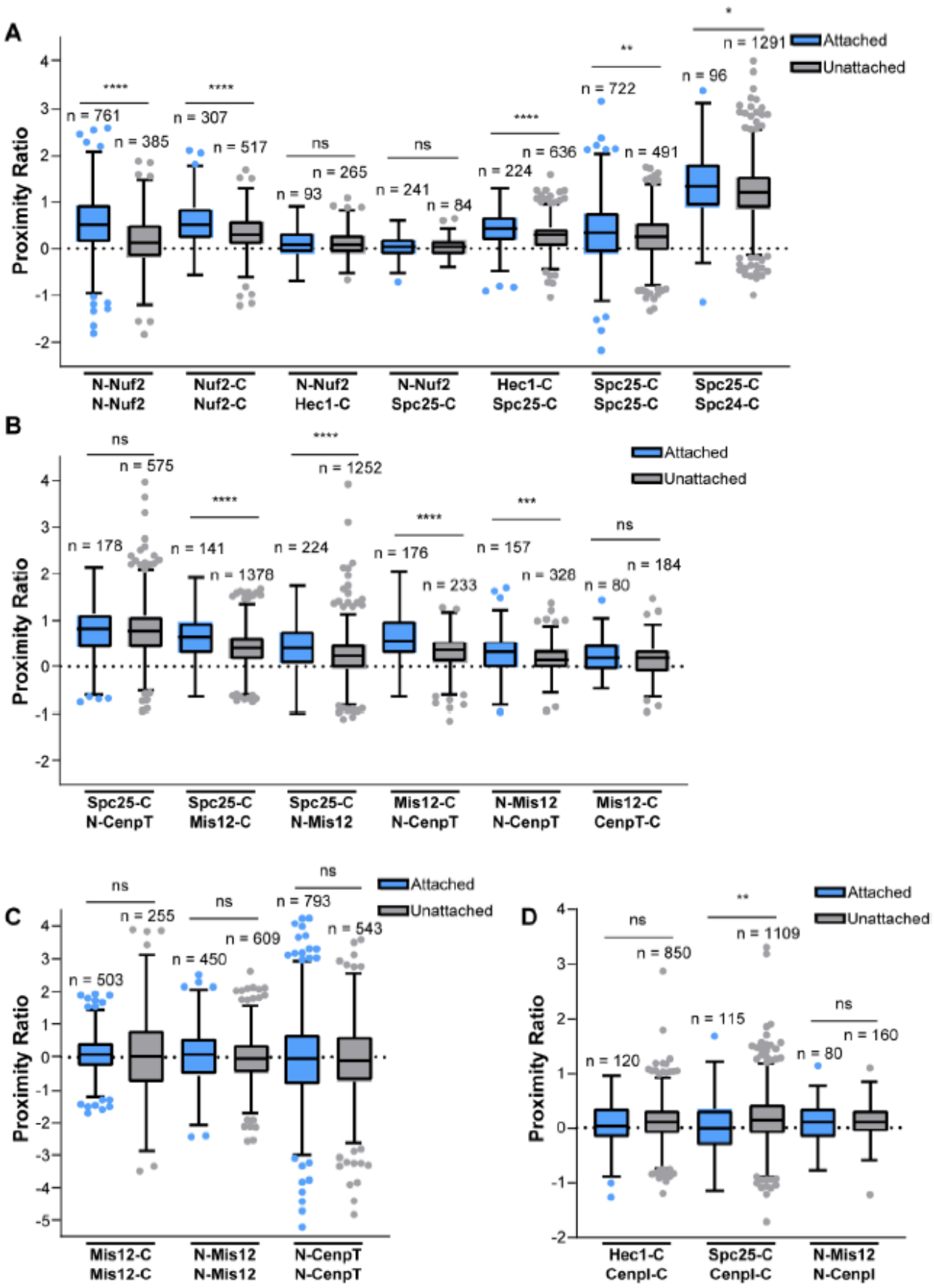
A
Proximity Ratio
Attached
Unattached
****
****
ns
ns
****
**
*
n = 761
n = 385
n = 307
n = 517
n = 93
n = 265
n = 241
n = 84
n = 224
n = 636
n = 722
n = 491
n = 96
n = 1291
N-Nuf2 N-Nuf2
Nuf2-C Nuf2-C
N-Nuf2 Hec1-C
N-Nuf2 Spc25-C
Hec1-C Spc25-C
Spc25-C Spc25-C
Spc25-C Spc24-C
B
Proximity Ratio
Attached
Unattached
ns
****
****
****
***
ns
n = 178
n = 575
n = 141
n = 1378
n = 224
n = 1252
n = 176
n = 233
n = 157
n = 328
n = 80
n = 184
Spc25-C N-CenpT
Spc25-C Mis12-C
Spc25-C N-Mis12
Mis12-C N-CenpT
N-Mis12 N-CenpT
Mis12-C CenpT-C
C
Proximity Ratio
Attached
Unattached
ns
ns
ns
n = 503
n = 255
n = 450
n = 609
n = 793
n = 543
Mis12-C Mis12-C
N-Mis12 N-Mis12
N-CenpT N-CenpT
D
Proximity Ratio
Attached
Unattached
ns
**
ns
n = 120
n = 850
n = 115
n = 1109
n = 80
n = 160
Hec1-C CenpI-C
Spc25-C CenpI-C
N-Mis12 N-CenpI

Supplementary Figure 2.5 Additional FRET Measurements of HeLa Cells Treated with Nocodazole, Related to Figure 2.4

(A) – (D) Tukey plots of the proximity ratio for the indicated FRET pairs. Light blue boxes are measurements from metaphase aligned kinetochores and gray boxes are measurements from nocodazole-treated, unaligned kinetochores. The number of measurements from fully occupied kinetochores is displayed above the boxes for members of Ndc80C (A), proteins involved in Ndc80C recruitment (B), members of Mis12C (C), and between the outer kinetochore and CenpI (D). Statistical significance was evaluated by a Mann Whitney test, ns = not significant; * = $p<0.05$; ** = $p<0.01$; *** = $p<0.001$; **** = $p<0.0001$.

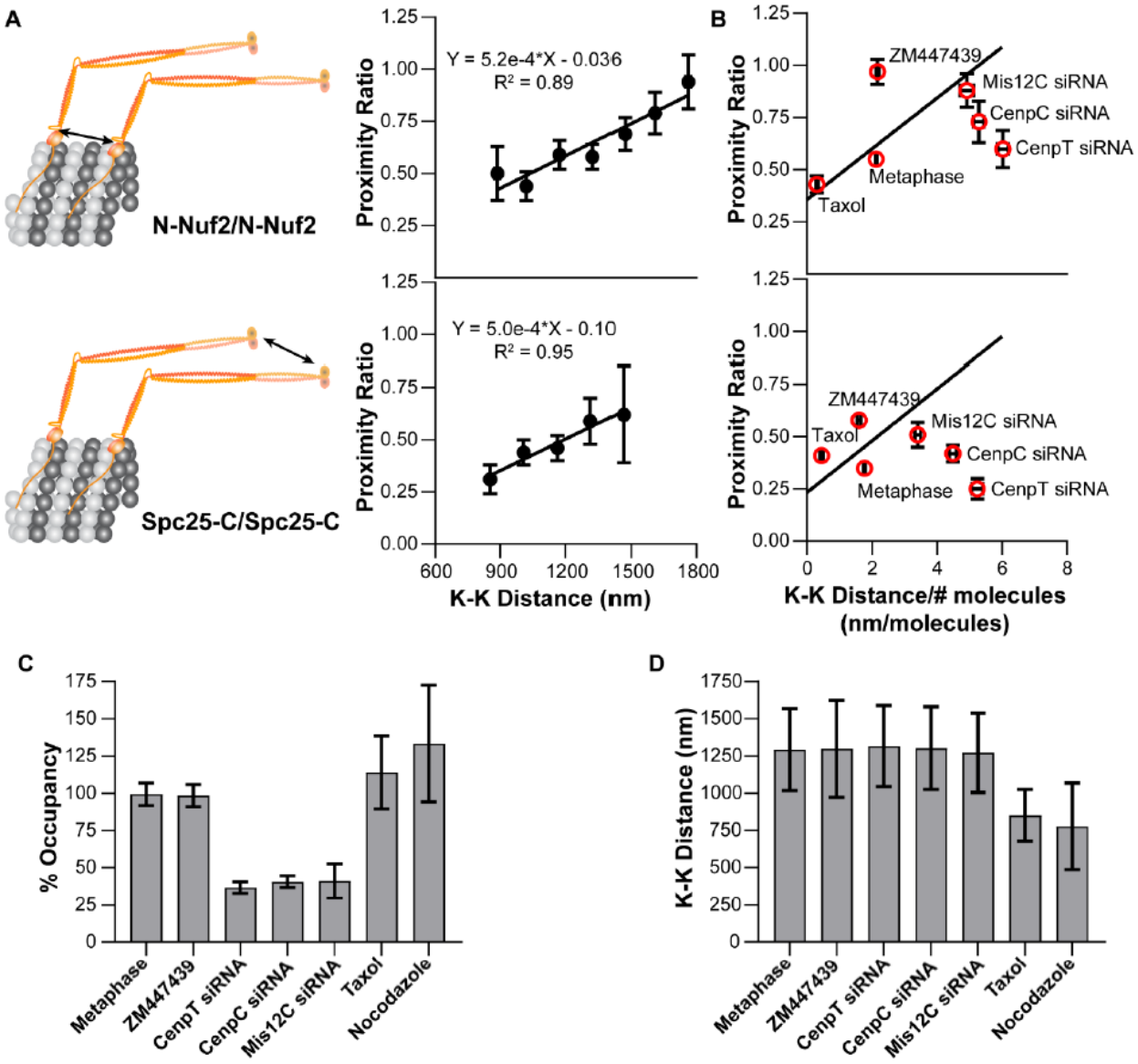

Supplementary Figure 2.6 The Relationship Between the Proximity Ratio and the Centromeric Tension per Molecule for Ndc80C with Various Drug and siRNA Treatments, Related to

(A) Cartoons for N-Nuf2/N-Nuf2 and Spc25-C/Spc25-C inter-complex FRET (left) and plots of the corresponding metaphase proximity ratios versus K-K distance (right, same as plots in Figure 2.5A). (B) The linear regressions in (A) were re-scaled by dividing the sister kinetochore distance by the average number of molecules in a metaphase kinetochore. Plotted alongside the regressions are the average proximity ratios for kinetochores after various treatments, including: untreated metaphase, Taxol-treated, Aurora B kinase inhibition (ZM447439), CenpT siRNA, CenpC siRNA, and Mis12C siRNA treated kinetochores. (C) The % occupancy and (D) the average sister kinetochore separation distance (both relative to untreated metaphase kinetochores) is plotted for N-Nuf2/N-Nuf2 expressing HeLa cells after the indicated drug or siRNA treatments. Error bars in (A) and (B) are ± S.E.M. Error bars in (C) and (D) are ± S.D.

2.10 References

Alushin, G. M., Musinipally, V., Matson, D., Tooley, J., Stukenberg, P. T., & Nogales, E. (2012). Multimodal microtubule binding by the Ndc80 kinetochore complex. *Nat Struct Mol Biol, 19*(11), 1161-1167. doi:10.1038/nsmb.2411

Alushin, G. M., Ramey, V. H., Pasqualato, S., Ball, D. A., Grigorieff, N., Musacchio, A., & Nogales, E. (2010). The Ndc80 kinetochore complex forms oligomeric arrays along microtubules. *Nature, 467*(7317), 805-810. doi:10.1038/nature09423

Aravamudhan, P., Felzer-Kim, I., Gurunathan, K., & Joglekar, A. P. (2014). Assembling the protein architecture of the budding yeast kinetochore-microtubule attachment using FRET. *Curr Biol, 24*(13), 1437-1446. doi:10.1016/j.cub.2014.05.014

Aravamudhan, P., Goldfarb, A. A., & Joglekar, A. P. (2015). The kinetochore encodes a mechanical switch to disrupt spindle assembly checkpoint signalling. *Nat Cell Biol, 17*(7), 868-879. doi:10.1038/ncb3179

Basilico, F., Maffini, S., Weir, J. R., Prumbaum, D., Rojas, A. M., Zimniak, T., . . . Musacchio, A. (2014). The pseudo GTPase CENP-M drives human kinetochore assembly. *Elife, 3*, e02978. doi:10.7554/eLife.02978

Becker, W. (2012). Fluorescence lifetime imaging--techniques and applications. *J Microsc, 247*(2), 119-136. doi:10.1111/j.1365-2818.2012.03618.x

Bock, L. J., Pagliuca, C., Kobayashi, N., Grove, R. A., Oku, Y., Shrestha, K., . . . De Wulf, P. (2012). Cnn1 inhibits the interactions between the KMN complexes of the yeast kinetochore. *Nat Cell Biol, 14*(6), 614-624. doi:10.1038/ncb2495

Bodor, D. L., Mata, J. F., Sergeev, M., David, A. F., Salimian, K. J., Panchenko, T., . . . Jansen, L. E. (2014). The quantitative architecture of centromeric chromatin. *Elife, 3*, e02137. doi:10.7554/eLife.02137

Cheeseman, I. M., Chappie, J. S., Wilson-Kubalek, E. M., & Desai, A. (2006). The conserved KMN network constitutes the core microtubule-binding site of the kinetochore. *Cell, 127*(5), 983-997. doi:10.1016/j.cell.2006.09.039

Cherry, L. M., Faulkner, A. J., Grossberg, L. A., & Balczon, R. (1989). Kinetochore size variation in mammalian chromosomes: an image analysis study with evolutionary implications. *J Cell Sci, 92 (Pt 2)*, 281-289. Retrieved from https://www.ncbi.nlm.nih.gov/pubmed/2674167

Cherry, L. M., & Johnston, D. A. (1987). Size variation in kinetochores of human chromosomes. *Hum Genet, 75*(2), 155-158. doi:10.1007/bf00591078

Ciferri, C., Pasqualato, S., Screpanti, E., Varetti, G., Santaguida, S., Dos Reis, G., . . . Musacchio, A. (2008). Implications for kinetochore-microtubule attachment from the

structure of an engineered Ndc80 complex. *Cell, 133*(3), 427-439. doi:10.1016/j.cell.2008.03.020

DeLuca, J. G., Gall, W. E., Ciferri, C., Cimini, D., Musacchio, A., & Salmon, E. D. (2006). Kinetochore microtubule dynamics and attachment stability are regulated by Hec1. *Cell, 127*(5), 969-982. doi:10.1016/j.cell.2006.09.047

Dhatchinamoorthy, K., Shivaraju, M., Lange, J. J., Rubinstein, B., Unruh, J. R., Slaughter, B. D., & Gerton, J. L. (2017). Structural plasticity of the living kinetochore. *J Cell Biol, 216*(11), 3551-3570. doi:10.1083/jcb.201703152

Dimitrova, Y. N., Jenni, S., Valverde, R., Khin, Y., & Harrison, S. C. (2016). Structure of the MIND Complex Defines a Regulatory Focus for Yeast Kinetochore Assembly. *Cell, 167*(4), 1014-1027 e1012. doi:10.1016/j.cell.2016.10.011

Dong, Y., Vanden Beldt, K. J., Meng, X., Khodjakov, A., & McEwen, B. F. (2007). The outer plate in vertebrate kinetochores is a flexible network with multiple microtubule interactions. *Nat Cell Biol, 9*(5), 516-522. doi:10.1038/ncb1576

Drpic, D., Almeida, A. C., Aguiar, P., Renda, F., Damas, J., Lewin, H. A., . . . Maiato, H. (2018). Chromosome Segregation Is Biased by Kinetochore Size. *Curr Biol, 28*(9), 1344-1356 e1345. doi:10.1016/j.cub.2018.03.023

Dumont, M., Gamba, R., Gestraud, P., Klaasen, S., Worrall, J. T., De Vries, S. G., . . . Fachinetti, D. (2020). Human chromosome-specific aneuploidy is influenced by DNA-dependent centromeric features. *EMBO J, 39*(2), e102924. doi:10.15252/embj.2019102924

Fanara, P., Turner, S., Busch, R., Killion, S., Awada, M., Turner, H., . . . Hellerstein, M. K. (2004). In vivo measurement of microtubule dynamics using stable isotope labeling with heavy water. Effect of taxanes. *J Biol Chem, 279*(48), 49940-49947. doi:10.1074/jbc.M409660200

Gascoigne, K. E., Takeuchi, K., Suzuki, A., Hori, T., Fukagawa, T., & Cheeseman, I. M. (2011). Induced ectopic kinetochore assembly bypasses the requirement for CENP-A nucleosomes. *Cell, 145*(3), 410-422. doi:10.1016/j.cell.2011.03.031

Helgeson, L. A., Zelter, A., Riffle, M., MacCoss, M. J., Asbury, C. L., & Davis, T. N. (2018). Human Ska complex and Ndc80 complex interact to form a load-bearing assembly that strengthens kinetochore-microtubule attachments. *Proc Natl Acad Sci U S A, 115*(11), 2740-2745. doi:10.1073/pnas.1718553115

Hill, T. L. (1985). Theoretical problems related to the attachment of microtubules to kinetochores. *Proc Natl Acad Sci U S A, 82*(13), 4404-4408. doi:10.1073/pnas.82.13.4404

Hinshaw, S. M., & Harrison, S. C. (2018). Kinetochore Function from the Bottom Up. *Trends Cell Biol, 28*(1), 22-33. doi:10.1016/j.tcb.2017.09.002

Hornung, P., Troc, P., Malvezzi, F., Maier, M., Demianova, Z., Zimniak, T., . . . Westermann, S. (2014). A cooperative mechanism drives budding yeast kinetochore assembly downstream of CENP-A. *J Cell Biol, 206*(4), 509-524. doi:10.1083/jcb.201403081

Huis In 't Veld, P. J., Jeganathan, S., Petrovic, A., Singh, P., John, J., Krenn, V., . . . Musacchio, A. (2016). Molecular basis of outer kinetochore assembly on CENP-T. *Elife, 5*. doi:10.7554/eLife.21007

Janczyk, P. L., Skorupka, K. A., Tooley, J. G., Matson, D. R., Kestner, C. A., West, T., . . . Stukenberg, P. T. (2017). Mechanism of Ska Recruitment by Ndc80 Complexes to Kinetochores. *Dev Cell, 41*(4), 438-449 e434. doi:10.1016/j.devcel.2017.04.020

Joglekar, A., Chen, R., & Lawrimore, J. (2013). A Sensitized Emission Based Calibration of FRET Efficiency for Probing the Architecture of Macromolecular Machines. *Cell Mol Bioeng, 6*(4), 369-382. doi:10.1007/s12195-013-0290-y

Joglekar, A. P., & Kukreja, A. A. (2017). How Kinetochore Architecture Shapes the Mechanisms of Its Function. *Curr Biol, 27*(16), R816-R824. doi:10.1016/j.cub.2017.06.012

Khandelia, P., Yap, K., & Makeyev, E. V. (2011). Streamlined platform for short hairpin RNA interference and transgenesis in cultured mammalian cells. *Proc Natl Acad Sci U S A, 108*(31), 12799-12804. doi:10.1073/pnas.1103532108

Kim, S., & Yu, H. (2015). Multiple assembly mechanisms anchor the KMN spindle checkpoint platform at human mitotic kinetochores. *J Cell Biol, 208*(2), 181-196. doi:10.1083/jcb.201407074

Klare, K., Weir, J. R., Basilico, F., Zimniak, T., Massimiliano, L., Ludwigs, N., . . . Musacchio, A. (2015). CENP-C is a blueprint for constitutive centromere-associated network assembly within human kinetochores. *J Cell Biol, 210*(1), 11-22. doi:10.1083/jcb.201412028

Kumar, N. (1981). Taxol-induced polymerization of purified tubulin. Mechanism of action. *J Biol Chem, 256*(20), 10435-10441. Retrieved from https://www.ncbi.nlm.nih.gov/pubmed/6116707

Logsdon, G. A., Barrey, E. J., Bassett, E. A., DeNizio, J. E., Guo, L. Y., Panchenko, T., . . . Black, B. E. (2015). Both tails and the centromere targeting domain of CENP-A are required for centromere establishment. *J Cell Biol, 208*(5), 521-531. doi:10.1083/jcb.201412011

Long, A. F., Udy, D. B., & Dumont, S. (2017). Hec1 Tail Phosphorylation Differentially Regulates Mammalian Kinetochore Coupling to Polymerizing and Depolymerizing Microtubules. *Curr Biol, 27*(11), 1692-1699 e1693. doi:10.1016/j.cub.2017.04.058

Magidson, V., He, J., Ault, J. G., O'Connell, C. B., Yang, N., Tikhonenko, I., . . . Khodjakov, A. (2016). Unattached kinetochores rather than intrakinetochore tension arrest mitosis in taxol-treated cells. *J Cell Biol, 212*(3), 307-319. doi:10.1083/jcb.201412139

Magidson, V., Paul, R., Yang, N., Ault, J. G., O'Connell, C. B., Tikhonenko, I., . . . Khodjakov, A. (2015). Adaptive changes in the kinetochore architecture facilitate proper spindle assembly. *Nat Cell Biol, 17*(9), 1134-1144. doi:10.1038/ncb3223

Malvezzi, F., Litos, G., Schleiffer, A., Heuck, A., Mechtler, K., Clausen, T., & Westermann, S. (2013). A structural basis for kinetochore recruitment of the Ndc80 complex via two distinct centromere receptors. *EMBO J, 32*(3), 409-423. doi:10.1038/emboj.2012.356

Manning, A. L., Bakhoum, S. F., Maffini, S., Correia-Melo, C., Maiato, H., & Compton, D. A. (2010). CLASP1, astrin and Kif2b form a molecular switch that regulates kinetochore-microtubule dynamics to promote mitotic progression and fidelity. *EMBO J, 29*(20), 3531-3543. doi:10.1038/emboj.2010.230

Mattiuzzo, M., Vargiu, G., Totta, P., Fiore, M., Ciferri, C., Musacchio, A., & Degrassi, F. (2011). Abnormal kinetochore-generated pulling forces from expressing a N-terminally modified Hec1. *PLoS One, 6*(1), e16307. doi:10.1371/journal.pone.0016307

McEwen, B. F., Ding, Y., & Heagle, A. B. (1998). Relevance of kinetochore size and microtubule-binding capacity for stable chromosome attachment during mitosis in PtK1 cells. *Chromosome Res, 6*(2), 123-132. Retrieved from https://www.ncbi.nlm.nih.gov/pubmed/9543015

McEwen, B. F., Heagle, A. B., Cassels, G. O., Buttle, K. F., & Rieder, C. L. (1997). Kinetochore fiber maturation in PtK1 cells and its implications for the mechanisms of chromosome congression and anaphase onset. *J Cell Biol, 137*(7), 1567-1580. doi:10.1083/jcb.137.7.1567

McIntosh, J. R. (1991). Structural and mechanical control of mitotic progression. *Cold Spring Harb Symp Quant Biol, 56*, 613-619. doi:10.1101/sqb.1991.056.01.070

McIntosh, J. R., O'Toole, E., Zhudenkov, K., Morphew, M., Schwartz, C., Ataullakhanov, F. I., & Grishchuk, E. L. (2013). Conserved and divergent features of kinetochores and spindle microtubule ends from five species. *J Cell Biol, 200*(4), 459-474. doi:10.1083/jcb.201209154

McKinley, K. L., Sekulic, N., Guo, L. Y., Tsinman, T., Black, B. E., & Cheeseman, I. M. (2015). The CENP-L-N Complex Forms a Critical Node in an Integrated Meshwork of

Interactions at the Centromere-Kinetochore Interface. *Mol Cell, 60*(6), 886-898. doi:10.1016/j.molcel.2015.10.027

Muller, E. G., Snydsman, B. E., Novik, I., Hailey, D. W., Gestaut, D. R., Niemann, C. A., . . . Davis, T. N. (2005). The organization of the core proteins of the yeast spindle pole body. *Mol Biol Cell, 16*(7), 3341-3352. doi:10.1091/mbc.e05-03-0214

Musacchio, A., & Desai, A. (2017). A Molecular View of Kinetochore Assembly and Function. *Biology (Basel), 6*(1). doi:10.3390/biology6010005

Ng, C. T., Deng, L., Chen, C., Lim, H. H., Shi, J., Surana, U., & Gan, L. (2019). Electron cryotomography analysis of Dam1C/DASH at the kinetochore-spindle interface in situ. *J Cell Biol, 218*(2), 455-473. doi:10.1083/jcb.201809088

Nishino, T., Rago, F., Hori, T., Tomii, K., Cheeseman, I. M., & Fukagawa, T. (2013). CENP-T provides a structural platform for outer kinetochore assembly. *EMBO J, 32*(3), 424-436. doi:10.1038/emboj.2012.348

Pesenti, M. E., Prumbaum, D., Auckland, P., Smith, C. M., Faesen, A. C., Petrovic, A., . . . Musacchio, A. (2018). Reconstitution of a 26-Subunit Human Kinetochore Reveals Cooperative Microtubule Binding by CENP-OPQUR and NDC80. *Mol Cell, 71*(6), 923-939 e910. doi:10.1016/j.molcel.2018.07.038

Petrovic, A., Keller, J., Liu, Y., Overlack, K., John, J., Dimitrova, Y. N., . . . Musacchio, A. (2016). Structure of the MIS12 Complex and Molecular Basis of Its Interaction with CENP-C at Human Kinetochores. *Cell, 167*(4), 1028-1040 e1015. doi:10.1016/j.cell.2016.10.005

Rago, F., Gascoigne, K. E., & Cheeseman, I. M. (2015). Distinct organization and regulation of the outer kinetochore KMN network downstream of CENP-C and CENP-T. *Curr Biol, 25*(5), 671-677. doi:10.1016/j.cub.2015.01.059

Redli, P. M., Gasic, I., Meraldi, P., Nigg, E. A., & Santamaria, A. (2016). The Ska complex promotes Aurora B activity to ensure chromosome biorientation. *J Cell Biol, 215*(1), 77-93. doi:10.1083/jcb.201603019

Roscioli, E., Germanova, T. E., Smith, C. A., Embacher, P. A., Erent, M., Thompson, A. I., . . . McAinsh, A. D. (2020). Ensemble-Level Organization of Human Kinetochores and Evidence for Distinct Tension and Attachment Sensors. *Cell Rep, 31*(4), 107535. doi:10.1016/j.celrep.2020.107535

Schleiffer, A., Maier, M., Litos, G., Lampert, F., Hornung, P., Mechtler, K., & Westermann, S. (2012). CENP-T proteins are conserved centromere receptors of the Ndc80 complex. *Nat Cell Biol, 14*(6), 604-613. doi:10.1038/ncb2493

Schmidt, J. C., Kiyomitsu, T., Hori, T., Backer, C. B., Fukagawa, T., & Cheeseman, I. M. (2010). Aurora B kinase controls the targeting of the Astrin-SKAP complex to bioriented kinetochores. *J Cell Biol, 191*(2), 269-280. doi:10.1083/jcb.201006129

Screpanti, E., De Antoni, A., Alushin, G. M., Petrovic, A., Melis, T., Nogales, E., & Musacchio, A. (2011). Direct binding of Cenp-C to the Mis12 complex joins the inner and outer kinetochore. *Curr Biol, 21*(5), 391-398. doi:10.1016/j.cub.2010.12.039

Smith, C. A., McAinsh, A. D., & Burroughs, N. J. (2016). Human kinetochores are swivel joints that mediate microtubule attachments. *Elife, 5*. doi:10.7554/eLife.16159

Suzuki, A., Badger, B. L., & Salmon, E. D. (2015). A quantitative description of Ndc80 complex linkage to human kinetochores. *Nat Commun, 6*, 8161. doi:10.1038/ncomms9161

Suzuki, A., Badger, B. L., Wan, X., DeLuca, J. G., & Salmon, E. D. (2014). The architecture of CCAN proteins creates a structural integrity to resist spindle forces and achieve proper Intrakinetochore stretch. *Dev Cell, 30*(6), 717-730. doi:10.1016/j.devcel.2014.08.003

Suzuki, A., Long, S. K., & Salmon, E. D. (2018). An optimized method for 3D fluorescence co-localization applied to human kinetochore protein architecture. *Elife, 7*. doi:10.7554/eLife.32418

Volkov, V. A., Huis In 't Veld, P. J., Dogterom, M., & Musacchio, A. (2018). Multivalency of NDC80 in the outer kinetochore is essential to track shortening microtubules and generate forces. *Elife, 7*. doi:10.7554/eLife.36764

Wan, X., O'Quinn, R. P., Pierce, H. L., Joglekar, A. P., Gall, W. E., DeLuca, J. G., . . . Salmon, E. D. (2009). Protein architecture of the human kinetochore microtubule attachment site. *Cell, 137*(4), 672-684. doi:10.1016/j.cell.2009.03.035

Wang, H. W., Long, S., Ciferri, C., Westermann, S., Drubin, D., Barnes, G., & Nogales, E. (2008). Architecture and flexibility of the yeast Ndc80 kinetochore complex. *J Mol Biol, 383*(4), 894-903. doi:10.1016/j.jmb.2008.08.077

Wei, R. R., Sorger, P. K., & Harrison, S. C. (2005). Molecular organization of the Ndc80 complex, an essential kinetochore component. *Proc Natl Acad Sci U S A, 102*(15), 5363-5367. doi:10.1073/pnas.0501168102

Weir, J. R., Faesen, A. C., Klare, K., Petrovic, A., Basilico, F., Fischbock, J., . . . Musacchio, A. (2016). Insights from biochemical reconstitution into the architecture of human kinetochores. *Nature, 537*(7619), 249-253. doi:10.1038/nature19333

Wendell, K. L., Wilson, L., & Jordan, M. A. (1993). Mitotic block in HeLa cells by vinblastine: ultrastructural changes in kinetochore-microtubule attachment and in centrosomes. *J Cell Sci, 104 (Pt 2)*, 261-274. Retrieved from https://www.ncbi.nlm.nih.gov/pubmed/8505360

Wynne, D. J., & Funabiki, H. (2015). Kinetochore function is controlled by a phospho-dependent coexpansion of inner and outer components. *J Cell Biol, 210*(6), 899-916. doi:10.1083/jcb.201506020

Wynne, D. J., & Funabiki, H. (2016). Heterogeneous architecture of vertebrate kinetochores revealed by three-dimensional superresolution fluorescence microscopy. *Mol Biol Cell, 27*(22), 3395-3404. doi:10.1091/mbc.E16-02-0130

Yoo, T. Y., Choi, J. M., Conway, W., Yu, C. H., Pappu, R. V., & Needleman, D. J. (2018). Measuring NDC80 binding reveals the molecular basis of tension-dependent kinetochore-microtubule attachments. *Elife, 7*. doi:10.7554/eLife.36392

Zaytsev, A. V., Mick, J. E., Maslennikov, E., Nikashin, B., DeLuca, J. G., & Grishchuk, E. L. (2015). Multisite phosphorylation of the NDC80 complex gradually tunes its microtubule-binding affinity. *Mol Biol Cell, 26*(10), 1829-1844. doi:10.1091/mbc.E14-11-1539

Zaytsev, A. V., Sundin, L. J., DeLuca, K. F., Grishchuk, E. L., & DeLuca, J. G. (2014). Accurate phosphoregulation of kinetochore-microtubule affinity requires unconstrained molecular interactions. *J Cell Biol, 206*(1), 45-59. doi:10.1083/jcb.201312107

Zhai, Y., Kronebusch, P. J., & Borisy, G. G. (1995). Kinetochore microtubule dynamics and the metaphase-anaphase transition. *J Cell Biol, 131*(3), 721-734. doi:10.1083/jcb.131.3.721

CHAPTER 3:

Stress Testing the Number of Ndc80 Complexes for Proper Spindle Assembly Checkpoint Silencing and Biorientation in Human Kinetochores

3.1 Abstract

The human kinetochore binds up to ~24 spindle microtubules to silence the spindle assembly checkpoint and segregate chromosomes. The Ndc80 complex plays crucial roles in both these functions. Interestingly, although the human kinetochore contains ~250 Ndc80 complexes, the number of microtubule-bound Ndc80 molecules fluctuates during mitosis. This raises the question: What is the minimum number of Ndc80 required for proper chromosome segregation? We address this question by titrating HeLa kinetochores with defective mutants of the Ndc80 complex. We find that the spindle assembly checkpoint is constitutively activated when kinetochores contain ≥40% of microtubule-binding defective Ndc80 mutants and silenced when occupied by ≥60% of a high microtubule-affinity mutant. Additionally, chromosome biorientation fails when kinetochores incorporate ≥20% of a high microtubule-affinity Ndc80 mutant. These observations suggest that the human kinetochore is built with an excess of Ndc80 and allow us to delineate the limits on this number for accurate chromosome segregation.

3.2 Introduction

To achieve accurate chromosome segregation, the kinetochore executes three principle functions: (1) spindle assembly checkpoint (SAC) signaling, which delays anaphase onset in the presence of unattached kinetochores (Foley & Kapoor, 2013; Sacristan & Kops, 2015); (2) error correction, which specifically detects and destabilizes non-productive attachments (Lampson & Grishchuk, 2017; Sarangapani & Asbury, 2014); and (3) force generation, which harnesses the energy of microtubule depolymerization to physically move chromosomes (Hill, 1985). Mechanistically, all three of these functions intersect at the microtubule-binding Ndc80 complex (Ndc80C), a central component of the core kinetochore scaffold (Ciferri et al., 2008; J. G. DeLuca et al., 2006; Joglekar & Kukreja, 2017). For example, SAC signaling is dictated by the competition between the Mps1 kinase, which activates the SAC via phosphorylation of kinetochore-localized targets, and microtubules for binding to Ndc80C (Hiruma et al., 2015; Ji, Gao, & Yu, 2015). During error correction, the Aurora B kinase weakens microtubule attachments via phosphorylation of Ndc80C (Chan, Jeyaprakash, Nigg, & Santamaria, 2012; Cimini, Wan, Hirel, & Salmon, 2006; Lampson & Cheeseman, 2011; Liu, Vader, Vromans, Lampson, & Lens, 2009; Schmidt et al., 2010; Welburn et al., 2010). Lastly, as a microtubule-binding protein, Ndc80C is essential to the process of force generation, participating in the formation and maintenance of microtubule plus end attachments (Cheeseman, Chappie, Wilson-Kubalek, & Desai, 2006; J. G. DeLuca et al., 2005; J. G. DeLuca et al., 2006; Joglekar & Kukreja, 2017; Volkov, Huis In 't Veld, Dogterom, & Musacchio, 2018; Wei, Al-Bassam, & Harrison, 2007).

The human kinetochore incorporates ~250 copies of Ndc80C to bind ~17 microtubules, suggesting that there are 14-15 Ndc80C molecules per microtubule attachment (Suzuki, Badger, & Salmon, 2015; Wendell, Wilson, & Jordan, 1993). However, evidence suggests that only a

fraction of the total Ndc80C at kinetochores actively participates in microtubule-binding, and that this bound fraction fluctuates in a manner that correlates with centromeric tension (Kukreja, Kavuri, & Joglekar, 2020; Yoo et al., 2018). Additionally, kinetochore microtubules turn-over and change polymerization states (Kabeche & Compton, 2013; McEwen, Ding, & Heagle, 1998; McEwen, Heagle, Cassels, Buttle, & Rieder, 1997; Zaytsev & Grishchuk, 2015), suggesting that the kinetochore must constantly regulate its attachments to maintain its connection with the spindle. It is unclear how the kinetochore orchestrates the dynamics of Ndc80C and microtubule binding, or how these dynamics affect the fidelity of chromosome segregation. Biochemical and structural characterization of many of the molecular players that regulate kinetochore-microtubule attachments have provided partial answers to these questions. However, to fully understand the binding dynamics of the kinetochore, the nanoscale architecture of its proteins must be considered (Joglekar & Kukreja, 2017). For example, the human kinetochore is built on a large centromeric DNA foundation (a ~200 nm diameter disk-like surface). Multiple centromere-specific nucleosomes (i.e., the CenpA nucleosome) bind this large surface, each one recruiting up to eight Ndc80C molecules through long, flexible protein linkers (Dong, Vanden Beldt, Meng, Khodjakov, & McEwen, 2007; Suzuki, Badger, Wan, DeLuca, & Salmon, 2014; Wendell et al., 1993). From this perspective, two alternative models emerge concerning the kinetochore's operation. In the repeat-subunit model, each centromeric subunit forms a discrete, independent binding site isolated from its neighbors. In the 'lawn model', the centromeric subunits operate like a lawn of long flexible linkers, allowing for coordination between the subunits in the binding of microtubules (Kukreja et al., 2020; Zaytsev, Sundin, DeLuca, Grishchuk, & DeLuca, 2014). While the true nature of the kinetochore remains elusive, each

model offers different conceptual frameworks for understanding the dynamics of Ndc80C and microtubule binding.

A handful of recent studies have begun to address how the binding dynamics of the human kinetochore affect its functions by focusing on the number of microtubule attachments. For instance, SAC signaling was found to remain active at individual kinetochores until they reach at least ~30% of their microtubule-binding capacity, suggesting a switch-like response of the SAC to a specific number of attachments (Etemad et al., 2019; Kuhn & Dumont, 2017, 2019). In another study, artificially lowering the number of microtubule attachments by ~1/3 resulted in only a modest effect on the accuracy of chromosome segregation (Dudka et al., 2018). This latter observation coincides with studies demonstrating that a single microtubule can transmit ~10-30 pN of force, whereas the force needed to move anaphase chromosomes is only ~0.1 pN (Helgeson et al., 2018; Huis In 't Veld, Volkov, Stender, Musacchio, & Dogterom, 2019; McIntosh, 2017; Nicklas, 1965; Volkov et al., 2013). Thus, the human kinetochore binds more microtubules than is necessary for many of its functions, calling into question why it has evolved such a high microtubule-binding capacity.

Equally important and less understood is how many Ndc80C molecules are necessary for kinetochore function. For example, how many Ndc80C molecules must bind the microtubule lattice to effectively silence the SAC? Will 30% of Ndc80C molecules suffice, like was observed for the number of microtubule attachments, or does this previous result reveal that 30% of microtubules are binding nearly 100% of Ndc80C molecules? Similarly, does the persistence of force generation and chromosome alignment under sub-saturating numbers of microtubule attachments reveal that only a subset of Ndc80C molecules is necessary for these kinetochore functions? Or do they reveal that these functions persist because a lower number of microtubules

is stabilized by a higher fraction of bound Ndc80C? To address these questions, we have adapted a method to challenge human kinetochores with microtubule binding mutants of Ndc80C to discover failure points in kinetochore function. Specifically, we titrate kinetochores with variants of the Ndc80C subunit, Hec1, which carry mutations in either of its two microtubule binding domains: the N-terminal, phospho-regulatable tail and the globular, non-regulatable calponin homology (CH) domain. These 'stress tests' reveal that human kinetochores can tolerate up to 40% of a non-binding Hec1 mutant before constitutively activating the SAC. Remarkably, this 40% threshold holds true for Hec1 mutants that possess either a weakened N-terminal tail or a weakened CH domain. We also find that Hec1 mutants engineered with high microtubule affinity tail domains cause failures in chromosome biorientation and segregation at as low as 20% kinetochore occupancy. When the strongest of these mutants reaches ≥60% occupancy, the cells exit mitosis more quickly than untreated cells, albeit with severe levels of chromosome missegregation. Thus, these cells have reached a threshold beyond which they cannot successfully implement SAC signaling or error correction. Finally, we titrate kinetochores with a chimeric Hec1 mutant that incorporates both a strong binding N-terminal tail and a weakened CH domain, finding that the Hec1 CH domain ultimately dictates the behavior of Ndc80C. These and other results demonstrate that robust kinetochore function relies on an excess of affinity-tunable Ndc80C molecules.

3.3 Results & Discussion

3.3.1 Quantitative Titration of Human Kinetochores with Variants of Ndc80C

To measure the effect of varying numbers of Ndc80C molecules on human kinetochore function, we developed an assay to titrate kinetochores with C-terminal GFP-tagged variants of Hec1, a subunit of Ndc80C (Figure 3.1A; Materials & Methods). As a first step, we engineered human cells to constitutively express the chromosome marker H2B-pHTomato and conditionally express Hec1-GFP from a doxycycline-inducible promoter. Upon induction, Hec1-GFP competes with endogenous, unlabeled Hec1 for kinetochore binding, resulting in kinetochores with varying levels of GFP fluorescence. Since the human kinetochore incorporates a discrete amount of Ndc80C, we calculate the percent occupancy of Hec1-GFP by comparison to a calibration cell line where kinetochores are fully-occupied by GFP-labeled Ndc80C (Figure 3.1B; Materials & Methods) (Kukreja et al., 2020; Suzuki et al., 2015).

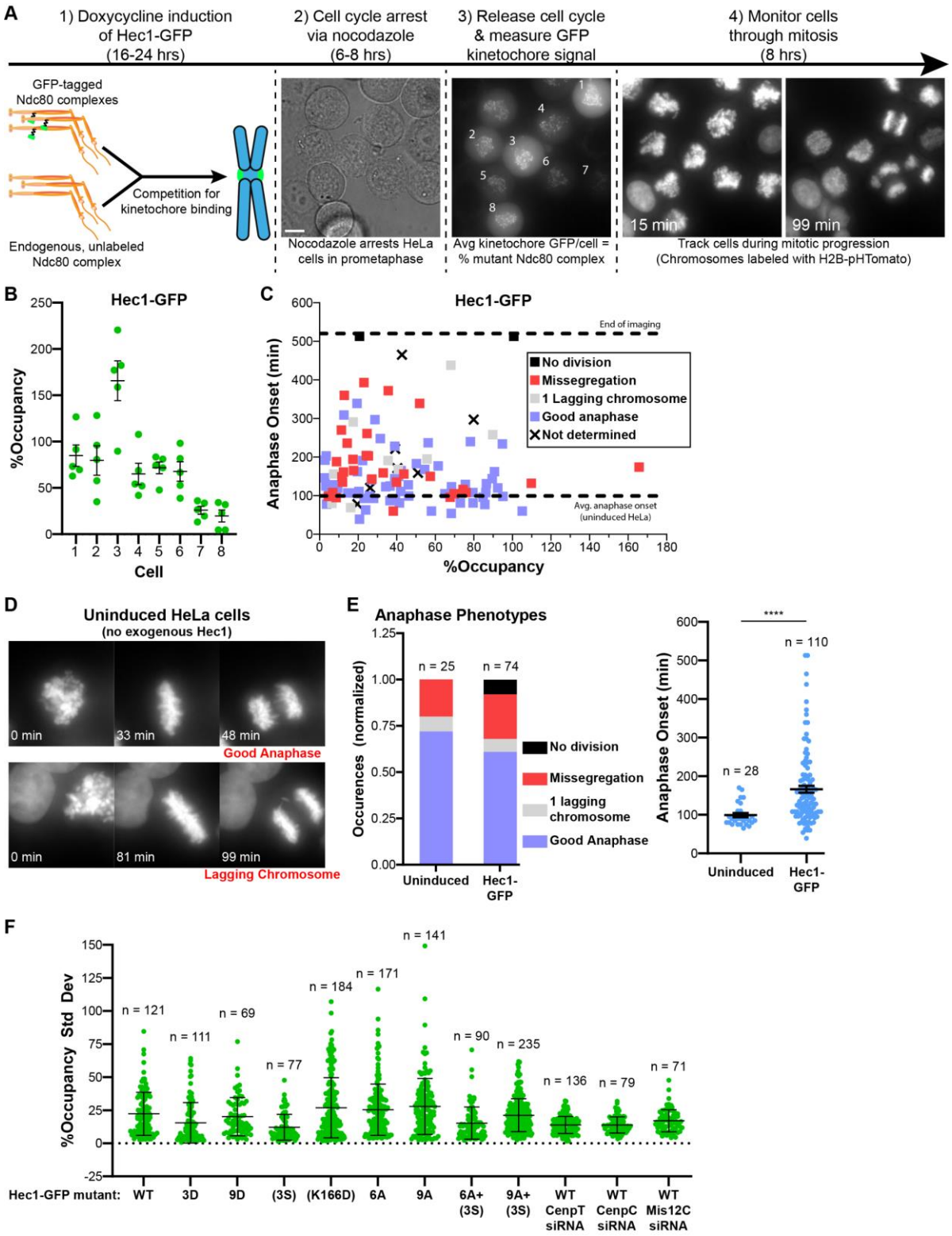

Figure 3.1 Titrating HeLa Kinetochores with Fluorophore-Tagged Ndc80C has Mild Effects on Anaphase Timing and Outcomes

(A) Outline of the methodology used in this study. A GFP-tagged version of the Ndc80 subunit, Hec1, is exogenously expressed in HeLa cells in the presence of endogenous, unlabeled Hec1. As the proteins compete for

kinetochore-binding, cells are synchronized in mitosis via nocodazole treatment. Upon nocodazole release, the level of Hec1-GFP at mitotic kinetochores is measured and chromosomes labeled with H2B-pHTomato are tracked for 8 hours as cells progress to anaphase. The trans-illuminated image (left), GFP image (middle) and pHTomato images (right most two images) are from cells expressing wildtype Hec1-GFP. The numbers in the GFP image correspond to panel B. For the pHTomato images, the time after nocodazole release is indicated. Scale bar indicates 10 μm. (B) The average % occupancy of wildtype Hec1-GFP (see Materials & Methods) at kinetochores in the cells indicated in panel A. For each cell, five kinetochores were measured. (C) Anaphase onset time versus the % occupancy of wildtype Hec1-GFP for nocodazole synchronized mitotic cells. The dashed lines indicate the maximum time for which cells were imaged (>8 hours) and the average anaphase onset time for cells expressing no transgenes (uninduced HeLa). Each data point corresponds to a single cell and is color-coded according to its segregation phenotype (legend on the right of the graph; see Materials & Methods). (D) Representative images of HeLa cells expressing no exogenous Hec1 protein. Chromosomes are labeled with H2B-pHTomato. The time after nocodazole release and anaphase phenotypes are indicated. Images are ~30x30 μm. (E) Anaphase phenotypes (left) and the average anaphase onset time (right) for uninduced and wildtype Hec1-GFP expressing cells after release from nocodazole. For the anaphase phenotypes of Hec1-GFP cells, only cells containing ≥20% of the exogenous protein at kinetochores are included. The number of cells analyzed in each graph is indicated. (F) The average standard deviation of % occupancy for individual cells expressing the indicated Hec1-GFP mutants. The number of measurements for each mutant is indicated. The error bars in (B) and (E) are SEM and in (F) they are SD. Statistical significance was evaluated using the Mann-Whitney test, ****$p<0.0001$.

Before measuring the percent occupancy of Hec1 at kinetochores, we synchronize cells at prometaphase via nocodazole treatment (Figure 3.1A, step 2). Upon nocodazole wash-out, we measure the Hec1-GFP fluorescence at kinetochores and track the corresponding chromosomes as cells proceed through mitosis. We take note of two specific features of these mitotic cells: 1) the elapsed time before they enter anaphase, and 2) the segregation behavior of their chromosomes (Figure 3.1C).

In our experiments, we express mutant variants of Hec1 which are defective in microtubule-binding, causing severe disruptions in normal cell and kinetochore function. Previous studies have noted that fluorophore-tagging of Hec1, particularly at its N-terminus, also causes defects in mitosis and chromosome segregation (Mattiuzzo et al., 2011). Therefore, we assessed the effect of wildtype Hec1-GFP expression on mitotic HeLa cells, using uninduced cells as a comparison (Figure 3.1D). Missegregation occurred in 28% of uninduced HeLa cells, compared to 31% in in cells expressing Hec1-GFP (Figure 3.1E, left; note that the general category of ‘Missegregation’ includes all missegregation events other than ‘1 lagging

chromosome' which is quantified separately). Additionally, 6 out of 74 Hec1-GFP expressing cells failed to divide by the end of imaging. We also noted that the average anaphase onset of uninduced HeLa cells increased significantly upon Hec1-GFP expression (99 ± 5.4 vs 166 ± 9.2 min (± SEM), respectively; Figure 3.1E, right). Thus, the expression of C-terminally tagged Hec1 causes minor defects on the cell cycle, consistent with previous studies (Diaz-Rodriguez, Sotillo, Schvartzman, & Benezra, 2008; Mattiuzzo et al., 2011).

As a final note, we highlight that we extrapolate the percent occupancy of relatively few kinetochores for the general occupancy of all kinetochores within a given cell. While the competition between labeled and unlabeled Hec1 yields kinetochores with varying levels of the Hec1-GFP, we find that the variation between kinetochores within a single cell is, on average, ~20% (Figure 3.1B and F). Thus, the percent occupancies we measure for various Hec1 mutants provide a gross analysis of the resulting mitotic behaviors of cells.

3.3.2 The SAC is Constitutively Activated in Kinetochores with ≥40% Non-Binding Ndc80C

The microtubule-binding activity of Ndc80C is encoded by three separate protein domains. Two of these are globular calponin homology (CH) domains, one from the Hec1 subunit and the other from the Nuf2 subunit. The other domain is an 80 amino acid disordered, basic tail at the N-terminus of Hec1 (Figure 3.2A) (Ciferri et al., 2005; Ciferri et al., 2008; Wei et al., 2007). The Hec1 tail provides electrostatic interactions with the microtubule lattice (Miller, Johnson, & Stukenberg, 2008; Tooley, Miller, & Stukenberg, 2011) and has proposed roles in recruiting additional microtubule-binding proteins and in cooperative Ndc80C binding (Alushin et al., 2012; Alushin et al., 2010; Wimbish et al., 2020). The tail is regulated by the Aurora B kinase via nine phospho-sites, allowing the kinetochore to fine-tune these activities (Cheeseman et al., 2002; J. G. DeLuca et al., 2006; K. F. DeLuca, Lens, & DeLuca, 2011;

Guimaraes, Dong, McEwen, & Deluca, 2008; Malik et al., 2009; Nousiainen, Sillje, Sauer, Nigg, & Korner, 2006; Wimbish & DeLuca, 2020; Zaytsev et al., 2015; Zaytsev et al., 2014). The globular Hec1 CH domain also provides a largely electrostatic interaction with the microtubule, but its affinity is not subject to any known regulation (Alushin et al., 2010; Tooley et al., 2011). However, the Mps1 kinase localizes to unattached kinetochores via its interaction with the Hec1 CH domain, making it crucial to proper SAC signaling (Guimaraes et al., 2008; Hiruma et al., 2015; Ji et al., 2015; Zhu et al., 2013).

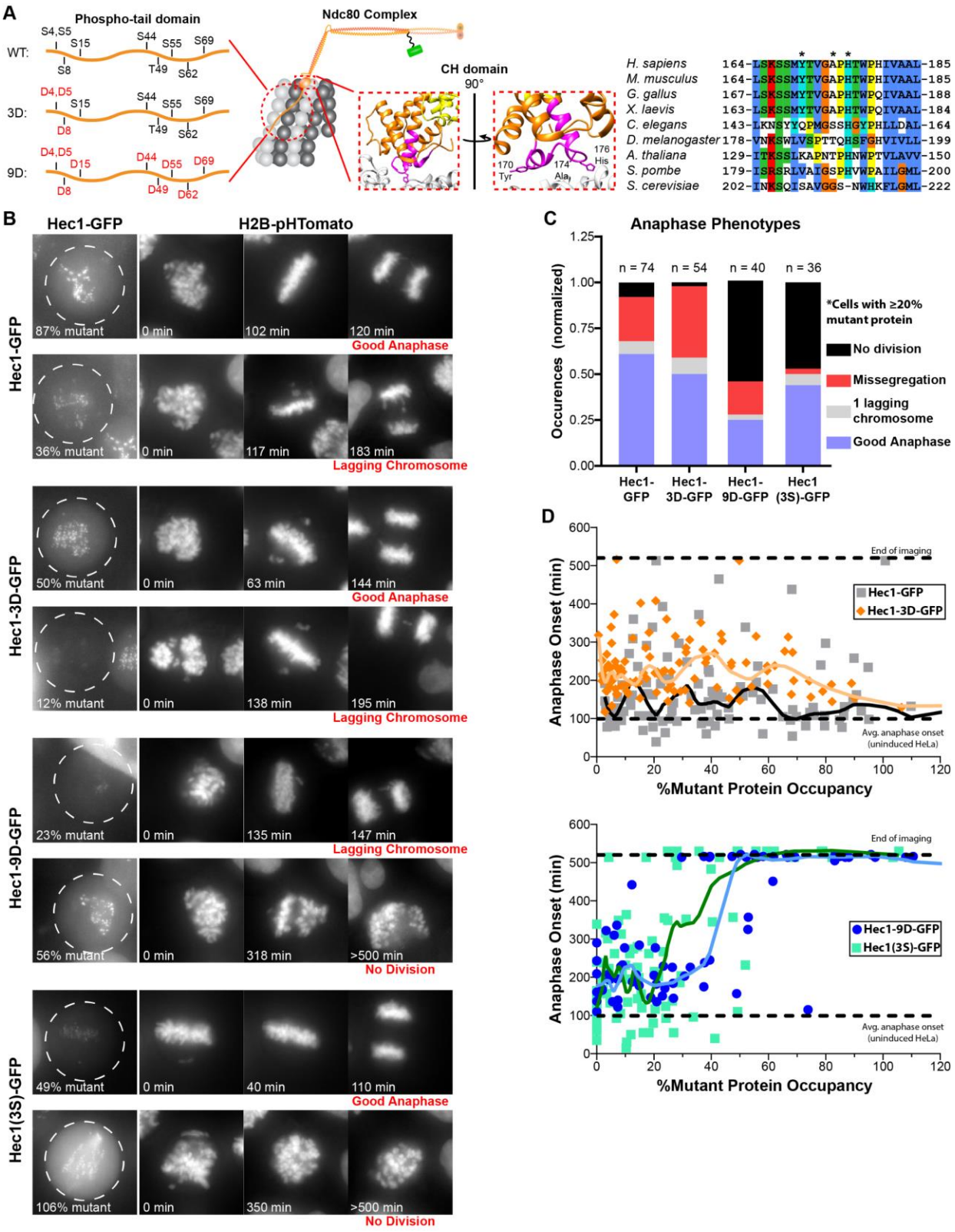

Figure 3.2 The Spindle Assembly Checkpoint is Constitutively Activated in Kinetochores with ≥40% Non-Binding Ndc80C Mutants

(A) Cartoon representation of Ndc80C highlighting two of three important domains related to its microtubule-binding activity: the N-terminal basic, disordered phospho-tail and the calponin homology (CH) domain of Hec1. Aurora B kinase phosphorylation sites within Hec1's tail domain as well as sites mutated to aspartic acids for the 3D and 9D mutants are shown (left). The crystal structure of the Hec1 CH domain (PDB: 3IZ0; middle) is shown with a rotated, enlarged view focusing on its interface with the microtubule (Hec1 in orange, alpha-tubulin in white, Nuf2 in yellow). Amino acids spanning L164—L185 are highlighted in magenta, and protein alignment for this region was performed with various eukaryotic sequences (right). Amino acids are colored according to the ClustalW color scheme. Residues mutated to serine in the Hec1-(3S) mutant are indicated with asterisks. (B) Representative images of mitotic HeLa cells expressing Hec1-GFP mutant proteins as they progress through anaphase. GFP images show the % occupancy of exogenous Hec1 at kinetochores. The H2B-pHTomato images show the corresponding chromosomes from these cells at different times after nocodazole release. The resulting anaphase phenotype is indicated below the final frame for each time series. Images are ~30x30 μm. (C) Anaphase phenotypes for mitotic cells expressing the indicated Hec1-GFP mutants after release from nocodazole. Only cells containing ≥20% of the mutant protein at kinetochores are included. The number of cells analyzed is indicated above the bars. (D) Anaphase onset time versus the % occupancy of wildtype Hec1-GFP (gray squares) and Hec1-3D-GFP (orange diamonds; top graph) and the % occupancy for Hec1-9D-GFP (blue circles) and Hec1(3S)-GFP (teal squares; bottom graph). All cells were synchronized in mitosis via nocodazole. The dashed lines indicate the maximum time for which cells were imaged (>8 hours) and the average anaphase onset time for cells expressing no transgenes (uninduced HeLa). Each data point corresponds to a single cell. The lines over the data points correspond to Loess smoothing of the data (Hec1-GFP = black line; Hec1-3D-GFP = light orange line; Hec1-9D-GFP = light blue line; Hec1(3S)-GFP = dark green line). Hec1-3D-GFP causes a slight increase in anaphase onset compared to wildtype Hec1-GFP, whereas the Hec1-9D-GFP and Hec1(3S)-GFP variants constitutively activate the SAC at around 40% occupancy. Note that two cells have been excluded from the Hec1-9D-GFP dataset, two from the Hec1-GFP dataset, and one from the Hec1-3D-GFP dataset.

To test the importance of the human kinetochore's ~250 Ndc80C molecules to chromosome segregation and SAC signaling, we titrated the kinetochore with low microtubule affinity mutants of Hec1. Two of these mutants consisted of phospho-mimicking amino acid substitutions that exchange Aurora B phospho-residues within the Hec1 tail (Hec1-3D and Hec1-9D; Figure 3.2A, left). In rescue experiments, where wildtype Hec1 is completely replaced by mutant protein, the Hec1-3D mutant has a relatively mild effect on chromosome segregation (Zaytsev et al., 2015; Zaytsev et al., 2014). Unsurprisingly, titrating Hec1-3D into human kinetochores only minorly perturbed mitotic cells, leading to a slight elevation in the rate of missegregation (31% vs 48% for Hec1-GFP and Hec1-3D-GFP, respectively) and a small, yet significant, increase in the average time to anaphase onset (166 ± 9 min. vs 229 ± 7 min. (± SEM); Figure 3.2B-D).

The Hec1-9D mutant, which has all its Aurora B phospho-sites mutated, has considerably weaker microtubule-binding affinity and a correspondingly stronger effect on disrupting kinetochore function (Guimaraes et al., 2008; Sundin, Guimaraes, & Deluca, 2011; Zaytsev et al., 2015; Zaytsev et al., 2014). We observed similar phenotypes as described previously for this mutant, with most cells failing to undergo cell division (Figure 3.2B & C). The lack of cell division indicates that many of the Hec1-9D cells are unable to silence the SAC, likely due to the large number of unattached kinetochores that result from such a low microtubule affinity mutant. Interestingly, human kinetochores tolerated moderate amounts of the Hec1-9D mutant before failing to complete cell division (Figure 3.2D, blue circles, bottom graph). As cells incorporated more Hec1-9D at kinetochores, a switch-like transition point was reached at ~40% mutant protein occupancy where cells failed to divide. Thus, the human kinetochore can tolerate up to 40% Ndc80C containing a weak-binding Hec1 tail.

In addition to the Hec1 tail mutants, we also engineered a variant of Hec1 with a weakened CH domain, replacing three non-polar (Y170 A174, and H176) residues with polar serine residues (termed 'Hec1(3S)'; Figure 3.2A, right). In designing this mutant, we were conscientious of the CH domain's dual-role in SAC signaling, choosing a helix-turn-helix region that contacts the microtubule lattice but is not predicted to interfere with the Mps1 interaction (Hiruma et al., 2015). As predicted, the Hec1(3S) mutant disrupted chromosome biorientation and resulted in many cells that fail to divide, similar to the Hec1-9D tail mutant (Figure 3.2B & C). Remarkably, the effects of the Hec1(3S) mutant were also titratable and produced a transition point at ~30-40% mutant protein occupancy beyond which cells failed to divide (Figure 3.2D, teal squares, bottom graph). The similarity of these results to the Hec1-9D mutant reinforce the

notion that the kinetochore can tolerate up to ~40% of a weak-binding variant of Ndc80C and also highlight the dual importance of Hec1's tail and CH domains.

Overall, these data imply that at least 40% of the Ndc80C at human kinetochores (~100 molecules) is dispensable for chromosome biorientation, segregation, and SAC function. Additionally, these data suggest that SAC activation does not occur if at least 60% of the available Ndc80C is capable of microtubule attachment. Given that kinetochores only need to bind 30% of their total microtubule capacity to shut-off SAC signaling, we propose that ~5-6 microtubules are bound by ~150 Ndc80C molecules to successfully silence the SAC (Etemad et al., 2019; Kuhn & Dumont, 2019; Suzuki et al., 2015). This stoichiometry suggests that as many as 25 Ndc80C molecules can participate in binding a single microtubule and therefore reflects key aspects of the 'lawn-like' model for kinetochore architecture (Kukreja et al., 2020; Zaytsev et al., 2014). The remaining ~100 unattached Ndc80C molecules either do not produce a strong enough SAC signal to prevent anaphase progression, or their SAC functions are silenced by some unknown mechanism. Regardless of how the kinetochore silences the SAC when almost 40% of its Ndc80C molecules are unbound, it is noteworthy that the transition to constitutive SAC activation is sharp (Etemad et al., 2019; Kuhn & Dumont, 2017, 2019). This suggests that the human kinetochore possesses a highly sensitive threshold to assess its attachment state.

3.3.3 Chromosome Biorientation Fails in Kinetochores with ≥20% High Affinity Ndc80C

The phospho-regulation of the Hec1 tail is an important mechanism to control the kinetochore's microtubule-binding affinity (Zaytsev et al., 2015; Zaytsev et al., 2014). The Aurora B kinase, which localizes between sister centromeres, provides fine control over the level of Hec1 phosphorylation in correlation with developing tension between sister kinetochores (Liu et al., 2009; Liu et al., 2010; Tanaka, 2005; Tanaka, Stark, & Tanaka, 2005; Welburn et al.,

2010; Zhu et al., 2013). As tension increases, the tail decreases in its phosphorylation level, allowing more Ndc80 molecules to engage with kinetochore-microtubules with greater affinity (Kukreja et al., 2020; Yoo et al., 2018). However, to adapt to changes in tension and allow for coordinated directional switches of oscillating, bioriented kinetochores, Aurora B must constantly adjust Ndc80C's microtubule-binding affinity via phosphorylation at metaphase aligned kinetochores (Burroughs, Harry, & McAinsh, 2015; K. F. DeLuca et al., 2011; Long, Udy, & Dumont, 2017; Nicklas & Koch, 1969; Nicklas, Ward, & Gorbsky, 1995; Roscioli et al., 2020). Additionally, Aurora B is crucial to error correction, whereby incorrect attachments are destabilized by virtue of their inability to develop tension between sister kinetochores (Cimini et al., 2006; Tanaka, 2010). To understand the importance of this regulation in the context of the ~250 Ndc80C molecules at the human kinetochore, we next performed a series of titration experiments using high microtubule affinity Hec1 mutants with reduced capacity for phosphorylation at its N-terminal tail.

For these experiments, we investigated the effect of two Hec1 tail mutants: Hec1-6A and Hec1-9A (Figure 3.3A). With six of its nine phospho-sites mutated to alanine residues, the Hec1-6A allows for reduced regulation of its microtubule-binding affinity. The Hec1-9A mutant, however, has no available regulation as all its sites are mutated. As noted in prior observations of these mutants, we observed high levels of unaligned chromosomes and missegregation, consistent with their strong microtubule-binding affinity (J. G. DeLuca et al., 2006; Sundin et al., 2011; Tooley et al., 2011; Zaytsev et al., 2014; Zhu et al., 2013) (Figure 3.3B). The majority of these missegregation events were in the form of tri- or multi-spindle separations, even for cells with as low as 20% occupancy of the Hec1-6A or Hec1-9A mutants (Figure 3.3A & B). Thus, the kinetochore has a low tolerance for strong microtubule-binding Hec1 mutants.

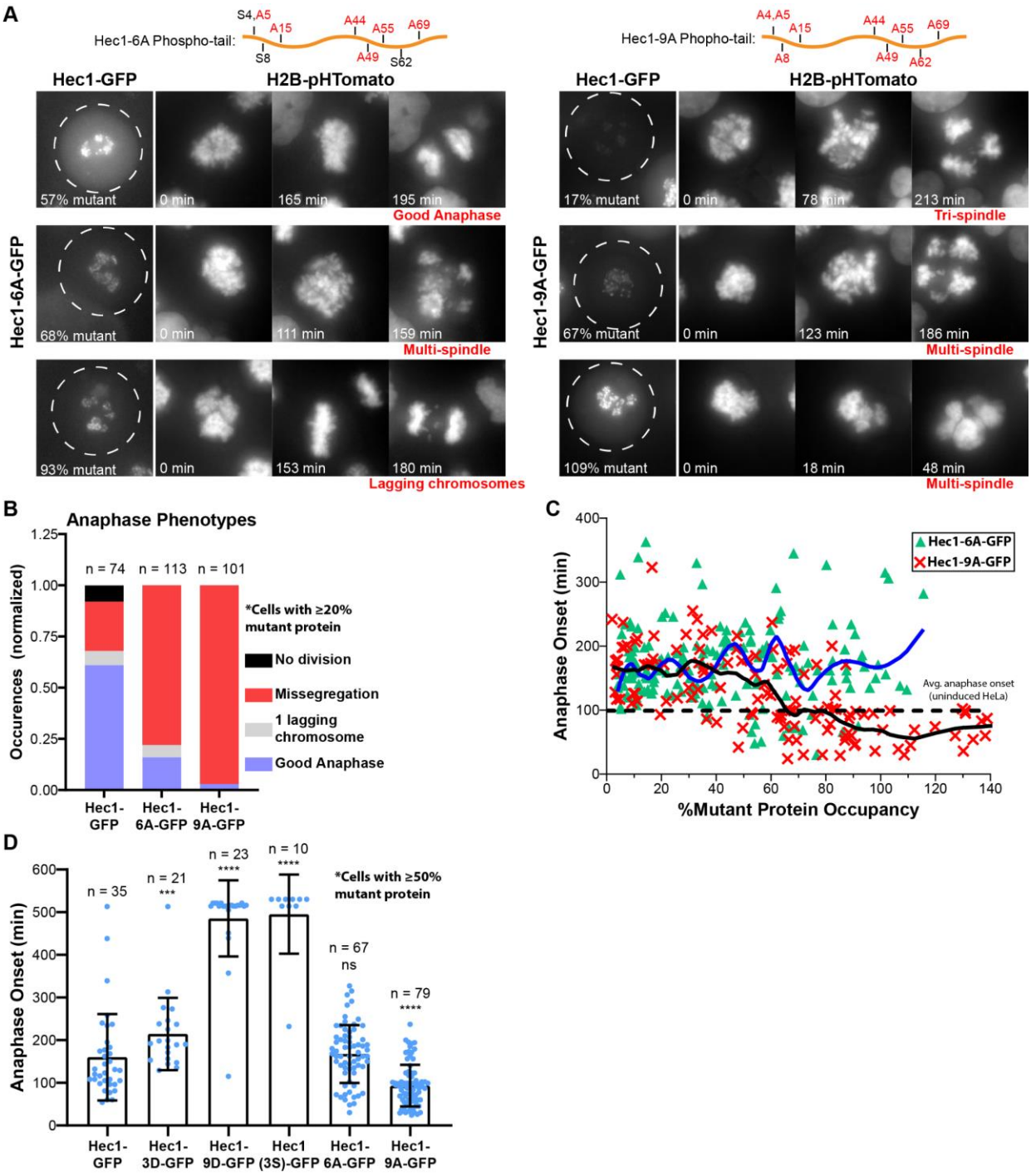

Figure 3.3 Chromosome Biorientation Fails in Kinetochores with ≥20% High Microtubule Affinity Ndc80C Mutants

(A) Top: Cartoon diagrams of the Hec1-6A and Hec1-9A phospho-tails, highlighting the residues that have been mutated to alanines. Bottom: Representative images of mitotic HeLa cells expressing Hec1-6A-GFP or Hec1-9A-GFP mutant proteins as they progress through anaphase. GFP images show the % occupancy of exogenous Hec1 at kinetochores. The H2B-pHTomato images show the corresponding chromosomes from these cells at different times after nocodazole release. The resulting anaphase phenotype is indicated below the final frame for each time series. Images are ~30x30 μm. (B) Anaphase phenotypes for mitotic cells expressing the indicated Hec1-GFP mutants after release from nocodazole. Only cells containing ≥20% of the mutant protein at kinetochores are included. The

number of cells analyzed is indicated above the bars. (C) Anaphase onset time versus the % occupancy of Hec1-6A-GFP (green triangles) and Hec1-9A-GFP (red X's). All cells were synchronized in mitosis via nocodazole. The dashed lines indicate the maximum time for which cells were imaged (>8 hours) and the average anaphase onset time for cells expressing no transgenes (uninduced HeLa). Each data point corresponds to a single cell. The lines over the data points correspond to Loess smoothing of the data (Hec1-6A-GFP = blue line; Hec1-9A-GFP = black line). The Hec1-6A-GFP protein does not change the anaphase onset time of HeLa cells, whereas Hec1-9A-GFP decreases the anaphase onset time at around ≥60% occupancy. Note that 13 cells have been removed from the Hec1-9A-GFP dataset. (D) Average anaphase onset time for the indicated Hec1-GFP mutants in cells that contain ≥50% of the mutant protein at kinetochores. Error bars are SD and then number of measurements for each mutant is indicated. Statistically significant difference between wildtype Hec1-GFP and each of the mutant Hec1 proteins was evaluated using the Mann-Whitney test, ns, not significant; $^{*}p < 0.05$; $^{**}p < 0.01$; $^{***}p < 0.001$; $^{****}p < 0.0001$.

When comparing the level of Hec1-9A kinetochore occupancy versus the anaphase onset time, we observed a subtle yet distinct transition point (Figure 3.3C). At ≥60% Hec1-9A mutant, cells begin to enter anaphase more quickly than wildtype Hec1-GFP expressing cells (93 ± 11 min. vs. 160 ± 17 min (± SEM) for cells with ≥50% occupancy, respectively; Figure 3.3D). Given the high microtubule affinity of this mutant, these results suggest that cells with ≥60% Hec1-9A satisfy the SAC more quickly than wildtype Hec1-GFP cells by more quickly establishing stabilized, albeit incorrect, attachments (Etemad, Kuijt, & Kops, 2015; Zhu et al., 2013). Notably, this ~60% transition point for SAC silencing coincides with the ~40% transition point for constitutive SAC activation that we observed with the weak-binding Hec1-9D and Hec1(3S) mutants (Figure 3.2B). Namely, the SAC is silenced when at least 60% of Ndc80C molecules bind strongly to microtubules and the SAC is constitutively activated when at least 40% of the Ndc80C molecules are not capable of forming strong attachments. Although phenotypically Hec1-6A was similar to Hec1-9A in terms of segregation outcomes, we did not observe any titratable effect on the timing of anaphase onset with this mutant (Figure 3.3B-D). This may be due to differences in the microtubule affinity of the Hec1-6A and 9A mutants, as well as the increased capacity for phospho-regulation on the Hec1-6A mutant.

3.3.4 Combining Low and High Affinity Mutant Domains in Ndc80C Shifts the Transition to Constitutive SAC Activation

The precise role of the Hec1 tail in microtubule attachment and biorientation for human kinetochores is still unresolved (Wimbish & DeLuca, 2020). Cells expressing tail-less Hec1 mutants form end-on microtubule attachments, albeit with reduced capacity to generate tension, defects in chromosome alignment, and delays in mitotic progression (Etemad et al., 2015; Guimaraes et al., 2008; Janczyk et al., 2017; Miller et al., 2008; Wimbish et al., 2020). These observations suggest that end-on attachments formed solely by the CH domains of Ndc80C are defective in silencing the SAC. Thus, the Hec1 tail is likely necessary for the displacement of Mps1 from the CH domains upon microtubule attachment (Ji et al., 2015). To investigate the importance of both the Hec1 tail and CH domains in SAC silencing further, we engineered chimeric Ndc80C mutants containing Hec1 with a strong-binding 6A or 9A tail and with a weak-binding ‘3S’ CH domain (termed Hec1-6A+(3S) or Hec1-9A+(3S), respectively; Figure 3.4A).

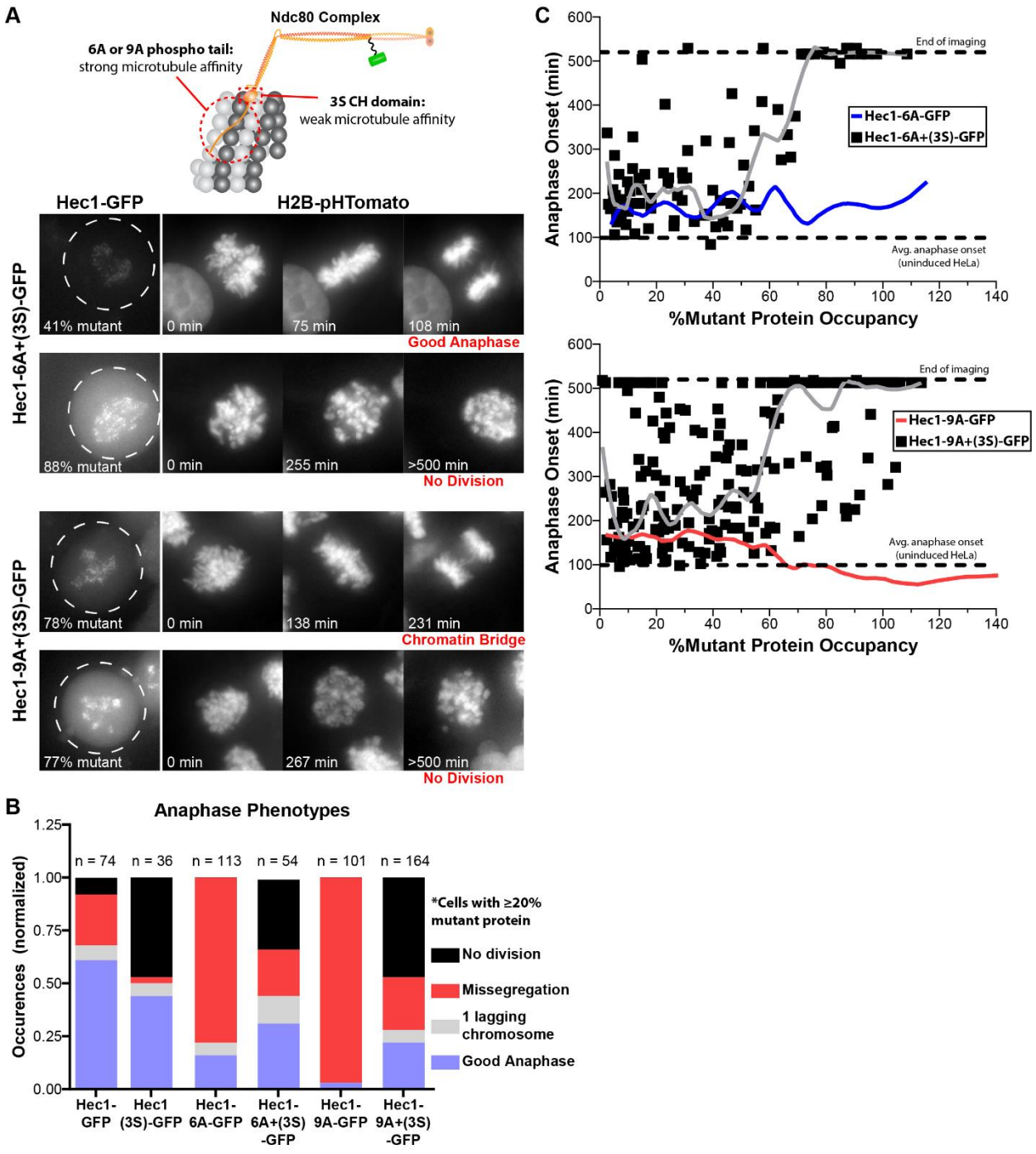

Figure 3.4 Combing Low and High Affinity Mutant Domains in Ndc80C Shifts the Transition to Constitutive SAC Activation

(A) Top: Cartoon of Ndc80C highlighting the phospho-tail domain of Hec1 which has been mutated to a high microtubule affinity state (6A or 9A) and the CH domain which has been mutated to a low affinity state (3S). Bottom: Representative images of mitotic HeLa cells expressing Hec1-6A+(3S)-GFP or Hec1-9A+(3S)-GFP mutant proteins as they progress through anaphase. GFP images show the % occupancy of exogenous Hec1 at kinetochores. The H2B-pHTomato images show the corresponding chromosomes from these cells at different times after nocodazole release. The resulting anaphase phenotype is indicated below the final frame for each time series. Images are ~30x30 µm. (B) Anaphase phenotypes for mitotic cells expressing the indicated Hec1-GFP mutants after release from nocodazole. Only cells containing ≥20% of the mutant protein at kinetochores are included. The

number of cells analyzed is indicated above the bars. (C) Anaphase onset time versus the % occupancy of Hec1-6A+(3S)-GFP (black squares; top graph) and Hec1-9A+(3S)-GFP (black squares; bottom graph). The dashed lines indicate the maximum time for which cells were imaged (>8 hours) and the average anaphase onset time for cells expressing no transgenes (uninduced HeLa). Each data point corresponds to a single cell. The lines over the data points correspond to Loess smoothing of the data (Hec1-6A+(3S)-GFP and Hec1-9A+(3S)-GFP = gray line; Hec1-6A-GFP = blue line; Hec1-9A-GFP = red line). The addition of the weak microtubule-binding (3S) mutation in the Hec1 CH domain overrides the strong microtubule binding 6A or 9A phospho-tail mutations.

Previous investigations combining a weak-binding CH domain and a strong-binding 9A tail demonstrated that the weakened CH domain ultimately dictates the chromosome alignment and microtubule attachment behavior of the kinetochore (Tooley et al., 2011). Similarly, we observed that the Hec1-6A+(3S) and Hec1-9A+(3S) mutants behaved much more like the Hec1(3S) mutant than either of the Hec1-6A or Hec1-9A mutants (Figure 3.4A & B). Compared to the Hec1-6A or 9A tail mutants, cells with ≥20% incorporation of the chimeric Hec1 mutants had more failures to divide, indicative of SAC activation. Additionally, the Hec1 chimeras had reduced levels of missegregation and a higher frequency of successful anaphases as compared to the Hec1-6A and Hec1-9A mutants. Thus, weakening Ndc80C's microtubule affinity via the 3S mutation in the Hec1 CH-domain negates the affinity enhancing effects of the 6A or 9A tail mutations.

Titrations with the Hec1 chimeras revealed a transition in the timing of anaphase onset. At ≥60% occupancy for either the Hec1-6A+(3S) or Hec1-9A+(3S) mutants cells no longer divide within the 500 min. observation window of our experiments (Figure 3.4C). This transition was better defined for the 6A Hec1 chimera than for the 9A chimera, which exhibited a more variable phenotype regarding the timing of anaphase onset (Figure 3.4C, bottom graph). Importantly, this transition is shifted relative to what we observed for Hec1(3S) expressing cells (Figure 3.2D, bottom graph). The Hec1(3S) cells transition at above ~30-40% occupancy whereas the addition of the 6A or 9A tail shifts the transition to ≥60% occupancy. This shift

implicates the tail in SAC silencing and suggests that a strong-binding, dephosphorylated tail is better at turning off SAC signaling. The exact mechanism by which the tail participates in SAC silencing is unclear. The tail may have a direct interaction with Mps1 and/or the CH domain, helping to disrupt Mps1/CH domain binding with decreasing levels of phosphorylation. Alternatively, by virtue of its increased microtubule affinity, a dephosphorylated tail may help the CH domain engage the microtubule lattice, thereby displacing Mps1 and silencing the SAC (Hiruma et al., 2015; Ji et al., 2015).

3.4 Future Directions

Thus far, this project has yielded significant insights into the role that the human kinetochore's ~250 copies of Ndc80C play in kinetochore function and the success of chromosome segregation. First, we have demonstrated that SAC satisfaction occurs even when all 250 molecules of the kinetochore are not actively engaged in microtubule binding (Figure 3.2). This result highlights an apparent discrepancy in the current understanding of SAC signaling, namely that unbound Ndc80C starts the SAC signaling cascade and that microtubule attachment extinguishes its SAC signaling capacity (Aravamudhan, Goldfarb, & Joglekar, 2015; Hiruma et al., 2015; Ji et al., 2015). Since Ndc80C's main role in SAC signaling is connected to its ability to bind the Mps1 kinase, which phosphorylates many proteins within the SAC signaling cascade, we will need to assess the level of Mps1 at kinetochores that are titrated with our weak-binding Hec1 mutants. We envision two possible outcomes. Either the level of Mps1 increases linearly with increasing amounts of mutant protein or there will be a sharp transition in the level of Mps1 at some threshold level of weak-binding Hec1. Distinguishing between these two possibilities will be important for further understanding the mechanism of SAC silencing

and the influence of the human kinetochore's 250 Ndc80C molecules in this process. Additionally, these experiments will allow us to perform an important control for the Hec1(3S) mutant that we introduce in this study. This mutant is heretofore uncharacterized, and while designed to avoid disruption of the Ndc80C/Mps1 interaction, it will be important to confirm that this interaction persists.

An intriguing implication of our result that human kinetochores can accommodate at least 40% weak-binding Ndc80C before constitutive SAC is that these kinetochores likely do not bind the full complement of microtubules. Taken a step further, previous studies have demonstrated that SAC silencing occurs when as little as 30% of the human kinetochores microtubule binding capacity is filled (Etemad et al., 2019; Kuhn & Dumont, 2019), suggesting that ~150 Ndc80C molecules can bind as few as ~5-6 microtubules. This stoichiometry is intriguing because it implies that 25-30 Ndc80C molecules can bind a single microtubule, whereas at full microtubule capacity the stoichiometry of the human kinetochores suggests that there are ~12-16 Ndc80C molecules per attachment. If the kinetochore can truly dedicate such a high number of Ndc80C molecules to a single microtubule attachment, this would further implicate the 'lawn' model of human kinetochore architecture rather than the discrete subunit model. To test this, we would need two measurements. First, we will measure how the number of kinetochore bound microtubules changes with increasing amounts of our Hec1 mutants (Figure 3.5A). We will also measure how FRET between microtubule-bound Ndc80C molecules changes with increasing amounts of our Hec1 mutants. We and others have already demonstrated that FRET between Ndc80C molecules increases with centromeric tension, and that this increase is due to a greater number of microtubule-bound Ndc80C molecules (Kukreja et al., 2020; Yoo et al., 2018). Since kinetochores can maintain SAC silencing at a sub-optimal microtubule-binding capacity, we

expect that FRET between Ndc80C molecules will not change much as the number of weak-binding Ndc80C mutants increases (and therefore the number of kinetochore-bound microtubules decreases). In fact, we have already indirectly demonstrated such a phenomenon when measuring FRET under conditions where the total amount of Ndc80C at the kinetochore is artificially reduced via siRNA (Kukreja et al., 2020). The titration method we have developed here will be an ideal assay to strengthen the notion that bioriented kinetochores maintain a certain level of microtubule-bound Ndc80C molecules, even when the number of microtubules fluctuates.

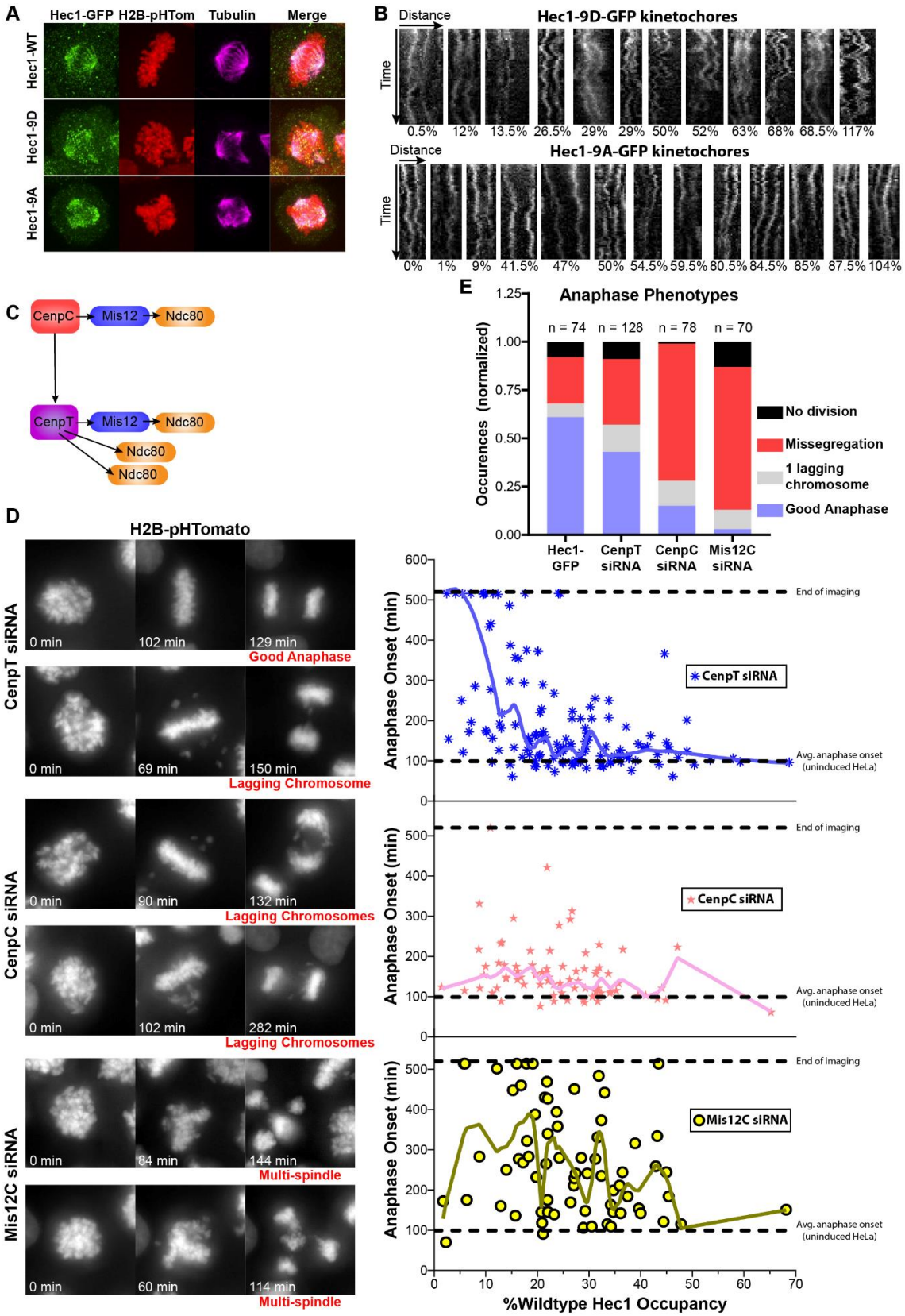
A
Hec1-GFP
H2B-pHTom
Tubulin
Merge
Hec1-WT
Hec1-9D
Hec1-9A
B
Distance
Time
Hec1-9D-GFP kinetochores
0.5% 12% 13.5% 26.5% 29% 29% 50% 52% 63% 68% 68.5% 117%
Hec1-9A-GFP kinetochores
0% 1% 9% 41.5% 47% 50% 54.5% 59.5% 80.5% 84.5% 85% 87.5% 104%
C
CenpC
Mis12
Ndc80
CenpT
Ndc80
Ndc80
D
H2B-pHTomato
CenpT siRNA
0 min
102 min
129 min
Good Anaphase
0 min
69 min
150 min
Lagging Chromosome
CenpC siRNA
0 min
90 min
132 min
Lagging Chromosomes
0 min
102 min
282 min
Lagging Chromosomes
Mis12C siRNA
0 min
84 min
144 min
Multi-spindle
0 min
60 min
114 min
Multi-spindle
E
Anaphase Phenotypes
n = 74
n = 128
n = 78
n = 70
Occurences (normalized)
No division
Missegregation
1 lagging chromosome
Good Anaphase
Hec1-GFP
CenpT siRNA
CenpC siRNA
Mis12C siRNA
Anaphase Onset (min)
End of imaging
CenpT siRNA
Avg. anaphase onset (uninduced HeLa)
CenpC siRNA
Mis12C siRNA
%Wildtype Hec1 Occupancy

Figure 3.5 Future Directions: Kinetochore Oscillations, Microtubule Binding, and Artificial Reduction in the Kinetochore's Capacity for Ndc80C
(A) Representative immunofluorescence images of mitotic HeLa cells staining with anti-GFP Alexfluor 488 to visualize Hec1-GFP mutants and anti-Tubulin Alexafluor 647 to visualize the spindle. Chromosomes are visualized with innate H2B-pHTomato fluorescence. The Hec1-9D-GFP and Hec1-9A-GFP cells show an abnormal tri-spindle morphology (B) Representative kymographs of HeLa kinetochores titrated with Hec1-9D-GFP and Hec1-9A-GFP. The % occupancy of the mutant proteins is listed below each micrograph. As kinetochores incorporate more Hec1-9D-GFP, oscillations become more erratic whereas greater incorporation of Hec1-9A-GFP leads to dampened oscillations. (C) Cartoon diagram of the recruitment scheme of Ndc80C. Centromeric proteins CenpT and CenpC, along with inner kinetochore protein complex Mis12C, each recruit a subset of the total Ndc80C. CenpT recruits three Ndc80C molecules, CenpC recruits one (via Mis12C), and Mis12C recruits two. Multiple of these recruitment motifs are bound by human centromeres. (D) Left: Representative images of mitotic HeLa cells progressing to anaphase. Cells express wildtype Hec1-GFP and are treated with siRNAs directed towards different members of the Ndc80C recruitment pathways. The H2B-pHTomato images show chromosomes at different times after nocodazole release. The resulting anaphase phenotype is indicated below the final frame for each time series. Images are ~30x30 μm. Right: Anaphase onset time versus the % occupancy of HeLa cells expressing wildtype Hec1-GFP and treated with CenpT siRNA (top graph; blue asterisks), CenpC siRNA (middle graph; pink stars), or Mis12C siRNA (bottom graph; yellow circles). The dashed lines indicate the maximum time for which cells were imaged (>8 hours) and the average anaphase onset time for cells expressing no transgenes (uninduced HeLa). Each data point corresponds to a single cell. The lines over the data points correspond to Loess smoothing of the data. Note that cells were also treated with siRNA targeting the endogenous, unlabeled Hec1 to encourage full occupancy of kinetochores with the exogenous Hec1-GFP. This measure allows us to assess the affect of siRNAs targeting the Ndc80C recruitment pathways. The effect of reducing Ndc80C depends upon the pathway that is perturbed. CenpT siRNA is still capable of SAC signaling at very low amounts of Ndc80C, CenpC siRNA abolishes SAC signaling, and Mis12C siRNA has an indeterminate effect. (E) Anaphase phenotypes for mitotic cells expressing wildtype Hec1-GFP and treated with the indicated siRNAs after release from nocodazole. For the untreated cells only, we include only those cells containing ≥20% of the Hec1-GFP protein at kinetochores. The number of cells analyzed is indicated above the bars.

Another significant finding has been that human kinetochores cannot tolerate ≥20% strong-binding Ndc80C molecules (Figure 3.3). This result highlights the importance of phospho-regulation on the Hec1 tail to tune the microtubule affinity of Ndc80C and demonstrates that the biorientation and force generation functions of the human kinetochore are much more sensitive to the total number of Ndc80C molecules than the SAC. Our assays so far provide a low-resolution look at kinetochore function, having only measured chromosome segregation phenotypes and the timing of anaphase onset for cells with varying levels of mutant Ndc80C incorporation at kinetochores. To deepen our analysis, we will also need to track the behavior of individual sister kinetochore pairs. We have already made some progress toward this aim, tracking the oscillations of bioriented kinetochores with varying levels of Hec1 mutant occupancy. For cells expressing the weak-binding Hec1-9D tail mutant, we observed that

chromosome oscillations become more erratic, exhibiting a higher frequency of directional switches and a decrease in the distance between sister kinetochores (Figure 3.5B, top row). For the strong-binding Hec1-9A tail mutant, oscillations dampen and sister kinetochore distances become fixed (Figure 3.5B, bottom row) (K. F. DeLuca et al., 2011; Zaytsev et al., 2014). Using a recently developed high-throughput kinetochore tracking software (Armond, Vladimirou, McAinsh, & Burroughs, 2016), we hope to provide a more detailed analysis of how increasing levels of various Hec1 mutants affect the behavior of bioriented kinetochores, including parameters such as: the amount of centromeric tension developed between sister kinetochores, the speed of oscillations, the frequency of directional switches and stalls, and the frequency of detachment from the spindle.

Our approach for investigating how the number of Ndc80C molecules influences human kinetochore functions relies on replacing functional Ndc80C with non-functional mutants. Although this approach has yielded many insights, doping the kinetochore with non-functional mutant protein may produce different results than simply lowering the number of Ndc80C molecules. To investigate the latter scenario, we have performed preliminary experiments where we knocked down different members of the Ndc80C recruitment pathways via siRNA (Figure 3.5C-E). Three proteins are directly involved in the recruitment of Ndc80C (Figure 3.5C). CenpC and CenpT are centromere binding proteins with long, flexible N-terminal tails that each bind to an adaptor complex called Mis12. The Mis12 complex directly binds one Ndc80C molecule. Additionally, the CenpT molecule can recruit up to two additional Ndc80C molecules via direction interaction with its N-terminal tail. RNAi of any one of these proteins results in an ~60% reduction in the total amount of Ndc80C at kinetochores (Kukreja et al., 2020; Suzuki et al., 2015). However, these knockdowns produced distinct results depending on which protein

was targeted (Figure 3.5D & E). For example, RNAi of CenpT, the protein receptor which recruits up to three Ndc80C molecules, only mildly effected chromosome segregation, increasing the missegregation rate to 48% versus 31% in wildtype Hec1-GFP expressing cells (Figure 3.5E). There was no effect on the timing of anaphase until the amount of wildtype Ndc80C dropped below 15% of normal, untreated kinetochores (Figure 3.5D). At this low point, the timing to anaphase onset increased with many cells failing to divide. Surprisingly, knockdown of either CenpC or the Mis12 complex, both of which recruit only one Ndc80C molecule, increased the missegregation rate to 84% (Figure 3.5E). However, the timing of anaphase onset was different for both proteins (Figure 3.5D). CenpC RNAi had almost no effect on the timing of anaphase onset, whereas knockdown of the Mis12 complex displayed unpredictable behavior where the timing of anaphase onset was uncorrelated with the occupancy of Ndc80C.

While our hope was that siRNA knockdowns of the Ndc80C recruitment pathways would reveal how kinetochore functions responds to reduced numbers of Ndc80C, these experiments instead demonstrate that there are pathway-specific effects on kinetochore function. This is likely due to the other roles that these proteins play in kinetochore assembly and function (Basilico et al., 2014; Gascoigne et al., 2011; Hara, Ariyoshi, Okumura, Hori, & Fukagawa, 2018; Hori et al., 2008; Klare et al., 2015; Malvezzi et al., 2013; Nishino et al., 2013; Nishino et al., 2012; Pesenti et al., 2018; Petrovic et al., 2016; Petrovic et al., 2014; Petrovic et al., 2010; Schleiffer et al., 2012; Screpanti et al., 2011; Weir et al., 2016). The most surprising of these results is the severe phenotype observed for knockdown of the Mis12 complex. This protein does not interact with the centromeric DNA like CenpC and CenpT, and therefore should have little influence on the integrity of the centromere (Suzuki et al., 2014). It is possible that the phenotypes from Mis12 complex knockdown are largely due to its role in recruiting the KNL1 protein, a direct target of

SAC signaling and involved in the activation of the Aurora B kinase (Caldas, DeLuca, & DeLuca, 2013). While many of these results are intriguing and deserve a thorough investigation, they are largely outside of the scope of this research project. Studying the effect of reduced numbers of Ndc80C at human kinetochores will require a different experimental approach, perhaps by expressing wildtype Hec1-GFP in a background where competition from the endogenous, unlabeled Hec1 is removed.

3.5 Materials & Methods

3.5.1 Culture Conditions for HeLa, U2OS, and HT1080 Cells

The parental HeLa A12, U2OS A13, or HT1080 A4 cell lines were maintained in DMEM media (GIBCO) supplemented with 10% FBS (Corning), 100 U/mL penicillin, and 100 µg/mL streptomycin (GIBCO). Parental cells stably-integrated with the dual-expression pERB131 plasmid were maintained in the same media supplemented with 1 µg/mL puromycin. Cells were grown in a 37 °C/5% CO_2 incubator. All plasmids integrated into the parental cell lines were verified via DNA sequencing, and stably-integrated cells were authenticated by selection for puromycin resistance and subsequent fluorescence microscopy for the proper localization of the fluorophore-tagged proteins.

3.5.2 Construction of Stable Integration Human Cell Lines for Dual Protein Expression

HeLa, U2OS, and HT1080 cell lines were generated from HeLa A12, U2OS A13, or HT1080 A4, respectively (gifts form the Lampson lab). These cells contain a chromosomal Cre/Lox integration site directly following the EF-1α promoter (Khandelia, Yap, & Makeyev, 2011). Cell lines were constructed essentially as described previously (Kukreja et al., 2020), using standard molecular cloning to engineer variants of the pERB131 plasmid backbone (gift from the Lampson lab). The pERB131 backbone harbors an expression cassette with two open reading frames (ORFs), one of which is constitutively expressed upon successful integration by the EF1-α promoter and another which is controlled by a tetracycline responsive element (Tet-ON). The cassette also contains a puromycin resistance gene which we used to select for successful transformants. A list of all cell lines generated for this study is provided in Table 3.1.

Integration was performed using the Lipofectamine 3000 Reagent kit (Thermo Fisher Scientific), the pERB131 plasmid cassette of interest, and a Cre-expression plasmid. Two days post-transfection, we added 2 μg/mL puromycin to the cell media to select for successful transformants. After two weeks of selection, surviving colonies were maintained in 1 μg/mL puromycin media. For cells not immediately ready for analysis after their construction, we created stocks by pelleting trypsinized cells (0.25% Trypsin – GIBCO) and resuspending cells in a 1:1 mixture of supplemented DMEM media (containing no puromycin) and 2x Freezing Media (50% FBS, 30% supplemented DMEM media without puromycin, 20% DMSO). Resuspended cells were placed in cryogenic vials and stored overnight at -80 °C before moving to liquid nitrogen for long-term storage.

3.5.3 Fluorescence Microscopy

Time-lapse imaging was performed on a Nikon Ti-E inverted microscope with a 1.4 NA, 100x, oil immersion objective. The microscope was equipped with XY linear encoders and a piezoelectric Z-stage (Prior). A Lumencor LED light engine (472/20 nm GFP excitation, 543/20 nm mCherry excitation) served as the laser power source. Images were acquired on an Andor iXon3 EMCCD camera (pixel size = 160 nm^2, 16-bit A/D converter). A Perfect Focus System (Nikon) was used to minimize axial drift during time-lapse imaging. Image acquisition was performed using the MetaMorph software (Molecular Devices).

Immunofluorescence was performed on a Nikon Ti-E inverted microscope with a 1.4 NA, 60x, oil immersion objective and 1.5x Optivar lens. The microscope was equipped with a side-arm X-Light V2 L-FOV spinning disk confocal (CrestOptics). A Lumencor Celesta light engine (475/28 nm GFP excitation, 555/28 nm mCherry excitation) served as the laser power source. Images were acquired on a Prime 95B sCMOS camera (Teledyne Photometrics; pixel size =

~122 nm^2, 16-bit A/D converter). Image acquisition was performed using the NIS-Elements software (Nikon).

3.5.4 Time-lapse Imaging for Anaphase Onset Timing

Cells were plated in 35 mm glass bottom dishes (MatTek) in DMEM media (GIBCO) supplemented with 10% FBS (Corning), 100 U/mL penicillin and 100 mg/mL streptomycin (GIBCO), 1 μg/mL puromycin. Approximately 26 hours prior to imaging, cells were induced with 2 μg/mL doxycycline and treated with 2.5 mM thymidine for synchronization in S-phase. Cells were released from thymidine and doxycycline treatments 16 hours later and replaced with fresh media. Four hours later, cells were treated with 100 ng/mL nocodazole for 6 hours. Immediately prior to imaging, nocodazole was washed out using FluoroBrite DMEM media (GIBCO) supplemented with 10% FBS (Corning), and 100 U/mL penicillin and 100 mg/mL streptomycin (GIBCO). The elapsed time between nocodazole wash-out and the beginning of time-lapse imaging was noted for all experiments.

For time-lapse experiments with siRNA-mediated knockdown of Ndc80C recruitment pathways, experiments were performed essentially as above except cells were double thymidine synchronized, with dox-induction and siRNA treatments occurring between the first and second thymidine treatment. Treatments with siRNA were performed using the Lipofectamine RNAiMAX kit (Invitrogen), using 60 pmol each of the recruitment pathway specific siRNA (either CenpT, CenpC, or Mis12C) and Hec1 siRNA targeting endogenous, unlabeled Hec1 (siRNAs listed in Table 3.2). Since these experiments were performed in cells with dox-inducible wildtype Hec1-GFP, the knockdown of endogenous Hec1 reduces the competition of Hec1-GFP for kinetochore binding (Kukreja et al., 2020). This lack of competition allowed us to

assess the efficiency of the CenpT, CenpC, or Mis12C knockdowns on reducing Ndc80C recruitment.

For all quantitative time-lapse experiments, a calibration was performed by imaging HeLa, U2OS, or HT1080 cells constitutively expressing Spc25-GFP. At least 24 hours prior to imaging, these cells were treated with 60 pmol Spc25 siRNA to knockdown endogenous, unlabeled Spc25. Cells were imaged immediately prior to time-lapse experiments, acquiring a 20 z-stack image series with 0.25 µm steps and GFP excitation at a 400 ms acquisition rate for each cell.

During imaging, cells were maintained in a heated chamber with CO_2 respirator and the objective was fit with a warming collar (Live Cell Instrument). For individual experiments, between 8 - 12 regions of interest (ROIs) were selected using the multidimensional acquisition app in MetaMorph. ROIs were imaged every 3 min for a total of 501 min. At each timepoint, a 13 z-stack image series with 1.5 µm steps was acquired using mCherry excitation and an acquisition rate of 10 ms. A single plane trans-light image was also acquired at each timepoint. Additionally, for the first timepoint only, acquired a 13 z-stack image series using GFP excitation and an acquisition rate of 400 ms. This GFP image was used to quantify the average amount of mutant protein at kinetochores.

3.5.5 Quantification of Hec1 Mutant Titrations and Anaphase Phenotypes

For time-lapse imaging to assess the timing of anaphase onset, image analysis was performed in FIJI. To estimate the GFP fluorescence corresponding to 100% kinetochore occupancy of Ndc80C, the calibration images collected from cells expressing Spc25-GFP were converted to a max intensity Z-projection. A 6x6 box was drawn and 5 random regions surrounding the metaphase plate were measured to estimate the average background. This same

box was positioned over kinetochores and used to measure their intensity. The brightness for 100% occupancy within a given cell was then defined as the average kinetochore intensity minus the average background signal. This was done for at least 15 cells for each time-lapse imaging experiment.

Measurements of cells titrated with Hec1 mutants was performed similarly. A max intensity z-projection was generated for the Hec1-GFP image, and a 6x6 box was used to measure the background signal from 5 regions surrounding the kinetochores. This same box was positioned over 5 kinetochores in the cell to estimate the average Hec1 mutant signal at kinetochores. This average intensity was divided by the average intensity determined in the calibration images to arrive at the average percent occupancy for GFP-labeled Hec1 at kinetochores within a given cell.

Trans and H2B-pHTomato images of the same cell were then observed over time, noting both the time of anaphase onset and general phenotypes of the chromosome segregation. Cells that went through anaphase without any abnormal spindle morphology, cell death, or lagging chromosomes were scored as “Good Anaphase”. Cells still in metaphase by the end of the movie were scored as “No Division” (movie lengths ~500 min). Cells with one observable lagging chromosome were scored as “1 Lagging Chromosome”. Cells with other segregation defects including more than 1 lagging chromosome, tri- or multi-spindles, micronuclei, and chromatin bridges were scored as “Missegregation”.

3.5.6 Dynamics of Kinetochore Oscillations

Cells were plated in a 4-chamber glass-bottom dish in supplemented DMEM media containing 1 μg/mL puromycin. Cells were double thymidine synchronized, with dox-induction (2 μg/mL) and siRNA treatments (60 pmol per protein specific siRNA) occurring between the

first and second thymidine treatment. At 8 hours after the release of the second thymidine treatment, cells were treated with 10 μM MG132 for 2 hours before imaging.

To monitor kinetochore oscillations, cells were imaged for 5 minutes at 5 second intervals. A 400 ms acquisition rate was used to acquire an initial frame of GFP to assess the amount of

3.5.7 Fixation and Antibody Staining for Immunofluorescence

Cells were plated in 2 mL 6-well dishes (Corning) atop 22 mm glass slides in supplemented DMEM media containing 1 μg/mL puromycin. Cells were double thymidine synchronized, with dox-induction (2 μg/mL) and siRNA treatments (60 pmol per protein specific siRNA) occurring between the first and second thymidine treatment. At 8 hours after the release of the second thymidine treatment, cells were treated with 10 μM MG132 for 3 hours.

For fixation, cells were rinsed with pre-warmed PHEM buffer (60 mM PIPES, 25 mM HEPES (pH 6.9 @ RT), 10 mM EGTA, 4 mM $MgSO_4$) and fixed for 1 min. in freshly prepared 4.0% paraformaldehyde/PHEM at RT. Cells were rinsed and permeabilized with 0.5% Triton X-100/PHEM for 5 min. at 37 °C. Cells were rinsed and then fixed for an additional 20 min. in 4.0% paraformaldehyde/PHEM at 37 °C. Cells were rinsed thrice in PBS-T (phosphate buffered saline with 0.05% Tween-20) for 5 min. each at RT. Blocking was for 30 min. in 5% boiled donkey serum (BDS)/PHEM at RT.

After blocking, cells were incubated with primary antibodies diluted in 5% BDS/PHEM at 4 °C overnight. Primary antibodies included polyclonal Rabbit anti-GFP (Invitrogen, Cat# PA1-980A; 1:200 dilution) and Dm1α (monoclonal IgG1 Mouse anti-αTubulin; EMD Millipore, Cat# 05-829; 1:500 dilution). Cells were rinsed four times in PBS-T for 5 min. each and then incubated in secondary antibodies (1:1000 in 5% BDS) for 1.5 hrs. at RT. Secondary antibodies

included Donkey anti-Rabbit Alexa Fluor 488 and Donkey anti-Mouse Alexa Fluor 647 (Both Invitrogen, Cat# A21206 and A31571, respectively). Cells were rinsed four times in PBS-T for 5 min. each and the coverslip was mounted to a glass slide with ProLong™ Diamond Antifade Mountant (Invitrogen, Cat# P36961). Slides were stored in the dark overnight to dry before imaging.

3.6 Acknowledgments

This chapter represents currently unpublished work, supported by NIGMS of the National Institutes of Health under award number: R35GM126983 to A.P.J. The authors would like to thank Dr. Jonathan Harrison, the Nigel Burroughs lab, and the Andrew McAinsh lab at the University of Warwick for help in using and trouble-shooting the KiT MATLAB package for tracking kinetochore oscillations.

3.7 Author Contributions

Conceptualization, Methodology, Writing – Original Draft, Writing – Review & Editing, Visualization, and Supervision, A.A.K. and A.J.P.; Formal Analysis and Investigation, A.A.K., J.A.O., and A.J.P.; Software, Resources, and Funding Acquisition, A.J.P.

Stress Testing the Number of Ndc80 Complexes for Proper Spindle Assembly Checkpoint Silencing and Biorientation in Human Kinetochores

Alexander A. Kukreja, Juan A. Orozco, and Ajit P. Joglekar. *In Manuscript. 2020.*

3.8 Tables

Table 3.1 List of Dual-Expression Plasmids
These plasmids were stably integrated into the HeLa genome via Cre/Lox recombination. ORF1 indicates genes that are under the control of a constitutive promoter (EF-1α) and ORF2 indicates genes that are under the control of doxycycline-inducible promoter.

Plasmid Name	Backbone	ORF1 gene (constitutive)	ORF2 gene (dox-inducible)
pAK026	pERB131	Spc25-GFP	Hec1-mCherry
pAK027	pERB131	Spc25-mCherry	Hec1-GFP
pAK101	pERB131	H2B-pHTomato	Hec1(3S)-GFP
pAK107	pERB131	H2B-pHTomato	Hec1-3D-GFP
pAK108	pERB131	H2B-pHTomato	Hec1-9D-GFP
pAK109	pERB131	H2B-pHTomato	Hec1-9A-GFP
pAK110	pERB131	H2B-pHTomato	Hec1(K166D)-GFP
pAK118	pERB131	H2B-pHTomato	Spc25-GFP
pAK120	pERB131	Spc25-mCherry	Hec1-9A-GFP
pAK121	pERB131	Spc25-mCherry	Hec1-9D-GFP
pAK122	pERB131	Spc25-mCherry	Hec1-3D-GFP
pAK138	pERB131	H2B-pHTomato	Hec1-9A+(3S)-GFP
pAK139	pERB131	H2B-pHTomato	Hec1-6A-GFP
pAK140	pERB131	H2B-pHTomato	CenpT(Δ1-230)-GFP
pAK141	pERB131	Spc25-mCherry	CenpT(Δ1-230)-GFP
pAK142	pERB131	H2B-pHTomato	Hec1-6A+(3S)-GFP
pAK146	pERB131	H2B-pHTomato	Hec1-GFP
pSK05	pERB131	Spc25-mCherry	Hec1(3S)-GFP
pSK07	pERB131	Spc25-mCherry	Hec1(K166D)-GFP

Table 3.2 List of siRNAs

Target Protein	Sequence	Target Sequence	Source	Reference
Hec1	UGUCUAGCAGAUACUUGCACGGUUU	5' UTR	Invitrogen	(Kukreja et al., 2020)
Spc25 (1)	UGCCUGCGAAGCAUUGUCCUACAUA	5' UTR	Invitrogen	(Kukreja et al., 2020)
Spc25 (2)	GCCUGCGAAGCAUUGUCCUACAUAA	5' UTR	Invitrogen	(Kukreja et al., 2020)
Mis12 (1)	GCAAAAUAAGCCAAGAUGUCU	ORF	Sigma Aldrich	(Kukreja et al., 2020)
Mis12 (2)	GUAUCUAUGCCAAAUUUGUUUU	ORF	Sigma Aldrich	(Kukreja et al., 2020)
Dsn1	GUCUAUCAGUGUCGAUUUA	ORF	Sigma Aldrich	(Kim & Yu, 2015)
Nsl1	CAUGAGCUCUUUCUGUUUA	ORF	Sigma Aldrich	(Kim & Yu, 2015)
CenpC (1)	GCACUCUUUCAGGUAGAAAGUCAA	ORF	Invitrogen	(Kukreja et al., 2020)
CenpC (2)	AACAUCUGGAAAUUUCAUCAUGACC	ORF	Invitrogen	(Kukreja et al., 2020)
CenpT (1)	AUCUCAAGAGCCUUCCUCUCCAUGG	ORF	Invitrogen	(Kukreja et al., 2020)
CenpT (2)	AACAGAGGCUGAGACUGUCAGUGUU	ORF	Invitrogen	(Kukreja et al., 2020)

3.9 References

Alushin, G. M., Musinipally, V., Matson, D., Tooley, J., Stukenberg, P. T., & Nogales, E. (2012). Multimodal microtubule binding by the Ndc80 kinetochore complex. *Nat Struct Mol Biol, 19*(11), 1161-1167. doi:10.1038/nsmb.2411

Alushin, G. M., Ramey, V. H., Pasqualato, S., Ball, D. A., Grigorieff, N., Musacchio, A., & Nogales, E. (2010). The Ndc80 kinetochore complex forms oligomeric arrays along microtubules. *Nature, 467*(7317), 805-810. doi:10.1038/nature09423

Aravamudhan, P., Goldfarb, A. A., & Joglekar, A. P. (2015). The kinetochore encodes a mechanical switch to disrupt spindle assembly checkpoint signalling. *Nat Cell Biol, 17*(7), 868-879. doi:10.1038/ncb3179

Armond, J. W., Vladimirou, E., McAinsh, A. D., & Burroughs, N. J. (2016). KiT: a MATLAB package for kinetochore tracking. *Bioinformatics, 32*(12), 1917-1919. doi:10.1093/bioinformatics/btw087

Basilico, F., Maffini, S., Weir, J. R., Prumbaum, D., Rojas, A. M., Zimniak, T., . . . Musacchio, A. (2014). The pseudo GTPase CENP-M drives human kinetochore assembly. *Elife, 3*, e02978. doi:10.7554/eLife.02978

Burroughs, N. J., Harry, E. F., & McAinsh, A. D. (2015). Super-resolution kinetochore tracking reveals the mechanisms of human sister kinetochore directional switching. *Elife, 4*. doi:10.7554/eLife.09500

Caldas, G. V., DeLuca, K. F., & DeLuca, J. G. (2013). KNL1 facilitates phosphorylation of outer kinetochore proteins by promoting Aurora B kinase activity. *J Cell Biol, 203*(6), 957-969. doi:10.1083/jcb.201306054

Chan, Y. W., Jeyaprakash, A. A., Nigg, E. A., & Santamaria, A. (2012). Aurora B controls kinetochore-microtubule attachments by inhibiting Ska complex-KMN network interaction. *J Cell Biol, 196*(5), 563-571. doi:10.1083/jcb.201109001

Cheeseman, I. M., Anderson, S., Jwa, M., Green, E. M., Kang, J., Yates, J. R., 3rd, . . . Barnes, G. (2002). Phospho-regulation of kinetochore-microtubule attachments by the Aurora kinase Ipl1p. *Cell, 111*(2), 163-172. doi:10.1016/s0092-8674(02)00973-x

Cheeseman, I. M., Chappie, J. S., Wilson-Kubalek, E. M., & Desai, A. (2006). The conserved KMN network constitutes the core microtubule-binding site of the kinetochore. *Cell, 127*(5), 983-997. doi:10.1016/j.cell.2006.09.039

Ciferri, C., De Luca, J., Monzani, S., Ferrari, K. J., Ristic, D., Wyman, C., . . . Musacchio, A. (2005). Architecture of the human ndc80-hec1 complex, a critical constituent of the outer kinetochore. *J Biol Chem, 280*(32), 29088-29095. doi:10.1074/jbc.M504070200

Ciferri, C., Pasqualato, S., Screpanti, E., Varetti, G., Santaguida, S., Dos Reis, G., . . . Musacchio, A. (2008). Implications for kinetochore-microtubule attachment from the structure of an engineered Ndc80 complex. *Cell, 133*(3), 427-439. doi:10.1016/j.cell.2008.03.020

Cimini, D., Wan, X., Hirel, C. B., & Salmon, E. D. (2006). Aurora kinase promotes turnover of kinetochore microtubules to reduce chromosome segregation errors. *Curr Biol, 16*(17), 1711-1718. doi:10.1016/j.cub.2006.07.022

DeLuca, J. G., Dong, Y., Hergert, P., Strauss, J., Hickey, J. M., Salmon, E. D., & McEwen, B. F. (2005). Hec1 and nuf2 are core components of the kinetochore outer plate essential for organizing microtubule attachment sites. *Mol Biol Cell, 16*(2), 519-531. doi:10.1091/mbc.e04-09-0852

DeLuca, J. G., Gall, W. E., Ciferri, C., Cimini, D., Musacchio, A., & Salmon, E. D. (2006). Kinetochore microtubule dynamics and attachment stability are regulated by Hec1. *Cell, 127*(5), 969-982. doi:10.1016/j.cell.2006.09.047

DeLuca, K. F., Lens, S. M., & DeLuca, J. G. (2011). Temporal changes in Hec1 phosphorylation control kinetochore-microtubule attachment stability during mitosis. *J Cell Sci, 124*(Pt 4), 622-634. doi:10.1242/jcs.072629

Diaz-Rodriguez, E., Sotillo, R., Schvartzman, J. M., & Benezra, R. (2008). Hec1 overexpression hyperactivates the mitotic checkpoint and induces tumor formation in vivo. *Proc Natl Acad Sci U S A, 105*(43), 16719-16724. doi:10.1073/pnas.0803504105

Dong, Y., Vanden Beldt, K. J., Meng, X., Khodjakov, A., & McEwen, B. F. (2007). The outer plate in vertebrate kinetochores is a flexible network with multiple microtubule interactions. *Nat Cell Biol, 9*(5), 516-522. doi:10.1038/ncb1576

Dudka, D., Noatynska, A., Smith, C. A., Liaudet, N., McAinsh, A. D., & Meraldi, P. (2018). Complete microtubule-kinetochore occupancy favours the segregation of merotelic attachments. *Nat Commun, 9*(1), 2042. doi:10.1038/s41467-018-04427-x

Etemad, B., Kuijt, T. E., & Kops, G. J. (2015). Kinetochore-microtubule attachment is sufficient to satisfy the human spindle assembly checkpoint. *Nat Commun, 6*, 8987. doi:10.1038/ncomms9987

Etemad, B., Vertesy, A., Kuijt, T. E. F., Sacristan, C., van Oudenaarden, A., & Kops, G. (2019). Spindle checkpoint silencing at kinetochores with submaximal microtubule occupancy. *J Cell Sci, 132*(12). doi:10.1242/jcs.231589

Foley, E. A., & Kapoor, T. M. (2013). Microtubule attachment and spindle assembly checkpoint signalling at the kinetochore. *Nat Rev Mol Cell Biol, 14*(1), 25-37. doi:10.1038/nrm3494

Gascoigne, K. E., Takeuchi, K., Suzuki, A., Hori, T., Fukagawa, T., & Cheeseman, I. M. (2011). Induced ectopic kinetochore assembly bypasses the requirement for CENP-A nucleosomes. *Cell, 145*(3), 410-422. doi:10.1016/j.cell.2011.03.031

Guimaraes, G. J., Dong, Y., McEwen, B. F., & Deluca, J. G. (2008). Kinetochore-microtubule attachment relies on the disordered N-terminal tail domain of Hec1. *Curr Biol, 18*(22), 1778-1784. doi:10.1016/j.cub.2008.08.012

Hara, M., Ariyoshi, M., Okumura, E. I., Hori, T., & Fukagawa, T. (2018). Multiple phosphorylations control recruitment of the KMN network onto kinetochores. *Nat Cell Biol, 20*(12), 1378-1388. doi:10.1038/s41556-018-0230-0

Helgeson, L. A., Zelter, A., Riffle, M., MacCoss, M. J., Asbury, C. L., & Davis, T. N. (2018). Human Ska complex and Ndc80 complex interact to form a load-bearing assembly that strengthens kinetochore-microtubule attachments. *Proc Natl Acad Sci U S A, 115*(11), 2740-2745. doi:10.1073/pnas.1718553115

Hill, T. L. (1985). Theoretical problems related to the attachment of microtubules to kinetochores. *Proc Natl Acad Sci U S A, 82*(13), 4404-4408. doi:10.1073/pnas.82.13.4404

Hiruma, Y., Sacristan, C., Pachis, S. T., Adamopoulos, A., Kuijt, T., Ubbink, M., . . . Kops, G. J. (2015). CELL DIVISION CYCLE. Competition between MPS1 and microtubules at kinetochores regulates spindle checkpoint signaling. *Science, 348*(6240), 1264-1267. doi:10.1126/science.aaa4055

Hori, T., Amano, M., Suzuki, A., Backer, C. B., Welburn, J. P., Dong, Y., . . . Fukagawa, T. (2008). CCAN makes multiple contacts with centromeric DNA to provide distinct pathways to the outer kinetochore. *Cell, 135*(6), 1039-1052. doi:10.1016/j.cell.2008.10.019

Huis In 't Veld, P. J., Volkov, V. A., Stender, I. D., Musacchio, A., & Dogterom, M. (2019). Molecular determinants of the Ska-Ndc80 interaction and their influence on microtubule tracking and force-coupling. *Elife, 8*. doi:10.7554/eLife.49539

Janczyk, P. L., Skorupka, K. A., Tooley, J. G., Matson, D. R., Kestner, C. A., West, T., . . . Stukenberg, P. T. (2017). Mechanism of Ska Recruitment by Ndc80 Complexes to Kinetochores. *Dev Cell, 41*(4), 438-449 e434. doi:10.1016/j.devcel.2017.04.020

Ji, Z., Gao, H., & Yu, H. (2015). CELL DIVISION CYCLE. Kinetochore attachment sensed by competitive Mps1 and microtubule binding to Ndc80C. *Science, 348*(6240), 1260-1264. doi:10.1126/science.aaa4029

Joglekar, A. P., & Kukreja, A. A. (2017). How Kinetochore Architecture Shapes the Mechanisms of Its Function. *Curr Biol, 27*(16), R816-R824. doi:10.1016/j.cub.2017.06.012

Kabeche, L., & Compton, D. A. (2013). Cyclin A regulates kinetochore microtubules to promote faithful chromosome segregation. *Nature, 502*(7469), 110-113. doi:10.1038/nature12507

Khandelia, P., Yap, K., & Makeyev, E. V. (2011). Streamlined platform for short hairpin RNA interference and transgenesis in cultured mammalian cells. *Proc Natl Acad Sci U S A, 108*(31), 12799-12804. doi:10.1073/pnas.1103532108

Kim, S., & Yu, H. (2015). Multiple assembly mechanisms anchor the KMN spindle checkpoint platform at human mitotic kinetochores. *J Cell Biol, 208*(2), 181-196. doi:10.1083/jcb.201407074

Klare, K., Weir, J. R., Basilico, F., Zimniak, T., Massimiliano, L., Ludwigs, N., . . . Musacchio, A. (2015). CENP-C is a blueprint for constitutive centromere-associated network assembly within human kinetochores. *J Cell Biol, 210*(1), 11-22. doi:10.1083/jcb.201412028

Kuhn, J., & Dumont, S. (2017). Spindle assembly checkpoint satisfaction occurs via end-on but not lateral attachments under tension. *J Cell Biol, 216*(6), 1533-1542. doi:10.1083/jcb.201611104

Kuhn, J., & Dumont, S. (2019). Mammalian kinetochores count attached microtubules in a sensitive and switch-like manner. *J Cell Biol, 218*(11), 3583-3596. doi:10.1083/jcb.201902105

Kukreja, A. A., Kavuri, S., & Joglekar, A. P. (2020). Microtubule Attachment and Centromeric Tension Shape the Protein Architecture of the Human Kinetochore. *Curr Biol*. doi:10.1016/j.cub.2020.09.038

Lampson, M. A., & Cheeseman, I. M. (2011). Sensing centromere tension: Aurora B and the regulation of kinetochore function. *Trends Cell Biol, 21*(3), 133-140. doi:10.1016/j.tcb.2010.10.007

Lampson, M. A., & Grishchuk, E. L. (2017). Mechanisms to Avoid and Correct Erroneous Kinetochore-Microtubule Attachments. *Biology (Basel), 6*(1). doi:10.3390/biology6010001

Liu, D., Vader, G., Vromans, M. J., Lampson, M. A., & Lens, S. M. (2009). Sensing chromosome bi-orientation by spatial separation of aurora B kinase from kinetochore substrates. *Science, 323*(5919), 1350-1353. doi:10.1126/science.1167000

Liu, D., Vleugel, M., Backer, C. B., Hori, T., Fukagawa, T., Cheeseman, I. M., & Lampson, M. A. (2010). Regulated targeting of protein phosphatase 1 to the outer kinetochore by KNL1 opposes Aurora B kinase. *J Cell Biol, 188*(6), 809-820. doi:10.1083/jcb.201001006

Long, A. F., Udy, D. B., & Dumont, S. (2017). Hec1 Tail Phosphorylation Differentially Regulates Mammalian Kinetochore Coupling to Polymerizing and Depolymerizing Microtubules. *Curr Biol, 27*(11), 1692-1699 e1693. doi:10.1016/j.cub.2017.04.058

Malik, R., Lenobel, R., Santamaria, A., Ries, A., Nigg, E. A., & Korner, R. (2009). Quantitative analysis of the human spindle phosphoproteome at distinct mitotic stages. *J Proteome Res, 8*(10), 4553-4563. doi:10.1021/pr9003773

Malvezzi, F., Litos, G., Schleiffer, A., Heuck, A., Mechtler, K., Clausen, T., & Westermann, S. (2013). A structural basis for kinetochore recruitment of the Ndc80 complex via two distinct centromere receptors. *EMBO J, 32*(3), 409-423. doi:10.1038/emboj.2012.356

Mattiuzzo, M., Vargiu, G., Totta, P., Fiore, M., Ciferri, C., Musacchio, A., & Degrassi, F. (2011). Abnormal kinetochore-generated pulling forces from expressing a N-terminally modified Hec1. *PLoS One, 6*(1), e16307. doi:10.1371/journal.pone.0016307

McEwen, B. F., Ding, Y., & Heagle, A. B. (1998). Relevance of kinetochore size and microtubule-binding capacity for stable chromosome attachment during mitosis in PtK1 cells. *Chromosome Res, 6*(2), 123-132. Retrieved from https://www.ncbi.nlm.nih.gov/pubmed/9543015

McEwen, B. F., Heagle, A. B., Cassels, G. O., Buttle, K. F., & Rieder, C. L. (1997). Kinetochore fiber maturation in PtK1 cells and its implications for the mechanisms of chromosome congression and anaphase onset. *J Cell Biol, 137*(7), 1567-1580. doi:10.1083/jcb.137.7.1567

McIntosh, J. R. (2017). Assessing the Contributions of Motor Enzymes and Microtubule Dynamics to Mitotic Chromosome Motions. *Annu Rev Cell Dev Biol, 33*, 1-22. doi:10.1146/annurev-cellbio-100616-060827

Miller, S. A., Johnson, M. L., & Stukenberg, P. T. (2008). Kinetochore attachments require an interaction between unstructured tails on microtubules and Ndc80(Hec1). *Curr Biol, 18*(22), 1785-1791. doi:10.1016/j.cub.2008.11.007

Nicklas, R. B. (1965). Chromosome Velocity during Mitosis as a Function of Chromosome Size and Position. *J Cell Biol, 25*, SUPPL:119-135. doi:10.1083/jcb.25.1.119

Nicklas, R. B., & Koch, C. A. (1969). Chromosome micromanipulation. 3. Spindle fiber tension and the reorientation of mal-oriented chromosomes. *J Cell Biol, 43*(1), 40-50. doi:10.1083/jcb.43.1.40

Nicklas, R. B., Ward, S. C., & Gorbsky, G. J. (1995). Kinetochore chemistry is sensitive to tension and may link mitotic forces to a cell cycle checkpoint. *J Cell Biol, 130*(4), 929-939. doi:10.1083/jcb.130.4.929

Nishino, T., Rago, F., Hori, T., Tomii, K., Cheeseman, I. M., & Fukagawa, T. (2013). CENP-T provides a structural platform for outer kinetochore assembly. *EMBO J, 32*(3), 424-436. doi:10.1038/emboj.2012.348

Nishino, T., Takeuchi, K., Gascoigne, K. E., Suzuki, A., Hori, T., Oyama, T., . . . Fukagawa, T. (2012). CENP-T-W-S-X forms a unique centromeric chromatin structure with a histone-like fold. *Cell, 148*(3), 487-501. doi:10.1016/j.cell.2011.11.061

Nousiainen, M., Sillje, H. H., Sauer, G., Nigg, E. A., & Korner, R. (2006). Phosphoproteome analysis of the human mitotic spindle. *Proc Natl Acad Sci U S A, 103*(14), 5391-5396. doi:10.1073/pnas.0507066103

Pesenti, M. E., Prumbaum, D., Auckland, P., Smith, C. M., Faesen, A. C., Petrovic, A., . . . Musacchio, A. (2018). Reconstitution of a 26-Subunit Human Kinetochore Reveals Cooperative Microtubule Binding by CENP-OPQUR and NDC80. *Mol Cell, 71*(6), 923-939 e910. doi:10.1016/j.molcel.2018.07.038

Petrovic, A., Keller, J., Liu, Y., Overlack, K., John, J., Dimitrova, Y. N., . . . Musacchio, A. (2016). Structure of the MIS12 Complex and Molecular Basis of Its Interaction with CENP-C at Human Kinetochores. *Cell, 167*(4), 1028-1040 e1015. doi:10.1016/j.cell.2016.10.005

Petrovic, A., Mosalaganti, S., Keller, J., Mattiuzzo, M., Overlack, K., Krenn, V., . . . Musacchio, A. (2014). Modular assembly of RWD domains on the Mis12 complex underlies outer kinetochore organization. *Mol Cell, 53*(4), 591-605. doi:10.1016/j.molcel.2014.01.019

Petrovic, A., Pasqualato, S., Dube, P., Krenn, V., Santaguida, S., Cittaro, D., . . . Musacchio, A. (2010). The MIS12 complex is a protein interaction hub for outer kinetochore assembly. *J Cell Biol, 190*(5), 835-852. doi:10.1083/jcb.201002070

Roscioli, E., Germanova, T. E., Smith, C. A., Embacher, P. A., Erent, M., Thompson, A. I., . . . McAinsh, A. D. (2020). Ensemble-Level Organization of Human Kinetochores and Evidence for Distinct Tension and Attachment Sensors. *Cell Rep, 31*(4), 107535. doi:10.1016/j.celrep.2020.107535

Sacristan, C., & Kops, G. J. (2015). Joined at the hip: kinetochores, microtubules, and spindle assembly checkpoint signaling. *Trends Cell Biol, 25*(1), 21-28. doi:10.1016/j.tcb.2014.08.006

Sarangapani, K. K., & Asbury, C. L. (2014). Catch and release: how do kinetochores hook the right microtubules during mitosis? *Trends Genet, 30*(4), 150-159. doi:10.1016/j.tig.2014.02.004

Schleiffer, A., Maier, M., Litos, G., Lampert, F., Hornung, P., Mechtler, K., & Westermann, S. (2012). CENP-T proteins are conserved centromere receptors of the Ndc80 complex. *Nat Cell Biol, 14*(6), 604-613. doi:10.1038/ncb2493

Schmidt, J. C., Kiyomitsu, T., Hori, T., Backer, C. B., Fukagawa, T., & Cheeseman, I. M. (2010). Aurora B kinase controls the targeting of the Astrin-SKAP complex to bioriented kinetochores. *J Cell Biol, 191*(2), 269-280. doi:10.1083/jcb.201006129

Screpanti, E., De Antoni, A., Alushin, G. M., Petrovic, A., Melis, T., Nogales, E., & Musacchio, A. (2011). Direct binding of Cenp-C to the Mis12 complex joins the inner and outer kinetochore. *Curr Biol, 21*(5), 391-398. doi:10.1016/j.cub.2010.12.039

Sundin, L. J., Guimaraes, G. J., & Deluca, J. G. (2011). The NDC80 complex proteins Nuf2 and Hec1 make distinct contributions to kinetochore-microtubule attachment in mitosis. *Mol Biol Cell, 22*(6), 759-768. doi:10.1091/mbc.E10-08-0671

Suzuki, A., Badger, B. L., & Salmon, E. D. (2015). A quantitative description of Ndc80 complex linkage to human kinetochores. *Nat Commun, 6*, 8161. doi:10.1038/ncomms9161

Suzuki, A., Badger, B. L., Wan, X., DeLuca, J. G., & Salmon, E. D. (2014). The architecture of CCAN proteins creates a structural integrity to resist spindle forces and achieve proper Intrakinetochore stretch. *Dev Cell, 30*(6), 717-730. doi:10.1016/j.devcel.2014.08.003

Tanaka, T. U. (2005). Chromosome bi-orientation on the mitotic spindle. *Philos Trans R Soc Lond B Biol Sci, 360*(1455), 581-589. doi:10.1098/rstb.2004.1612

Tanaka, T. U. (2010). Kinetochore-microtubule interactions: steps towards bi-orientation. *EMBO J, 29*(24), 4070-4082. doi:10.1038/emboj.2010.294

Tanaka, T. U., Stark, M. J., & Tanaka, K. (2005). Kinetochore capture and bi-orientation on the mitotic spindle. *Nat Rev Mol Cell Biol, 6*(12), 929-942. doi:10.1038/nrm1764

Tooley, J. G., Miller, S. A., & Stukenberg, P. T. (2011). The Ndc80 complex uses a tripartite attachment point to couple microtubule depolymerization to chromosome movement. *Mol Biol Cell, 22*(8), 1217-1226. doi:10.1091/mbc.E10-07-0626

Volkov, V. A., Huis In 't Veld, P. J., Dogterom, M., & Musacchio, A. (2018). Multivalency of NDC80 in the outer kinetochore is essential to track shortening microtubules and generate forces. *Elife, 7*. doi:10.7554/eLife.36764

Volkov, V. A., Zaytsev, A. V., Gudimchuk, N., Grissom, P. M., Gintsburg, A. L., Ataullakhanov, F. I., . . . Grishchuk, E. L. (2013). Long tethers provide high-force coupling of the Dam1 ring to shortening microtubules. *Proc Natl Acad Sci U S A, 110*(19), 7708-7713. doi:10.1073/pnas.1305821110

Wei, R. R., Al-Bassam, J., & Harrison, S. C. (2007). The Ndc80/HEC1 complex is a contact point for kinetochore-microtubule attachment. *Nat Struct Mol Biol, 14*(1), 54-59. doi:10.1038/nsmb1186

Weir, J. R., Faesen, A. C., Klare, K., Petrovic, A., Basilico, F., Fischbock, J., . . . Musacchio, A. (2016). Insights from biochemical reconstitution into the architecture of human kinetochores. *Nature, 537*(7619), 249-253. doi:10.1038/nature19333

Welburn, J. P., Vleugel, M., Liu, D., Yates, J. R., 3rd, Lampson, M. A., Fukagawa, T., & Cheeseman, I. M. (2010). Aurora B phosphorylates spatially distinct targets to differentially regulate the kinetochore-microtubule interface. *Mol Cell, 38*(3), 383-392. doi:10.1016/j.molcel.2010.02.034

Wendell, K. L., Wilson, L., & Jordan, M. A. (1993). Mitotic block in HeLa cells by vinblastine: ultrastructural changes in kinetochore-microtubule attachment and in centrosomes. *J Cell Sci, 104 (Pt 2)*, 261-274. Retrieved from https://www.ncbi.nlm.nih.gov/pubmed/8505360

Wimbish, R. T., & DeLuca, J. G. (2020). Hec1/Ndc80 Tail Domain Function at the Kinetochore-Microtubule Interface. *Front Cell Dev Biol, 8*, 43. doi:10.3389/fcell.2020.00043

Wimbish, R. T., DeLuca, K. F., Mick, J. E., Himes, J., Jimenez-Sanchez, I., Jeyaprakash, A. A., & DeLuca, J. G. (2020). The Hec1/Ndc80 tail domain is required for force generation at kinetochores, but is dispensable for kinetochore-microtubule attachment formation and Ska complex recruitment. *Mol Biol Cell, 31*(14), 1453-1473. doi:10.1091/mbc.E20-05-0286

Yoo, T. Y., Choi, J. M., Conway, W., Yu, C. H., Pappu, R. V., & Needleman, D. J. (2018). Measuring NDC80 binding reveals the molecular basis of tension-dependent kinetochore-microtubule attachments. *Elife, 7*. doi:10.7554/eLife.36392

Zaytsev, A. V., & Grishchuk, E. L. (2015). Basic mechanism for biorientation of mitotic chromosomes is provided by the kinetochore geometry and indiscriminate turnover of kinetochore microtubules. *Mol Biol Cell, 26*(22), 3985-3998. doi:10.1091/mbc.E15-06-0384

Zaytsev, A. V., Mick, J. E., Maslennikov, E., Nikashin, B., DeLuca, J. G., & Grishchuk, E. L. (2015). Multisite phosphorylation of the NDC80 complex gradually tunes its microtubule-binding affinity. *Mol Biol Cell, 26*(10), 1829-1844. doi:10.1091/mbc.E14-11-1539

Zaytsev, A. V., Sundin, L. J., DeLuca, K. F., Grishchuk, E. L., & DeLuca, J. G. (2014). Accurate phosphoregulation of kinetochore-microtubule affinity requires unconstrained molecular interactions. *J Cell Biol, 206*(1), 45-59. doi:10.1083/jcb.201312107

Zhu, T., Dou, Z., Qin, B., Jin, C., Wang, X., Xu, L., . . . Yao, X. (2013). Phosphorylation of microtubule-binding protein Hec1 by mitotic kinase Aurora B specifies spindle checkpoint kinase Mps1 signaling at the kinetochore. *J Biol Chem, 288*(50), 36149-36159. doi:10.1074/jbc.M113.507970

CHAPTER 4:

Discussion and Future Directions

4.1 Nanoscale Architecture of the Human Kinetochore: Summary of Key Findings

The kinetochore is among the most complex naturally occurring molecular machines in biology. With its crucial role in chromosome segregation and the proper replication of cells, it is perhaps unsurprising that the kinetochore contains >50 unique proteins, all present in multiple copies and with dynamic localization throughout cell division (Cheeseman, 2014; Cheeseman, Drubin, & Barnes, 2002). Mis-regulation of any of these proteins can cause chromosome missegregation and aneuploidy, which is responsible for a multitude of developmental diseases, a common source of miscarriage, and a hallmark of cancer cells (Bakhoum & Compton, 2012; Bharadwaj & Yu, 2004; Hassold & Hunt, 2001; Jia et al., 2015; Naylor & van Deursen, 2016; Weaver & Cleveland, 2006; Yuen, Montpetit, & Hieter, 2005). While the function and structure of a majority of kinetochore proteins are known, an integrated view of how the entire kinetochore network coordinates to give rise to the emergent functions of high-fidelity chromosome segregation is lacking. To achieve such an understanding, we must elucidate the protein architecture of the kinetochore (Joglekar & Kukreja, 2017).

In chapter 2 of this thesis, I developed a unique FRET-based methodology to probe a critical and heretofore unexplored area of the human kinetochore's architecture: the nanoscale

organization of proteins around individual kinetochore-microtubule attachments. Given its central role in all the kinetochore's main functions (spindle assembly checkpoint signaling, error correction, microtubule attachment and force generation), I focused my studies on the Ndc80 complex (Ndc80C). My measurements provide a map of the proximity of Ndc80C and several of its interaction partners in relation to each other and to the microtubule plus-end under a variety of kinetochore functional states. Importantly, the architectural model I synthesize from these measurements leads to several significant insights regarding how the kinetochore operates.

4.1.1 The Organization of Microtubule-Bound Ndc80C is Shaped by Centromeric Tension and Microtubule Attachment

In microtubule-attached kinetochores, I found that Ndc80C molecules cluster and that this clustering increases with centromeric tension. Using chemical assays to alter the kinetochore's microtubule-attachment state, I discovered that microtubule polymerization dynamics and the number of microtubule-bound Ndc80C molecules both play a role in the increased clustering of Ndc80C with centromeric tension. These observations suggest several important concepts regarding how the kinetochore regulates its attachments to generate force and maintain its connection to the spindle. Ndc80C clustering is reminiscent of *in vitro* studies that demonstrate the ability of Ndc80C molecules to transduce greater amounts of force when more molecules are collectively engaged in microtubule binding (Helgeson et al., 2018; Huis In 't Veld, Volkov, Stender, Musacchio, & Dogterom, 2019; Powers et al., 2009; Volkov, Huis In 't Veld, Dogterom, & Musacchio, 2018; Volkov et al., 2013). The correlation between Ndc80C binding and tension is regulated by the Aurora B kinase and phosphatases, allowing kinetochore-microtubule attachments to strengthen under increasing load (Akiyoshi et al., 2010). This latter point is supported by assays I performed with an inhibitor of the Aurora B kinase, resulting in

high levels of Ndc80C binding (Yoo et al., 2018). Additionally, I observed that Ndc80C clustering is reduced when microtubule dynamics are dampened. This is reminiscent of the force-coupling mechanism of kinetochore-microtubule attachments, where depolymerizing microtubule protofilaments push the kinetochore's microtubule-binding proteins towards the microtubule minus-end to generate movement (Grishchuk, Molodtsov, Ataullakhanov, & McIntosh, 2005; Hill, 1985; Inoue & Salmon, 1995).

I also found that Ndc80C clustering vanishes when kinetochores are unattached, suggesting that the microtubule lattice acts a scaffold upon which Ndc80C molecules can effectively cluster. The lack of clustering at unattached kinetochores indicates that Ndc80C molecules are further apart from one another when unbound. This dispersed arrangement of Ndc80C molecules effectively increases the surface area of the kinetochore, a feature that would benefit a 'search and capture'-like mechanism for the initial formation of attachments (Magidson et al., 2015; Roscioli et al., 2020; Tanaka, Stark, & Tanaka, 2005).

4.1.2 Artificially Lowering the Amount of Ndc80C at Kinetochores Does Not Disrupt Clustering, Suggesting a 'Lawn'-Like Mode of Microtubule Binding

Another key finding from this study was the persistence of Ndc80C clustering when its centromeric receptors are reduced. This result was counter-intuitive to our expectations; reducing the number of Ndc80C receptors leads to kinetochores with fewer Ndc80C molecules and therefore fewer microtubule attachments (Suzuki, Badger, & Salmon, 2015). Thus, we expected Ndc80C clustering to reduce. This would certainly be the case in a 'repeat-subunit' model of the human kinetochore (Blower, Sullivan, & Karpen, 2002; Vargiu et al., 2017; Zinkowski, Meyne, & Brinkley, 1991), where large mammalian kinetochores that bind multiple microtubules are conceptualized as mere repetitions of the fundamental budding yeast kinetochore subunit: one

centromeric nucleosome that recruits all the kinetochore components necessary to bind exactly one microtubule (Joglekar, Bouck, et al., 2008). While vertebrate kinetochores are certainly composed of biochemical subunits centered on centromere-specific nucleosomes (Musacchio & Desai, 2017; Pesenti et al., 2018; Weir et al., 2016), the notion that these nucleosome subunits constitute single microtubule sites has been challenged in the 'lawn' model of the kinetochore (Dong, Vanden Beldt, Meng, Khodjakov, & McEwen, 2007; Zaytsev, Sundin, DeLuca, Grishchuk, & DeLuca, 2014). The lawn model proposes that the kinetochore behaves as a network of adaptable attachment sites that form due to the cooperation of its multiple nucleosome subunits. Importantly, our data provide support for this latter interpretation of the kinetochore architecture. The cooperation of multiple nucleosome subunits in microtubule binding explains how Ndc80C clustering persists even when the number of Ndc80C molecules is reduced.

4.1.3 Human and Budding Yeast Kinetochores Use Divergent Centromeric Blueprints to Build Similar Microtubule-Binding Architectures

Our final key insight comes from a comparison of the human and budding yeast kinetochore architectures. The point centromere of the budding yeast kinetochore has a denser organization than the regional centromere of the human kinetochore. This dense organization is a potential consequence of the small size of the budding yeast centromere (~125 bp) and its incorporation of exactly one centromeric nucleosome to bind exactly one microtubule (Aravamudhan, Felzer-Kim, & Joglekar, 2013; Cheeseman et al., 2002; Joglekar, Bouck, Molk, Bloom, & Salmon, 2006; Joglekar, Salmon, & Bloom, 2008). By comparison, the vastly larger human centromere (an ~200 nm diameter disk-like surface composed of megabase pairs of DNA) contains many hundreds of centromeric nucleosomes and dynamically binds between 12-

25 microtubules (Bodor et al., 2014; Kabeche & Compton, 2013; Wendell, Wilson, & Jordan, 1993).Since the distribution of centromere proteins dictates the spatial arrangement of Ndc80C molecules, the sparser organization of the human centromere may reflect functional requirements for forming multiple microtubule attachments.

Human and budding yeast kinetochores also differ in their organization of microtubule-bound Ndc80C. Whereas budding yeast kinetochores maintain a collinear arrangement of Ndc80C around the microtubule circumference, human kinetochores stagger their Ndc80C molecules between 20-30 nm along the microtubule lattice. While these organizations may arise due to differences in how each organism recruits Ndc80C, the potential functional consequences of these spatial arrangements provide some intriguing possibilities. For example, budding yeast kinetochores use a unique ring-like complex called Dam1 to encircle the microtubule (Franck et al., 2007; Lampert, Hornung, & Westermann, 2010; Lampert, Mieck, Alushin, Nogales, & Westermann, 2013; Tien et al., 2010; Westermann et al., 2005). The Dam1 ring binds behind Ndc80C's microtubule-attachment domain (Aravamudhan, Felzer-Kim, Gurunathan, & Joglekar, 2014), allowing it to transmit the force of depolymerizing protofilaments to Ndc80C and the kinetochore. By virtue of its interaction with Ndc80C, the Dam1 ring would also restrict the distribution of Ndc80C molecules to a narrow region on the microtubule lattice. Thus, the collinear arrangement of budding yeast Ndc80C molecules appears to be imposed by the functional requirements of budding yeast kinetochore-microtubule attachments. While human kinetochores possess no such ring-like molecule, the staggered arrangement of human Ndc80C may also occur due to its interactions with its own unique set of microtubule-binding proteins (e.g., the Ska complex and Astrin/SKAP) (Friese et al., 2016; Helgeson et al., 2018; Huis In 't Veld et al., 2019; Janczyk et al., 2017; Wimbish et al., 2020). Additionally, staggering may

represent a unique solution to increase the microtubule tip-tracking ability of Ndc80C molecules (Volkov et al., 2018). While the organization of budding yeast and human kinetochores exhibit several architectural differences, there is one remarkable similarity: both display a comparable degree of clustering between the microtubule-binding ends of their Ndc80C molecules. This conservation in Ndc80C architecture suggests that, despite the different challenges for chromosome segregation in budding yeast and human cells, there are shared principles for how kinetochores engage the spindle.

4.2 The Role of Multiple Ndc80 Complexes in Kinetochore Function: Summary of Key Findings

The research presented in Chapter 2 of this thesis is largely descriptive, providing an architectural model of kinetochore proteins and how this architecture responds to the physical state of the kinetochore. The importance of such architectural studies is that they inform a mechanistic understanding of kinetochore function. For my second project presented in Chapter 3 of this thesis, my goal has been to directly study the functional consequences of a particular aspect of the human kinetochore's architecture. Namely, I am attempting to answer the question: why does the human kinetochore contain ~250 copies of the Ndc80 complex? While the question may appear self-evident, there are a few key observations that motivate such a study. First, during my FRET-based studies of human kinetochore architecture I observed that: 1) kinetochores still attach to the spindle, align at the metaphase plate, and produce normal amounts of tension when the number of Ndc80C molecules is artificially reduced, and 2) the number of microtubule-bound Ndc80C molecules fluctuates throughout the course of mitosis. Additionally, others have observed that chromosomes still segregate with very few errors when the number of microtubule attachments is artificially reduced (Dudka et al., 2018), and the spindle assembly

checkpoint (SAC) is satisfied when kinetochores bind only 30% of their microtubule capacity (Etemad et al., 2019; Kuhn & Dumont, 2019). These observations suggest that the human kinetochore employs an excess of Ndc80C molecules, leading us to not only ask why the kinetochore contains 250 Ndc80C molecules, but also what is the minimum number necessary for the proper execution of each of its functions. To answer this question, I developed an approach to titrate the human kinetochore with functionally-impaired Ndc80C mutants. By doping human kinetochores with increasing amounts of mutant Ndc80C, I have been able to perform a series of 'stress tests' to determine the failure point of the kinetochore's various functions.

4.2.1 The Spindle Assembly Checkpoint Exhibits A Switch-Like Operation to a Threshold Number of Microtubule-Bound Ndc80C Molecules

The first set of tests I performed were aimed at delineating the number of Ndc80C molecules needed for SAC activation. By titrating kinetochores with microtubule-binding defective Ndc80C mutants, I found that cells progress to anaphase when kinetochores contain, on average, as much as 40% unbound Ndc80C. Beyond this threshold, there is an immediate switch-like transition to constitutive SAC activation where cells no longer divide. This simple observation provides several insights and brings up many questions regarding the mechanism of SAC activation.

First, cell cycle progression does not require all the kinetochore's ~250 Ndc80C molecules to be actively bound to microtubules. Since unbound Ndc80C molecules participate in SAC signaling (Aravamudhan, Goldfarb, & Joglekar, 2015; Hiruma et al., 2015; Ji, Gao, & Yu, 2015), it is unclear how cells containing 40% unbound Ndc80C per kinetochore avoid SAC arrest. One possibility is that the collective signaling strength of these unbound Ndc80C

molecules is not strong enough to delay the cell cycle. This interpretation, however, poses a major problem. If the *average* number of unbound Ndc80C molecules per kinetochore is below the 40% threshold, cells will divide. Thus, cells could contain a low number of unattached kinetochores without ever crossing this threshold, leading to chromosome missegregation. For this mechanism to operate, individual kinetochores would need to exponentially scale the strength of their SAC signal with the number of unbound Ndc80C molecules (Chen et al., 2019). Alternatively, it is possible that kinetochores possess a mechanism to inactivate the SAC signaling function of their unbound Ndc80C molecules beyond a threshold level of attachment. In this scenario, the SAC signaling capacity of kinetochores would slowly be extinguished as their number of unattached Ndc80C molecules fell below the 40% threshold. This mechanism leaves open the possibility that a single unattached kinetochore can produce an SAC signal strong enough to delay the cell cycle. How partially attached kinetochores would silence the SAC activity of their unbound Ndc80C molecules, however, is unknown.

The other surprising feature of this titration experiment is the rapid transition to constitutive SAC activation. Such a sharp transition demonstrates that the kinetochore is acutely sensitive to the number of unbound Ndc80C molecules. How the kinetochore precisely discriminates the number of unbound Ndc80C molecules to achieve this switch-like response is unknown. However, this response is consistent with previous studies showing a similar, rapid transition in SAC activation when kinetochores drop below 30% of their microtubule binding capacity (Etemad et al., 2019; Kuhn & Dumont, 2019). Combining these results with my own, the kinetochore needs between 150-175 of its Ndc80C molecules engaged with at least 5-6 microtubules to meet the SAC's requirement for attachment.

4.2.2 Chromosome Alignment and Segregation Rely on the Precise, Coordinated Regulation of Kinetochore-Microtubule Attachment Strength

In a second set of tests, I investigated the sensitivity of chromosome segregation to the kinetochore's ability to fine-tune the strength of its microtubule attachments. The predominate method by which kinetochores tune their microtubule binding strength is through phospho-regulation of Ndc80C's microtubule-binding affinity (DeLuca, Lens, & DeLuca, 2011; Long, Udy, & Dumont, 2017; Welburn et al., 2010). I found that cells exhibit severe defects in chromosome alignment and segregation when their kinetochores contain as little as 20% of a strong-binding Ndc80C mutant whose microtubule affinity cannot be regulated. This incredible sensitivity of chromosome segregation on the regulation Ndc80C's binding strength shows that the formation of kinetochore-microtubule attachments is not a one step process. The kinetochore must constantly detach and reform its connection with the spindle to biorient chromosomes on the metaphase plate. The fact that such a small amount of strong-binding Ndc80C disrupts the entire alignment process highlights the fragility of the kinetochore's microtubule-binding apparatus and emphasizes the dexterity with which the kinetochore simultaneously regulates its ~250 molecules to produce coordinated, coherent chromosome movement.

While the preliminary results from this project leave many open-ended questions, one clear takeaway is that different kinetochore functions exhibit varying degrees of reliance on the human kinetochore's pool of 250 Ndc80C molecules. The titration assay I developed for this project provides a direct means for quantitatively defining this reliance in terms of failure limits. Importantly, the existence of such failure limits indicates that the kinetochore incorporates an excess of Ndc80C molecules, allowing the kinetochore to operate with definable margins of error. In Chapter 3, I layout several future directions for this study to deepen the insights we have

already attained and to explore more functional consequences of the human kinetochore's 250 Ndc80C molecules. For this reason, I will forgo such a discussion here.

4.3 The Interplay Between Kinetochore Architecture and Kinetochore Function: Future Directions

The central theme of my studies is the interconnected relationship between the kinetochore's architecture and its function. In Chapter 2 of my thesis, I mapped the nanoscale organization of the human kinetochores microtubule attachments, revealing several key insights into how the kinetochore forms attachments. In Chapter 3, I dissect a particular aspect of the kinetochore's architecture, the necessity of its ~250 Ndc80C molecules, revealing that the number of Ndc80C molecules is dictated by the kinetochore's functional demands. Deepening our understanding of the kinetochore's mechanisms will certainly continue to expose this reciprocal relationship. Below, I layout several key areas for the future study of kinetochore architecture and function

4.3.1 Changes in Kinetochore Architecture with the State of Its Attachments

In Chapter 2, I demonstrated that the organization of Ndc80C molecules changes both upon the initial formation of microtubule attachments and in response to increasing centromeric tension. There are several other functionally important attachment states which may reveal important changes to the organization of Ndc80C and its interaction partners at the kinetochore (Figure 4.1A). In particular, two such attachment states are of keen interest: syntelically attached kinetochores and anaphase kinetochores.

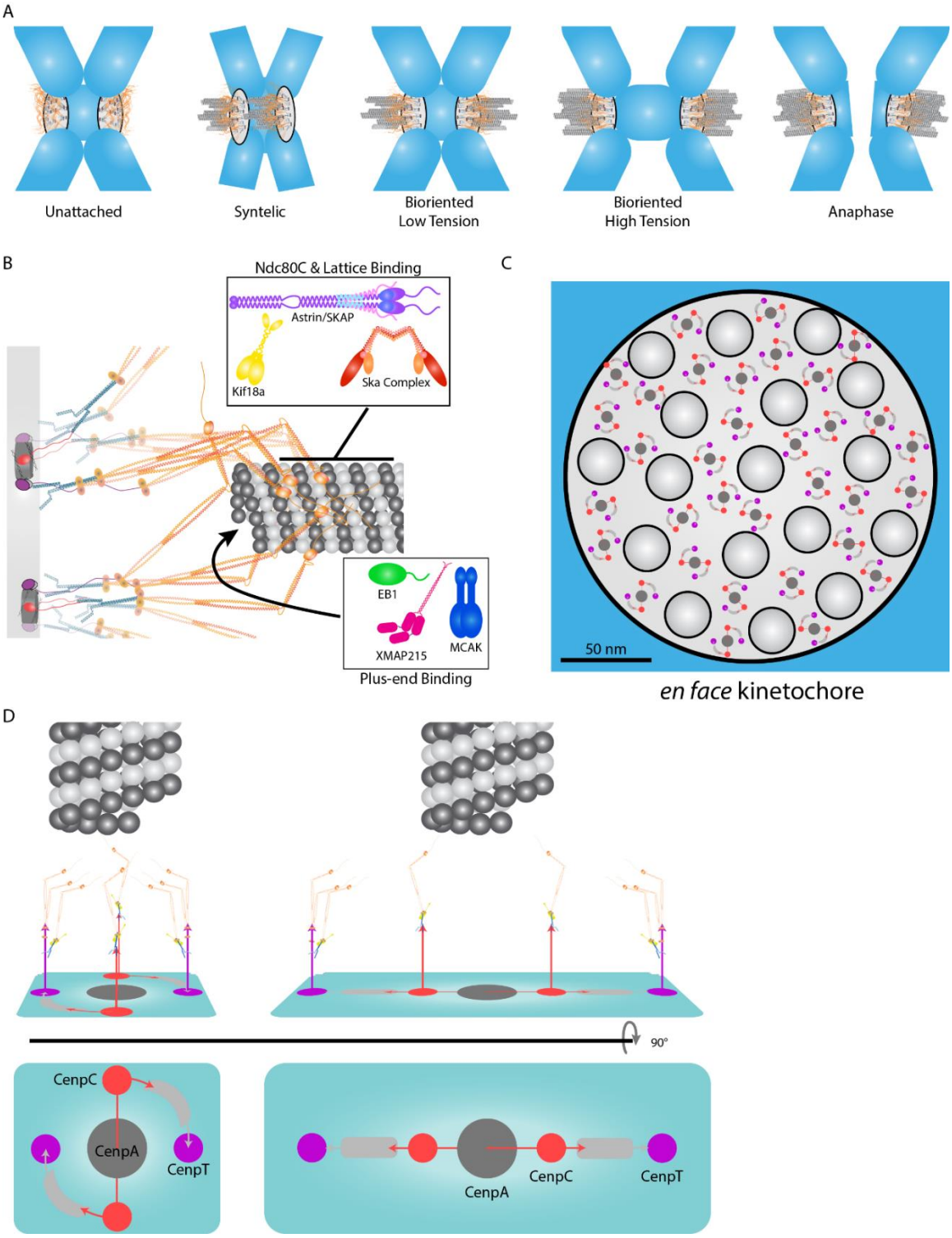

Figure 4.1 Future Frontiers in the Architecture & Function of Human Kinetochores
(A) Different attachment states of the human kinetochore will influence the architecture of its protein components. Investigating these architectural changes will be an important step in understanding the kinetochore's functional mechanisms. (B) The end-on kinetochore-microtubule attachment has several accessory proteins that do not constitute the main kinetochore scaffold but nonetheless participate in the regulation of attachments and force generation. Proteins like the Ska complex, SKAP/Astrin, and Kif18a either directly interact with Ndc80C or bind the

microtubule lattice. XMAP215, MCAK, and EB1 are importantly regulators of plus-end polymerization dynamics and mediate the transition from poleward and anti-poleward movement. The spatial relationship and physical interaction of these proteins with the kinetochore will provide insights into the coordination and regulation of the human kinetochore's multiple microtubule attachments. (C) *En face* views of the kinetochore demonstrate an apparent regularity in the spacing of its microtubule attachments (microtubules, light gray circles with black outlines). To understand this regularity, the spatial organization of the microtubule-binding centromeric nucleosome subunits that decorate the centromeric surface must be mapped (centromeric nucleosome subunits, regular patterns of dark gray, red, and purple circles). (D) Possible spatial organizations of the centromeric nucleosome (CenpA, dark gray circle) and the CenpC and CenpT molecules (red and purple circles, respectively) which anchor Ndc80C to the centromere. Unraveling the precise geometry of these interactions will highlight how centromeric nucleosomes arrange Ndc80C molecules for microtubule-binding (microtubule, gray and white spheres at the top of the cartoon) and how multiple such nucleosomes may cooperate in the formation of attachments.

Syntely, a condition where both kinetochores in a sister chromatid pair are attached to the same spindle pole, are specifically destabilized by the kinetochore's error correction mechanism (Cimini, Wan, Hirel, & Salmon, 2006; Gregan, Polakova, Zhang, Tolic-Norrelykke, & Cimini, 2011; Nicklas, Ward, & Gorbsky, 1995; Tanaka, 2010). Such attachments satisfy the SAC and therefore do not delay cell cycle progression. Nonetheless, these attachments will lead to chromosome missegregation if allowed to persist. A key question has been what is the precise signature recognized by the kinetochore to distinguish syntelic attachments from productive bioriented attachments. Since the syntelic attachment geometry fails to develop tension between its sister kinetochores, it is largely believed that this is the key signal being sensed by the kinetochore (Lampson & Grishchuk, 2017). However, how the kinetochore senses this lack of tension is unknown. Even more intriguing is the fact that bioriented kinetochores also often exist in states of low tension, further complicating how the error correction distinguishes these two attachments types. Understanding how the protein architecture of syntelic attachments differs from low-tension bioriented kinetochores will certainly lend insights into the nature of the error correction mechanism's shrewd ability to destabilize incorrect attachments.

Anaphase kinetochores also present a unique study for how the kinetochore adapts to the state of its attachments. At the onset of anaphase, kinetochores are maximally bound by spindle

microtubules as the tension between sister chromatids reduces significantly due to the loss of cohesion (McEwen, Heagle, Cassels, Buttle, & Rieder, 1997). Myself and others have shown that the kinetochore strengthens its attachments via tension-induced mechanisms (Akiyoshi et al., 2010; DeLuca et al., 2011; S. A. Miller, Johnson, & Stukenberg, 2008; Yoo et al., 2018). However, the regulatory mechanisms controlling attachment strength reduce at anaphase onset (Afonso et al., 2019), and the microtubule-generated segregation forces produced at anaphase kinetochores are considerably low (~0.1 pN; (Nicklas, 1965, 1983; Nicklas & Koch, 1969)). Studying the architecture of these anaphase attachments will shed light on how the kinetochore maintains robust connections to the spindle during this vital stage of chromosome segregation and how microtubule depolymerization forces are transmitted to kinetochore proteins when there is little to no opposing force.

4.3.2 The Influence of the Spatial Relationship Between Ndc80C and Accessory Microtubule-Binding Proteins on Kinetochore-Microtubule Attachments

The FRET-based architectural study I presented in Chapter 2 is far from exhaustive. However, a complete survey of the spatial relationships between all the kinetochore's proteins would present a sizable undertaking that may lack the appropriate focus to yield significant insights. For my studies, I limited my investigations to the organization of Ndc80C, allowing me to emphasize the relationship between kinetochore architecture and microtubule-attachment. While Ndc80C is a nexus for all the kinetochore's principal functions, several other proteins are involved in the execution of these functions. In particular, the persistence of the kinetochore's microtubule attachments and its ability to manipulate their polymerization dynamics are directly tied to the interactions between Ndc80C and a diverse set of accessory microtubule-binding proteins (Figure 4.1B). Mapping the spatial relationship between these accessory proteins and

Ndc80C will be necessary to understand how the kinetochore regulates its attachments and force generation.

One important class of microtubule-binding proteins are those that directly bind Ndc80C to enhance the geometry and strength of its attachment to the microtubule lattice (Figure 4.1B). For example, the SKAP/Astrin complex localizes to kinetochore-microtubule attachments via interactions with Ndc80C (Friese et al., 2016; Kern, Monda, Su, Wilson-Kubalek, & Cheeseman, 2017), and may aid in the conversion of lateral to end-on microtubule attachments (Kern, Nicholls, Page, & Cheeseman, 2016; Shrestha et al., 2017). Additionally, the Ska complex binds to Ndc80C and microtubules, strengthening microtubule attachment and the tip-tracking abilities of both complexes (Helgeson et al., 2018; Huis In 't Veld et al., 2019; Janczyk et al., 2017; Welburn et al., 2009; Wimbish et al., 2020; Zhang et al., 2012). The role of the Ska complex at human kinetochores has been likened to the budding yeast Dam1 ring-like complex, although Ska has not been observed to form higher order oligomeric structures. However, the subunit composition of the Ska complex incorporates at least two copies of an Ndc80C interaction domain, raising the intriguing possibility that this complex may simultaneously coordinate multiple Ndc80C molecules at microtubule-attached human kinetochores. Thus, it will be important to address how such coordination influences the clustering and staggering of Ndc80C. Another interesting lattice-binding protein is the kinesin motor, Kif18a (Stumpff, von Dassow, Wagenbach, Asbury, & Wordeman, 2008; Stumpff, Wagenbach, Franck, Asbury, & Wordeman, 2012). While an interaction between Kif18a and Ndc80C has not been investigated, loss of Kif18a from kinetochores results in tension-less attachments that activate an SAC-mediated arrest (Janssen et al., 2018). Inactivating the SAC, however, allows these tension-less kinetochores to proceed to anaphase without any change in the rate of chromosome

missegregation. Given that Ndc80C participates in SAC signaling and is a target for the destabilization of low-tension attachments, these phenotypes suggest that Kif18a plays an important role in the functional mechanisms of Ndc80C.

In addition to maintaining robust attachments, the kinetochore must coordinate the polymerization dynamics of ~15-20 microtubule attachments to achieve coherent chromosome movement. In this regard, a host of kinetochore-specific plus-end binding proteins are of particular interest in unraveling the regulatory mechanisms of kinetochore-microtubule dynamics (Figure 4.1B). The EB1 (for End Binding 1) protein specifically localizes to the plus-ends of polymerizing microtubules. During mitosis, this protein displays a remarkable localization pattern at kinetochores: EB1 is only found at bioriented kinetochores with anti-poleward motion, switching between sister kinetochores as they oscillate about the metaphase plate (Tirnauer, Canman, Salmon, & Mitchison, 2002). While this localization makes sense with EB1's microtubule-binding properties, it will be important to determine how this localization influences the dynamics of kinetochore-microtubule attachments and if there are other features of anti-poleward kinetochores that encourage EB1 to localize at kinetochores versus elsewhere in the spindle. Several other kinetochore-specific end-binding proteins present intriguing phenotypes the regarding the coordination of kinetochore-microtubule dynamics. MCAK and XMAP215 are both potent microtubule destabilizing enzymes, promoting the conversion from growing to shrinking microtubule plus-ends (Ayaz, Ye, Huddleston, Brautigam, & Rice, 2012; Humphrey, Felzer-Kim, & Joglekar, 2018; Kosco et al., 2001; M. P. Miller, Asbury, & Biggins, 2016; M. P. Miller et al., 2019; Wordeman, Wagenbach, & von Dassow, 2007). Additionally, CLASP proteins are targeted to the plus-end of kinetochore microtubules by the kinetochore protein CENP-E, and may also play a functional role in the microtubule-binding mechanisms of

SKAP/Astrin (Maffini et al., 2009; Maiato et al., 2003; Maiato, Khodjakov, & Rieder, 2005; Manning et al., 2010; Pereira et al., 2006). Importantly, a crucial missing piece of information is a logical framework that connects and regulates the activities of this assortment of end-binding proteins. Mapping the dynamic spatial relationship of these proteins to each other and to the main kinetochore scaffold will enhance our understanding of how the kinetochore regulates its attachments to facilitate coherent chromosome movement.

4.3.3 Centromeric Protein Architecture Dictates the Rules of Engagement Between Human Kinetochores and the Mitotic Spindle

The future studies presented thus far, and my architectural study in Chapter 2, has focused on the spatial relationships between kinetochore proteins at individual microtubule attachments. However, the human kinetochore simultaneously binds 15-20 microtubules (Dudka et al., 2018; Wendell et al., 1993), leading to the question of how these attachments are coordinated for unified kinetochore function. Electron micrographs of *en face* views of the mammalian kinetochore present a striking regularity in the spacing of microtubule attachments (Figure 4.1C) (McEwen, Ding, & Heagle, 1998; Rieder, 1982). To understand how this regularity is enforced and the functional consequences of this spacing, a macroscale view of kinetochore proteins across the entire centromere surface will need to be developed.

The human kinetochore is composed of repeating biochemical subunits centered on the centromere-specific CenpA nucleosome (Allu et al., 2019; Bodor et al., 2014; Pesenti et al., 2018; Weir et al., 2016). A single CenpA nucleosome seeds the recruitment of all the protein components necessary for kinetochore formation, including the Ndc80C centromeric receptors, CenpC and CenpT (Basilico et al., 2014; Gascoigne et al., 2011; Hori et al., 2008; Kato et al., 2013; Klare et al., 2015; Logsdon et al., 2015; Nishino et al., 2012). Due to their ability to recruit

Ndc80C, the spatial distribution of CenpC and CenpT molecules will set up the entire microtubule-binding interface of the kinetochore (Figure 4.1D; (Dimitrova, Jenni, Valverde, Khin, & Harrison, 2016; Huis In 't Veld et al., 2016; Nishino et al., 2013; Petrovic et al., 2016; Rago, Gascoigne, & Cheeseman, 2015; Schleiffer et al., 2012; Screpanti et al., 2011)). Thus, two specific aspects of the organization of human centromere proteins are pertinent: 1) The spatial relationship of proteins centered about a single CenpA nucleosome, and 2) the spatial relationship between neighboring CenpA nucleosomes.

Significant progress has been made towards this first goal, predominately through an impressive array of biochemical and structure based studies (Allu et al., 2019; Hinshaw & Harrison, 2019, 2020; Kato et al., 2013; Pesenti et al., 2018; Weir et al., 2016; Yan et al., 2019). These studies demonstrate that centromere proteins are densely organized around the CenpA nucleosome, forming an ~20 nm diameter sphere-like globule. However, a nucleosome structure containing both CenpC and CenpT has yet to be solved, preventing insight into the spacing of the recruitment domains for Ndc80C and how they may be coordinated with the nucleosome structure.

The spatial organization of multiple CenpA nucleosomes across the human centromere surface presents an even more challenging goal. Human centromeres contain megabase pairs of repetitive DNA sequence and CenpA nucleosomes do not display strong sequence-specific binding (Kixmoeller, Allu, & Black, 2020; Musacchio & Desai, 2017). Additionally, centromeres are interspersed with CenpA nucleosomes and canonical nucleosomes, and the centromere incorporates an excess of CenpA nucleosomes that do not directly participate in kinetochore formation (Bodor et al., 2014). Thus, the rules regulating CenpA deposition at the human centromere have remained intractable to current methodological approaches.

Complicating this picture further, CenpA can form functional centromeres at ectopic chromosomal locations (i.e., 'neocentromeres') and researchers have even artificially bypassed the need for CenpA to form functional kinetochores (Bodor et al., 2014; Gascoigne et al., 2011).

One potential strategy that could help elucidate how CenpA molecules are organized relative to the kinetochore's microtubule attachment sites is to perform super-resolution microscopy of the *en face* kinetochore (Figure 4.1C). The human centromere is a ~200 nm diameter disk (Wendell et al., 1993), making it a suitable structure for super-resolution studies. Because the centromere contains hundreds of CenpA nucleosomes, not all of which participate in kinetochore formation, labeling this protein will not provide a requisite strategy to reveal the spacing of the kinetochore's nucleosome-centered biochemical subunits. However, one of the lower copy-number centromere proteins that interacts with CenpA for kinetochore formation may provide a suitable target for labeling. At ~80 molecules per human kinetochore, CenpT or members of the CenpHIKM complex make perfect targets for this enterprise. Considering the surface area of the centromere, the subunit stoichiometry of the CenpA biochemical subunits, and assuming a uniform distribution of these molecules across the centromere surface, we can expect that to find biochemical subunits spaced ~11-16 nm apart. Although these dimensions approach the limits of current super-resolution methodologies, they will allow us to observe the macroscopic distribution of these proteins across the centromere face.

In summary, the intimate relationship between human kinetochore architecture and function is akin to the architecture/function relationship of any macroscopic machine. Understanding the operation of any machine requires knowledge of the spatial relationship and interaction of its constituent pieces. Likewise, building a machine for a specific purpose places restrictions on its potential design. With successful chromosome segregation being the absolute

guiding principle of the architecture/function of the human kinetochore, continuing to elucidate the nature of this relationship will yield deeper insight into one of cellular biology's most fundamental problems.

4.4 References

Afonso, O., Castellani, C. M., Cheeseman, L. P., Ferreira, J. G., Orr, B., Ferreira, L. T., . . . Maiato, H. (2019). Spatiotemporal control of mitotic exit during anaphase by an aurora B-Cdk1 crosstalk. *Elife, 8*. doi:10.7554/eLife.47646

Akiyoshi, B., Sarangapani, K. K., Powers, A. F., Nelson, C. R., Reichow, S. L., Arellano-Santoyo, H., . . . Biggins, S. (2010). Tension directly stabilizes reconstituted kinetochore-microtubule attachments. *Nature, 468*(7323), 576-579. doi:10.1038/nature09594

Allu, P. K., Dawicki-McKenna, J. M., Van Eeuwen, T., Slavin, M., Braitbard, M., Xu, C., . . . Black, B. E. (2019). Structure of the Human Core Centromeric Nucleosome Complex. *Curr Biol*. doi:10.1016/j.cub.2019.06.062

Aravamudhan, P., Felzer-Kim, I., Gurunathan, K., & Joglekar, A. P. (2014). Assembling the protein architecture of the budding yeast kinetochore-microtubule attachment using FRET. *Curr Biol, 24*(13), 1437-1446. doi:10.1016/j.cub.2014.05.014

Aravamudhan, P., Felzer-Kim, I., & Joglekar, A. P. (2013). The budding yeast point centromere associates with two Cse4 molecules during mitosis. *Curr Biol, 23*(9), 770-774. doi:10.1016/j.cub.2013.03.042

Aravamudhan, P., Goldfarb, A. A., & Joglekar, A. P. (2015). The kinetochore encodes a mechanical switch to disrupt spindle assembly checkpoint signalling. *Nat Cell Biol, 17*(7), 868-879. doi:10.1038/ncb3179

Ayaz, P., Ye, X., Huddleston, P., Brautigam, C. A., & Rice, L. M. (2012). A TOG:alphabeta-tubulin complex structure reveals conformation-based mechanisms for a microtubule polymerase. *Science, 337*(6096), 857-860. doi:10.1126/science.1221698

Bakhoum, S. F., & Compton, D. A. (2012). Chromosomal instability and cancer: a complex relationship with therapeutic potential. *J Clin Invest, 122*(4), 1138-1143. doi:10.1172/JCI59954

Basilico, F., Maffini, S., Weir, J. R., Prumbaum, D., Rojas, A. M., Zimniak, T., . . . Musacchio, A. (2014). The pseudo GTPase CENP-M drives human kinetochore assembly. *Elife, 3*, e02978. doi:10.7554/eLife.02978

Bharadwaj, R., & Yu, H. (2004). The spindle checkpoint, aneuploidy, and cancer. *Oncogene, 23*(11), 2016-2027. doi:10.1038/sj.onc.1207374

Blower, M. D., Sullivan, B. A., & Karpen, G. H. (2002). Conserved organization of centromeric chromatin in flies and humans. *Dev Cell, 2*(3), 319-330. doi:10.1016/s1534-5807(02)00135-1

Bodor, D. L., Mata, J. F., Sergeev, M., David, A. F., Salimian, K. J., Panchenko, T., . . . Jansen, L. E. (2014). The quantitative architecture of centromeric chromatin. *Elife, 3*, e02137. doi:10.7554/eLife.02137

Cheeseman, I. M. (2014). The kinetochore. *Cold Spring Harb Perspect Biol, 6*(7), a015826. doi:10.1101/cshperspect.a015826

Cheeseman, I. M., Drubin, D. G., & Barnes, G. (2002). Simple centromere, complex kinetochore: linking spindle microtubules and centromeric DNA in budding yeast. *J Cell Biol, 157*(2), 199-203. doi:10.1083/jcb.200201052

Chen, C., Whitney, I. P., Banerjee, A., Sacristan, C., Sekhri, P., Kern, D. M., . . . Joglekar, A. P. (2019). Ectopic Activation of the Spindle Assembly Checkpoint Signaling Cascade Reveals Its Biochemical Design. *Curr Biol, 29*(1), 104-119 e110. doi:10.1016/j.cub.2018.11.054

Cimini, D., Wan, X., Hirel, C. B., & Salmon, E. D. (2006). Aurora kinase promotes turnover of kinetochore microtubules to reduce chromosome segregation errors. *Curr Biol, 16*(17), 1711-1718. doi:10.1016/j.cub.2006.07.022

DeLuca, K. F., Lens, S. M., & DeLuca, J. G. (2011). Temporal changes in Hec1 phosphorylation control kinetochore-microtubule attachment stability during mitosis. *J Cell Sci, 124*(Pt 4), 622-634. doi:10.1242/jcs.072629

Dimitrova, Y. N., Jenni, S., Valverde, R., Khin, Y., & Harrison, S. C. (2016). Structure of the MIND Complex Defines a Regulatory Focus for Yeast Kinetochore Assembly. *Cell, 167*(4), 1014-1027 e1012. doi:10.1016/j.cell.2016.10.011

Dong, Y., Vanden Beldt, K. J., Meng, X., Khodjakov, A., & McEwen, B. F. (2007). The outer plate in vertebrate kinetochores is a flexible network with multiple microtubule interactions. *Nat Cell Biol, 9*(5), 516-522. doi:10.1038/ncb1576

Dudka, D., Noatynska, A., Smith, C. A., Liaudet, N., McAinsh, A. D., & Meraldi, P. (2018). Complete microtubule-kinetochore occupancy favours the segregation of merotelic attachments. *Nat Commun, 9*(1), 2042. doi:10.1038/s41467-018-04427-x

Etemad, B., Vertesy, A., Kuijt, T. E. F., Sacristan, C., van Oudenaarden, A., & Kops, G. (2019). Spindle checkpoint silencing at kinetochores with submaximal microtubule occupancy. *J Cell Sci, 132*(12). doi:10.1242/jcs.231589

Franck, A. D., Powers, A. F., Gestaut, D. R., Gonen, T., Davis, T. N., & Asbury, C. L. (2007). Tension applied through the Dam1 complex promotes microtubule elongation providing a direct mechanism for length control in mitosis. *Nat Cell Biol, 9*(7), 832-837. doi:10.1038/ncb1609

Friese, A., Faesen, A. C., Huis in 't Veld, P. J., Fischbock, J., Prumbaum, D., Petrovic, A., . . . Musacchio, A. (2016). Molecular requirements for the inter-subunit interaction and kinetochore recruitment of SKAP and Astrin. *Nat Commun, 7*, 11407. doi:10.1038/ncomms11407

Gascoigne, K. E., Takeuchi, K., Suzuki, A., Hori, T., Fukagawa, T., & Cheeseman, I. M. (2011). Induced ectopic kinetochore assembly bypasses the requirement for CENP-A nucleosomes. *Cell, 145*(3), 410-422. doi:10.1016/j.cell.2011.03.031

Gregan, J., Polakova, S., Zhang, L., Tolic-Norrelykke, I. M., & Cimini, D. (2011). Merotelic kinetochore attachment: causes and effects. *Trends Cell Biol, 21*(6), 374-381. doi:10.1016/j.tcb.2011.01.003

Grishchuk, E. L., Molodtsov, M. I., Ataullakhanov, F. I., & McIntosh, J. R. (2005). Force production by disassembling microtubules. *Nature, 438*(7066), 384-388. doi:10.1038/nature04132

Hassold, T., & Hunt, P. (2001). To err (meiotically) is human: the genesis of human aneuploidy. *Nat Rev Genet, 2*(4), 280-291. doi:10.1038/35066065

Helgeson, L. A., Zelter, A., Riffle, M., MacCoss, M. J., Asbury, C. L., & Davis, T. N. (2018). Human Ska complex and Ndc80 complex interact to form a load-bearing assembly that strengthens kinetochore-microtubule attachments. *Proc Natl Acad Sci U S A, 115*(11), 2740-2745. doi:10.1073/pnas.1718553115

Hill, T. L. (1985). Theoretical problems related to the attachment of microtubules to kinetochores. *Proc Natl Acad Sci U S A, 82*(13), 4404-4408. doi:10.1073/pnas.82.13.4404

Hinshaw, S. M., & Harrison, S. C. (2019). The structure of the Ctf19c/CCAN from budding yeast. *Elife, 8*. doi:10.7554/eLife.44239

Hinshaw, S. M., & Harrison, S. C. (2020). The Structural Basis for Kinetochore Stabilization by Cnn1/CENP-T. *Curr Biol, 30*(17), 3425-3431 e3423. doi:10.1016/j.cub.2020.06.024

Hiruma, Y., Sacristan, C., Pachis, S. T., Adamopoulos, A., Kuijt, T., Ubbink, M., . . . Kops, G. J. (2015). CELL DIVISION CYCLE. Competition between MPS1 and microtubules at kinetochores regulates spindle checkpoint signaling. *Science, 348*(6240), 1264-1267. doi:10.1126/science.aaa4055

Hori, T., Amano, M., Suzuki, A., Backer, C. B., Welburn, J. P., Dong, Y., . . . Fukagawa, T. (2008). CCAN makes multiple contacts with centromeric DNA to provide distinct pathways to the outer kinetochore. *Cell, 135*(6), 1039-1052. doi:10.1016/j.cell.2008.10.019

Huis In 't Veld, P. J., Jeganathan, S., Petrovic, A., Singh, P., John, J., Krenn, V., . . . Musacchio, A. (2016). Molecular basis of outer kinetochore assembly on CENP-T. *Elife, 5*. doi:10.7554/eLife.21007

Huis In 't Veld, P. J., Volkov, V. A., Stender, I. D., Musacchio, A., & Dogterom, M. (2019). Molecular determinants of the Ska-Ndc80 interaction and their influence on microtubule tracking and force-coupling. *Elife, 8*. doi:10.7554/eLife.49539

Humphrey, L., Felzer-Kim, I., & Joglekar, A. P. (2018). Stu2 acts as a microtubule destabilizer in metaphase budding yeast spindles. *Mol Biol Cell, 29*(3), 247-255. doi:10.1091/mbc.E17-08-0494

Inoue, S., & Salmon, E. D. (1995). Force generation by microtubule assembly/disassembly in mitosis and related movements. *Mol Biol Cell, 6*(12), 1619-1640. doi:10.1091/mbc.6.12.1619

Janczyk, P. L., Skorupka, K. A., Tooley, J. G., Matson, D. R., Kestner, C. A., West, T., . . . Stukenberg, P. T. (2017). Mechanism of Ska Recruitment by Ndc80 Complexes to Kinetochores. *Dev Cell, 41*(4), 438-449 e434. doi:10.1016/j.devcel.2017.04.020

Janssen, L. M. E., Averink, T. V., Blomen, V. A., Brummelkamp, T. R., Medema, R. H., & Raaijmakers, J. A. (2018). Loss of Kif18A Results in Spindle Assembly Checkpoint Activation at Microtubule-Attached Kinetochores. *Curr Biol, 28*(17), 2685-2696 e2684. doi:10.1016/j.cub.2018.06.026

Ji, Z., Gao, H., & Yu, H. (2015). CELL DIVISION CYCLE. Kinetochore attachment sensed by competitive Mps1 and microtubule binding to Ndc80C. *Science, 348*(6240), 1260-1264. doi:10.1126/science.aaa4029

Jia, C. W., Wang, L., Lan, Y. L., Song, R., Zhou, L. Y., Yu, L., . . . Wang, S. Y. (2015). Aneuploidy in Early Miscarriage and its Related Factors. *Chin Med J (Engl), 128*(20), 2772-2776. doi:10.4103/0366-6999.167352

Joglekar, A. P., Bouck, D., Finley, K., Liu, X., Wan, Y., Berman, J., . . . Bloom, K. S. (2008). Molecular architecture of the kinetochore-microtubule attachment site is conserved between point and regional centromeres. *J Cell Biol, 181*(4), 587-594. doi:10.1083/jcb.200803027

Joglekar, A. P., Bouck, D. C., Molk, J. N., Bloom, K. S., & Salmon, E. D. (2006). Molecular architecture of a kinetochore-microtubule attachment site. *Nat Cell Biol, 8*(6), 581-585. doi:10.1038/ncb1414

Joglekar, A. P., & Kukreja, A. A. (2017). How Kinetochore Architecture Shapes the Mechanisms of Its Function. *Curr Biol, 27*(16), R816-R824. doi:10.1016/j.cub.2017.06.012

Joglekar, A. P., Salmon, E. D., & Bloom, K. S. (2008). Counting kinetochore protein numbers in budding yeast using genetically encoded fluorescent proteins. *Methods Cell Biol, 85*, 127-151. doi:10.1016/S0091-679X(08)85007-8

Kabeche, L., & Compton, D. A. (2013). Cyclin A regulates kinetochore microtubules to promote faithful chromosome segregation. *Nature, 502*(7469), 110-113. doi:10.1038/nature12507

Kato, H., Jiang, J., Zhou, B. R., Rozendaal, M., Feng, H., Ghirlando, R., . . . Bai, Y. (2013). A conserved mechanism for centromeric nucleosome recognition by centromere protein CENP-C. *Science, 340*(6136), 1110-1113. doi:10.1126/science.1235532

Kern, D. M., Monda, J. K., Su, K. C., Wilson-Kubalek, E. M., & Cheeseman, I. M. (2017). Astrin-SKAP complex reconstitution reveals its kinetochore interaction with microtubule-bound Ndc80. *Elife, 6*. doi:10.7554/eLife.26866

Kern, D. M., Nicholls, P. K., Page, D. C., & Cheeseman, I. M. (2016). A mitotic SKAP isoform regulates spindle positioning at astral microtubule plus ends. *J Cell Biol, 213*(3), 315-328. doi:10.1083/jcb.201510117

Kixmoeller, K., Allu, P. K., & Black, B. E. (2020). The centromere comes into focus: from CENP-A nucleosomes to kinetochore connections with the spindle. *Open Biol, 10*(6), 200051. doi:10.1098/rsob.200051

Klare, K., Weir, J. R., Basilico, F., Zimniak, T., Massimiliano, L., Ludwigs, N., . . . Musacchio, A. (2015). CENP-C is a blueprint for constitutive centromere-associated network assembly within human kinetochores. *J Cell Biol, 210*(1), 11-22. doi:10.1083/jcb.201412028

Kosco, K. A., Pearson, C. G., Maddox, P. S., Wang, P. J., Adams, I. R., Salmon, E. D., . . . Huffaker, T. C. (2001). Control of microtubule dynamics by Stu2p is essential for spindle orientation and metaphase chromosome alignment in yeast. *Mol Biol Cell, 12*(9), 2870-2880. doi:10.1091/mbc.12.9.2870

Kuhn, J., & Dumont, S. (2019). Mammalian kinetochores count attached microtubules in a sensitive and switch-like manner. *J Cell Biol, 218*(11), 3583-3596. doi:10.1083/jcb.201902105

Lampert, F., Hornung, P., & Westermann, S. (2010). The Dam1 complex confers microtubule plus end-tracking activity to the Ndc80 kinetochore complex. *J Cell Biol, 189*(4), 641-649. doi:10.1083/jcb.200912021

Lampert, F., Mieck, C., Alushin, G. M., Nogales, E., & Westermann, S. (2013). Molecular requirements for the formation of a kinetochore-microtubule interface by Dam1 and Ndc80 complexes. *J Cell Biol, 200*(1), 21-30. doi:10.1083/jcb.201210091

Lampson, M. A., & Grishchuk, E. L. (2017). Mechanisms to Avoid and Correct Erroneous Kinetochore-Microtubule Attachments. *Biology (Basel), 6*(1). doi:10.3390/biology6010001

Logsdon, G. A., Barrey, E. J., Bassett, E. A., DeNizio, J. E., Guo, L. Y., Panchenko, T., . . . Black, B. E. (2015). Both tails and the centromere targeting domain of CENP-A are required for centromere establishment. *J Cell Biol, 208*(5), 521-531. doi:10.1083/jcb.201412011

Long, A. F., Udy, D. B., & Dumont, S. (2017). Hec1 Tail Phosphorylation Differentially Regulates Mammalian Kinetochore Coupling to Polymerizing and Depolymerizing Microtubules. *Curr Biol, 27*(11), 1692-1699 e1693. doi:10.1016/j.cub.2017.04.058

Maffini, S., Maia, A. R., Manning, A. L., Maliga, Z., Pereira, A. L., Junqueira, M., . . . Maiato, H. (2009). Motor-independent targeting of CLASPs to kinetochores by CENP-E promotes microtubule turnover and poleward flux. *Curr Biol, 19*(18), 1566-1572. doi:10.1016/j.cub.2009.07.059

Magidson, V., Paul, R., Yang, N., Ault, J. G., O'Connell, C. B., Tikhonenko, I., . . . Khodjakov, A. (2015). Adaptive changes in the kinetochore architecture facilitate proper spindle assembly. *Nat Cell Biol, 17*(9), 1134-1144. doi:10.1038/ncb3223

Maiato, H., Fairley, E. A., Rieder, C. L., Swedlow, J. R., Sunkel, C. E., & Earnshaw, W. C. (2003). Human CLASP1 is an outer kinetochore component that regulates spindle microtubule dynamics. *Cell, 113*(7), 891-904. doi:10.1016/s0092-8674(03)00465-3

Maiato, H., Khodjakov, A., & Rieder, C. L. (2005). Drosophila CLASP is required for the incorporation of microtubule subunits into fluxing kinetochore fibres. *Nat Cell Biol, 7*(1), 42-47. doi:10.1038/ncb1207

Manning, A. L., Bakhoum, S. F., Maffini, S., Correia-Melo, C., Maiato, H., & Compton, D. A. (2010). CLASP1, astrin and Kif2b form a molecular switch that regulates kinetochore-microtubule dynamics to promote mitotic progression and fidelity. *EMBO J, 29*(20), 3531-3543. doi:10.1038/emboj.2010.230

McEwen, B. F., Ding, Y., & Heagle, A. B. (1998). Relevance of kinetochore size and microtubule-binding capacity for stable chromosome attachment during mitosis in PtK1 cells. *Chromosome Res, 6*(2), 123-132. Retrieved from https://www.ncbi.nlm.nih.gov/pubmed/9543015

McEwen, B. F., Heagle, A. B., Cassels, G. O., Buttle, K. F., & Rieder, C. L. (1997). Kinetochore fiber maturation in PtK1 cells and its implications for the mechanisms of chromosome congression and anaphase onset. *J Cell Biol, 137*(7), 1567-1580. doi:10.1083/jcb.137.7.1567

Miller, M. P., Asbury, C. L., & Biggins, S. (2016). A TOG Protein Confers Tension Sensitivity to Kinetochore-Microtubule Attachments. *Cell, 165*(6), 1428-1439. doi:10.1016/j.cell.2016.04.030

Miller, M. P., Evans, R. K., Zelter, A., Geyer, E. A., MacCoss, M. J., Rice, L. M., . . . Biggins, S. (2019). Kinetochore-associated Stu2 promotes chromosome biorientation in vivo. *PLoS Genet, 15*(10), e1008423. doi:10.1371/journal.pgen.1008423

Miller, S. A., Johnson, M. L., & Stukenberg, P. T. (2008). Kinetochore attachments require an interaction between unstructured tails on microtubules and Ndc80(Hec1). *Curr Biol, 18*(22), 1785-1791. doi:10.1016/j.cub.2008.11.007

Musacchio, A., & Desai, A. (2017). A Molecular View of Kinetochore Assembly and Function. *Biology (Basel), 6*(1). doi:10.3390/biology6010005

Naylor, R. M., & van Deursen, J. M. (2016). Aneuploidy in Cancer and Aging. *Annu Rev Genet, 50*, 45-66. doi:10.1146/annurev-genet-120215-035303

Nicklas, R. B. (1965). Chromosome Velocity during Mitosis as a Function of Chromosome Size and Position. *J Cell Biol, 25*, SUPPL:119-135. doi:10.1083/jcb.25.1.119

Nicklas, R. B. (1983). Measurements of the force produced by the mitotic spindle in anaphase. *J Cell Biol, 97*(2), 542-548. doi:10.1083/jcb.97.2.542

Nicklas, R. B., & Koch, C. A. (1969). Chromosome micromanipulation. 3. Spindle fiber tension and the reorientation of mal-oriented chromosomes. *J Cell Biol, 43*(1), 40-50. doi:10.1083/jcb.43.1.40

Nicklas, R. B., Ward, S. C., & Gorbsky, G. J. (1995). Kinetochore chemistry is sensitive to tension and may link mitotic forces to a cell cycle checkpoint. *J Cell Biol, 130*(4), 929-939. doi:10.1083/jcb.130.4.929

Nishino, T., Rago, F., Hori, T., Tomii, K., Cheeseman, I. M., & Fukagawa, T. (2013). CENP-T provides a structural platform for outer kinetochore assembly. *EMBO J, 32*(3), 424-436. doi:10.1038/emboj.2012.348

Nishino, T., Takeuchi, K., Gascoigne, K. E., Suzuki, A., Hori, T., Oyama, T., . . . Fukagawa, T. (2012). CENP-T-W-S-X forms a unique centromeric chromatin structure with a histone-like fold. *Cell, 148*(3), 487-501. doi:10.1016/j.cell.2011.11.061

Pereira, A. L., Pereira, A. J., Maia, A. R., Drabek, K., Sayas, C. L., Hergert, P. J., . . . Maiato, H. (2006). Mammalian CLASP1 and CLASP2 cooperate to ensure mitotic fidelity by regulating spindle and kinetochore function. *Mol Biol Cell, 17*(10), 4526-4542. doi:10.1091/mbc.e06-07-0579

Pesenti, M. E., Prumbaum, D., Auckland, P., Smith, C. M., Faesen, A. C., Petrovic, A., . . . Musacchio, A. (2018). Reconstitution of a 26-Subunit Human Kinetochore Reveals Cooperative Microtubule Binding by CENP-OPQUR and NDC80. *Mol Cell, 71*(6), 923-939 e910. doi:10.1016/j.molcel.2018.07.038

Petrovic, A., Keller, J., Liu, Y., Overlack, K., John, J., Dimitrova, Y. N., . . . Musacchio, A. (2016). Structure of the MIS12 Complex and Molecular Basis of Its Interaction with CENP-C at Human Kinetochores. *Cell, 167*(4), 1028-1040 e1015. doi:10.1016/j.cell.2016.10.005

Powers, A. F., Franck, A. D., Gestaut, D. R., Cooper, J., Gracyzk, B., Wei, R. R., . . . Asbury, C. L. (2009). The Ndc80 kinetochore complex forms load-bearing attachments to dynamic microtubule tips via biased diffusion. *Cell, 136*(5), 865-875. doi:10.1016/j.cell.2008.12.045

Rago, F., Gascoigne, K. E., & Cheeseman, I. M. (2015). Distinct organization and regulation of the outer kinetochore KMN network downstream of CENP-C and CENP-T. *Curr Biol, 25*(5), 671-677. doi:10.1016/j.cub.2015.01.059

Rieder, C. L. (1982). The formation, structure, and composition of the mammalian kinetochore and kinetochore fiber. *Int Rev Cytol, 79*, 1-58. Retrieved from https://www.ncbi.nlm.nih.gov/pubmed/6185450

Roscioli, E., Germanova, T. E., Smith, C. A., Embacher, P. A., Erent, M., Thompson, A. I., . . . McAinsh, A. D. (2020). Ensemble-Level Organization of Human Kinetochores and Evidence for Distinct Tension and Attachment Sensors. *Cell Rep, 31*(4), 107535. doi:10.1016/j.celrep.2020.107535

Schleiffer, A., Maier, M., Litos, G., Lampert, F., Hornung, P., Mechtler, K., & Westermann, S. (2012). CENP-T proteins are conserved centromere receptors of the Ndc80 complex. *Nat Cell Biol, 14*(6), 604-613. doi:10.1038/ncb2493

Screpanti, E., De Antoni, A., Alushin, G. M., Petrovic, A., Melis, T., Nogales, E., & Musacchio, A. (2011). Direct binding of Cenp-C to the Mis12 complex joins the inner and outer kinetochore. *Curr Biol, 21*(5), 391-398. doi:10.1016/j.cub.2010.12.039

Shrestha, R. L., Conti, D., Tamura, N., Braun, D., Ramalingam, R. A., Cieslinski, K., . . . Draviam, V. M. (2017). Aurora-B kinase pathway controls the lateral to end-on conversion of kinetochore-microtubule attachments in human cells. *Nat Commun, 8*(1), 150. doi:10.1038/s41467-017-00209-z

Stumpff, J., von Dassow, G., Wagenbach, M., Asbury, C., & Wordeman, L. (2008). The kinesin-8 motor Kif18A suppresses kinetochore movements to control mitotic chromosome alignment. *Dev Cell, 14*(2), 252-262. doi:10.1016/j.devcel.2007.11.014

Stumpff, J., Wagenbach, M., Franck, A., Asbury, C. L., & Wordeman, L. (2012). Kif18A and chromokinesins confine centromere movements via microtubule growth suppression and spatial control of kinetochore tension. *Dev Cell, 22*(5), 1017-1029. doi:10.1016/j.devcel.2012.02.013

Suzuki, A., Badger, B. L., & Salmon, E. D. (2015). A quantitative description of Ndc80 complex linkage to human kinetochores. *Nat Commun, 6*, 8161. doi:10.1038/ncomms9161

Tanaka, T. U. (2010). Kinetochore-microtubule interactions: steps towards bi-orientation. *EMBO J, 29*(24), 4070-4082. doi:10.1038/emboj.2010.294

Tanaka, T. U., Stark, M. J., & Tanaka, K. (2005). Kinetochore capture and bi-orientation on the mitotic spindle. *Nat Rev Mol Cell Biol, 6*(12), 929-942. doi:10.1038/nrm1764

Tien, J. F., Umbreit, N. T., Gestaut, D. R., Franck, A. D., Cooper, J., Wordeman, L., . . . Davis, T. N. (2010). Cooperation of the Dam1 and Ndc80 kinetochore complexes enhances microtubule coupling and is regulated by aurora B. *J Cell Biol, 189*(4), 713-723. doi:10.1083/jcb.200910142

Tirnauer, J. S., Canman, J. C., Salmon, E. D., & Mitchison, T. J. (2002). EB1 targets to kinetochores with attached, polymerizing microtubules. *Mol Biol Cell, 13*(12), 4308-4316. doi:10.1091/mbc.e02-04-0236

Vargiu, G., Makarov, A. A., Allan, J., Fukagawa, T., Booth, D. G., & Earnshaw, W. C. (2017). Stepwise unfolding supports a subunit model for vertebrate kinetochores. *Proc Natl Acad Sci U S A, 114*(12), 3133-3138. doi:10.1073/pnas.1614145114

Volkov, V. A., Huis In 't Veld, P. J., Dogterom, M., & Musacchio, A. (2018). Multivalency of NDC80 in the outer kinetochore is essential to track shortening microtubules and generate forces. *Elife, 7*. doi:10.7554/eLife.36764

Volkov, V. A., Zaytsev, A. V., Gudimchuk, N., Grissom, P. M., Gintsburg, A. L., Ataullakhanov, F. I., . . . Grishchuk, E. L. (2013). Long tethers provide high-force coupling of the Dam1 ring to shortening microtubules. *Proc Natl Acad Sci U S A, 110*(19), 7708-7713. doi:10.1073/pnas.1305821110

Weaver, B. A., & Cleveland, D. W. (2006). Does aneuploidy cause cancer? *Curr Opin Cell Biol, 18*(6), 658-667. doi:10.1016/j.ceb.2006.10.002

Weir, J. R., Faesen, A. C., Klare, K., Petrovic, A., Basilico, F., Fischbock, J., . . . Musacchio, A. (2016). Insights from biochemical reconstitution into the architecture of human kinetochores. *Nature, 537*(7619), 249-253. doi:10.1038/nature19333

Welburn, J. P., Grishchuk, E. L., Backer, C. B., Wilson-Kubalek, E. M., Yates, J. R., 3rd, & Cheeseman, I. M. (2009). The human kinetochore Ska1 complex facilitates microtubule

depolymerization-coupled motility. *Dev Cell, 16*(3), 374-385. doi:10.1016/j.devcel.2009.01.011

Welburn, J. P., Vleugel, M., Liu, D., Yates, J. R., 3rd, Lampson, M. A., Fukagawa, T., & Cheeseman, I. M. (2010). Aurora B phosphorylates spatially distinct targets to differentially regulate the kinetochore-microtubule interface. *Mol Cell, 38*(3), 383-392. doi:10.1016/j.molcel.2010.02.034

Wendell, K. L., Wilson, L., & Jordan, M. A. (1993). Mitotic block in HeLa cells by vinblastine: ultrastructural changes in kinetochore-microtubule attachment and in centrosomes. *J Cell Sci, 104 (Pt 2)*, 261-274. Retrieved from https://www.ncbi.nlm.nih.gov/pubmed/8505360

Westermann, S., Avila-Sakar, A., Wang, H. W., Niederstrasser, H., Wong, J., Drubin, D. G., . . . Barnes, G. (2005). Formation of a dynamic kinetochore- microtubule interface through assembly of the Dam1 ring complex. *Mol Cell, 17*(2), 277-290. doi:10.1016/j.molcel.2004.12.019

Wimbish, R. T., DeLuca, K. F., Mick, J. E., Himes, J., Jimenez-Sanchez, I., Jeyaprakash, A. A., & DeLuca, J. G. (2020). The Hec1/Ndc80 tail domain is required for force generation at kinetochores, but is dispensable for kinetochore-microtubule attachment formation and Ska complex recruitment. *Mol Biol Cell, 31*(14), 1453-1473. doi:10.1091/mbc.E20-05-0286

Wordeman, L., Wagenbach, M., & von Dassow, G. (2007). MCAK facilitates chromosome movement by promoting kinetochore microtubule turnover. *J Cell Biol, 179*(5), 869-879. doi:10.1083/jcb.200707120

Yan, K., Yang, J., Zhang, Z., McLaughlin, S. H., Chang, L., Fasci, D., . . . Barford, D. (2019). Structure of the inner kinetochore CCAN complex assembled onto a centromeric nucleosome. *Nature, 574*(7777), 278-282. doi:10.1038/s41586-019-1609-1

Yoo, T. Y., Choi, J. M., Conway, W., Yu, C. H., Pappu, R. V., & Needleman, D. J. (2018). Measuring NDC80 binding reveals the molecular basis of tension-dependent kinetochore-microtubule attachments. *Elife, 7*. doi:10.7554/eLife.36392

Yuen, K. W., Montpetit, B., & Hieter, P. (2005). The kinetochore and cancer: what's the connection? *Curr Opin Cell Biol, 17*(6), 576-582. doi:10.1016/j.ceb.2005.09.012

Zaytsev, A. V., Sundin, L. J., DeLuca, K. F., Grishchuk, E. L., & DeLuca, J. G. (2014). Accurate phosphoregulation of kinetochore-microtubule affinity requires unconstrained molecular interactions. *J Cell Biol, 206*(1), 45-59. doi:10.1083/jcb.201312107

Zhang, G., Kelstrup, C. D., Hu, X. W., Kaas Hansen, M. J., Singleton, M. R., Olsen, J. V., & Nilsson, J. (2012). The Ndc80 internal loop is required for recruitment of the Ska complex to establish end-on microtubule attachment to kinetochores. *J Cell Sci, 125*(Pt 13), 3243-3253. doi:10.1242/jcs.104208

Zinkowski, R. P., Meyne, J., & Brinkley, B. R. (1991). The centromere-kinetochore complex: a repeat subunit model. *J Cell Biol, 113*(5), 1091-1110. doi:10.1083/jcb.113.5.1091